Report Prepared by:
Francisco J. Presuel-Moreno
With
Yanbo Liu*
Yu-You Wu**
Wendy Arias*

Final Report

Analysis and Estimation of Service Life of Corrosion Prevention Materials Using Diffusion, Resistivity and Accelerated Curing for New Bridge Structures - Volume 2: Accelerated Curing of Concrete with High Volume Pozzolans (Resistivity, Diffusivity, and Compressive Strength)

(BDK79-977-02)

submitted to

Florida Department of Transportation Research Center
605 Suwannee Street
Tallahassee, Florida 32399

submitted by

Francisco Presuel-Moreno
Center for Marine Materials
Department of Ocean and Mechanical Engineering
Florida Atlantic University – Sea Tech
101 North Beach Road
Dania Beach, Florida 33004

December 2013

* Graduate Student
** Post-Doctoral Research Associate

Disclaimer

The opinions, findings, and conclusions expressed in this publication are those of the author and not necessarily those of the State of Florida Department of Transportation.

SI* (MODERN METRIC) CONVERSION FACTORS

APPROXIMATE CONVERSIONS TO SI UNITS

Symbol	When You Know	Multiply By	To Find	Symbol
		LENGTH		
in	inches	25.4	millimeters	mm
ft	feet	0.305	meters	m
yd	yards	0.914	meters	m
mi	miles	1.61	kilometers	km
		AREA		
in^2	square inches	645.2	square millimeters	mm^2
ft^2	square feet	0.093	square meters	m^2
yd^2	square yard	0.836	square meters	m^2
ac	acres	0.405	hectares	ha
mi^2	square miles	2.59	square kilometers	km^2
		VOLUME		
fl oz	fluid ounces	29.57	milliliters	mL
gal	gallons	3.785	liters	L
ft^3	cubic feet	0.028	cubic meters	m^3
yd^3	cubic yards	0.765	cubic meters	m^3
		NOTE: volumes greater than 1000 L shall be shown in m^3		
		MASS		
oz	ounces	28.35	grams	g
lb	pounds	0.454	kilograms	kg
T	short tons (2000 lb)	0.907	megagrams (or "metric ton")	Mg (or "t")
		TEMPERATURE (exact degrees)		
°F	Fahrenheit	5 (F-32)/9 or (F-32)/1.8	Celsius	°C
		ILLUMINATION		
fc	foot-candles	10.76	lux	lx
fl	foot-Lamberts	3.426	$candela/m^2$	cd/m^2
		FORCE and PRESSURE or STRESS		
lbf	poundforce	4.45	newtons	N
lbf/in^2	poundforce per square inch	6.89	kilopascals	kPa

APPROXIMATE CONVERSIONS FROM SI UNITS

Symbol	When You Know	Multiply By	To Find	Symbol
		LENGTH		
mm	millimeters	0.039	inches	in
m	meters	3.28	feet	ft
m	meters	1.09	yards	yd
km	kilometers	0.621	miles	mi
		AREA		
mm^2	square millimeters	0.0016	square inches	in^2
m^2	square meters	10.764	square feet	ft^2
m^2	square meters	1.195	square yards	yd^2
ha	hectares	2.47	acres	ac
km^2	square kilometers	0.386	square miles	mi^2
		VOLUME		
mL	milliliters	0.034	fluid ounces	fl oz
L	liters	0.264	gallons	gal
m^3	cubic meters	35.314	cubic feet	ft^3
m^3	cubic meters	1.307	cubic yards	yd^3
		MASS		
g	grams	0.035	ounces	oz
kg	kilograms	2.202	pounds	lb
Mg (or "t")	megagrams (or "metric ton")	1.103	short tons (2000 lb)	T
		TEMPERATURE (exact degrees)		
°C	Celsius	1.8C+32	Fahrenheit	°F
		ILLUMINATION		
lx	lux	0.0929	foot-candles	fc
cd/m^2	$candela/m^2$	0.2919	foot-Lamberts	fl
		FORCE and PRESSURE or STRESS		
N	newtons	0.225	poundforce	lbf
kPa	kilopascals	0.145	poundforce per square inch	lbf/in^2

*SI is the symbol for the International System of Units. Appropriate rounding should be made to comply with Section 4 of ASTM E380.
(Revised March 2003)

Technical Report Documentation Page

1. Report No.	2. Government Accession No.	3. Recipient's Catalog No.
4. Title and Subtitle Analysis and Estimation of Service Life of Corrosion Prevention Materials Using Diffusion, Resistivity and Accelerated Curing for New Bridge Structures -- Volume 2: Accelerated Curing Of Concrete With High Volume Pozzolans (Resistivity, Diffusivity And Compressive Strength)		5. Report Date December, 2013 6. Performing Organization Code FAU-OE-CMM-08-3
7. Author(s) Francisco Presuel-Moreno, Yanbo Liu, Yu-You Wu, Wendy Arias		8. Performing Organization Report No. BDK79-977-02
9. Performing Organization Name and Address Center for Marine Materials Florida Atlantic University – Sea Tech Campus 101 North Beach Road Dania Beach, Florida 33004		10. Work Unit No. (TRAIS) 11. Contract or Grant No. BDK79-977-02
12. Sponsoring Agency Name and Address Florida Department of Transportation 605 Suwannee Street, MS 30 Tallahassee, FL 32399		13. Type of Report and Period Covered Final Report April 2010 – December 30, 2013 14. Sponsoring Agency Code
15. Supplementary Notes		

16. Abstract

This investigation presents results of the temperature effect via accelerated curing on durability properties (resistivity and diffusivity) and compressive strength of concrete with pozzolans or slag and the effect of these admixtures on microstructure and chemical compositions of concrete pore solution. Temperature dependence of electrical resistivity and chloride diffusivity was studied by dynamic temperature tests in the case of resistivity and by testing chloride migration coefficient (D_{nssm}) at multiple temperatures on specimens of the same composition. For both type of tests, mature specimens were used (older than one year). Accelerated curing regimes involved curing concrete specimens in 35°C lime water for different periods of time. Compressive strength test, resistivity measurement, bulk diffusion (D_{app}), and rapid chloride migration (RCM) tests were performed. Additionally, a leaching method was used to measure pH and conductivity of concrete pore solution. Based on the results, general normalization equations were developed to describe the temperature effect on resistivity and diffusivity of concrete. The accelerated curing regimes were found to increase the compressive strength and resistance to chloride ion penetration in the short and long terms. With the developed correlation between resistivity and migration coefficients, it is possible to employ the resistivity measurement as an alternative of the RCM test to evaluate resistance of chloride ion penetration of concrete. Bulk diffusion values were also correlated to resistivity values for the different mixtures. Pozzolanic admixtures were found to decrease both pH and conductivity of concrete pore solution as the replacement ratio increased. Moreover, the migration coefficients were found to be greatly correlated to the microstructure properties of concrete, such as porosity, formation factor, and tortuosity.

17. Key Word	18. Distribution Statement
Bridge substructures, concrete, bulk diffusion, accelerated curing, compression strength, resistivity, migration coefficient	No restrictions. This document is available to the public through NTIS, Springfield, VA 22161

19. Security Classification. (of this report) Unclassified	20. Security Classif. (of this page) Unclassified	21. No. of Pages 226	22. Price

Form DOT F 1700.7 (8-72) Reproduction of completed page authorized

ACKNOWLEDGEMENTS

The authors are indebted to the FDOT State Materials Office for assisting in preparing the different concrete specimens and conducting several tests at SMO for this study and, in particular, Mr. Mario Paredes, Mr. Ronald Simmons, and several SMO Technicians (Richard Delorenzo, Pat Carlton, Thomas Frank, Jason Burchfield). The assistance of several undergraduate students that worked as research assistants is also acknowledged.

EXECUTIVE SUMMARY

This investigation presents results of the temperature effect via accelerated curing on durability properties (resistivity and diffusivity) and compressive strength of concrete with pozzolans or slag and the effect of these admixtures on microstructure and chemical compositions of concrete pore solution. Temperature dependence of electrical resistivity and chloride diffusivity was studied by dynamic temperature tests (the cylinders were subjected to multiple temperatures until stable and the resistivity then measured) in the case of resistivity and by testing chloride migration coefficient (D_{nssm}) at multiple temperatures on specimens of the same composition. For both type of tests, mature specimens were used (older than one year). Accelerated curing regimes involved curing concrete specimens in 35°C lime water for different periods of time (including 2 days room temperature, RT, and 26 days elevated temperature, ET: 2RT/26ET, 7RT/21ET, 14RT/14ET, 2RT/ET). Compressive strength tests, resistivity measurements, bulk diffusion (D_{app}) tests, and rapid chloride migration (RCM) tests were performed. Additionally, a leaching method was used to measure pH and conductivity of concrete pore solution on selected specimens. Based on the results, general normalization equations were developed to describe the temperature effect on resistivity and diffusivity of concrete. The accelerated curing regimes were found to increase the compressive strength and resistance to chloride ion penetration (via resistivity measurements) at short-term and long-term. With the developed correlation between resistivity and migration coefficients, it is possible to employ the resistivity measurement as an alternative of the RCM test to evaluate resistance of chloride ion penetration of concrete. Bulk diffusion values were also correlated to resistivity values for the different mixtures. Pozzolanic admixtures were found to decrease both pH and conductivity of concrete pore solution as the replacement ratio increased. However, pH for the same composition subjected to different curing regimes showed very similar values. Moreover, the migration coefficients were found to be greatly correlated to the microstructure properties of concrete, such as porosity, formation factor and tortuosity.

TABLE OF CONTENTS

LIST OF FIGURES

LIST OF TABLES

NOMENCLATURE

a	Constant in Archie's law; electrode spacing of Wenner method.
c_i	Concentration of ion species i
C_T	Critical chloride threshold
D	Diffusion coefficient
D_{app}	Apparent diffusion coefficient
D_{eff}	Effective diffusion coefficient
D_i	Diffusivity of ion species i
D_T	Diffusion coefficient at temperature T
$D(t)$	Diffusion coefficient at age t
D_{Cl}	Diffusion coefficient of chloride ions
D_{nssm}	Non-steady-state migration coefficient
$D_{nssm,T}$	Non-steady-state migration coefficient at temperature T
$E_{a,\rho}$	Activation energy for resistivity
$E_{a,D}$	Activation energy for diffusivity
F	Formation factor
I	Electric current
I_i	Electric current contribution of ion species i
$I_{corr}(T)$	Corrosion current density at temperature T
$K_{D,\rho}$	Constant of diffusivity and resistivity
$K_{\rho,g}$	Geometry factor for electrical resistivity of concrete
$K_{\rho,T}$	Temperature factor on resistivity
$K_{D,T}$	Temperature factor on diffusivity

m	Aging factor; tortuosity constant
Q	Electric quantity
Q_i	Electric quantity contribution of ion species i
R	Gas constant
t_i	Transference number of ion species i
T	Temperature
T_i	Time to corrosion imitation
T_p	Time of corrosion propagation
Z_i	Charge of species ion i
α	Temperature coefficient
σ	Conductivity
σ_i	Conductivity of ion species i
σ_0	Conductivity of pore solution
ϕ	Porosity
λ_i	Molar conductivity of ion species i
ρ	Electrical resistivity
ρ_{app}	Apparent electrical resistivity
ρ_T	Electrical resistivity at temperature T
$\rho(t)$	Electrical resistivity at age t
τ	Tortuosity

1. INTRODUCTION AND OBJECTIVES

Concrete is one of the most widely used construction materials in the world. Concrete is strong in compression and relatively weak in tension, so reinforcing steel (rebar) is usually used to increase the tensile strength of concrete. Due to the high alkalinity (pH>12.5) of the concrete pore solution, a passive oxide film is formed on the rebar surface. This passive layer initially protects the rebar from corrosion[1]. However, the presence of chloride ions could destroy the passive layer even at high alkalinity once it exceeds a certain concentration (critical chloride threshold C_T)[2]. Once C_T is exceeded, corrosion initiates and then propagates. The volume of the corrosion products is several times that of the parent steel. The products build up and cause tensile stresses, eventually leading to cracking and spalling of the concrete cover[3]. Chloride-induced corrosion on reinforcing steel is the major cause of the deterioration of reinforced concrete structures exposed to seawater or deicing salt.

Chloride diffusivity into concrete is usually considered the most important parameter that determines the service life of reinforced concrete structures. According to Tutti's model, the service life of reinforced concrete structures consists of two stages: 1) time to corrosion initiation (T_i); and 2) time of corrosion propagation (T_p)[4]. The initiation period is the time it takes for chloride ions to ingress into concrete to the reinforcement and reach C_T for corrosion initiation. T_i is strongly related to the chloride ion permeability of concrete. The corrosion propagation period is the time from corrosion initiation to the end service of structures, which is controlled by the corrosion rate.

Transport of chloride ions into concrete involves complex physical and chemical processes[5]. Diffusion is the main mechanism to transport chlorides into water-saturated concrete from the concrete surface to the rebar surface[6]. The corrosion rate is usually mainly controlled by the electrical resistivity of concrete[7-9] once corrosion has initiated. However, both diffusion of chloride ions and corrosion rate of depassivated steel are temperature dependent. It is necessary to take into account the temperature effect while predicting service life of reinforced concrete structures.

Various test procedures have been developed to evaluate the chloride penetration resistance of concrete. These tests are classified into three categories[5]: 1) diffusion tests including AASHTO T259 (salt ponding test), NT BUILD 433 (bulk diffusion test) and other natural long-term full-immersion tests; 2) migration tests, including ASTM C1202 (rapid chloride permeability test) and NT Build 492 (chloride

migration test); 3) indirect tests, such as electrical resistivity measurement[10-13]. Duration of the test methods ranges from minutes (resistivity method) to several years (diffusion test).

Over the last couple of decades there has been an increasing interest in measuring the electrical resistivity (conductivity) on water-saturated concrete specimens to evaluate concrete durability. It has been found that electrical concrete resistivity correlates well with the concrete chloride diffusivity. The Florida Department of Transportation (FDOT) has replaced the rapid chloride permeability (RCP) test (ASTM C1202) with a surface resistivity (SR) test (Florida Method, FM5-578) using a four pin Wenner probe array[14]. FDOT's research found a good correlation between RCP test values and SR measurements for specimens that were wet cured in a controlled environment (or under full immersion) at room temperature (RT)[15]. Resistivity of concrete has also been correlated to corrosion rate of depassivated reinforcement[9, 16].

Pozzolans and other supplementary cementing materials (SCM) including fly ash (FA), ultra-fine fly ash (UFFA), Metakaolin (MK), silica fume (SF), and ground granulated blast-furnace slag (GGBS) have been used as partial replacement of cement to improve the durability of reinforced concrete structures. The long term concrete permeability has been found to be significantly reduced by using pozzolanic and SCM admixtures. However, it has been found that concrete which contains some of these pozzolans and SCM, such as GGBS and Class F FA has slower reaction rates compared with ordinary Portland cement concrete (OPC), which is reflected by both lower strength and lower chloride resistance properties at early age (e.g. 28 days) [17-21]. The quality control tests, such as compressive test and diffusivity test, are usually carried out at 28 days, which is not long enough for concrete with slow reacting pozzolans to achieve passing values. High performance concretes (HPC) with Class F FA or slag as the only pozzolans or SCM present usually shows slow hydration. As time passes the hydration of concrete with these pozzolans reduce the pore size and pore connectivity (in the order of a few months to a few years). Resistivity measurement can be used to monitor the concrete hydration.

The SR test (FM 5-578) is usually performed after 28 days of moist curing the concrete sample. However, 28 days is usually not long enough for the reactions in these HPC to develop a low permeability, especially when FA or Slag is used in large replacement ratios (≥20% and ≥50% respectively by weight of total cementitious material).

Elevated temperature curing has been widely used in precast concrete structures to develop or test high early strength properties[17, 22]. As concrete permeability is an important characteristic indicating the durability of concrete, there is a need to develop accelerated curing regimes to develop or test low

permeability at early ages[23]. To obtain passing RCP test values, the Virginia Department of Transportation (VDOT) developed accelerated curing regimes and results show that long term permeability properties (6 months and beyond) were obtained at 28 days[17]. However, the concrete resistivity was not included in VDOT's study. Typically RCP or RMT tests (or similar tests) are used to evaluate the chloride permeability as these test periods are relatively short compared with the diffusion method. The resistivity method was rarely used to study the diffusion properties for concrete under accelerated curing.

Use of pozzolanic admixture changes not only the microstructures of concrete, but also the chemical compositions of the pore solution (pH and conductivity)[24-26]. The pH of concrete is important because it affects the threshold of $[Cl^-]$ for corrosion initiation and alkali silica reaction (ASR).

In this investigation, concrete with large volume pozzolans (FA and Slag) up to 70% by mass were studied. Temperature dependence of electrical resistivity and chloride diffusion were studied by dynamic temperature tests in Chapter 3 and Chapter 6, respectively; accelerated curing by elevated temperature was studied in Chapter 4; correlation between electrical resistivity and bulk diffusion was studied in Chapter 4; correlation between electrical resistivity and chloride migration coefficients was studied in Chapter 5, and the effect of pozzolanic and slag admixtures on pore solution pH and conductivity was studied in Chapter 7.

The objectives of this research include:

1. Study the temperature effect on electrical resistivity of saturated and unsaturated concrete specimens, and develop a more precise method to normalize resistivity measured corresponding to temperature.
2. Study the temperature effect on the chloride migration coefficients in concrete, and develop a more precise method to predict chloride migration coefficients at different temperatures.
3. Develop and evaluate accelerated curing regimes to obtain low permeability properties at early ages (28 days) for concrete with high volume of pozzolans, and identify the appropriateness of the replacement ratio of pozzolans and accelerated curing regimes to achieve early and long-term low permeability
4. Use resistivity measurements to evaluate the permeability development over time under different curing regimes.
5. Study the correlation between electrical resistivity and chloride migration coefficients, and develop a method to predict chloride migration coefficients by resistivity measurement.

6. Study the correlation between electrical resistivity and apparent diffusion coefficients,
7. Study the effect of pozzolanic and slag admixtures on pH and conductivity of concrete pore solution.

2. LITERATURE REVIEW

2.1 Concrete and its Composition

Concrete is a composite heterogeneous material that consists of coarse granular material (the aggregate or filler) embedded in a hard matrix material (the cement or binder combine with fine aggregate and water) that fills the space between the aggregate particles and glues them together[2]. Concrete has a number of advantages compared with other construction materials as it can be cast to any desired shape, and in massive sections if needed. Concrete is also deemed as a durable construction material.

2.1.1 Chemical Composition of Ordinary Portland Cement (OPC)

Ordinary Portland cement is the most commonly used hydraulic cement for making concrete. Four compounds are usually regarded as the main constituents of Portland cement as shown in Table 2.1, which are C_3S, C_2S, C_3A and C_4AF. A small amount of gypsum is added to control the early reactions of C_3A called flash setting. The chemical composition of OPC is traditionally written in an oxide notation as shown in Table 2.2.

Table 2.1 Typical Composition of Ordinary Portland Cement [2]

Chemical Name	Chemical Formula	Shorthand Notation	Weight Percent
Tricalcium silicate	$3CaO{\cdot}SiO_2$	C_3S	50
Dicalcium Silicate	$2CaO{\cdot}SiO_2$	C_2S	25
Tricalcium aluminate	$3CaO{\cdot}Al_2O_3$	C_3A	12
Tetracalcium Aluminoferrite	$4CaO{\cdot}Al_2O_3{\cdot}Fe_2O_3$	C_4AF	8
Calcium sulfate dihydrate (gypsum)	$CaSO_4{\cdot}H_2O$	$C\bar{S}H_2$	3.5

Table 2.2: Typical Oxide Composition of Ordinary Portland Cement [2]

Oxide	Notation	Name	Weight Percent
CaO	C	Lime	63
SiO_2	S	Silica	22
Al_2O_3	A	Alumina	6
Fe_2O_3	F	Ferric oxide	2.5
MgO	M	Magnesia	2.6
K_2O	K	Alkalis	0.6
Na_2O	N		0.3
SO_3	$\bar{S}$	Sulfur trioxide	2.0
H_2O	H	Water	-

2.1.2 Hydration of Portland Cement

The hydration of Portland cement involves the reaction of the anhydrous calcium silicate and aluminate phases with water to form hydrated phases. However, for the purpose of a clearer description of the chemical and physical changes during hydration, the reactions of the silicate phases (C_3S and C_2S) and the aluminate phases (C_3A and C_4AF) are usually considered separately[27].

Both C_3S and C_2S react with water to produce an amorphous calcium silicate hydrate (C-S-H) gel which is the main component which binds the sand and aggregate particles together in concrete. The following equations summarize the hydration reactions silicates[2]:

$$2C_3S + 6H \rightarrow C_3S_2H_3 + 3CH \quad (2\text{-}1)$$

Tricalcium Silicate water C-S-H Calcium Hydroxide

$$2C_2S + 4H \rightarrow C_3S_2H_3 + CH \quad (2\text{-}2)$$

Dicalcium Silicate water C-S-H Calcium Hydroxide

Under standard ambient temperature conditions of 20ºC, C_3S is much more reactive than C_2S. Approximately half of the C_3S present in typical cement will be hydrated in 3 days and 80% in 28 days. However, the hydration of C_2S is not significant until 14 days after cast.

In the absence of soluble calcium sulfate, C_3A reacts rapidly to form the phases C_2AH_8 and C_4AH_{19}, which subsequently convert to C_2AH_6. This is a rapid and highly exothermic reaction. In Portland cement, the hydration of C_3A involves reactions with sulfate ions which are supplied by the dissolution of gypsum. The primary initial reaction of C_3A is:

$$C_3A + 3C\bar{S}H_2 + 26H \rightarrow C_6A\bar{S}_3H_{32} \quad (2\text{-}3)$$

Tricalcium aluminate gypsum water ettringite

If the sulfate is all consumed before the C_3A has completely hydrated, then ettringite transforms to another calcium sulfo-aluminate hydrate containing less sulfate:

$$2C_3A + C_6A\bar{S}_3H_{32} + 4H \rightarrow 3C_4\bar{S}H_{12} \quad (2\text{-}4)$$

C_4AF forms the same sequence of hydration products as does C_3A, with or without gypsum. The reactions are slower and involve less heat. These reactions are shown below:

$$C_4AF + 3C\bar{S}H_2 + 21H \rightarrow C_6(A,F)\bar{S}_3H_{32} + (A,F)H_3 \quad (2\text{-}5)$$

$$C_4AF + C_6(A,F)\bar{S}_3H_{32} + 7H \rightarrow 3C_4(A,F)\bar{S}H_{12} + (A,F)H_3 \quad (2\text{-}6)$$

Characteristics of the major hydration products in hardened cement paste are shown in Table 2.3.

Table 2.3: Hydration Products in Cement Paste [24]

Hydration products	Volume percentage	Formation Rate	Strength
$C_6AS_3H_{32}$	15-20	Fast	Low
C-S-H	50-60	Slow	High
$Ca(OH)_2$	20-25	Slow	-

2.2 Durability of Reinforced Concrete

2.2.1 Reinforced Concrete

Concrete is a material which is strong in compression but relatively weak in tension, so it is usually reinforced with steel bars (rebar) to increase its tensile strength. Carbon steel rebars are traditionally used in reinforced concrete, but alternative reinforcements including duplex and austenitic stainless steel, stainless steel clad, as well as galvanized steel bar are also used.

2.2.2 Corrosion of Steel in Concrete

Due to the high alkalinity (pH>12.5) of the concrete pore solution, steel bar in concrete is usually protected by a passive layer. The passive layer of reinforcing steel exhibits a relatively noble potential and mainly consists of γ-Fe_2O_3[28]. However, when concrete is exposed to seawater or deicing salt, chloride ions slowly diffuse from the concrete surface to the rebar. Once the chloride concentration at the rebar surface exceeds a critical concentration (critical chloride threshold, C_T) the passive layer breaks down and corrosion initiates.

The corrosion of steel in concrete is an electrochemical process and two reaction cells are formed: anodic and cathodic regions, connected thru the metal and by the electrolyte in the form of the concrete pore water, as shown in Figure 2.1.

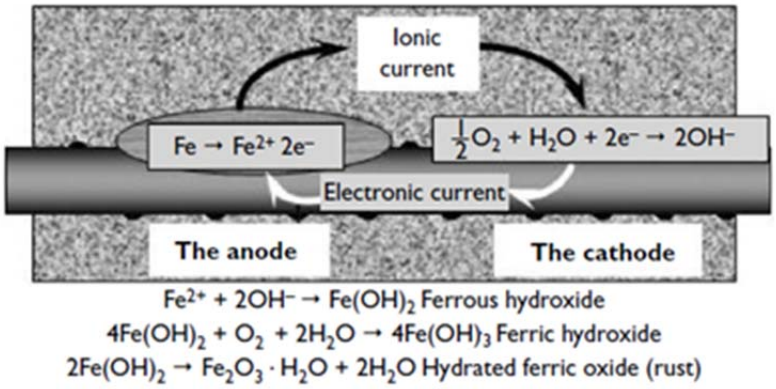

Figure 2.1: Illustration of anodic and cathodic reaction for corrosion of steel in concrete [3]

The anodic reactions:

$$Fe \rightarrow Fe^{++} + 2e^{-} \tag{2-7}$$

$$Fe^{++} + 2(OH)^{-} \rightarrow Fe(OH)_2 \text{ (ferrous hydroxide)} \tag{2-8}$$

$$4Fe(OH)_2 + 2H_2O + O_2 \rightarrow Fe(OH)_3 \text{ (ferric hydroxide)} \tag{2-9}$$

And the major cathodic reaction is:

$$4e^{-} + 2H_2O + O_2 \rightarrow 4(OH)^{-} \tag{2-10}$$

As the electrochemical cell requires a connection between the anode and cathode thru the pore water (ionic path), as well as thru the reinforcing steel itself (electric path), thus, the electrical resistivity of concrete controls the flow of the ionic current once corrosion has initiated.

Corrosion of reinforcement is one of the major causes of the deterioration of reinforced concrete. The specific volume of the corrosion products is several times of the reactants from which they are formed. Consequently, as the corrosion products accumulate within the pore structure, tensile stresses develop inside the concrete and ultimately cracking and spalling takes place. The relative volume of iron, iron hydroxide and iron oxides formed during corrosion are shown in Figure 2.2.

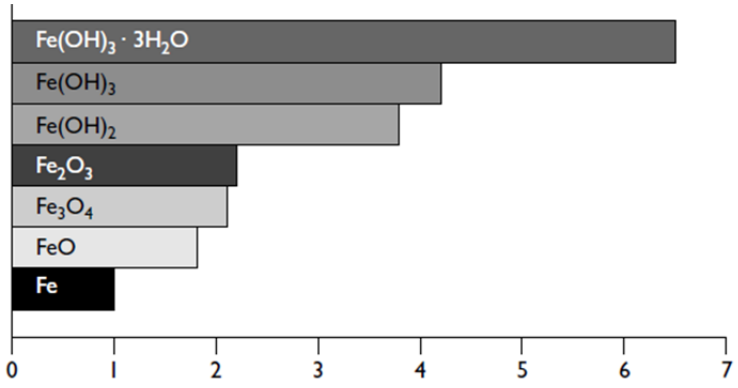

Figure 2.2: Relative volumes of ion and ion oxides [3]

Little damage occurs in very dry concrete because of the absence of water, nor is there much damage in continuously water-saturated concrete due to the limited oxygen available as a result of slow oxygen transport through the liquid phase compared with air. Unsaturated concrete, especially the tidal and splash zone areas which are exposed to alternate wetting and drying, allows more rapidly transporting oxygen and chloride to the steel surface which is needed to initiate and maintain corrosion. This explains why the splash zone is especially susceptible to corrosion damage.

2.2.3 Chloride Diffusivity in Concrete

Concrete is a porous material. The pores are of various small diameters sizes and lengths. Chloride ions, water, other aggressive ions, and gases (e.g., O_2 and CO_2) are able to penetrate into concrete through the connected pores. In marine environments, chloride diffusivity is the most important parameter which determines the durability of reinforced concrete. According to Tutti's model, service life of reinforced concrete structures consists of two stages: 1) time to corrosion initiation (T_i); and 2) time of corrosion propagation (T_p), as shown in Figure 2.3[4, 29]. During T_i, diffusivity determines the time it takes for the chloride ions to reach C_T at the rebar surface to initiate corrosion. Once corrosion has initiated, during T_p, resistivity and moisture content controls the available amount of water and/or O_2 which affects the corrosion rates.

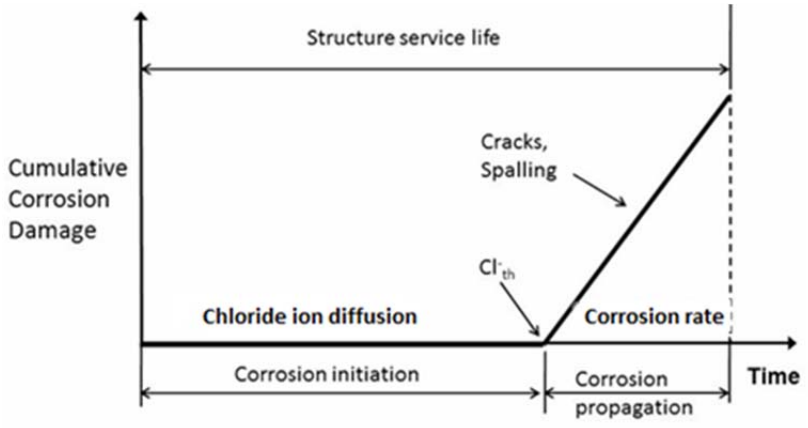

Figure 2.3: Schematic illustrations of the initiation and propagation stage in reinforced concrete

Despite the complicated transport mechanisms of chloride ion in concrete, interactions with other ions and/or chloride binding are usually not included. The chloride transport into concrete is generally treated using Fick's second law. Assuming that the apparent diffusion coefficient constant and that the chloride ion transport is one dimensional semi-infinite, Fick's second law is described as:

$$\frac{\partial C}{\partial t} = D_{app} \frac{\partial^2 C}{\partial x^2} \tag{2-11}$$

Where t is time; x the depth in the chloride diffusion path; D_{app} (m^2/s) is the apparent diffusion coefficient; C is the chloride concentration at a specific exposure time and concrete depth. Assuming C ($t = 0$) = 0, the solution of Equation (2-11) is:

$$C(x,t) = C_s \left(1 - erf \frac{x}{2\sqrt{D_{app} t}} \right) \tag{2-12}$$

C_s is the surface chloride concentration; erf is the Gaussian error function. D_{app} is usually calculated through curve fitting to chloride concentration profiles obtained experimentally.

As described in chapter 1, various tests have been developed to evaluate the chloride penetration resistance of concrete. These methods include ASTM C1202 (rapid chloride permeability test), AASHTO T259 (salt ponding test), NT BUILD 433 (bulk diffusion test), NT Build 492(chloride migration test) and others[10-13]. The test duration ranges from 6 hours to several years excluding specimen preparation time.

Bulk Diffusion Test

Bulk diffusion test, designated as NT Build 433 or ASTM C1556, is a test method used to determine the apparent chloride diffusion coefficient of concrete[12, 30]. In this method, chloride ions penetrate into concrete only through diffusion, as shown in Figure 2.4. The exposure time for this test is at least 35 days for low quality concrete and 90 days for high quality concrete. Longer exposure times up to 1 to 3 years are also used.

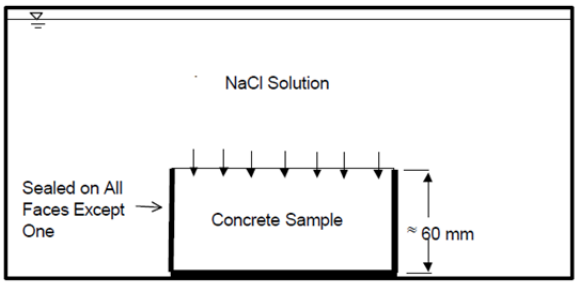

Figure 2.4 Schematic illustrations of bulk diffusion test [31]

Rapid Chloride Migration Test

Rapid Chloride Migration (RCM) test is designed according to NT Build 492[13]. The setup for this test is shown in Figure 2.5. A potential ranging from 10V-60V is used to accelerate the penetration of chlorides and the test period ranges from 6 to 96 hours. The duration and applied voltage depends on the quality of concrete. The averaged chloride penetration depth is obtained by splitting the specimen and spraying 0.1N $AgNO_3$ as a color indicator at the cross section. Non-steady-state migration coefficient (D_{nssm}) is obtained with the following equation:

$$D_{nssm} = \frac{0.0239(273+T)L}{(U-2)t}\left(x_d - 0.0238\sqrt{\frac{(273+T)Lx_d}{U-2}}\right) \quad (2\text{-}13)$$

where:

D_{nssm}: non-steady-state migration coefficient, $\times 10^{-12}$ m^2/s;
U: absolute value of the applied voltage, V;
T: average value of the initial and final temperatures in the anolyte solution, °C;
L: thickness of the specimen, mm;
x_d: average value of the penetration depths, mm;
t: test duration, hour.

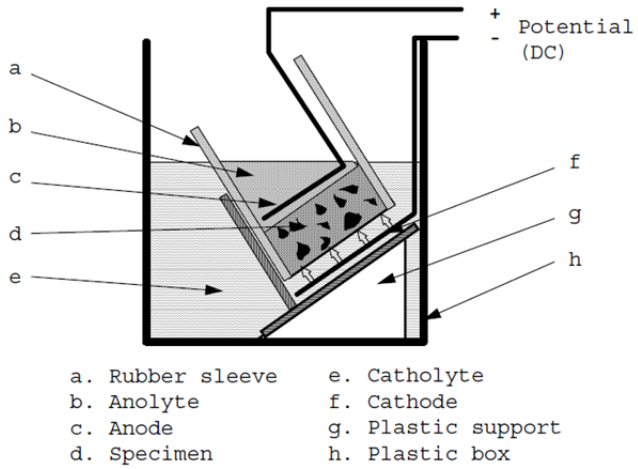

Figure 2.5: Schematic illustrations of RCM test setup [31]

Based on results from RCM test, the resistance to chloride penetration can be assessed by the relationship shown in Table 2.4, which was suggested by Nilsson et al. [32].

Table 2.4: Relationship between non-steady-state migration coefficients and resistance to chloride penetration [32].

D_{nssm} $\times 10^{-12}$ m^2/s	Resistance to chloride penetration
>15	Low
10-15	Moderate
5-10	High
2.5-5	Very high
<2.5	Extremely high

2.2.4 Time-Dependence of Chloride Diffusivity in Concrete

Regardless of the test methods for chloride diffusivity in concrete, it has been found that chloride diffusion coefficient (D_{Cl}) is time-dependent[7, 8, 21, 33-36]. Generally, D_{Cl} decreases with time, which is due to the refinement of pore structures caused by further hydration. The time-dependence of chloride diffusion coefficient is described as [33, 34]:

$$D(t) = D_0 \left(\frac{t_0}{t} \right)^m \tag{2-14}$$

Where $D(t)$ is the diffusion coefficient at time t; D_0 is the diffusion coefficient at reference time t_0; m (usually $0 \leq m \leq 1$) is the aging factor which is dependent on the mix properties of concrete. The

suggested values of m range from 0.32 to 0.91, depending on the mix properties of concrete [8, 21, 34, 36].

The aging factor plays an important role while determining the diffusion coefficients by chloride profiles both in the laboratory and field. In the laboratory, the bulk diffusion test is usually started on specimens at 28 days and the exposure period ranges from 35 days to one year and even longer. Due to the aging effect, the diffusion coefficient determined from bulk diffusion test is the apparent diffusion coefficient (D_{app}), which is the average diffusion coefficient of the exposure period. The aging effect also happens on in-situ concrete structures when determining diffusion coefficients by chloride profiles from cores drilled from bridges. In this case, the apparent diffusion coefficient is the average of the total exposure period (age of the bridge at the time of coring and environmental conditions).

Due to the importance of the aging factor for the life prediction of reinforced concrete structure, various investigations have been performed to determine the values of aging factor [21, 36]. Rather than using diffusion coefficients to calculate the aging factors, Andrade etc. calculated aging factor by using the resistivity method [34, 37]. Due to the wide range of m values reported in the literature, it is necessary to perform further investigation to study the aging factor.

2.2.5 Concrete Resistivity

The electrical resistivity (ρ) or conductivity (σ) of concrete indicates the resistance of concrete against the flow of electrical current. The determination of electrical resistivity of concrete has become an established non-destructive measurement technique in the assessment of the durability of concrete structures.

Electrical resistivity of concrete is affected by a number of factors such as pore structure (continuity and tortuosity), pore solution composition, moisture content and temperature [38-42]. Pore structure of concrete varies with water to cementitious material (w/cm) ratio, degree of hydration, and use of mineral admixtures such as blast furnace slag, fly ash and silica fume [38, 43-46]. Concrete pore solution contains K^+, Na^+, Ca^{2+}, SO_4^{2-}, and OH^- [43-46]. Chloride ion may also appear due to the deicing salt or seawater. The use of mineral admixture could change the composition and concentration of ions in pore solution [43, 46]. However, it has been found that changes in pore structure exerted a greater influence on the measured resistivity than changes in pore solution composition and concentration [47]. Degree of hydration affects resistivity as further hydration reduces the concrete porosity [43]. When concrete resistivity is measured, the electrical current is mainly due to the ion mobility, ion-ion and ion-

solid interactions[38, 48]. Moisture content plays an important role in concrete resistivity as electrical current in the concrete is carried by the pore water. Electrical resistivity increases with decreasing moisture content[45, 49].

Temperature change was found to have a significant effect on electrical resistivity of concrete, and usually, an increase in temperature leads to decrease in resistivity. Temperature affects resistivity by changing the ion mobility, ion-ion and ion-solid interactions, as well as the ion concentration in pore solution.

Various techniques have been developed to measure the resistivity of concrete. Two-electrode method and four-electrode method are the most used methods.

Two-electrode method

Resistivity can be measured by the following formula:

$$\rho = R \cdot \frac{A}{L} \tag{2-15}$$

Where R is the resistance of a prismatic or cylinder specimen; A is the area of the cross-section, and L is the length of the specimen, as shown in Figure 2.6.

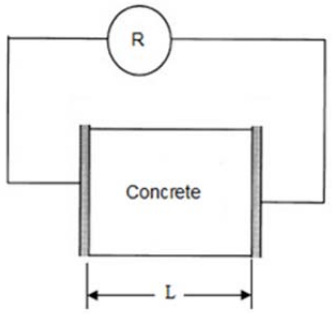

Figure 2.6: Schematic illustration of concrete resistivity measurement by two-plate method

Four-electrode Method

Four-electrode method, also known as the Wenner method, is one of most widely used techniques to measure concrete resistivity, particularly in the field. This method was originally developed by Wenner to measure soil resistivity[50]. The Wenner method consists of placing four equally spaced

electrodes on the concrete surface. A current is induced at the two outer electrodes and the potential is measured at the two inner electrodes, as shown in Figure 2.7. An alternating current (AC) between 50-1000 Hz is usually used. It has been reported that DC is not recommended as it may add errors due to polarization[38].

If the concrete geometry dimensions can be considered semi-infinite, the resistivity is given by the following equation[50]:

$$\rho = \frac{2\pi \cdot a \cdot V}{I} \tag{2-16}$$

Where a is the electrode spacing, V is potential between inner electrodes, and I is the induced current between the outer electrodes.

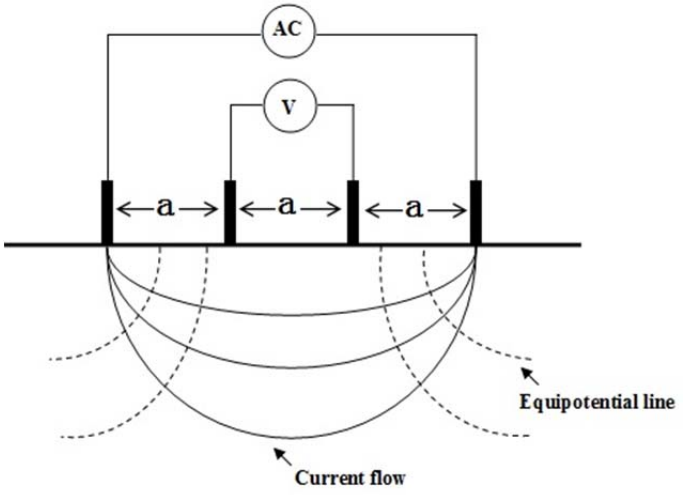

Figure 2.7: Schematic illustration of concrete resistivity measurement by Wenner method [38]

Equation 2-16 is valid only if the measured concrete geometry approaches semi-infinite dimensions. However, in practice, most concrete samples measured in the laboratory have finite dimensions, such as 10cm diameter × 20cm long cylinders. It has been found that finite geometry has a large effect on the measured resistivity, and hence an additional geometry correction is needed. In most cases, the measured resistivity is the apparent resistivity (ρ_{app}) rather than the real resistivity (ρ). To convert to bulk resistivity, an additional geometry correction (cell constant) $K_{\rho,g}$ is usually applied:

$$\rho = \frac{\rho_{app}}{K_{\rho,g}} \tag{2-17}$$

Where ρ is the real resistivity, ρ_{app} is the measured resistivity, and $K_{\rho,g}$ the cell constant dependent on the specimens geometry, electrodes spacing, measuring position and rebar location[19, 51]. The presence of conductive rebars can also significantly affect the measured resistivity value. The effect is greater the smaller the concrete cover is[19].

2.2.6 Correlation between Concrete Resistivity and Diffusivity

During T_i, diffusivity is the controlling parameter which determines the time it takes for chloride ions to diffuse into concrete and reach the critical chloride threshold (C_T) for corrosion imitation. However, most test methods, such as the rapid chloride migration (RCM) test, rapid chloride permeability test (RCPT) or bulk diffusion (BD) method, are either expensive or time-consuming for determining the concrete permeability properties, which limits their use as routine quality control tool. Recently, electrical resistivity of concrete has been applied as an indirect method to evaluate concrete chloride permeability, based on both theoretical analysis and experimental results.

2.2.6.1 Theoretical Background

In dilute electrolytes solutions, correlation between diffusivity (D_i) of an ion species i and its partial conductivity σ_i (or resistivity ρ_i) could be expressed by the Nernst-Einstein equation[52]:

$$D_i = \frac{RT\sigma_i}{Z_i^2 F^2 C_i} \tag{2-18}$$

Where D_i is the diffusivity of ion i (m^2/s); σ_i is the partial conductivity of ion i (S/m); R is the gas constant (8,314J/mol); T is absolute temperature (K); Z_i is the charge of ion i ; F is the Faraday's constant (96500 Coulombs/mole) and C_i is the concentration of ion i (mol/m^2). In the case that the partial conductivity σ_i (or resistivity ρ_i) and the concentration C_i are determined, the diffusivity of ion i can be in principle calculated from equation 2-18. The partial conductivity is:

$$\sigma_i = t_i \sigma \tag{2-19}$$

Where σ is the conductivity of the concrete and t_i is the transference number of the ion species *i,* which is defined as:

$$t_i = \frac{Q_i}{Q} = \frac{I_i}{I} \tag{2-20}$$

where Q_i and I_i are the electric charge quantity and current contribution of ion species *i* to the total electric charge quantity Q and current I. Equation 2-18 can also be written as:

$$D_i = \frac{RT\lambda_i}{Z_i^2 F^2} \tag{2-21}$$

Where λ_i is the molar conductivity of species *i* and $\lambda_i = \frac{\sigma_i}{C_i}$. In a simplified form, Equation 2-21 can be written as[53]:

$$D_i = \frac{K_{D,\rho}}{\rho} \tag{2-22}$$

Where $K_{D,\rho}$ is the constant parameter for the correlation of diffusivity and resistivity; ρ is the resistivity of concrete. When the conductivity of pore solution and concrete are known, Nernst-Einstein equation can be written as follow[54-56]:

$$\frac{D_{eff}}{D_0} = \frac{\sigma}{\sigma_0} = \frac{\rho_0}{\rho} = \frac{\phi}{\tau} \tag{2-23}$$

Where D_{eff} is the effective chloride diffusion coefficient of concrete; D_0 is the chloride ion diffusion coefficient is the pore solution; ρ is the bulk resistivity of concrete; ρ_0 is the resistivity of pore solution; σ is the bulk conductivity of concrete; σ_0 is the conductivity of pore solution; ϕ is porosity of concrete and τ is the tortuosity of concrete.

As concrete is also a porous material, Archie's law could be applied to describe the correlation between the bulk resistivity (or conductivity), pore solution resistivity (or conductivity) and porosity [53, 57]:

$$F = \frac{\rho}{\rho_0} = \frac{\sigma_0}{\sigma} = a \cdot \phi^{-m} \tag{2-24}$$

where F is formation factor; a and m are constants. m is named as tortuosity constant which is dependent on tortuosity of concrete. The values of m have been found to be 1.5 to 3.2[57].

With Equation 2-23 or Equation 2-24, the Nernst-Einstein equation and Archie's law are combined as:

$$F = \frac{D_0}{D_{eff}} \tag{2-25}$$

2.2.6.2 Experimental Background

In recent years, various investigations have performed experiments to study the correlation between concrete resistivity and chloride diffusivity. The Florida Department of Transportation (FDOT) performed experiments to study the correlation between resistivity and Rapid Chloride Permeability results[15]. In this investigation, resistivity was measured using the Wenner method[50]. This research reported a good correlation between RCP test and resistivity results for specimens that were wet cured in a controlled environment or cured in lime water, as shown in Figure 2.8. Based on this correlation, FDOT developed a surface resistivity method (FDOT FM5-578[14] and then an AASHTO test method TP-95[59]) to characterize concrete permeability and proposed a relationship between resistivity and chloride permeability as shown in Table 2.5 [14].

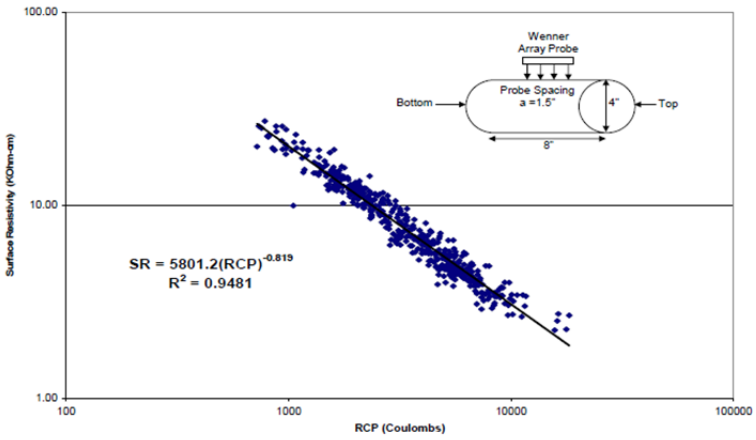

Figure 2.8: Relationship between RCP and surface resistivity [15]

Table 2.5: Correlation between surface resistivity and chloride ion permeability [13]

RCP versus Surface Resistivity				
Chloride Ion Permeability	RCP Test Charged Passed (coulombs)	Surface Resistivity Test		
		4 X 8 Cylinder (Kohm-cm) a=1.5 k=1.8 (Measured)	6 X 12 Cylinder (KOhm-cm) a=1.5 k=1.41 (Measured)	Semi-Infinite Slab (Real)
High	>4,000	< 12	< 9.5	< 6.7
Moderate	2,000-4,000	12 - 21	9.5 - 16.5	6.7 - 11.7
Low	1,000-2,000	21 - 37	16.5 – 29	11.7 - 20.6
Very Low	100-1,000	37 - 254	29 – 199	20.6 - 141.1
Negligible	<100	> 254	> 199	> 141.1

The Louisiana Transportation Research Center (LTRC) recently performed a similar investigation to evaluate surface resistivity measurement as an alternative to the rapid chloride permeability (RCP) test for quality assurance and acceptance[58]. A good correlation between resistivity and RCP test was also found and concrete permeability classes corresponding to surface resistivity values were recommended similar to those in Table 2.5.

A round-robin test was carried-out in which several departments of transportation and industry laboratories participated [58b] to assess the precision of resistivity measurements on different concrete compositions, the findings from this investigation provided similar results than those from FDOT. As a result of the this round robin, the American Association of State Highway and Transportation Officials (AASHTO) published a provisional method TP 95-11 “Surface Resistivity Indication of Concrete's Ability to Resist Chloride Ion Penetration”[59].

Besides investigations carried out on laboratory specimens, research has also been performed on field results to correlate electrical resistivity and apparent diffusivity coefficients (D_{app}). Figure 2.9a shows correlation between apparent diffusivity and resistivity reported by several authors. Results are scattered in Figure 2.9a as the exposure environments are more complex due to different humidity, temperature and the elevation from water level. As D_{app} is usually obtained after a long period of exposure ranging from months to years and even longer, the aging effect needs to be considered as concrete diffusivity changes with time. Figure 2.9b shows additional apparent diffusivity vs. resistivity results corresponding to field data on Florida bridges by Presuel et al., from a recent investigation[60]. It shows that when resistivity was measured under saturated condition, a better correlation was found between resistivity and apparent diffusivity.

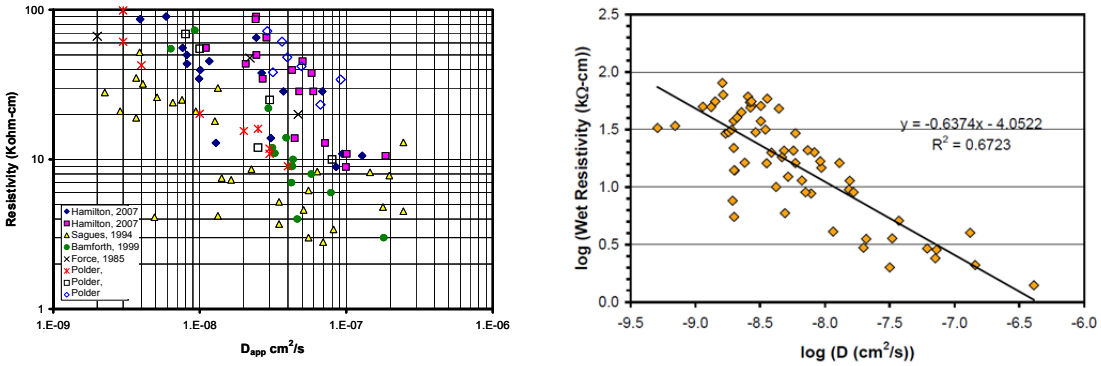

(a) (b)

Figure 2.9: Relationship between apparent diffusivity coefficients and resistivity

An investigation conducted by European Union–Brite EuRam III reported a correlation between Rapid Chloride Migration (RCM) coefficients and electrolytic (electrical) resistivity measured by two-electrode method, as shown in Figure 2.10 [7]. A similar correlation between RCM coefficient and resistivity measured by Wenner method was reported by Vries [61]. With this correlation, it would be possible to employ the resistivity measurement as an alternative or replacement of the RCM test to evaluate chloride permeability of concrete indirectly. However, more experiments are needed to verify this correlation.

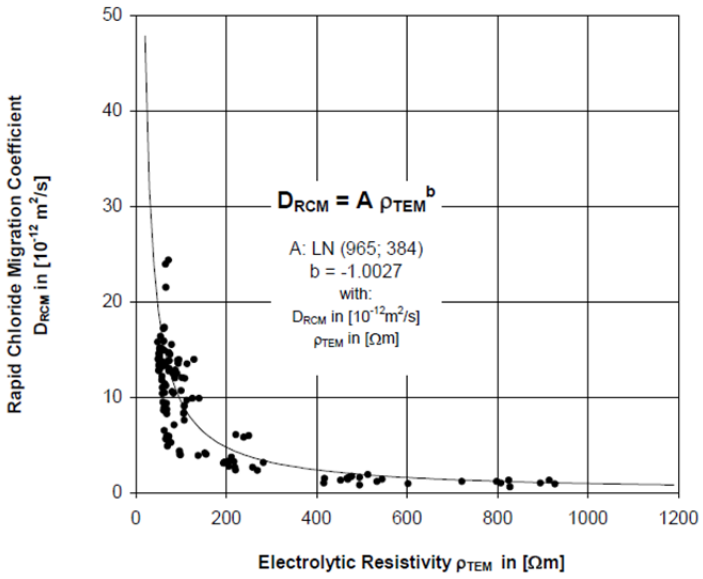

Figure 2.10: Correlation between Rapid Chloride Migration coefficient and electrolytic resistivity measured by two-electrode method [7]

2.2.7 Correlation between Concrete Resistivity and Corrosion Rates

During the propagation stage (T_p), rebar is depassivated and corrosion has initiated. In this stage, the most important parameter is corrosion rate which determines how fast the reinforced concrete structure is deteriorating. Figure 2.11 by Andrade et al. shows the relationship between decreases of rebar cross-section and corrosion rate[62]. It indicates that the propagation stage of concrete structures could be significantly increased by reducing the corrosion rate.

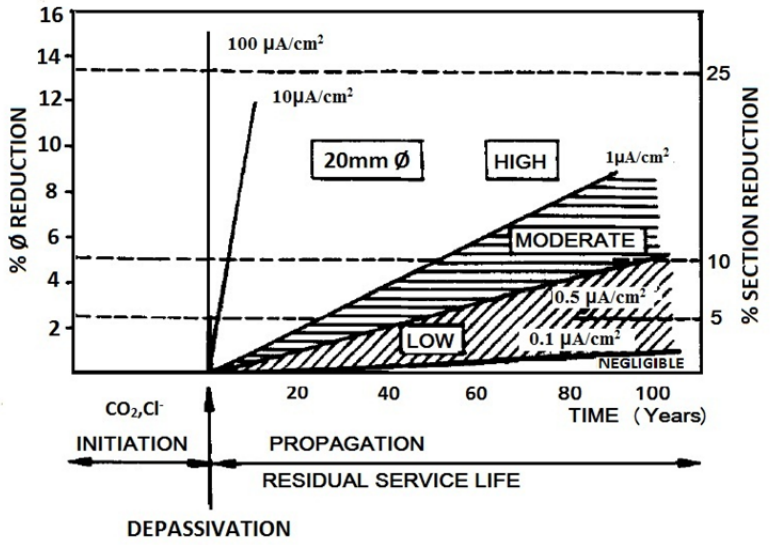

Figure 2.11: Decrease of rebar diameter/rebar cross-section as a function of corrosion rate during propagation period [62]

Once corrosion is initiated by chloride ions, corrosion rate is dependent on numerous parameters such as relative humidity (RH), oxygen availability, ratio of anodic/cathodic area, concrete resistivity and so on, as shown in Figure 2.12 [63]. When concrete is under water or concrete cover is thick, corrosion rate of steel in concrete is usually considered to be under cathodic control, that is, corrosion rate is dependent on the availability of O_2 [9]. When concrete is under aerated condition, such as the splash zone, the O_2 flux into concrete is usually enough to support the anodic current. In this condition, cathodic control no longer exists and the factor limiting the corrosion rate is the flow of ionic current through concrete, that is, the electrical resistivity of concrete[9, 63]. Resistive control describes the relationship between corrosion rate and electrical resistivity of concrete (or mortar), which has been studied by various investigations[9, 42]. For example, Glass et al. proposed a theory named as anodic resistance control, that is, the corrosion rate of steel in concrete is under anodic control with the anodic reaction being limited by the resistivity of mortar[64]. Investigations performed by Bertolini et al. and Morris et al. found concrete

resistivity not only affect corrosion rate, but also the corrosion potential, which support Glass's anodic resistance theory[42, 65].

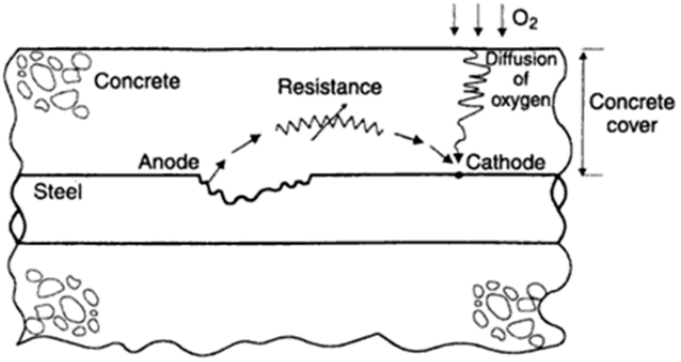

Figure 2.12: Schematic descriptions of factors which may affect corrosion rate of steel in concrete: (i) O2 availability and (ii) electrical resistance of concrete[63]

The correlation between the corrosion rate of depassivated steel and concrete resistivity has been reported in various research works [9, 42, 62, 66]. Most of these investigations found a linear relationship between corrosion rate and concrete conductivity (inverse of resistivity). Figure 2.13 shows the relationship between corrosion rate and electrical resistivity of carbonated mortars by Andrade et al. [62]. The slope will be different in case of chloride presence as the corrosion rate will be affected by $[Cl^-]/[OH^-]$[62]. Bertolini found that the slope varied with different concrete cover depth as well as different concrete types[42]. In Bertolini's investigation, electrical resistivity was changed by dynamic temperature tests performed at different relative humidity.

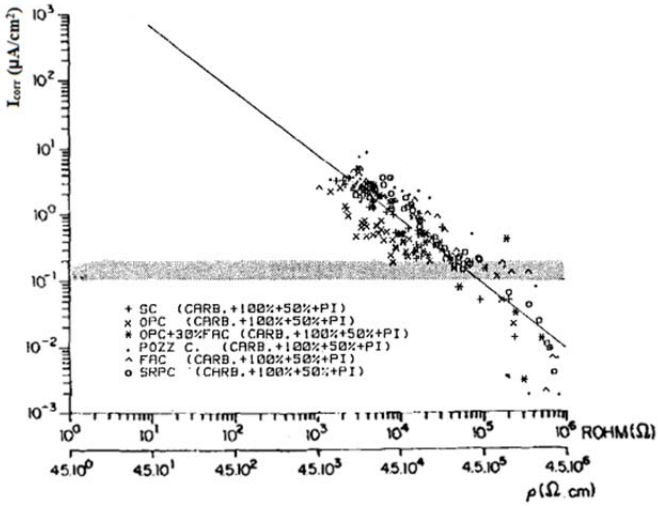

Figure 2.13: Dependence of Icorr on electrical resistivity of carbonated mortars with several cement types [62]

An empirical equation describing relation between corrosion rate and resistivity was proposed by Andrade et al. [67]:

$$I_{corr} \cong \frac{3 \cdot 10^3}{\rho} \tag{2-26}$$

with I_{corr} in μA/cm^2 and ρ in Ω·cm. DuraCrete and LIFECON proposed similar models describing the relationship between corrosion rate and various parameters [7, 8]:

$$I_{corr} = \frac{k_0}{\rho(t)} \cdot F_{Cl} \cdot F_{Galv} \cdot F_{O_2} \tag{2-27}$$

Where

I_{corr}	corrosion rate in μA/cm^2
k_0	constant regression parameter in μm·Ωm/a
$\rho(t)$	actual resistivity at time t in Ωm
F_{Cl}	accounting for the influence of the chloride content
F_{Galv}	influence of galvanic effect
F_{O_2}	availability of oxygen

In most cases, F_{Galv} and F_{O_2} equals to 1 and F_{Cl} is dependent on the chloride concentration at the corrosion spot. The value of k_0 was proposed to be k_0 =882 by DuraCrete when corrosion is initiated by chlorides[7]:

Langford also proposed a relationship between corrosion rate of depassivated steel reinforcement and resistivity as shown in Table 2.6.

Table 2.6: Relationship between resistivity and corrosion rate of depassivated steel reinforcement in concrete [39]

Resistivity: kΩ cm	Corrosion rate
< 5	Very high
5- 10	High
10-20	Low/moderate
> 20	Low

2.2.8 Temperature Effect on Electrical Resistivity, Chloride Diffusivity and Corrosion Rate.

Electrical Resistivity vs. Temperature

Concrete is a porous material with electrolytes filling the pores. Current flowing through is carried by ions dissolved in the pore solution. Temperature change has been found to have a significant effect on electrical resistivity of concrete, and usually, an increase in temperature leads to a decrease in resistivity. Temperature affects resistivity by changing the ion mobility, ion-ion and ion-solid interactions, as well as the ion concentration in pore solution [38, 39, 48]. Temperature effect on resistivity of bulk pore solution was found to be significantly different from that of cement paste or mortar with the same ion concentration in the pores, which was possibly due to the strong ion-solid interactions in cement paste or mortar[68]. Various researches have reported effect of temperature on resistivity experimentally [39, 42, 45, 69]. Elkey reported that, for Portland Cement Concrete (PCC), under 30% saturation, resistivity changes by 5% per °C at 21°C, whereas 3% per °C under 70% saturation [45]. For simplicity, at the temperature between 0°C to 40°C, a change of 3% to 5% on resistivity at per °C change has been suggested [38, 45]. A linear relationship between resistivity and temperature has been proposed[48, 69, 70]:

$$\rho = \rho_0(1 + \alpha \cdot \Delta T) \tag{2-28}$$

Where: ρ: resistivity at temperature T (°C)

ρ_0 : resistivity at reference temperature T_0.

ΔT : temperature deference between T and T_0 ($\Delta T = T_0 - T$)

α: temperature coefficient.

Values of α have been reported between 0.022-0.035/°C [48, 69, 70]. In Equation 2-28, the measured resistivity at temperature T can be standardized to the resistivity at a reference temperature T_0 (e.g., 21°C), however, it was found that this equation is only applicable in a narrow temperature interval about the reference temperature ($T_0 \pm 5$°C) [48, 69, 70].

An exponential dependence on temperature of resistivity has also been developed by dynamic temperature tests [39, 42]:

$$\rho = A \cdot e^{B \cdot T} \tag{2-29}$$

Where ρ is resistivity at temperature T (°C); A and B are empirical coefficients and A>0, B < 0.

DuraCrete proposed another model describing correlation between resistivity ρ_T at temperature T (°C) and resistivity ρ_{20} at 20°C[7]:

$$\rho_T = K_T \cdot \rho_{20} \tag{2-30}$$

where K_T is characteristic value of the temperature factor for resistivity and K_T is defined as:

$$K_T = \frac{1}{1 + K(T - 20)} \tag{2-31}$$

K is the characteristic value of a factor describing the temperature dependency in °C^{-1}. Values of K are defined in Table 2.7:

Table 2.7: Characteristic values of the temperature factor [31]

Variable	Condition	Characteristic value	Unit
K	Temperature below 20°C	0.025	°C^{-1}
K	Temperature above 20°C	0.073	°C^{-1}

Correlation between K_T and T according to Equation 2-31 is shown in Figure 2.14.

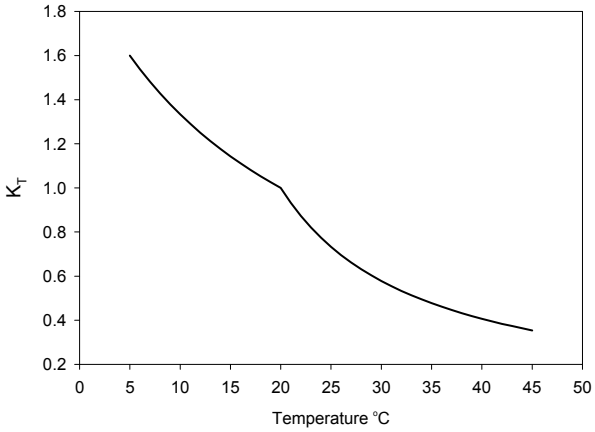

Figure 2.14: Characteristic values of the temperature factor by LIFECON [7]

There is a wide agreement on the application of Arrhenius equation [39, 47, 48, 69, 71]:

$$\rho = A \cdot \exp\left(\frac{E_{a,\rho}}{R \cdot T}\right) \tag{2-32}$$

Where ρ is the resistivity at temperature T (K), and A is the resistivity when $T \to +\infty$. A modified form of Equation 2-32 can be written as the following:

$$\rho_T = \rho_0 \cdot \exp\left[\frac{E_{a,\rho}}{R}\left(\frac{1}{T} - \frac{1}{T_0}\right)\right] \tag{2-33}$$

Where:

ρ_T : resistivity measured at temperature T (K);

ρ_0 : resistivity at a reference temperature T_0(K);

R: gas constant (8.314 kJ^{-1} mol^{-1})

$E_{a,\rho}$: activation energy for resistivity (J/mol)

Values of $E_{a,\rho}$ have been reported ranging from 16.9 J/mol to 42.77J/mol [47, 48, 69]. Use of pozzolanic materials was found to increase the activation energy relative to the OPC mixes [47]. Similar results were also found when decreasing the degree of water saturation of the concrete [45, 48, 69]. In general, activation energy is found to be dependent on the moisture content, mix design, age of hydration, etc. Due to the variation of reported activation energy values, using a global activation energy value is found to be not applicable and could lead to errors [69, 72].

Chloride Diffusivity vs. Temperature

Diffusivity of chloride ions in concrete has been found to be dependent on temperature as described the Arrhenius equation [73-78]:

$$D_T = D_0 \exp\left[\frac{E_{a,D}}{R}\left(\frac{1}{T_0}-\frac{1}{T}\right)\right] \tag{2-34}$$

Where D_T is the diffusion coefficient at temperature T (K) and D_0 is the diffusion coefficient at a reference temperature T_0 (K); $E_{a,D}$ is the activation energy for diffusivity and R is gas constant. Values of $E_{a,D}$ have been found to be dependent on water to cement ratio and cement type [75-77]. Page reported $E_{a,D}$ from 25kJ/mol to 45 kJ/mol[77]. Samson reported $E_{a,D}$ from 17.9 kJ/mol to 21.2kJ/mol by migration test[79]. Yuan reported $E_{a,D}$ from 15.5 kJ/mol to 26.7 kJ/mol by migration test and 17.9 kJ/mol to 39.9 kJ/mol by diffusion test[76]. Nguyen reported $E_{a,D}$ values of 35.7 kJ/mol for CEM-I mortar and 32.3 kJ/mol for CEM-V mortar[78]. LIFECON uses an $E_{a,D}$ = 39.9kJ/mol to model the temperature effect on chloride diffusivity, this $E_{a,D}$ value is the average $E_{a,D}$ value obtained by Page[77]. In Life-365's service life prediction model, an activation energy value of 35 kJ/mol is used[80].

Corrosion Rate vs. Temperature

Electrical resistivity is one of the most important parameters determining the corrosion rate of steel in concrete as described in Equation 2-30. By combining Equation 2-30 and Equation 2-34, temperature effect on corrosion can also be described by Arrhenius equation:

$$I_{corr}(T) = I_{corr}(T_0)\exp\left[\frac{E_{a,\rho}}{R}\left(\frac{1}{T_0}-\frac{1}{T}\right)\right] \tag{2-35}$$

where $I_{corr}(T)$ is the corrosion current density at temperature T (K) and $I_{corr}(T_0)$ is the corrosion current density at a reference temperature T_0. $E_{a,\rho}$ is activation energy for resistivity which is the same as in Equation 2-33. However, Equation 2-35 is a simplified equation describing the temperature effect on corrosion rates which considers only the effect from resistivity. Other factors such as galvanic potential may also change with temperature and then affect the corrosion rates.

2.3 Pozzolanic and Supplementary Cementing Materials in Concrete

2.3.1 Pozzolanic and Supplementary Cementing Materials

The utilization of pozzolanic and supplementary cementing materials to produce high performance concrete (in addition to or in partial replacement of Portland cement) has risen sharply in the past decades. The application of pozzolanic and supplementary cementing materials usually improve the workability of harsh mixes, lower the total heat evolved during curing, and more importantly, it improves the durability of concrete under various chemical attacks. Pozzolan is defined in ASTM C 618-94a as "a siliceous or siliceous and aluminous material, which in itself possesses little or no cementitious value but which will, in finely divided form and in the presence of moisture, chemically react with calcium hydroxide at ordinary temperatures to form compounds possessing cementitious properties" [81]. Pozzolanic admixtures can be either natural or artificial.

Suplementary cementitious materials include pozzolanic and non-pozzolanic materials. Pozzolanic admixtures in use include fly ash (FA), ultra-fine fly ash (UFA), silica fume (SF), and Metakaolin (MK); non-pozzolanic materials in use include, ground granulated blast furnace slag (GGBS). In the US these materials are used as partial replacement of Portland cement. These pozzolanic and supplementary cementing materials affect the progress of hydration as a consequence of their chemical composition, reactivity, particle size distribution, and particle shape[82]. The applicability of pozzolanic materials used as admixtures in cement is determined by pozzolanic activity which is strongly related to the amount of active components such as SiO_2, Al_2O_3, and Fe_2O_3.

Fly Ash

Fly ash is the ash precipitated electrostatically or mechanically from the exhaust gases of coal-fired power stations[82]. Fly ash consists of spherical and glassy particles with a very high fineness. The particle size of fly ash ranges from 1μm to 100 μm. According to ASTM C618, fly ash is classified by the total amount of (SiO_2+ Al_2O_3+ Fe_2O_3) as shown in Table 2.8 [81].

Class F fly ash is normally produced from burning bituminous coal which only shows pozzolanic properties. Class C fly ash is normally produced from lignite or subbituminous coal. Compared with Class F fly ash, the presence of high lime in Class C FA makes it both pozzolanic and cementitious properties, and hence allows the pozzolanic reaction to start earlier for Class C FA than for Class F FA.

Class N fly ash is raw or claimed natural pozzolans such as some diatomaceous earths, opaline cherts and shales, clays and shales, tuffs and volcanic ashes or pumicites.

Table 2.8: Fly ash classification according to ASTM C618.

		Class		
		N	F	C
$SiO_2+Al_2O_3+Fe_2O_3$	min%	70	50	70
SO_3	max%	4	5	5
Moisture content	max%	3	3	3
Loss on ignition	max%	10	6	6

Ground Granulated Blastfurnace Slag (GGBS)

Ground granulated blastfurnace slag is a by-product produced in the manufacture of iron in a blast-furnace. The chemical composition of GGBS varies by the source and the processing conditions. The major composition of GGBS is CaO, SiO_2 and Al_2O_3. GGBS has similar oxides than those that make up ordinary Portland cement but with different proportions as shown in Table 2.9. ASTM C 989 classifies slag depending on the mortar strengths when mixed with equal weight of Portland cement and compared to that of pure Portland cement mortar [83].

Table 2.9: Typical composition of GGBS compared with Portland cement [82]

Oxide	Composition (%)	
	Portland Cement	GGBS
CaO	64	40
SiO_2	21	36
Al_2O_3	6.0	10
Fe_2O_3	3.0	0.5
MgO	1.5	8.0
SO_3	2.0	0.2
K_2O	0.8	0.7
Na_2O	0.5	0.4

Silica Fume

The use of silica fume (SF) has significantly increased since 1980s. SF is a very fine power with glassy spherical particles having diameters 100 times finer than Portland cement [84]. The particle size ranges from 0.1 μm to 0.2 μm. The silica (SiO_2) content of SF varies from 85% to 98%. ASTM C 1240

requires a minimum silica content of 85%. Surface area of SF is at the order of 20 to 23 m^2/g, which is 13 to 20 times higher than the specific surface area of other pozzolanic materials. FDOT standard specification 346 allows the use of 7% to 9% SF by mass as replacement of cementitious materials [85].

The extremely small size and spherical shape of glassy SF particles makes it a highly reactive pozzolan which appreciably improves the properties of concrete both in fresh and hardened state after a short time [82].

2.3.2 The Pozzolanic Reaction

During the hydration reaction of Portland cement and water, C-S-H and CH are formed. In water filled capillaries, concretes containing pozzolanic admixtures undergo a pozzolanic reaction with the CH released during cement hydration to form additional C-S-H:

$$CH + S + H \rightarrow C\text{-}S\text{-}H \tag{2-36}$$

Reactive alumina in pozzolans also can react with CH:

$$CH + A + H \rightarrow C\text{-}A\text{-}H \tag{2-37}$$

Other compounds may also form depending on the compositions of cements and pozzolans, such as C_2AH, C_2ASH_8 or monosulfoaluminate. As a result, the capillary pore system in the cement/admixture paste is further reduced and a finer and less inter-connected pore system is formed. These reaction leads to a reduction in the permeability of the concrete and an increase in compressive strength. Cement paste with pozzolanic admixtures show fairly good strength, long-term durability and corrosion resistance.

The pozzolanic reaction of fly ash is described in Figure 2.15 [86]. Portland cement grain first starts hydration and the C-S-H with spiny shape is formed, at the same time calcium hydroxide is formed as a by-product of hydration. The pH of the pore water increases as the calcium hydroxide accumulates and dissolves into the pore water. When the pH of pore water increases and exceeds a pH threshold, the pozzolanic reaction is activated. Fly ash particles react with calcium hydroxide and additional C-S-H is formed that then fill the interstitial spaces. Due to the physical effect of filling voids by pozzolanic reaction products which cause pore refinement and reduces micro-cracks at the transitional zone, additional improvement of strength (higher) and diffusion (lower) properties are achieved [84].

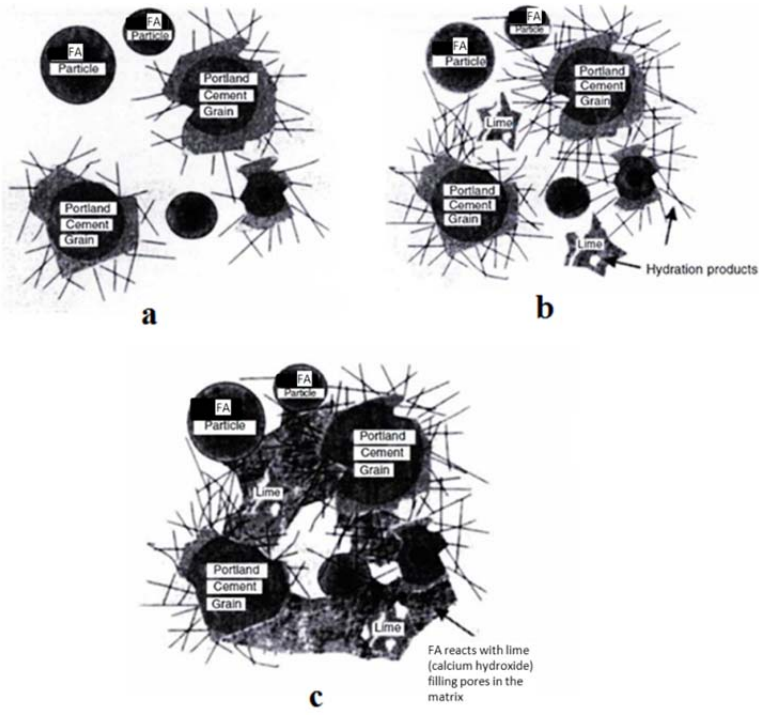

Figure 2.15: Schematic illustrations of pozzolanic reaction in concrete. (a) Hydration of Portland cement; (b) Calcium hydroxide (lime) is formed as a by-product of hydration; (c) The pozzolanic reaction initiates and forms additional hydration products to fill the pore systems [86]

It has been found that for some of pozzolans such as Class F fly ash, the pozzolanic reactions initiates when the pH of pore water is higher than 13.2[82]. A shorter delay has been reported for granulated blast furnace slag. As a result, overall concrete hydration rate at early age is delayed, which leads to lower strength development and high permeability properties during the short term. The advantage of using Class F fly ash or blast furnace slag for strength or permeability properties is usually reflected at longer-term ages. The rate of strength development of concrete with pozzolanic admixtures is dependent upon factors such as admixture types, mix proportions, ambient temperatures, and curing conditions. Figure 2.16 shows an example of strength development between OPC concrete and OPC+FA concrete hydrated at 20°C[86].

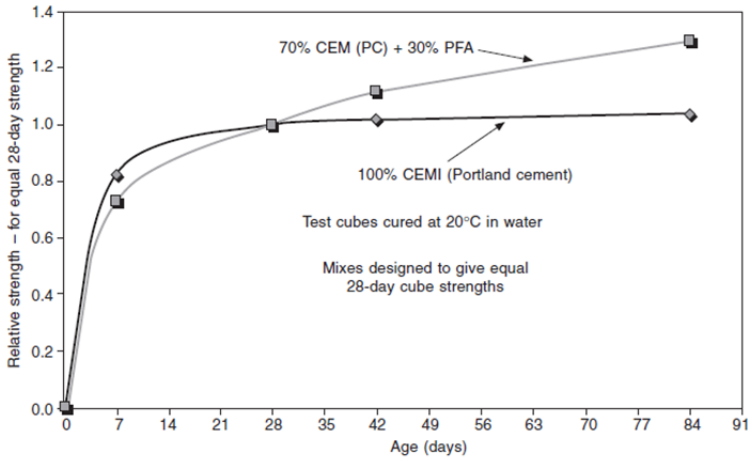

Figure 2.16: Strength development of OPC and OPC with 30% fly ash [86]

Figure 2.17 shows the development of electrical resistivity with on concretes with OPC and OPC+Class F FA under moist curing at 21ºC[19]. It indicates that for concrete with 20%FA, the resistivity is lower than concrete with OPC during the early age (< 28 days). However, after 28 days, the resistivity of 20%FA concrete is significantly higher than OPC concrete.

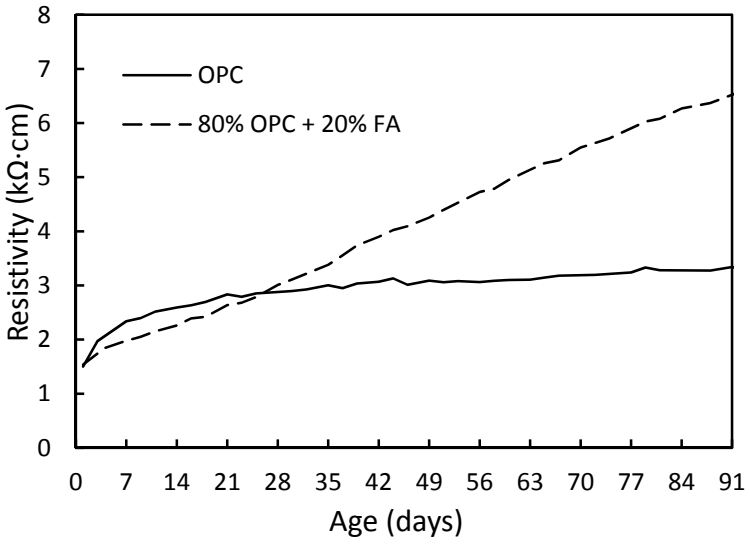

Figure 2.17: Electrical resistivity development of concrete with OPC and OPC/FA under moisture curing at 21ºC

2.3.3 Effect of Pozzolanic Admixture on Chemical Composition of Pore Solution

Use of pozzolanic admixtures and supplementary cementing materials changes the microstructures of concrete as a result of pozzolanic reaction. As the pozzolanic reaction consumes the Ca $(OH)_2$ in the pore solution to form additional C-S-H gel, the chemical composition of the pore solution is changed. Researchers have found that pozzolanic admixtures could significantly reduce the pH of concrete pore solution[24-26, 87]. Diamond studied cement paste with OPC and OPC blended with 30%FA, and found that use of fly ash decreased the concentration of OH^-, Na^+ and K^+[26]. Shehata et al. studied 2-year old cement paste with high alkalinity Portland cement blended with fly ash and found that the pH of concrete decreased with increasing replacement ratio of FA, as shown in Figure 2.18[25]. However, Shehata also stated that the decrease of pH was a combined result of dilution effect, replacement ratio of FA and alkalinity of the FA [25]. As the ion concentration in the pore solution is decreased when pozzolanic admixtures are used, the pore solution conductivity is also reduced. However, Nokken stated that FA and Slag did not affect the pore solution conductivity, other than by dilution in an amount approximately equal to the volume replacement of cement[88].

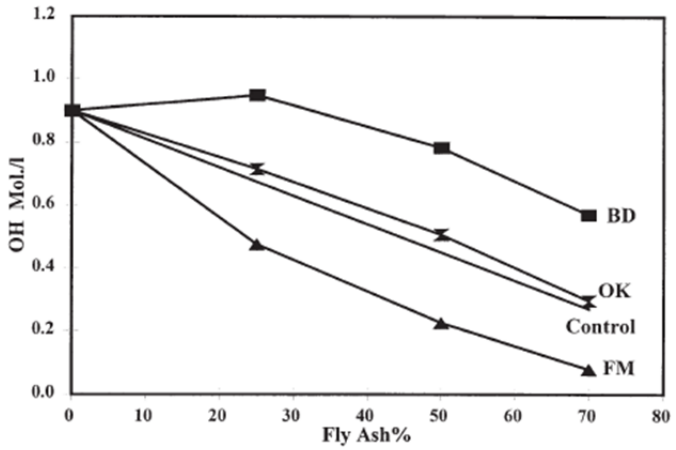

Figure 2.18: Effect of replacement ration of FA on the alkalinity of concrete pore solution.(BD, OK, FM: type of FA)[25]

2.3.4 Replacement Ratio of Pozzolans

ACI 318-08 limits the total replacement ratio of pozzolans to 50% by weight, as shown in Table 2.10 [89]. However, the limitation for fly ash and silica fume is usually 25% and 10% by weight, respectively. FDOT specifies 18%-22% Class F fly ash replacement ratio for regular concrete structures

and 18%-50% for mass concrete, and 7%-9% by weight for silica fume[85]. High volume fly ash (HVFA) concretes with replacement ratio up to 85% by mass have been reported.

Table 2.10: Limitations of pozzolan replacement under Exposure Class III [89]

Cementitious materials	Maximum percent of total cementitious materials by weight
Fly ash or other pozzolans conforming to ASTM C618	25
Slag conforming to ASTM C989	50
Total of fly ash or other pozzolans, slag and silica fume	10
Silica fume conforming to ASTM C1240	50
Total of fly ash or other pozzolans and silica fume	35

2.4 Accelerated Curing (AC) of Concrete by Elevated Temperature (ET)

2.4.1 Temperature Effect on Compressive Strength and Durability of Concrete

The curing temperature of concrete has a significant effect on the rate of hydration. It has been found that for OPC concrete, a higher curing temperature increases the hydration rates and results in higher compressive strength at the early age, however, it has been reported that the long term compressive strength is decreased. Figure 2.19 shows the effect of curing temperature during the first 28 days on the compressive strength[82]. At higher temperatures (32°C -49°C), the compressive strength is higher up to 7 days, however, the long term (> 28 days)compressive strength is lower than those cured at low temperatures (<23°C). At the initial high rate of hydration there is insufficient time available for the hydration products to diffuse away from the cement particles, which explains the adverse effects of a high early curing temperature on the later compressive strength is that. As a result, the products of hydration builds up in the vicinity of the hydrating particles and thus retard the subsequent hydration and adversely affect the long term compressive strength[82]. In addition, the non-uniform distribution of hydration products during high early curing temperatures leads to higher volumes of pores especially the larger pores (>150 nm in diameter) which is of great importance for concrete durability[90].

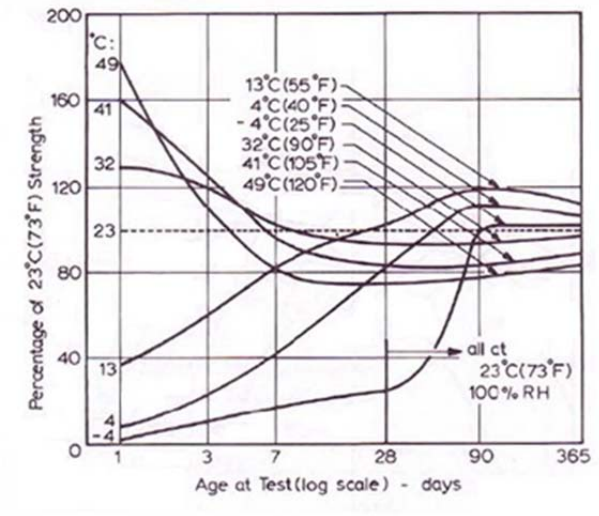

Figure 2.19: Effect of curing temperature during the first 28 days on the compressive strength of OPC concrete [82]

Under high curing temperatures(usually >30°C), concrete made with OPC shows higher early age compressive strength and lower long term compressive strength, however, concrete containing fly ash has been found to behave significantly differently. Figure 2.20 shows the 28-day compressive strength of OPC concrete and concrete containing fly ash under different curing temperatures[91]. It indicates that under higher curing temperatures, both early age and long term compressive strength were obtained for concrete containing fly ash, which is different from what has been observed on OPC concrete. Studies by Ozturan and Bastopcu also found that concrete with Class C fly ash subjected to 7 days of 30°C water bath curing had higher durability performance at 28 days and 56 days than those cured at 20°C all the time, as shown in Figure 2.21 [92].

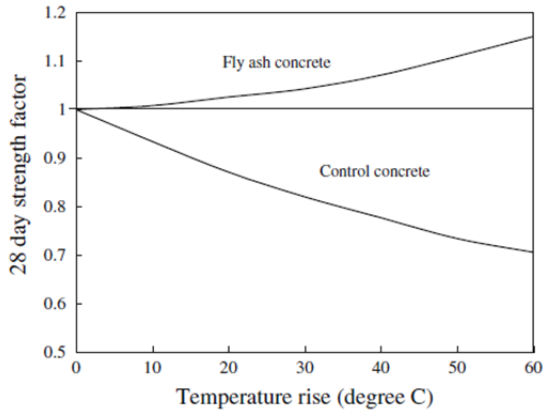

Figure 2.20: Effect of curing temperature on the 28-day compressive strength of OPC concrete and concrete with fly ash [91]

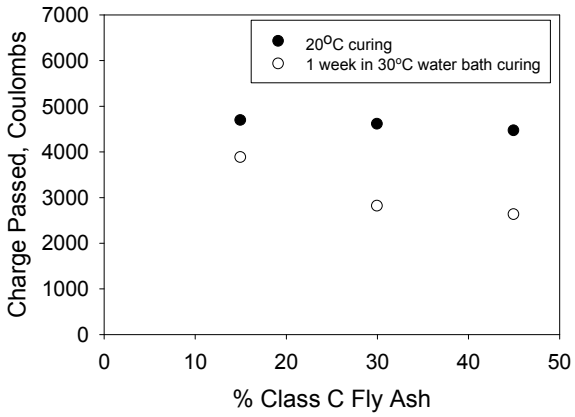

Figure 2.21: Effect of curing temperature on chloride ion permeability of concrete with Class C fly ash at 28 days [92]

2.4.2 Accelerated Curing of Concrete by Elevated Temperature

Accelerated curing of concrete by elevated temperature has been extensively used in the production of concrete structural members for over 100 years. The primary purpose of accelerated curing of concrete has been to study the early development of strength. Accelerated curing of concrete by elevated temperature can be applied not only to all types of cements described in ASTM C150, but also to the blended cements described in ASTM C595. The optimum accelerated curing regime depends in part on the type and source of cements selected. Accelerated curing and testing of concrete was developed because of the need for faster evaluation of the quality control of the concrete, which allows early prediction to be made based on testing at 28 days[93]. Accelerated curing is frequently used in cold areas where slow hydration is caused by low temperatures. In the manufacture of precast/ prestressed concrete structures, heat curing is regularly employed for accelerating strength gain which allows the timely release of prestressing force and turnaround of casting beds. Both production cycle and cost is reduced[94].

In recent years, supplementary cemetitious materials (SCMs) like fly ash, GGBS and silica fume have been used more frequently as blended materials to improve the properties of concrete. Concrete with some of the SCMs, such as Class F FA and GGBS, it usually takes a longer time to achieve the improved properties in the case of FA due to the slower pozzolanic reaction during hydration. Accelerated curing by elevated temperature and full immersion could expedite the pozzolanic reaction of concrete with FA.

Concrete under accelerated curing by elevated temperature usually achieves a higher early-strength. However, researchers have found that the long-term strength and resistance to chloride ingress decreased. Verbeck and Helmuth stated that because of the low solubility and diffusivity/mobility, cement hydration products cannot diffuse to a significant distance from the cement grain in the timeframe allowed by rapid hydration[95]. This results in microstructure that consists of relatively dense "shells" of hydrated products surrounding the cement grains and an open pore structure between the grains with a corresponding reduction in strength and high diffusivity properties[96-98]. It is important to note that the temperature at which the accelerated curing is carried out as well as its duration might play an important role in affecting the diffusion of hydration products.

Various methods of accelerated curing with elevated temperature have been developed. These methods involve samples being immersed in warm/hot water curing and high/low pressure stream curing[99]. One of the advantages of these methods is that sufficient moisture is provided for hydration during curing. A modified curing method consists of samples exposed in high temperature and high moisture. There are other curing methods used to accelerate concrete curing at elevated temperature, such as hot oil heating, electric resistance heating, microwave heating and infrared methods have also been developed [100, 101].

ASTM C684 provides four accelerated curing methods based on different curing regimes and tests are carried after 24, 28.5, 49.5 and 5 hours of casting.

-Procedure A: warm water method, 24 hours at 35°C ± 3°C.

-Procedure B: boiling water method, 23 hours at 21°C and 3.5 hours at 100°C.

-Procedure C: autogenous curing method.

-Procedure D: elevated temperature and pressure (K-5) method, 5 hours at 150°C ± 3°C.

British Standards

The British Standards, BS 1881 Part 12, provides three curing temperatures for accelerating the rate of gain of strength.

• 35°C method:

immediately after casting and sealing, cubes are immersed in water at 35°C ± 2°C for 24 hours ± 15mins. De-mold and label the cubes in 15 minutes and then the test is carried out immediately after removal from tank.

• 55°C method:

after casting and sealing, cubes are left undisturbed at 20°C ± 5°C between 1 to 1.5 hours. Between 1.5 to 3.5 hours after mixing, the cubes are immersed in water at 55°C ± 2°C for not less than 19hours 50 minutes. De-molding and labeling the cubes is completed by not more than 20hours 10 minutes after mixing. The cubes are immersed in water in a cooling tank at 20°C±5°C for 1 to 2 hours. Cubes are tested immediately after removal from the cooling tank.

• 82°C method:

after casting and sealing, cubes are left undisturbed at 20°C±5°C for at least one hour and then placed in an empty tank which is then filled with tap water at 5°C-20°C. The water temperature is raised to 82°C±2°C within 2 hours ± 15 minutes and maintained at this temperature for 14 hours ± 15 minutes. Hot water is drained off in 15 minutes and cubes are removed, de-molded and labeled. Tests are carried-out on the cubes immediately while still hot.

All the curing regimes described in the ASTM and British methods adopt short heating periods, usually less than 24 hours. Moreover, more complex accelerated curing regimes have been developed which involve longer curing period and wider ranges of curing temperatures[17]. Both OPC and other blended cement concrete with pozzolanic materials have been tested. Table 2.11 shows a list of elevated temperature curing regimes found in the literature.

Table 2.11: List of accelerated curing by elevated temperature in the literature.

Name	Year	Cement	Pozzolan	w/c or w/c+f	Temperature	Test methods	Curing Period
Klieger, P. [102]	1958	Type I, Type II, Type III	none		25, 40, 55, 73, 90, 105, 120 F	Compressive test	365 days
Detwiler R. J. et al. [96]	1991	OPC	none	0.4,0.5, 0.58	5, 20, 50 ℃	Back scattered electron images chloride permeability test , chloride penetration test	Typically 10-31days
Freyne, S. F. et al. [94]	2003	TypeIII	C fly ash, SF, Slag	0.24 to 0.31	23,30,42,60, 71℃	Compressive test	Up to 56days
Gardner, N. J. [103]	1990	Type I, Type III,	F fly ash	0.55,0. 35	0,10,20,30℃	Dynamic modulus test, compressive test	Up to 112days
Detwiler R. J. et al. [97]	1994	OPC	SF, Slag	0.4,0.5	23,50,70℃		2-10 days
Ozyildirim, C. [104]	1994	Type II, Type III,	F fly ash, SF	0.4,0.4 5	23 to 38℃	Compressive test, chloride permeability test	28 days
Ezziane, K. etc [98]	2010	OPC	Blast furnace slag, natural pozzolan, limestone power	0.47	20,40,60℃	Compressive strength tests, setting time by EN 196-3 method	90 days
Ahmed, H. E. H. [18]	2005	Type I, TypeV	F PFA, SF	0.4, 0.44, 0.53	35℃	Compressive test	Up to 90 days
Tokyay, M. [105]	1999	OPC	HL FA, LL FA	0.48,0. 27,0.26 ,0.25	35,100℃	Compressive tests	Up to 90 days
Yazici, H. [106]	2004	OPC	C fly ash	0.40	65℃	Compressive test, length change, setting time	Up to 90 days
Ozkul, M. H. [107]	2001	OPC	Tress cement	0.3 to 0.65	35,100℃	Compressive test	Up to 28 days

Table 2.11 (continued)

Siviero, E. [108]	1994	Portland 325, Portland 425,	Pozzolana 315, FA	0.42-0.84	36, 76 °C	Compressive test	>17 hours
Naik, T. R. [109]	1979	Four types of cement	none		100 F	Compressive test	Up to 28days
Ozyildirim, C. [17]	1998	OPC,OPC/ slag, OPC/FA,OPC/SF	Slag, SF, fly ash	0.33 to 0.45	5,10,23,38, 50 °C and combined	Compressive test, permeability test	Up to 1 year
Chini. A. R. [110]	2003	Type II,	F fly ash, blast furnace slag	0.41	73,160,200F	Compressive test, chloride penetration test, time to corrosion test, density and percentage of voids	Up to 56 days
Newlon Jr, H. [111]	1971	Type II, Type III	none	variable	95F, 212F	Compressive test	Up to 28 days
Nasser, K. W. [112]	1985	Type V	C fly ash	0.6	11,21,71,121 ,149,177, 232 °C		Up to 6 months
D.M. Roy [136]	1985	OPC	GBS, SF		27,38,60, 250 °C	Permeability, SEM, compressive test, mercury porosimetry test, calorimetry test	Up to 28 days
Johnston, C. D. [113]	1992	OPC	SF	0.43, 0.36 0.39	23,45,65 °C	Compressive test, chloride permeability test	Up to 28days
Kanda, T. [114]	1992	OPC	SF	0.25	25,45,55,65, 75°C	Compressive test	Up to 28 days
Poon, C. S. [115]	1997	OPC	F fly ash	0.27-0.49	15, 27°C	Compressive test, water permeability test, chloride penetration test, mercury intrusion porosimetry test,	Up to 90 days

Detwiler [96] studied the effect of curing temperature on the microstructure and properties with plain cement concrete of 0.4, 0.5 and 0.58 w/c cured either in 5°C, 20°C or 50°C. Backscattered electron images were taken and chloride diffusion tests were performed. Detwiler concluded that in plain cement concrete, elevated temperatures result in a coarser pore structure and a corresponding decrease in the resistance to chloride diffusion. Klieger [102] also studied Portland cement concrete cured between 23ºC and 49ºC, and found that higher curing temperature provided higher early strength but lower ultimate strength at later ages. Similar results were also found by Freyne [94] using concrete with type III cement.

Researchers have shown that the elevated temperature curing effect on concrete with fly ash/slag is different from plain cement concrete. Detwiler [97] studied concrete with slag and silica fume cured at 23°C, 50°C and 70°C up to 70% of hydration. Detwiler concluded that under elevated curing temperature, both slag and silica fume decreased concrete diffusivity properties, however, high temperature increased the penetration of chloride irons. Ozyildirim [116] studied concrete made with Type II and Type III cement combined with Class F fly ash and silica fume. Specimens were cured at 23°C and 38°C with various curing periods. Ozyildirim concluded that increasing the curing temperature from at 23°C and 38°C greatly decreased the coulomb values in specimens containing pozzolans. Gardner [103] studied concrete made with Type I, Type III, Type I/FA cured at 0ºC, 10ºC, 20ºC and 30ºC up to 112 days. Early strength of all the specimens increased at higher curing temperatures. However, type III cement concrete were not affected by curing temperature at ages of three days or more. Long term strength is slightly decreased for type I cement concrete at curing temperature of 30ºC. For concrete made with Type I/FA, both the short and long term strength were benefited from higher curing temperatures.

Concrete with SF were studied by Kanda [114] and Johnston [113]. Kanda studied concrete specimens with SF cured at 25ºC, 45ºC, 55ºC and 75ºC up to 28 days and concluded that at higher curing temperatures the 1-week strength was higher but the strength development from 1 week to 4 weeks tended to be lower. Johnston studied concrete specimens cured at 23ºC, 45ºC and 65ºC. Johnston's results showed that a curing temperature of 65ºC had a tendency to adversely affect resistance to chloride permeability and a less severe 45ºC curing temperature on reduced these adverse effects while improving long-term strength development almost to the levels achieved with normal moist curing.

Concrete with slag was studied by Hou [117] using: synchrotron radiation accelerator (SRA) observations, SEM tests, Mercury intrusion porosimetry (MIP) tests, permeability test, electrical resistance test and electrical permeability tests. Hou concluded that slag added to concrete produced more C-S-H gel than concrete without slag. Hou's results reported that lower permeability, enhanced strength, higher electrical resistance and low permeability of chloride ions were achieved for slag at later ages. However, temperature effect on curing was not investigated. Ma[118] studied the pore structure of low lime fly ash activated by $Ca(OH)_2$ and $CaSO_4 \cdot H_2O$ at 25 ºC, 60 ºC, 80 ºC, 100 ºC and 180 ºC. Ma found that the volumes of pores having average radii of about 19 A increased with thermal treatment for low lime fly ash with $Ca(OH)_2$, and the surface area increased as a result of treatment at elevated temperature. C-S-H was found to be responsible for the change of surface area.

3. TEMPERATURE DEPENDENCE OF CONCRETE RESISTIVITY

3.1 Introduction and Research Objectives

Electrical resistivity measurement has been employed as a method to estimate corrosion rate of depassivated steel in concrete as well as an indirect method to estimate chloride ion permeability of concrete. Higher resistivity usually indicates lower corrosion rate (when corrosion is initiated) and higher resistance to chloride ion penetration. However, resistivity of concrete is temperature dependent and an increase in temperature usually leads to a decrease of resistivity.

Temperature effect is important in predicting service life of reinforced concrete structures during both the initiation and propagation periods. Higher temperature will increase both chloride ion penetration rates and corrosion rates of steel in concrete. Temperature effect is also important when resistivity measurement is adopted as a quality control method for estimating chloride ion permeability. As resistivity measurement could be made under different temperatures, it is necessary to standardize the measured values corresponding to a reference temperature (i.e., 21°C). As described in section 2.2.7, the present methods in the literature could not provide a general solution to describe temperature effect on concrete with a wide range of resistivity values.

Under in-situ environment, degree of saturation also has a significant effect on concrete resistivity. To study the temperature effect on resistivity, it is necessary to keep the tested concrete specimens under saturated condition or under a fixed relative humidity (RH) environment.

The objectives of this research include:

- Study temperature effect on concrete with various intrinsic resistivity, mix design, and alkalinity under saturated and unsaturated conditions.
- Study temperature effect on hydrating and full hydrated concretes.
- Develop a method which could be applied to describe or standardize concrete resistivity corresponding to temperature under saturated or fixed RH conditions.

3.2 Experimental Procedure

3.2.1 Materials

Four groups of concrete specimens were prepared in this investigation. All the specimens were Φ10×20cm (4×8in) cylinders. Mix designs for Group 1 are shown in Table 3.1. Specimens in this group were initially prepared to study alkali-silica reaction (ASR). Two types of cements were used: OPC (F1) cement and HA cement. NaOH was added to increase the alkalinity of the pore solution. All the mixes had water to cementitious materials ratio (w/cm) of 0.41. Class F fly ash was used in all the mixes reported here with a cement replacement ratio of 19% by mass. The chemical compositions of the cements and fly ash are listed in Table 3.2. Seven types of coarse aggregates were used. $LiNO_3$ was used as an inhibitor to ASR in some sets. More details of the mix properties are included in the report of the project[119]. Concrete cylinders were demolded after 24 hours of casting, and then kept in sealed plastic containers at 95% RH and 38°C. Six years later, the concrete were transferred to room temperature environment (about 21°C) and immersed in fresh water for more than three months, which assured the cylinders were close to or fully hydrated and saturated.

Specimens in Group 2 were prepared as part a round-robin test for evaluating precision of electrical resistivity measurement on water-saturated concrete cylinders[120]. Eleven mixes were prepared in this group. Type I/II cement with different amount of pozzolanic admixtures, fine and coarse aggregates, and w/cm were used. Details of mix design are shown in Table 3.3. More details are included in the final report of the research[120]. The concrete cylinders were demolded after one day and then were cured in lime water at room temperature (around 21°C) for more than three months. Thereafter, two cylinders were kept in fresh water at 45°C for two months to accelerate the hydration process.

Table 3.1: Mix designs in Group 1

Mix No.	Cement Type	Agg. Type	Cement (kg/m^3)	FA (kg/m3)	Water (kg/m3)	Fine agg. SSD (kg/m^3)	Coarse agg. SSD (kg/m^3)	Air Adm. ml/m^3	LiNO3 Dosage	NaOH (kg/m^3)
00	F1	F1	363	83	178	607	1005	110	-	-
01	F1	NG	363	83	178	607	1085	218	-	-
02	HA	NG	363	83	178	607	1085	436	-	-
03	HA	F1	363	83	178	607	1085	436	-	-
05	F1	GG	363	83	178	607	1085	436	-	-
06	F1	F2	363	83	178	607	994	218	-	-
07	HA	F2	363	83	178	607	994	218	-	-
16	F1	GG	363	83	178	607	1085	436	1	3.42
17	F1	GG	363	83	178	607	1085	436	1.5	3.42
18	F1	GG	363	83	178	607	1085	436	1	4.57
19	F1	GG	363	83	178	607	1085	436	1.5	4.57
22	F1	NG	363	83	178	607	1085	436	1	3.42
23	F1	NG	363	83	178	607	1085	436	1.5	4.57
30	F1	H1	363	83	178	607	1105	218	-	-
33	F1	H1	363	83	178	607	1105	218	1	3.42
34	F1	H1	363	83	178	607	1105	218	1.5	3.42
36	F1	H1	363	83	178	607	1105	218	1.5	4.57
37	HA	H1	363	83	178	607	1105	218	-	-
38	F1	H2	363	83	178	607	1113	218	-	-
41	F1	H2	363	83	178	607	1113	327	1	3.42
42	F1	H2	363	83	178	607	1113	327	1	4.57
43	HA	H2	363	83	178	607	1113	327	-	-
44	F1	F3	363	83	178	607	917	-	-	-
45	F1	F3	363	83	178	607	917	-	-	3.42
47	F1	F3	363	83	178	607	917	218	1	3.42
49	HA	F3	363	83	178	607	917	-	-	-

Table 3.2: Chemical composition of cement of FA for Group 1 (percentage by mass)

Designation	SiO_2	$A1_2O_3$	Fe_2O_3	CaO	SO_3	Na_2O	K_2O	Na_2Oe
F1	19.09	5.59	4.17	63.87	3.55	0.148	0.6	0.544
HA	20.08	4.95	3.05	61.98	4.2	0.278	1.15	1.037
FA	52.82	21.9	6.06	4.92	0.27	0.284	1.49	1.267

Table 3.3: Mix designs in Group 2

Mix No.	Cement kg/m^3	FA kg/m^3	SF kg/m^3	MK kg/m^3	CA1 kg/cm^3	CA2 kg/m^3	Fine agg. Kg/cm^3	Water kg/m^3	Total Cementitious	% FA	% SF	% MK	w/cm
R2	285	71	-	-	282	854	824	144	356	20	-	-	0.40
R3	392	119	-	-	785	-	724	199	510	23	-	-	0.39
R4	279	178	-	-	940	-	793	158	457	39	-	-	0.35
R5	308	103	-	-	909	-	879	164	411	25	-	-	0.40
R6	390	-	-	-	1068	-	712	145	390	-	-	-	0.37
R7	296	80	24	-	532	528	687	160	401	20	-	-	0.40
R8	335	84	-	-	-	-	-	163	418	20	-	-	0.39
R9	291	65	15	-	1032	-	697	151	371	18	4	-	0.41
R10	297	153	-	-	1009	-	638	180	450	34	-	-	0.40
R11	430	95	-	-	1033	-	577	157	525	18	-	-	0.30
R12	402	-	-	45	1009	-	624	156	446	-	10	10	0.35

FA: fly ash; SF: silica fume; MK: metakaolin; CA: coarse aggregate

Concrete cylinders for Group 3 were from a previous investigation for studying resistivity of concrete. Mix design for Group 3 is listed in Table 3.4. Class F FA and SF were used in the mixes. Three mix designs were included with w/c of 0.40. More details on these mixes were described in the thesis[19]. All the specimens were kept either in a fog room with around 100 %RH or in sealed plastic containers with around 95% RH at room temperature for three years. Thereafter, three cylinders from each mix were selected and immersed in fresh water for at least three months.

Table 3.4: Mix designs in Group 3

Mix No.	Cement	Coarse agg.	Cement (kg/m^3)	FA (kg/m^3)	Water (kg/m^3)	Fine agg. SSD (kg/m^3)	Coarse agg. SSD (kg/m^3)	% FA	% SF
1C1	type I/II	Limestone	390	-	156	734	996	-	-
1C2	type I/II	Limestone	312	78	156	734	996	20%	-
1C3	type I/II	Limestone	281	78	31	734	996	20%	8%

Mix designs for Group 4 are listed in Table 4.2. Two types of coarse aggregates were used: limestone and granite. Class F FA was used with replacement ratio ranging from 20% to 50%. Slag was also used with replacement ratio of 50% and 70%. In some specimens, 10%FA+60%Slag and 20%FA+50%Slag were used. More details regarding mix properties and curing regimes are described in Chapter 4.

Two cylinders were selected for each mix in Group 1 to 3 for dynamic temperature test. Eight cylinders cured under different curing regimes (two per curing regime) were selected for each mix in Group 4. Details of the curing regimes are described in Chapter 4.

3.2.2 Dynamic Temperature Test

Resistivity is affected by temperature as well as degree of hydration and saturation. To study the temperature dependence of concrete resistivity, it is necessary to perform dynamic temperature test on specimens at a fixed degree of hydration and saturation. The degree of hydration of the four groups of specimens was different, so two different temperature ranges were used.

Table 3.5 lists the degree of hydration of specimens (based on resistivity evolution with age) when dynamic temperature test was performed and tested temperature range. Resistivity measurements were performed using a Wenner probe device according to FM 5-578[14]. The electrode spacing used was 3.8 cm (1.5in) and the geometry cell constant $K_{\rho,g}$ was 1.89. All the resistivity values shown in here are the geometry normalized resistivity values.

Table 3.5: Degree of hydration and range of dynamic temperature test

Group #	Hydration status	Range of dynamic temperature test
1	fully hydrated	10°C-45°C
2	close to or fully hydrated	10°C-45°C
3	close to or fully hydrated	10°C-45°C
4	not fully hydrated	10°C-35°C

As specimens in group 1, 2 and 3 were close to or fully hydrated, a higher maximum temperature (up to 45°C) was used. To minimize effect of further hydration due to elevated temperature during the test, the highest tested temperature for group 4 was 35 °C. Two water bath tanks were used for the test: a warm water tank and a cool water tank. Both tanks were filled with tap water deep enough to completely immerse all the specimens. Inside of the warm tank, a heater controlled by a thermostat was used to adjust the water temperature (21°C to 35°C or 45°C). A pump was also used to help water and heat circulation. For the cool water tank, a chiller controlled by a thermostat was used to adjust the water temperature from 10°C to 21°C.

Resistivity was measured at least two hours after water temperature had stabilized. Concrete cylinders were momentarily taken out of water and surface-dried by a towel. Resistivity was measured immediately thereafter and water temperature was recorded. Water temperature was changed every 2°C for Group 1, 2, 3 and every 5 °C for Group 4. It usually took one week to finish a cycle of measurement for Group 1, 2, 3 (10°C to 45°C) and three days for Group 4(10°C to 35°C). Multiple cycles of measurements were performed for specimens in Group 1, 2 and 3 to verify the reproducibility of resistivity values obtained from different cycles testing. For specimens in Group 4, resistivity at room temperature (21°C) was measured before and after dynamic temperature test to verify no additional (or very modest increase) hydration happened during the test.

Besides dynamic temperature test performed for saturated specimens, some cylinders from Group 1 and Group 3 were selected for dynamic temperature test under controlled RH conditions. The selected specimens were put in a humidity-temperature environmental chamber. The specimens were first in the chamber under 92% RH at 40°C for more than two months until the weight was stable. Then dynamic temperature test was performed at the temperature between 10°C and 45°C under fixed 92%RH. Temperature was changed every 5°C and resistivity was measured every 24 hours. Thereafter, the specimens were put in the chamber under 85%RH at 40°C and same procedures were repeated as those on 92%RH.

3.3 Results and Discussion

3.3.1 Resistivity vs. Temperature

Resistivity vs. Temperature on Saturated Specimens.

Representative results of the measured resistivity during dynamic temperature test on saturated specimens are shown in Figure 3.1. The plots in Figure 3.1 indicate that the resistivity values follow a trend of exponential decay with increasing temperature. In Figure 3.1a, the resistivity value of the two cylinders from the same mix cured under the same curing regimes is similar or overlapped. However, in Figure 3.1b, two groups were obtained with different range of resistivity values, which is attributed to different degrees of hydration based on the corresponding curing regimes (D24&25 under 2RT/ET and D26&27 under 2RT/26ET/RT).

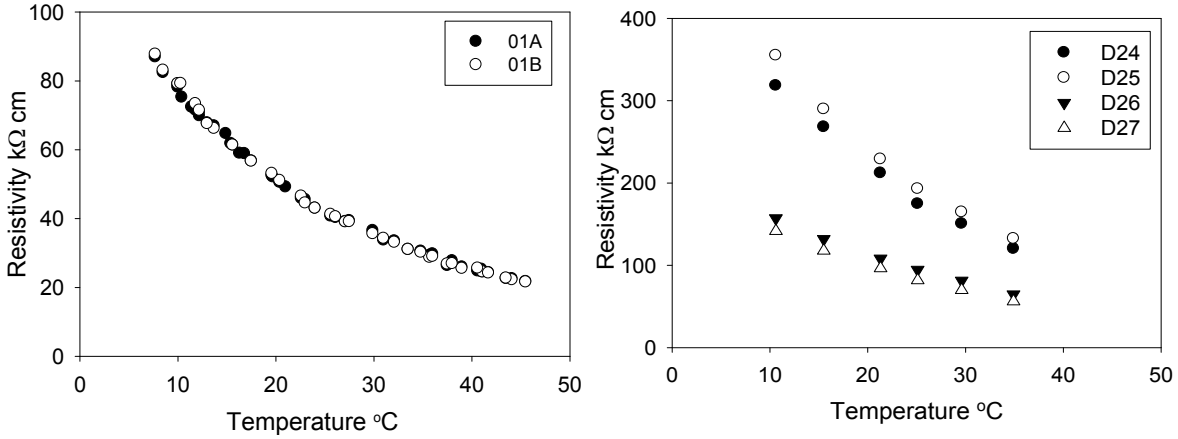

Figure 3.1: Evolution of resistivity with temperature of saturated specimens.

Figure 3.2 shows the measured resistivity with temperature on specimens with different intrinsic resistivity. The observed trends show that temperature effect is different on concrete with different resistivity values, and it indicates that temperature has a more significant effect on concrete with higher resistivity values than on concrete with lower resistivity values.

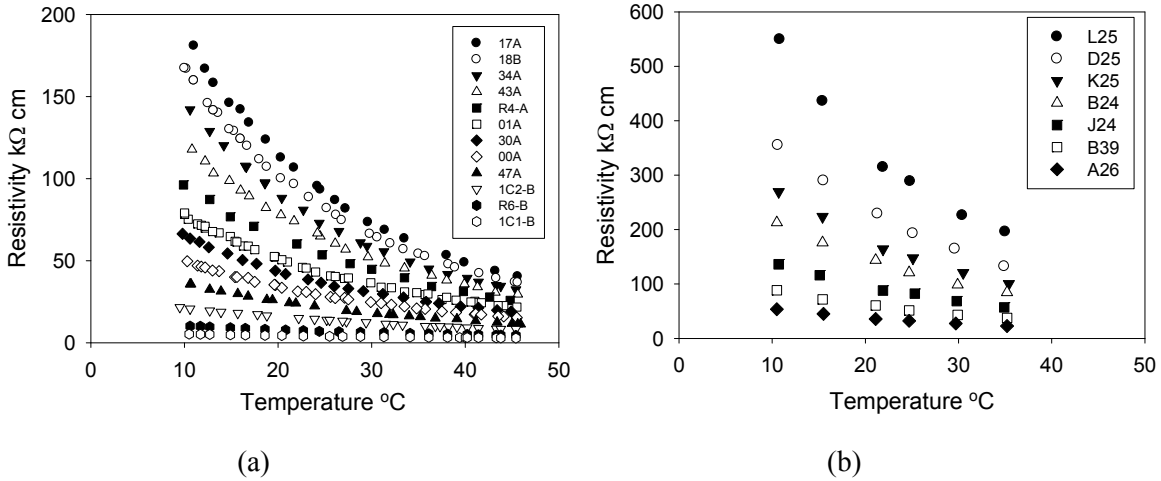

Figure 3.2: Evolution of resistivity with temperature on saturated specimens with typical resistivity values.

Resistivity vs. Temperature on Unsaturated Specimens.

Figure 3.3 shows typical results of resistivity evolution with temperature under 85% RH, 92% RH and under saturated condition. It shows that concrete resistivity is higher at lower RH conditions. Under exposure at 92% and 85% RH condition, resistivity decreases with increasing temperature, which is somewhat similar to the results under saturated condition.

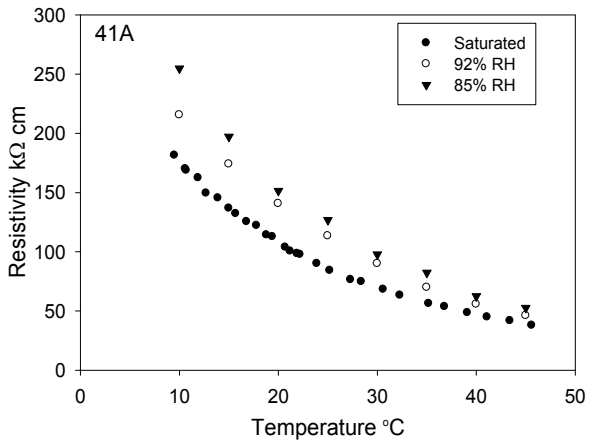

Figure 3.3: Comparison of resistivity evolution with temperature on specimens under saturated and unsaturated (85%RH and 92%RH) conditions.

3.3.2 Calculation of Activation Energy

As previously stated in Chapter 2, various methods have been proposed to describe temperature effect on concrete resistivity. As Arrhenius equation is the most widely accepted method, the modified Arrhenius equation was employed to analyze the experimental results:

$$\rho = A \cdot \exp\left[\frac{E_{a,\rho}}{R \cdot (T + 273.15)}\right] \tag{3-1}$$

where A is the resistivity when $T(°C) \rightarrow +\infty$, which is the intrinsic property of concrete. The value of activation energy for resistivity ($E_{a,\rho}$) determines the slope of the decay, which reflects the sensitivity of resistivity change with temperature. Equation 3-1 was used for curve fitting on the measured results to obtain parameters A and $E_{a,\rho}$. Examples of the curve fitting are shown in Figure 3.4 Parameters calculated from curve fitting from Group 1 to Group 4 are shown in Figure 3.6 to Figure 3.9. Table 3.10 and Table 3.11 lists the results on specimens under 92%RH and 85%RH.

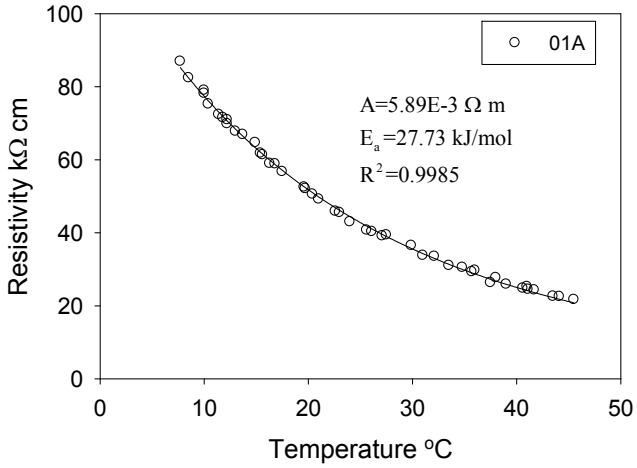

Figure 3.4: Examples of curve fitting using Arrhenius equation on specimen 01A.

Table 3.6: Parameters calculated with Arrhenius equation on specimens in Group 1

Specimen No.	A Ω m	$E_{a,\rho}$ kJ/mol	ρ at 21°C kΩ cm	R^2	Specimen No.	A Ω m	$E_{a,\rho}$ kJ/mol	ρ at 21°C kΩ cm	R^2
00A	1.09E-02	25.26	33.35	0.9988	30A	6.73E-03	27.02	42.30	0.9990
00B	1.50E-02	24.29	30.89	0.9991	30B	7.33E-03	26.75	41.26	0.9994
01A	5.89E-03	27.74	49.80	0.9985	33A	2.64E-03	31.67	111.32	0.9987
01B	4.78E-03	28.27	50.00	0.9983	33B	2.71E-03	31.62	112.07	0.9983
02A	9.86E-03	26.09	42.32	0.9993	34A	1.41E-03	32.61	87.15	0.9995
02B	3.88E-03	28.88	52.09	0.9992	34B	1.48E-03	32.44	85.45	0.9994
03A	6.03E-03	27.60	47.97	0.9983	36A	1.46E-03	32.58	88.86	0.9993
03B	5.43E-03	27.98	50.62	0.9995	36B	1.14E-03	33.31	94.19	0.9985
05A	6.40E-03	27.46	48.24	0.9988	37A	4.91E-03	28.38	53.94	0.9980
05B	6.10E-03	27.55	47.71	0.9989	37B	4.19E-03	28.72	52.74	0.9990
06A	1.05E-02	25.65	37.69	0.9982	38A	7.04E-03	27.52	54.32	0.9994
06B	7.50E-03	26.55	38.87	0.9989	38B	7.07E-03	27.57	55.57	0.9996
07A	6.86E-03	27.19	46.22	0.9996	41A	1.48E-03	32.92	103.68	0.9988
07B	8.30E-03	26.71	46.03	0.9987	41B	1.70E-03	32.54	102.24	0.9988
16A	2.05E-03	31.80	90.88	0.9993	42A	1.02E-03	33.99	111.18	0.9987
16B	2.20E-03	31.64	91.47	0.9996	42B	1.46E-03	33.10	110.42	0.9989
17A	1.35E-03	33.30	110.25	0.9989	43A	3.11E-03	30.31	75.03	0.9991
17B	1.22E-03	33.60	113.66	0.9988	43B	2.67E-03	30.50	69.69	0.9988
18A	1.54E-03	32.77	101.20	0.9993	44A	2.54E-02	22.07	21.08	0.9984
18B	1.46E-03	32.83	98.62	0.9993	44B	2.39E-02	21.74	17.37	0.9966
19A	1.91E-03	32.16	98.10	0.9990	45A	1.25E-02	24.16	24.42	0.9991
19B	1.68E-03	32.46	97.32	0.9990	45B	1.18E-02	24.45	25.92	0.9994
22A	1.63E-03	32.00	78.38	0.9991	47A	1.21E-02	24.27	24.68	0.9988
22B	1.31E-03	32.83	88.96	0.9981	47B	1.30E-02	23.65	20.62	0.9994
23A	1.23E-03	33.53	110.95	0.9984	49A	1.69E-02	23.69	27.18	0.9986
23B	1.20E-03	33.39	102.07	0.9988	49B	1.57E-02	23.84	26.93	0.9986

Table 3.7: Parameters calculated with Arrhenius equation on specimens in Group 2

Specimen No.	A Ω m	$E_{a,\rho}$ kJ/mol	ρ at 21°C kΩ cm	R^2	Specimen No.	A Ω m	$E_{a,\rho}$ kJ/mol	ρ at 21°C kΩ cm	R^2
R2A	2.22E-02	24.42	48.16	0.9963	R8A	1.16E-02	28.81	151.26	0.9992
R2B	2.57E-02	23.91	45.24	0.9969	R8B	1.66E-02	27.86	147.74	0.9987
R3A	1.25E-02	26.06	53.03	0.9980	R9A	1.42E-02	25.31	44.48	0.9976
R3B	1.63E-02	25.28	50.33	0.9952	R9B	1.45E-02	25.43	47.59	0.9980
R4A	7.01E-03	27.84	61.72	0.9987	R10A	2.09E-02	27.66	170.26	0.9991
R4B	5.09E-03	28.56	60.01	0.9966	R10B	1.91E-02	27.78	163.49	0.9968
R5A	1.69E-02	23.44	24.52	0.9984	R11A	1.22E-02	26.87	72.41	0.9979
R5B	1.50E-02	23.72	24.42	0.9987	R11B	2.61E-02	24.95	70.33	0.9970
R6A	4.99E-02	18.20	8.50	0.9983	R12A	3.65E-02	22.14	31.27	0.9982
R6B	5.88E-02	17.57	7.74	0.9976	R12B	3.36E-02	22.53	33.64	0.9983
R7A	7.48E-03	29.07	108.79	0.9990					
R7B	8.51E-03	28.73	107.70	0.9992					

Table 3.8: Parameters calculated with Arrhenius equation on specimens in Group 3

Specimen No.	A Ω m	$E_{a,\rho}$ kJ/mol	ρ at 21°C kΩ cm	R^2
1C1A	1.90E-01	13.26	4.30	0.9967
1C1B	1.94E-01	13.19	4.27	0.9978
1C1C	1.60E-01	13.84	4.57	0.9957
1C2A	2.74E-02	21.35	16.92	0.9989
1C2B	3.61E-02	20.43	15.35	0.9981
1C2C	2.73E-02	21.40	17.22	0.9977
1C3A	8.60E-03	27.07	55.07	0.9993
1C3B	7.08E-03	27.53	54.82	0.9992

Table 3.9: Parameters calculated with Arrhenius equation on specimens in Group 4

Specimen No.	A Ω m	$E_{a,\rho}$ kJ/mol	ρ at 21°C kΩ cm	R^2	Specimen No.	A Ω m	$E_{a,\rho}$ kJ/mol	ρ at 21°C kΩ cm	R^2
Ai24	6.83E-03	27.68	56.25	0.9986	F24	1.41E-02	26.35	67.06	0.9989
Ai25	8.99E-03	26.95	54.91	0.9997	F25	1.77E-02	25.81	67.62	0.9994
Ai26	1.12E-02	25.45	36.88	0.9956	F26	1.77E-02	24.67	42.70	0.9992
Ai27	1.27E-02	25.20	38.06	0.9998	F27	1.35E-02	25.48	45.40	0.9945
Ai37	1.24E-02	26.12	53.97	0.9988	F37	1.83E-02	25.63	65.39	0.9982
Ai38	1.02E-02	26.69	56.15	0.9994	F38	1.75E-02	25.86	68.49	0.9987
Ai39	1.21E-02	25.34	38.28	0.9987	F39	1.44E-02	25.22	43.39	0.9989
Ai40	1.79E-02	24.35	37.79	0.9974	F40	2.14E-02	24.13	41.13	0.9998
Bi24	8.38E-03	29.74	160.26	0.9987	I24	1.87E-02	26.88	110.68	0.9970
Bi25	6.12E-03	30.38	152.26	0.9990	I25	2.14E-02	26.56	111.66	0.9985
Bi26	1.38E-02	26.89	82.15	0.9984	I26	2.15E-02	25.06	60.55	0.9994
Bi27	9.35E-03	27.69	77.30	0.9981	I27	1.53E-02	25.96	62.55	0.9993
Bi37	6.19E-03	30.27	146.81	0.9981	I37	3.36E-02	25.41	109.27	0.9973
Bi38	8.91E-03	29.47	152.53	0.9946	I38	2.26E-02	26.33	107.09	0.9985
Bi39	1.23E-02	27.03	77.61	0.9978	I39	2.31E-02	24.83	59.40	0.9992
Bi40	1.09E-02	27.33	77.53	0.9983	I40	1.80E-02	25.40	58.46	0.9998
A24	1.00E-02	26.52	51.13	0.9997	H24	1.93E-02	27.52	148.48	0.9984
A25	1.61E-02	25.45	53.18	0.9984	H25	1.41E-02	28.12	138.55	0.9986
A26	1.13E-02	25.40	36.66	0.9984	H26	2.69E-02	25.07	76.04	0.9993
A27	1.54E-02	24.63	36.48	0.9989	H27	2.14E-02	25.68	77.83	0.9984
A37	1.09E-02	26.48	54.68	0.9987	H37	3.06E-02	26.18	136.46	0.9929
A38	1.22E-02	26.19	54.47	0.9980	H38	2.64E-02	26.58	138.69	0.9980
A39	1.56E-02	24.58	36.00	0.9980	H39	2.61E-02	24.98	71.07	0.9951
A40	1.18E-02	25.29	36.59	0.9967	H40	2.18E-02	25.43	71.51	0.9983
B24	1.75E-02	27.63	140.78	0.9980	C24	6.36E-03	29.35	103.50	0.9997
B25	1.30E-02	28.31	138.91	0.9931	C25	1.15E-02	27.87	102.65	0.9997
B27	2.40E-02	24.97	65.31	0.9988	C26	1.46E-02	26.67	79.47	0.9996
B28	2.17E-02	25.19	64.48	0.9989	C27	1.57E-02	26.43	77.43	0.9997
B37	1.37E-02	28.12	134.98	0.9974	C37	1.18E-02	27.75	99.46	0.9992
B38	1.43E-02	28.00	133.98	0.9977	C38	1.50E-02	27.08	96.53	0.9995
B39	1.64E-02	25.68	59.46	0.9969	C39	1.20E-02	26.91	71.82	0.9992
B40	1.56E-02	25.83	60.39	0.9976	C40	1.35E-02	26.66	73.41	0.9997
J24	2.41E-02	25.83	93.03	0.9974	K24	1.15E-02	29.13	171.17	0.9977
J25	2.07E-02	26.10	89.32	0.9977	K25	1.00E-02	29.51	174.33	0.9985
J26	1.50E-02	25.53	51.36	0.9954	K26	1.25E-02	27.75	106.00	0.9980
J27	1.94E-02	24.94	52.03	0.9943	K27	1.55E-02	27.30	109.06	0.9996
J37	1.44E-02	27.03	91.12	0.9989	K37	7.37E-03	30.07	161.01	0.9988
J38	1.46E-02	26.99	90.70	0.9978	K38	8.12E-03	29.76	156.76	0.9987
J39	2.34E-02	24.50	52.46	0.9995	K39	1.28E-02	27.45	96.36	0.9970
J40	2.09E-02	24.75	51.97	0.9984	K40	1.25E-02	27.45	93.74	0.9955
D24	1.65E-02	28.74	209.93	0.9965	L24	1.23E-02	30.31	297.70	0.9960
D25	1.46E-02	29.26	229.86	0.9996	L25	6.62E-03	32.16	339.67	0.9972
D26	3.33E-02	25.40	108.08	0.9977	L26	1.99E-02	27.50	152.04	0.9983
D27	1.60E-02	26.88	95.27	0.9981	L27	1.57E-02	28.06	150.61	0.9958
D37	1.73E-02	28.68	214.57	0.9910	L37	8.92E-03	31.07	293.51	0.9909
D38	1.45E-02	29.14	217.00	0.9964	L38	7.85E-03	31.67	330.52	0.9921
D39	2.19E-02	26.46	109.55	0.9980	L39	9.11E-03	29.29	145.07	0.9938
D40	3.12E-02	25.44	102.76	0.9912	L40	1.06E-02	28.81	139.26	0.9954
E24	8.89E-03	26.11	38.59	0.9990	G24	8.13E-03	26.37	39.15	0.9998
E25	1.32E-02	25.08	37.57	0.9988	G25	5.06E-03	27.43	37.67	0.9987
E26	1.26E-02	24.35	26.53	0.9976	G26	5.28E-03	26.63	28.32	0.9996
E27	1.22E-02	24.44	26.54	0.9979	G27	5.38E-03	26.61	28.59	0.9994
E37	1.27E-02	25.30	39.40	0.9977	G37	8.54E-03	25.85	33.23	0.9989
E38	1.31E-02	25.23	39.63	0.9989	G38	6.15E-03	26.56	32.04	0.9989
E39	8.20E-03	25.50	27.69	0.9959	G39	1.73E-02	23.66	27.57	0.9960
E40	7.35E-03	25.76	27.59	0.9973	G40	6.13E-03	26.11	26.60	0.9995

Table 3.10: Parameters calculated with Arrhenius equation on specimens at 92% RH

Specimen No.	A Ω m	$E_{a,\rho}$ kJ/mol	ρ at 21°C kΩ cm	R^2	Specimen No.	A Ω m	$E_{a,\rho}$ kJ/mol	ρ at 21°C kΩ cm	R^2
1C1A	1.16E-01	15.30	6.04	0.9972	33A	7.07E-04	35.13	122.39	0.9986
1C1B	1.28E-01	15.09	6.13	0.9874	33B	1.11E-03	34.03	122.61	0.9994
1C2A	1.76E-02	23.93	31.27	0.9985	36A	1.05E-03	34.03	116.30	0.9994
1C2B	2.11E-02	23.35	29.57	0.9932	36B	1.07E-03	34.05	119.51	0.9988
1C3A	8.10E-03	27.97	75.14	0.9989	41A	2.52E-03	32.19	131.22	0.9966
1C3B	8.00E-03	28.12	78.95	0.9998	41B	2.66E-03	32.03	129.84	0.9985
03A	3.62E-03	29.48	62.26	0.9991	43A	8.41E-04	34.11	96.05	0.9984
03B	2.82E-03	30.19	64.75	0.9987	43B	1.37E-03	32.87	94.21	0.9996
30A	9.09E-03	27.20	61.55	0.9980	45A	8.01E-03	26.28	37.23	0.9983
30B	1.17E-02	26.50	59.54	0.9952	45B	7.41E-03	26.63	39.65	0.9984

Table 3.11: Parameters calculated with Arrhenius equation on specimens at 85% RH

Specimen No.	A Ω m	$E_{a,\rho}$ kJ/mol	ρ at 21°C kΩ cm	R^2	Specimen No.	A Ω m	$E_{a,\rho}$ kJ/mol	ρ at 21°C kΩ cm	R^2
3A	4.04E-03	29.72	76.53	0.9993	41A	1.54E-03	33.70	148.44	0.9987
3B	4.70E-03	29.43	79.14	0.9985	41B	1.72E-03	33.39	146.58	0.9998
30A	1.10E-02	27.08	70.70	0.9994	43A	1.46E-03	33.10	110.04	0.9993
30B	9.13E-03	27.39	66.86	0.9979	43B	1.46E-03	33.07	109.02	0.9990
33A	1.40E-03	33.66	132.22	0.9995	45A	1.06E-02	26.01	44.15	0.9996
33B	1.18E-03	34.14	136.33	0.9980	45B	9.57E-03	26.41	46.85	0.9993
36A	1.22E-03	34.01	133.34	0.9992					
36B	1.07E-03	34.34	134.99	0.9992					

3.3.3 Discussion

3.3.3.1 Correlation between ρ_{21} and $E_{a,\rho}$

Saturated Specimens

Results in Table 3.6 to Table 3.9 show that, the resistivity of saturated specimens at 21°C ranges from 4.3 kΩ cm (1C1A) to 340 kΩ cm (L25) and the values of activation energy range from 13.2 kJ/mol (1C1A) to 32.2 kJ/mol (L25). The values of activation energy from this investigation are in agreement with the reported values in the literature (16.9 kJ/mol to 42.77 kJ/mol)[47, 48, 69]. The correlation between 21°C resistivity and activation energy for all the specimens is plotted in Figure 3.5. The plots show that activation energy values increase with concrete resistivity. Depending on the concrete mix

property, two equations describing the correlation between 21°C resistivity (ρ_{21}) and activity energy for resistivity ($E_{a,\rho}$) are proposed:

$$E_{a,\rho} = 6.0157 \ln(\rho_{21}) + 4.3141 \quad (3\text{-}2)$$

$$E_{a,\rho} = 3.7738 \ln(\rho_{21}) + 9.7518 \quad (3\text{-}3)$$

Where ρ_{21} in kΩ cm and $E_{a,\rho}$ in kJ/mol.

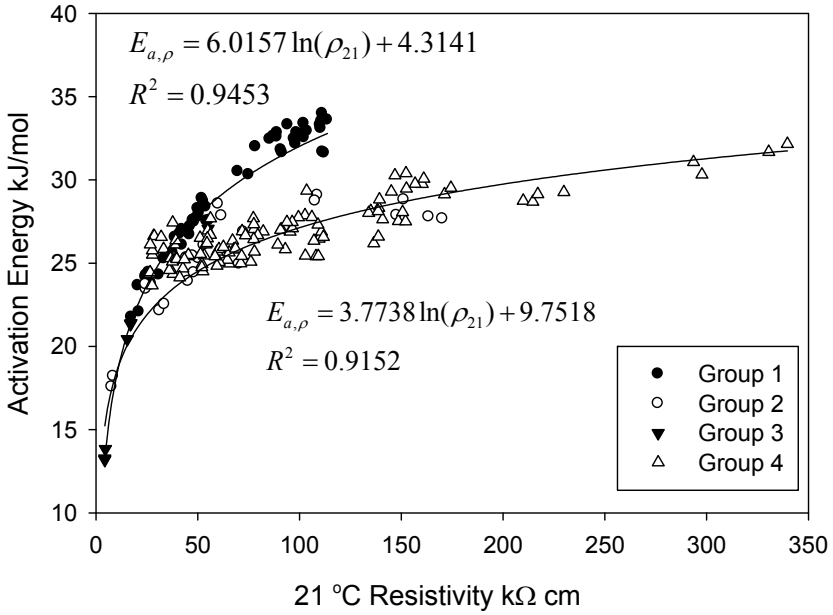

Figure 3.5: Correlation between 21 °C resistivity and activation energy on saturated specimens

The application of the proposed Equation 3-2 and 3-3 depends on concrete alkalinity, type of pozzolanic admixture and its replacement ratio. A simplified grouping method is suggested in Table 3.12. In general, Equation 3-2 is applicable for concrete with ≤ 20% FA or ≤50% slag, and Equation 2-3 is applicable for concrete with >20% FA or >70% (Slag+FA).

Table 3.12: Grouping of specimens by mix property for application of general equations

Equation	Concrete property
Equation 3-2	OPC concrete; high alkalinity concrete; concrete with <20% FA; concrete with ≤ 50% Slag.
Equation 3-3	concrete with ≥20% FA; concrete with >50%Slag.

Unsaturated Specimens

Figure 3.6 shows comparison of 21 °C resistivity vs. activation energy on saturated and unsaturated specimens. Results for saturated specimens are those that follow Equation 3-2 and the results for unsaturated specimens under 92%RH and 85% RH (Table 3.5and Table 3.6). The data shows that, values of resistivity and activation energy are higher at unsaturated conditions than at saturated conditions. Moreover, at unsaturated conditions and under a constant RH condition, the correlation between 21°C resistivity and activation energy still follows the curve developed from saturated specimens (Equation 3-2).

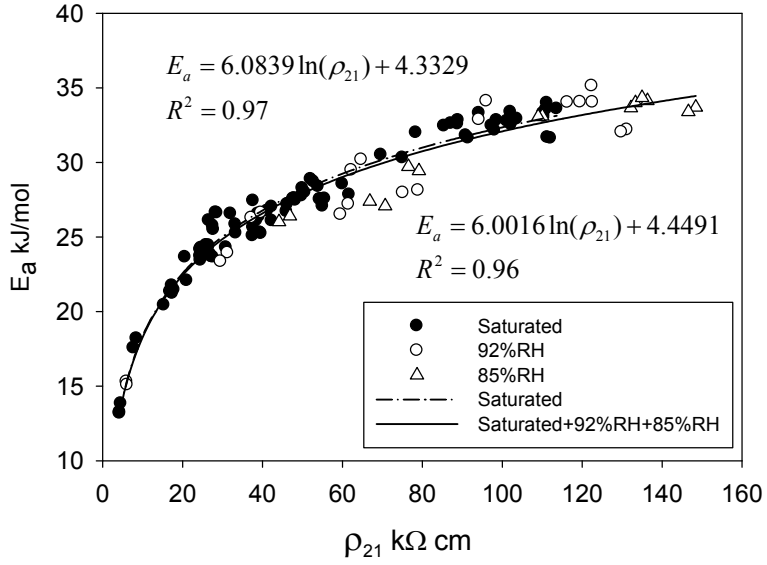

Figure 3.6: Comparison of 21°C resistivity vs. activation energy between saturated and unsaturated specimens (92% RH and 85% RH)

3.3.3.2 Development of General Resistivity Normalization Equations

With the correlation between ρ_{21} and $E_{a,\rho}$ described in Equation 3-2 and 3-3, it is possible to generate general equations to normalize concrete resistivity corresponding to temperature. In Equation 2-33, by taking $T_0 = 21$°C, it becomes:

$$\rho_T = \rho_{21} \cdot \exp\left[\frac{E_{a,\rho}}{R}\left(\frac{1}{T+273.15} - \frac{1}{294.15}\right)\right] \tag{3-4}$$

Where T in °C, $E_{a,\rho}$ in J/mol, ρ_T and ρ_{21} in Ω m, and R=8.314 J/mol/°C. To make the units the same as in Equation 3-4, Equation 3-2 and 3-3 can be rewritten as:

$$E_{a,\rho} = \left[6.0157\ln(\rho_{21}/10) + 4.3141\right] \times 1000 \tag{3-5}$$

$$E_{a,\rho} = \left[3.7738\ln(\rho_{21}/10) + 9.7518\right] \times 1000 \tag{3-6}$$

Where $E_{a,\rho}$ in J/mol and ρ_{21} in Ω m.

Development of General Resistivity Normalization Equation with Equation 3-5:

By substituting Equation 3-5 into Equation 3-4, it leads to:

$$\rho_T = \rho_{21} \cdot \exp\left[1000 \cdot \frac{6.0157\ln(\rho_{21}/10) + 4.3141}{8.314} \times \left(\frac{1}{T+273.15} - \frac{1}{294.15}\right)\right] \tag{3-7}$$

In equation 3-7, taking ρ_T and T as constant, ρ_{21} as variable, it is solved by MATLAB as the following expression:

$$\rho_{21} = 10 \cdot \exp\left[\frac{0.4 \cdot \log(10/\rho_T) \cdot T + 109.26 \cdot \log(10/\rho_T) + 148.18 - 0.705621 \cdot T}{0.583937 \cdot T - 129.923}\right] \tag{3-8}$$

With Equation 3-8, the 21°C resistivity ρ_{21} could be calculated by the resistivity ρ_T measured at temperature *T*. By substituting the calculated ρ_{21} into equation 3-7, the resistivity values at other temperatures could be calculated. The procedure includes the following steps:

1) Resistivity ρ_T measured at T.
2) Putting ρ_T and T into Equation 3-6 to calculate ρ_{21}.
3) Putting ρ_{21} into Equation 3-7.
4) Calculate resistivity at any temperature T with Equation 3-7.

Caution should be used that the temperature T in Equation 3-8 is the temperature at which resistivity is measured, whereas the temperature T in Equation 3-7 is the temperature at which the measured resistivity is normalized to. It is important to note that the units in Equation 3-7 and Equation 3-8 are in J/mol (E_a) and Ω m (ρ).

Development of General Resistivity Normalization Equation with Equation 3-6:

Similarly, a general equation for resistivity normalization could also be generated with Equation 3-6. By substitute Equation 3-6 into Equation 3-4, it becomes:

$$\rho_T = \rho_{21} \cdot \exp\left[1000 \times \frac{3.7738 \ln(\rho_{21}/10) + 9.7518}{8.314} \times \left(\frac{1}{T + 273.15} - \frac{1}{294.15}\right)\right] \quad (3\text{-}9)$$

In equation 3-9, taking ρ_T and T as constant, ρ_{21} as variable, it is solved by MATLAB as the following results:

$$\rho_{21} = 10 \cdot \exp\left[\frac{0.2 \cdot \log(10/\rho_T) \cdot T + 54.63 \cdot \log(10/\rho_T) + 16.7477 - 0.7975096 \cdot T}{0.1086242 \cdot T - 61.1111}\right] \quad (3\text{-}10)$$

Equation 3-9 and 3-10 are the general equation for resistivity normalization on concrete with >20% FA or ≥70% (Slag+FA). The calculation procedures are the same as previously stated.

3.3.3.3 Validation of General Resistivity Normalization Equations

To validate the general equations for resistivity normalization, measured resistivity values from dynamic temperature test were normalized to 21°C. Figure 3.7 shows results of measured resistivity and normalized resistivity using general equations developed from Equation 3-2 and Equation 3-3. It can be observed in Figure 3.7a that, because Mix 1A has OPC and 20%FA, both general equations are applicable. In Figure 3.7b, Mix 17A has higher alkalinity, so normalized values obtained by applying Equation 3-2 are better than by applying Equation 3-3. In Figure 3.7c and Figure 3.7d, results obtained by applying Equation 3.3 are better because the specimen compositions (34%FA in R10A and 50% FA in D25). Figure 3.8 shows the measured resistivity and normalized resistivity using Equation 3-2 on specimens 41A under saturated and unsaturated conditions. Results in Figure 3.8 indicate that the general equations can also be applied on unsaturated specimens at a fixed RH.

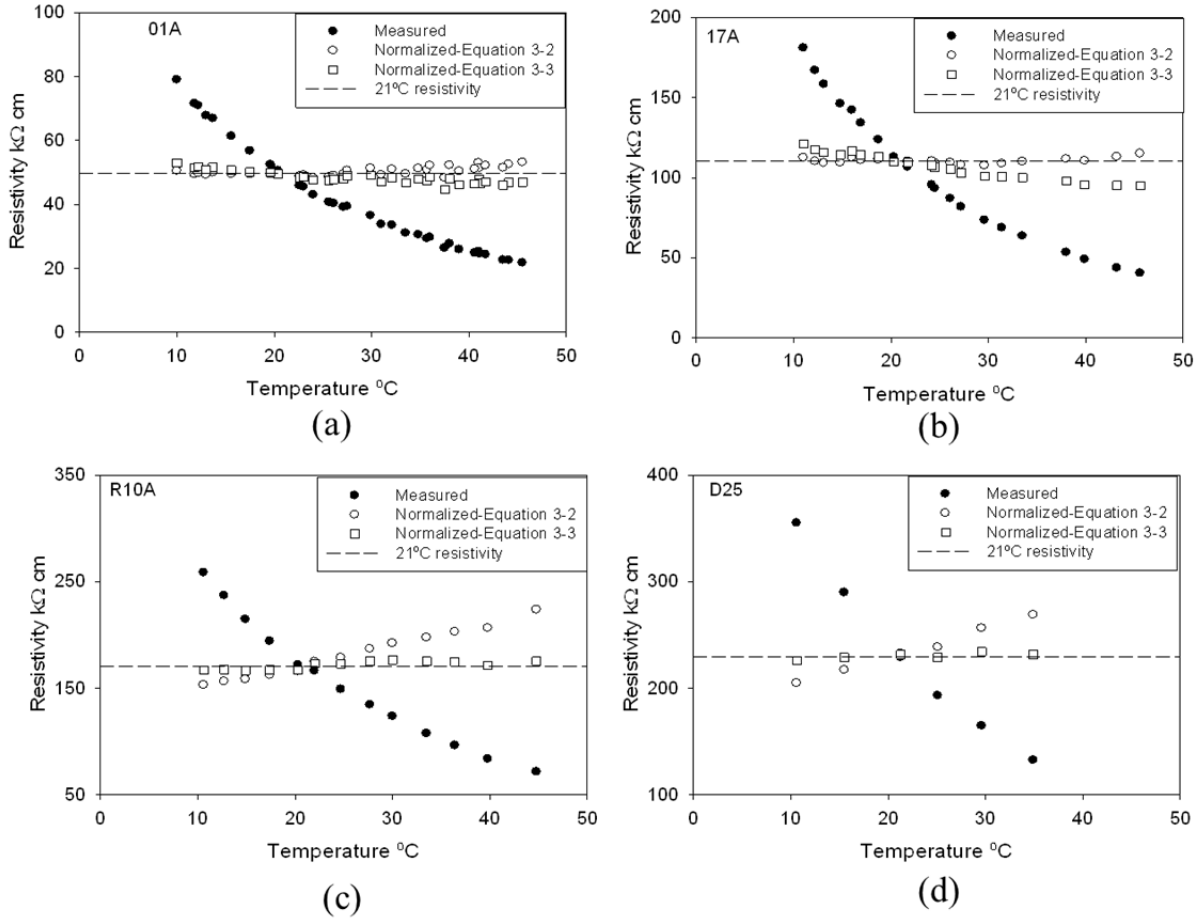

Figure 3.7: Evolution of resistivity with temperature and normalized resistivity (to 21°C) using Equation 3-2 and Equation 3-3 for selected saturated specimens

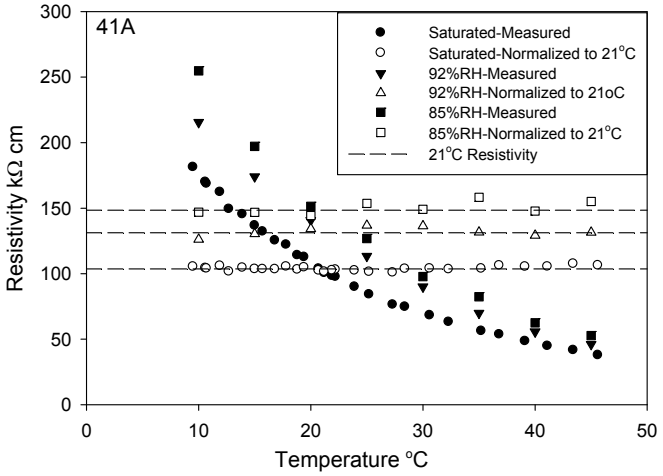

Figure 3.8: Evolution of resistivity with temperature and normalized resistivity (to 21°C) using Equation 3-2 on specimen under saturated and unsaturated conditions

3.3.3.4 Comparison with Methods in the Literature

Figure 3.9 and Figure 3.10 show the ratios of measured resistivity (ρ_T) at temperature T and 21°C resistivity (ρ_{21}) for concrete with various resistivity values using different general normalization equations. Plots from the two figures show that, for concrete with the same ρ_{21}, temperature effect is more significant in Figure 3.9 than in Figure 3.10. In Figure 3.9, for concrete with $\rho_{21} = 20$ kΩ cm, the resistivity at 10°C is $1.43\rho_{21}$, however, in Figure 3.10, it is $1.40\rho_{21}$. This difference increases for concrete with higher resistivity values. For concrete with $\rho_{21} = 200$ kΩ cm, the resistivity at 10°C is $1.78\rho_{21}$ in Figure 3.9 and $1.60\rho_{21}$ in Figure 3.10 respectively.

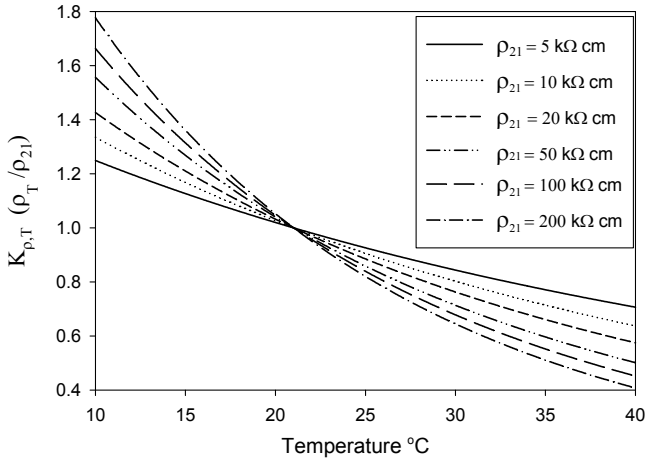

Figure 3.9: Temperature factor for resistivity on concrete with different resistivity values calculated from Equation 3-2

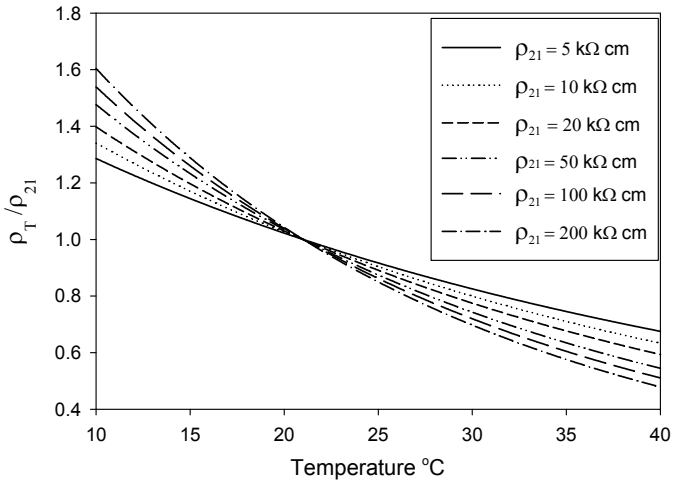

Figure 3.10: Temperature factor for resistivity on concrete with different resistivity values calculated from Equation 3-3

Table 3.13 shows the percentage change per °C of concrete with difference resistivity at different temperatures using Equation 3-2 and 3-3. It is found that when ρ_{21} is as low as 10 kΩ cm, Equation 3-2 and 3-3 gives the same percentage change in resistivity per °C. When ρ_{21} increases, the percentage change of resistivity per °C provided by Equation 3-2 is higher than 3-3. It also shows that the percentage change of resistivity per °C will increase more significantly with higher concrete resistivity. For example, when using Equation 3-2, the percentage change per °C for concrete with ρ_{21}=10 kΩ cm at 21°C is 2.6%, but for ρ_{21}=100 kΩ, the value is 4.5%.. The percentage change of resistivity per °C is more significant at lower temperatures than at higher temperatures. For example, when using Equation 3-2, the percentage change per °C for concrete with ρ_{21}=40 kΩ cm at 10°C is 4.3%, but the percentage change at 40°C is 3.5%.

Table 3.13: Percentage change of resistivity per °C of concrete with different resistivity at different temperatures

ρ_{21} kΩ cm	$(\rho_{T-1}-\rho_T)/\rho_T \times 100\%$					
	10°C		21°C		40°C	
	Eq 3-2	Eq 3-3	Eq 3-2	Eq 3-3	Eq 3-2	Eq 3-3
10	2.8	2.8	2.6	2.6	2.3	2.3
50	4.3	3.7	3.9	3.5	3.5	3
100	4.9	4.1	4.5	3.8	4	3.4
200	5.6	4.6	5.1	4.2	4.6	3.7

The percentage change of resistivity per °C in Table 3.7 ranges from 2.3% to 5.6%, which is in agreement with the reported values(3%-5%)[38, 45]. However, as the change of resistivity with temperature is dependent on concrete's intrinsic resistivity, normalizing concrete resistivity based on the measured concrete resistivity and temperature is suggested. The linear relationship in Equation 2-29 provides 2.2% to 3.5% change in resistivity per °C[48, 69, 70]. Equation 2-29 would be applicable for concrete with resistivity less than 50 kΩ cm and for a small temperature range.

Figuer 3.11 shows temperature factors generated by Equation 3-2 (a), Equation 3-3 (b) and DuraCrete corresponding to resistivity at 20°C. It indicates that under 20°C, the temperature factor from DuraCrete is similar to the factor from concrete with ρ_{21} =15 kΩ cm generated from Equation 3-2 and 3-3. For temperatures higher than 20°C, the temperature factor from DuraCrete is similar to the factor for concrete with ρ_{21} higher than 200 kΩ cm. The above comparison shows that DuraCrete's equation is only applicable for concrete with ρ_{21} =15 kΩ cm when temperature is under 20°C and for concrete with ρ_{21} higher than 200 kΩ cm for temperature higher than 20°C.

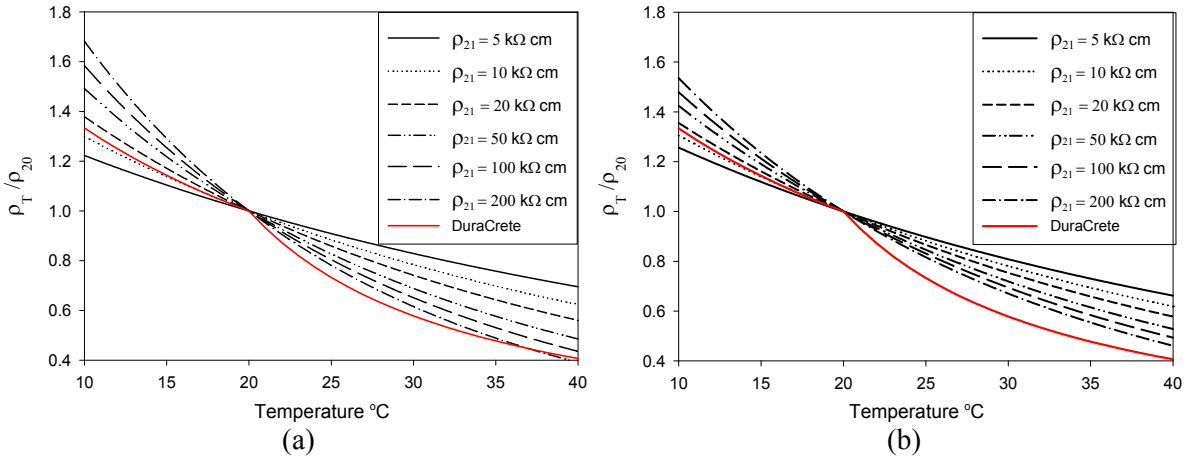

Figure 3.11: Comparison of temperature factors generated by (a) Equation 3-2, (b) Equation 3-3 and DuraCrete

Figure 3.12 shows comparison of ρ_{21} vs. $E_{a,\rho}$ from this investigation for concrete with ≤ 20%FA under saturated and unsaturated conditions (85% and 92%RH) with results from Villagran Zaccardi. for mortar with OPC and silica sand under saturated, 75% and 55% RH conditions (determined using embedded probes) [48]. In Villagran Zaccardi's results, resistivity of the mortar under saturated conditions was around 12 kΩ cm and the activation energy is 15 kJ/mol, however, under a 55% RH

condition, the resistivity is as high as 473 kΩ cm and the activation energy is 43.8 k kΩ cm. By combining the results from concrete with ≤20% FA with Villagran Zaccardi's results, a new equation describing correlation between ρ_{21} and $E_{a,\rho}$ is obtained:

$$E_{a,\rho} = 6.2182\ln(\rho_{21}) + 3.4816 \tag{3-11}$$

Equation 3-11 is quite similar to Equation 3-2, which proves that the general equations (Equation 3-7 and equation 3-8) generated from Equation 3-2 are also applicable on experimental results from Villagran Zaccardi.

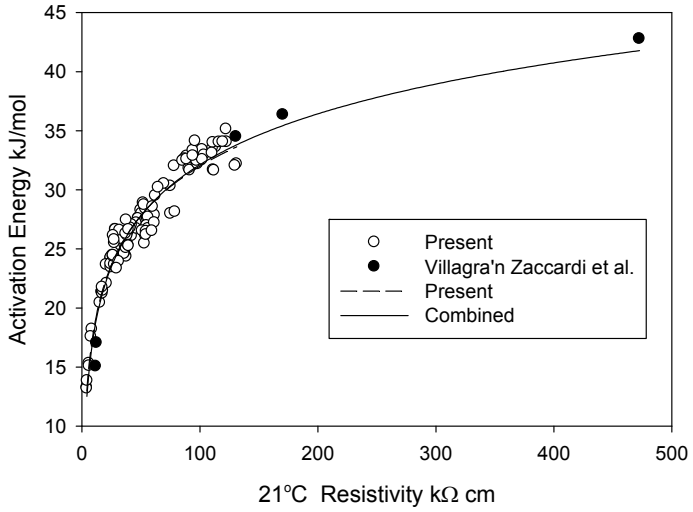

Figure 3.12: Comparison of correlation between and with results from Villagran Zaccardi

Instead of using fixed parameters to normalize the temperature effect on concrete resistivity, general equations proposed in this investigation showed advantages in resistivity normalization. It is reported in the literature that activation energy is different on concrete with different intrinsic resistivity values and the value of activation energy is dependent on degree of saturation, degree of hydration and mix properties. As a result, using fixed parameters (e.g. a fixed value of activation energy) would cause an over-estimate or under-estimate of the temperature effect (as shown in Figure 3.9), which would lead to misleading results in predicting the service life of reinforced concrete structures.

Results from this investigation found that the value of resistivity is dependent on the intrinsic value of concrete resistivity. The resistivity-dependent general equations proposed in this paper based on

the correlation between 21°C resistivity and activation energy show significant advantages for normalization of temperature on resistivity. As the intrinsic resistivity of concrete is a combined result of concrete mix properties, degree of hydration and degree of saturation, the resistivity-dependent general equations could be applied for resistivity normalization regardless of concrete's degree of hydration and saturation. Once the cement type (alkalinity) and replacement ratio of pozzolanic admixtures are known, the temperature effect on concrete resistivity could be normalized using the appropriate equations regardless of w/cm, type/amount of aggregates, etc.

It is necessary to note that, the proposed equations are only applicable on saturated specimens or specimens under a fixed RH condition. For the in-situ conditions, RH of the air usually changes with temperature and therefore the concrete's degree of saturation changes. In this case, the general equations would not be applicable as the saturation factor needs to be considered.

3.4 Conclusions

The effect of temperature on electrical resistivity of concrete was investigated in this paper. It was found that the temperature effect is different on concrete with different intrinsic resistivity values, and temperature shows more significant effect on concrete with higher intrinsic values than on those with lower values. The value of activation energy in this investigation ranged from 14 kJ/mol to 34 kJ/mol, and it was found to increase with increasing intrinsic resistivity of concrete. Based on the developed correlation between 21°C resistivity and activation energy, general equations were proposed for normalizing temperature effect on resistivity. Once the cement type (alkalinity) and replacement ratio of pozzolanic admixtures are known, the resistivity-dependent general equations could provide a more simple and precise method for resistivity normalization regardless of concrete's degree of hydration, degree of saturation and other mix properties.

4. ACCELERATED CURING ON CONCRETE WITH HIGH VOLUME POZZOLANS BY ELEVATED TEMPERATURE

4.1 Introduction

Pozzolanic admixtures have been widely used to increase the durability properties of reinforced concrete. The principal components of pozzolans, such as SiO_2, Al_2O_3, and Fe_2O_3, react with Ca $(OH)_2$ (CH) formed during the early cement hydration in the capillary pores, and also form additional CSH. The additional CSH can further decrease the porosity and tortuosity of concrete.

Performance-based test methods, such as the rapid chloride permeability test, are usually carried-out at 28 days of moist curing the concrete sample. However, 28 days is usually not long enough for concrete with pozzolanic admixtures to develop the low permeability properties (that these concretes are known to reach), especially when large cement replacement ratios are used (>20% by mass). To obtain passing RCP test values at 28 days, the Virginia Department of Transportation (VDOT) developed an accelerated curing regime which involves 7 days wet cure at 23ºC (73ºF) followed by 21 days in wet cure at 38ºC(100ºF). VDOT's results show that with this accelerated curing regime, long term permeability (6 months and beyond) was obtained at 28 days. It has been found for OPC concrete, elevated temperature curing leads to lower long term compressive strength and decreased durability properties. It is not clear from the reviewed literature if both trends would remain the same for concretes with pozzolanic admixtures. Hence it is necessary to study the effect of elevated temperature curing regarding both compressive strength and durability properties on concrete with various pozzolanic admixtures and replacement ratios.

The objectives of this part of the investigation include:

- Develop curing regimes by using 35°C lime water bath to accelerate the hydration of concrete with SCMs admixtures.
- Determine how many days would be needed at room temperature curing to achieve the 28 days accelerated curing resistivity measurement value
- Establish the electrical resistivity evolution with time for specimens cured under different curing regimes.
- Establish correlations between electrical resistivity and non-steady-state migration diffusion coefficients.

4.2 Experimental Procedure

4.2.1 Materials

Two types of SCMs admixtures were used in this investigation: Class F fly ash (FA) and GGBS. Most of the concrete mixes prepared were binary blends, i.e. FA +OPC or GGBS +OPC. Replacement ratio of FA is 20%, 30%, 40% and 50% by mass. For GGBS, the replacement ratio is 50% and 70% by mass. From this point forwards GGBS will be called Slag. Additionally, two ternary blends were prepared and the ternary blends consisted of 10%FA+60%Slag and 20%FA+50%Slag. Type I/II cement was used for all the mixes and the w/cm was 0.41. Chemical composition of cement and FA are listed in Table 4.1. The Slag used in this investigation was ASTM C-989 Grade 120 Slag. The coarse aggregate for most mixes was Florida limestone. Granite was used on four concrete mixes to investigate its effect on the properties of concrete. The fine aggregate was Florida river sand. Details of the mix designs are listed in Table 4.2.

Table 4.1: Chemical composition of cement and fly ash

	SiO_2	$A1_2O_3$	Fe_2O_3	CaO	MgO	SO_3	Na_2O	K_2O	Na_2Oe
Cement	19.60	5.30	3.70	64.00	0.90	3.10	0.14	0.40	0.40
Fly Ash	54.07	27.75	6.67	2.11	0.96	0.19	0.07	2.28	1.57

Table 4.2: Mix design of specimens

Mix. NO.	Coarse agg.	Cement kg/m^3	FA kg/m^3	Slag kg/m^3	Fine agg. kg/m^3	Coarse agg. kg/m^3	FA %	Slag %	Air %	W/CM
Ai	Limestone	312	78	-						
Bi	Limestone	234	156	-						
A	Limestone	312	78	-	777	930	20	-	5.8	0.41
J	Limestone	273	117	-	739	951	30	-	5.8	0.41
B	Limestone	234	156	-	712	916	40	-	7.6	0.41
D	Limestone	195	195	-	720	927	50	-	4.8	0.41
E	Limestone	195	-	195	739	951	-	50	4.5	0.41
F	Limestone	117	-	273	736	947	-	70	3.6	0.41
I	Limestone	117	39	234	732	943	10	60	4.6	0.41
H	Limestone	117	78	195	732	942	20	50	5.2	0.41
C	Granite	312	78	-	736	1061	20	-	9.0	0.41
K	Granite	273	117	-	720	1038	30	-	7.5	0.41
L	Granite	195	195	-	709	1023	50	-	4.6	0.41
G	Granite	195	-	195	739	1067	-	50	4.2	0.41

Note: 1 kg/m^3=1.69 lb/yd^3; - = not measured items.

Additionally Ai and Bi mixes were prepared that contained a higher entrained air % than target

4.2.2 Experimental Methods

The geometry selected for the specimens were ϕ10 cm x 20 cm (4x8 in) cylinders. All concrete specimens were prepared at the State Material Office (SMO) of the Florida Department of Transportation (FDOT) in Gainesville, Florida. Fifty-one cylinders were cast per concrete mix. One day after the specimens were cast, cylinders #1 to #21 were demolded and kept in lime water at room temperature (21°C) for curing in FDOT. One day after the specimens were cast, cylinders #22 to #51 were transported to the Marine Materials Lab in the SeaTech campus of Florida Atlantic University (FAU) in Dania Beach, Florida. Two days after the specimens were cast, cylinders #22 to #51 were demolded and immersed in saturated lime water, and then cylinders #22 to #34 were kept in an elevated temperature room with air temperature around 38°C (100 °F). Cylinders #35 to #47 were moved into room temperature curing and then transferred to the hot room after they reach 7 days age. Similarly, cylinders #48 to #51 were kept at room temperature and then transferred to the elevated temperature room after they reached the 14 days age. All the specimens cured in elevated room were in saturated lime water with water temperature around 35±2°C. Figure 4.1 shows specimens under RT limewater curing regimes in FDOT and ET limewater curing regimes in FAU-SeaTech.

Resistivity measurements were performed at 2, 7, 14, 21, and 28 days and every four weeks thereafter on cylinders #22 to #51. Cylinders #22, #35, #48 were prepared with an embedded type T thermocouple to monitor the inside temperature. Resistivity of cylinder #1 to #6 was measured every two weeks during the first month and every two months thereafter.

(a) (b)

Figure 4.1: Specimens under (a) RT limewater curing at FDOT and (b) ET limewater curing at FAU

For cylinders cured in lime water at room temperature and elevated temperature, resistivity was measured immediately after the specimen was removed from water and surface-dried with a towel. Water temperature was recorded simultaneously. All the resistivity measurements were performed according to FM 5-578 with 1.5in (3.8cm) electrode spacing[14]. The cell constant of $K_{\rho,g} = 1.89$ was employed to normalize the geometry effect. When resistivity was measured on the specimens cured at elevated temperatures, cylinders were taken from the lime water (around 35°C) and surface-dried immediately with a towel, and measurements were performed subsequently as soon as possible to minimize surface temperature and moisture changes. Simultaneously, water temperature was measured and recorded with a thermocouple. For specimens cured at room temperature, a similar procedure for resistivity measurement was performed. As the resistivity was measured at different temperatures (even water temperature in the lab fluctuates with time), all measured resistivity values were normalized to the resistivity at 21°C using the general equations developed in Chapter 3. As previously stated, the general normalization equation that needs to be applied is dependent on the mix design.

At the age of 28 days, cylinders #16 to #18 were subjected to compressive test and cylinders #13 to #15 were taken out from the curing tank and prepared for the bulk diffusion test. When average resistivity of cylinders #4 to #6 (which were cured at RT) reached the average 28-day resistivity of cylinders #22 to #25 (which were cued 2RT/26ET), cylinders #4 to #6 were cut and subjected to the bulk diffusion test for a one-year exposure period and cylinders #16 to #18 were tested for compressive strength.

At about one-year age (Table 4.3), cylinders #7 to #9 were subjected to bulk diffusion test with a one-year exposure period. Also upon reaching one year of age, cylinders #10, #11, #24 to #27 and #37 to #40 were subjected to the RCM test according to NT Build 492. Details of the RCM test are introduced in Chapter 5, and the details of the curing regimes, test methods and the corresponding test date are described in Table 4.3.

All the bulk diffusion tests were performed according to NT Build 443 with a one-year exposure period at FDOT. The slicing procedure of concrete cylinders is shown in Figure 4.2. Rather than using a single exposure solution, two solutions with different NaCl content were used. Of the two slices from each specimen, all the top slices were exposed to 165g/L NaCl solution (2.83mol NaCl/L) and all the bottoms slices were exposed to 30g/L NaCl solution (0.51mol NaCl/L). Figure 4.3 shows the exposure tank and specimens exposed in NaCl solution.

Table 4.3: Curing regimes and test methods for specimens

	Cylinder #	Curing Regime	Test method and age	
FDOT	1-3	RT	Resistivity	Resistivity
	4-6	RT	Resistivity	BD test when SR@RT=SR@28ET
	7-9	RT	Resistivity	BD test @ 1 year
	10-11	RT	Resistivity	RCMT @ 1 year
	12	RT	Resistivity	Extra Specimen
	13-15	RT	-	BD @ 28 days
	16-18	RT	-	Compression test @ 28 days
	19-21	RT	-	Compression test when SR@RT=SR@28ET
FAU-SeaTech	22-23	2RT/ET	Resistivity	Resistivity
	24-25	2RT/ET	Resistivity	RCMT @ 1 year
	26-27	2RT/26ET/RT	Resistivity	RCMT @ 1 year
	28	2RT/26ET/RT	Resistivity	Resistivity
	29-31	2RT/26ET	Resistivity	Compression test @ 28 days
	32-34	2RT/26ET	Resistivity	BD @ 28 days* actually ~170 days of age
	35-36	7RT/ET	Resistivity	Resistivity, 35 Compression, 36 BD> 600 days
	37-38	7RT/ET	Resistivity	RCMT @ 1 year
	39-40	7RT/21ET/RT	Resistivity	RCMT @ 1 year
	41	7RT/21ET/RT	Resistivity	Resistivity
	42-44	7RT/21ET	Resistivity	Compression test @ 28 days
	45-47	7RT/21ET	Resistivity	BD test @ 28 days actually ~170 days
	48,49	14RT/ET	Resistivity	Resistivity, Compression @ > 600 days
	50	14RT/14ET	Resistivity	Compression test @ 28 days
	51	14RT/14ET	Resistivity	BD test @ 28 days actually ~170 days

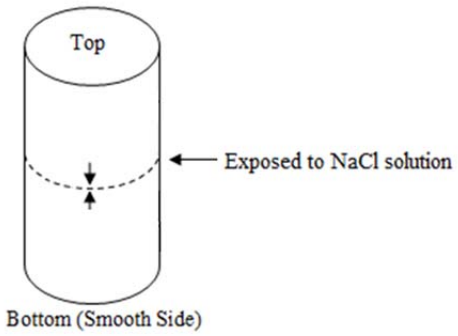

Figure 4.2: Illustration of slicing specimens for bulk diffusion test

Figure 4.3: Exposure tank for bulk diffusion test at FDOT

4.3 Results and Discussion

4.3.1 Normalization of Measured Resistivity

As the specimens in this investigation were cured under various curing regimes and hence resistivity was measured at the corresponding temperatures, all the measured resistivity was normalized to 21°C using general equations for resistivity normalization generated from Equation 3-2 and Equation 3-3. **Error! Reference source not found.** lists the mix designs and the corresponding general equations applied for resistivity normalization. Figure 4.4 shows typical results that compare the measured and normalized resistivity on specimens from Group A which were cured under room temperature and elevated temperatures. All subsequent figures with resistivity values show the normalized values to 21°C.

Table 4.4: Mix designs and the corresponding general equation for resistivity normalization

Mix No.	General equation for resistivity normalization
G, E	Equation 3-2
Ai, Bi, A, B,J, D,F,H, I,C,K, L	Equation 3-3

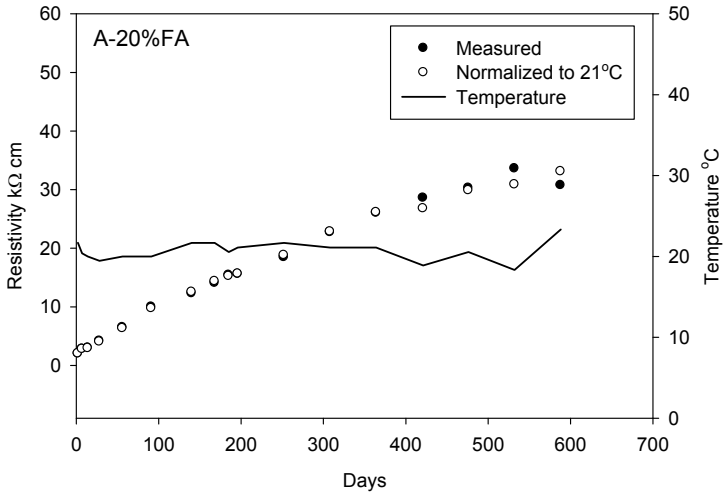

(a)

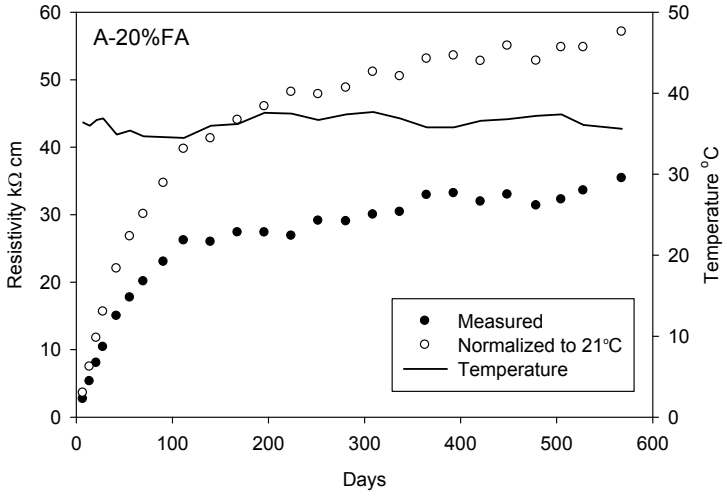

(b)

Figure 4.4: Measured and normalized resistivity for concrete cured under (a) room temperature and (b) elevated temperature

Figure 4.5 shows the results of resistivity development on specimens with FA/Limestone under various curing regimes up-to 1000 days. Plots for the resistivity evolution for the other mixes are included in the Appendix A. For all the mixes, the normalized resistivity values of specimens subjected to ET curing regimes are higher than the resistivity values of those cured under room temperatures at both short term (28 days) and long-term(up to 2.5 years) .

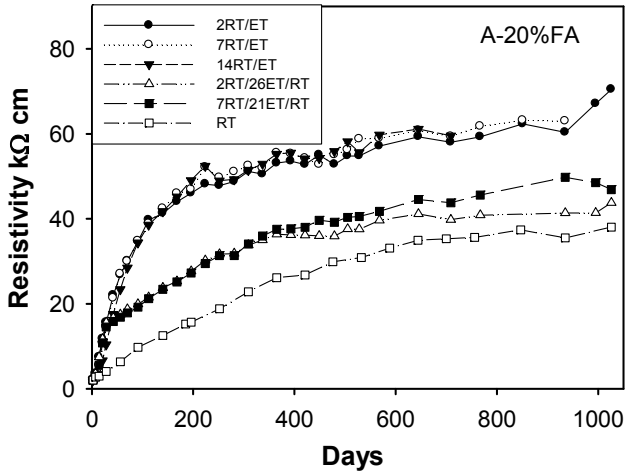

Figure 4.5: Resistivity development of specimens with 20%FA/limestone

4.3.2 Compressive Strength

Compressive strength test was performed at 28-day on specimens cured at 28RT, 2RT/26ET, 7RT/21ET and 14RT/14ET curing regimes. Additionally, compressive strength tests were performed on specimens cured under room temperature once the resistivity reached the 28-day resistivity of concrete under 2RT/26ET ($\rho_{RT} = \rho_{2RT/26ET}$). Figure 4.6 illustrates the resistivity evolution on specimens with 20% FA and limestone (Mix A), in which compressive strength test was performed at 28 days on specimens cured under 2RT/26ET and at 185 days on specimens cured under RT once $\rho_{RT} = \rho_{2RT/26ET}$.

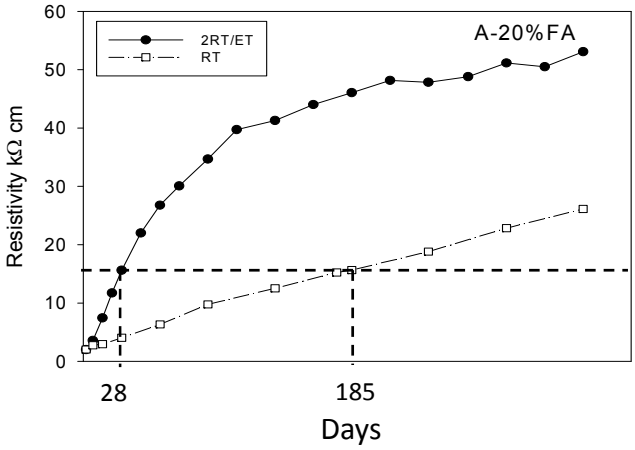

Figure 4.6: Illustration of compressive strength test performed on specimens cured under RT when RT resistivity value reached the 2RT/26ET resistivity value

The values of $\rho_{2RT/26ET}$ for all the mixes are listed in Table 4.5, which are the target resistivity values of the specimens cured under RT. Table 4.5 also lists the actual measured resistivity values ($\rho_{RT} = \rho_{2RT/26ET}$) and the experimentally determined equivalent age ($t_{\text{equivalent}}$) of specimens cured at RT.

Table 4.5: Lists of ρ_{RT} and $t_{\text{equivalent}}$ of RT cured specimens when ρ_{RT} reached $\rho_{2RT/26ET}$.

Mix No.	Resistivity kΩ cm		Days
	Target (2RT/26ET)	RT	$t_{equivalent}$
Ai*	13.4	14.5	168
Bi*	27.3	27.0	320
A	15.6	15.2	185
J	20.7	21.3	196
B	26.6	26.5	329
D	28.0	30.3	308
E	19.5	19.7	370
F	30.0	28.8	420
I	36.3	35.6	420
H	45.5	48.6	420
C	26.7	26.4	252
K	35.3	35.5	277
L	49.3	45.3	420
G**	22.7	17.3	551

*: Trial mixes with higher air content

**: Compressive strength was performed at 551 days

Results of compressive strength performed on specimens at different ages and under different regimes are listed in Table 4.6 The table include test performed on cylinder that were cured for an extended period of time at ET (last two columns indicate age and strength respectively).

Table 4.6: Values of compressive strength on specimens under various curing regimes

	Compressive Strength MPa					Age	MPa
Mix No.	28RT	2RT/26ET	7RT/21ET	14RT/14ET	RT**	14RT/ET	14RT/ET
Ai*	33.9	44.9	42.7	36.0	42.1		
Bi*	24.1	35.7	37.6	33.0	41.9		
A	51.9	66.4	64.8	65.0	65.3	740	68.8
J	48.1	67.7	68.0	66.2	68.7	667	77.6
B	34.0	55.7	52.7	51.0	58.6	740	57.0
D	31.8	59.0	55.7	52.0	63.0	711	63.9
E	64.6	79.7	81.6	78.0	82.1	661	84.7
F	67.3	77.2	79.7	76.4	81.5	711	82.4
I	60.5	71.3	73.2	76.4	76.2	698	82.3
H	56.5	73.1	73.1	72.5	74.1	698	79.3
C	46.7	73.4	76.9	78.2	69.7	667	78.0
K	40.8	62.5	60.3	60.1	67.8	661	70.6
L	23.5	51.2	49.4	47.9	55.9	632	71.3
G***	58.0	63.1	65.6	58.2	89.8	632	63.1

*:Trial mixes with higher air content

**: Compressive strength at RT when ρ_{RT} reached $\rho_{2RT/26ET}$.

***: ρ_{RT} did not reach $\rho_{2RT/26ET}$ when compressive strength was performed

4.3.3 Rapid Chloride Migration Coefficients

Two cylinders from each curing regime (RT, 2RT/ET, 2RT/26ET/RT, 7RT/ET and 7RT/21ET/RT) were selected upon reaching one year of age for RCM tests. Results of RCM test and the corresponding 21°C resistivity values measured before performing RMT tests are listed in Table 4.7, in which the D_{nssm} of each specimen was the average of the two center slices.

Table 4.7: Chloride migration coefficients and resistivity at 1-year of age

Specimen No.	ρ_{21} kΩ cm	D_{nssm} $10^{-12}m^2/s$	Specimen No.	ρ_{21} kΩ cm	D_{nssm} $10^{-12}m^2/s$	Specimen No.	ρ_{21} kΩ cm	D_{nssm} $10^{-12}m^2/s$
Ai10	28.7	4.21	D10	55.7	2.10	C10	41.2	1.64
Ai11	30.0	3.88	D11	50.6	1.76	C11	43.3	1.37
Ai24	54.8	2.20	D24	196.7	0.64	C24	104.5	0.94
Ai25	55.8	2.68	D25	214.6	0.56	C25	102.0	0.96
Ai26	36.9	2.98	D26	112.4	1.08	C26	77.6	1.39
Ai27	37.5	3.38	D28	99.8	0.99	C27	76.2	1.35
Ai37	52.1	2.50	D37	199.8	0.66	C37	97.6	0.88
Ai38	54.7	2.20	D38	198.1	0.49	C38	93.9	0.93
Ai39	39.5	3.76	D39	109.7	1.03	C39	71.3	1.62
Ai40	38.7	3.09	D40	101.4	0.85	C40	72.4	1.15
Bi10	41.7	2.46	E10	21.4	3.64	K10	58.6	0.98
Bi11	41.9	1.88	E11	21.2	3.72	K11	53.7	1.04
Bi24	153.8	0.94	E24	39.9	3.11	K24	171.6	0.47
Bi25	141.8	0.92	E25	38.9	2.26	K25	178.8	0.47
Bi26	81.9	2.02	E26	26.5	3.28	K26	114.1	0.70
Bi27	76.3	1.82	E27	27.3	2.77	K27	117.2	0.57
Bi37	104.9	0.99	E37	40.4	1.96	K37	160.1	0.48
Bi38	113.8	0.98	E38	39.5	2.17	K38	162.6	0.52
Bi39	74.9	1.54	E39	27.0	3.01	K39	103.7	0.71
Bi40	74.4	1.59	E40	26.9	3.32	K40	101.2	0.59
A10	28.5	3.21	F10	30.0	2.93	L10	51.6	1.36
A11	29.7	3.83	F11	29.2	2.43	L11	53.8	1.45
A24	49.9	2.15	F24	63.8	1.33	L24	316.0	0.24
A25	50.9	2.17	F25	61.8	1.38	L25	344.2	0.23
A26	36.8	2.76	F26	40.1	2.64	L26	165.5	0.46
A27	36.6	2.79	F28	40.5	2.51	L27	165.8	0.43
A37	51.9	2.26	F37	61.7	1.20	L37	291.7	0.25
A38	52.4	1.87	F38	65.0	1.22	L38	326.1	0.19
A39	36.5	2.60	F39	40.6	1.87	L39	153.5	0.51
A40	37.0	3.03	F40	39.1	2.00	L40	153.7	0.53
J10	35.8	2.36	I10	36.3	2.03	G10	16.5	3.45
J11	35.2	2.41	I11	37.7	2.32	G11	16.2	3.36
J24	90.6	0.85	I24	106.3	0.81	G24	38.4	1.90
J25	86.5	1.21	I25	105.6	0.92	G25	36.6	1.93
J26	48.9	1.26	I26	57.4	1.79	G26	28.1	2.32
J27	49.9	1.55	I27	59.6	1.73	G27	28.5	2.45
J37	89.8	0.83	I37	102.1	0.90	G37	33.0	2.34
J38	85.1	1.04	I38	105.6	0.96	G38	31.5	2.25
J39	51.0	1.56	I39	57.6	2.04	G39	25.9	2.47
J40	49.9	2.28	I40	56.1	1.86	G40	25.7	2.52
B10	35.6	2.52	H10	42.8	2.05			
B11	35.8	2.67	H11	44.9	2.24			
B24	131.5	0.83	H24	144.9	0.70			
B25	134.6	0.82	H25	136.8	0.79			
B26	68.7	1.22	H26	80.6	1.59			
B27	68.7	1.42	H27	79.5	1.72			
B37	130.0	0.74	H37	132.4	0.89			
B38	140.7	0.68	H38	138.1	0.81			
B39	63.8	1.62	H39	66.5	1.33			
B40	57.4	1.50	H40	68.1	1.78			

4.3.4 Bulk Diffusion Coefficients

After one-year exposure period was reached, the specimens were removed from the testing solution. Shortly after removing the samples the epoxy was cut-off, then the specimens were cut to slices with nominal thickness of 0.25in (0.64cm) in parallel to the exposure surface (Note: in some cases the waiting between removal and cutting/slicing was of several months). Seven (or eight) slices were cut for each specimen. The slices were then pulverized and the concrete powders were subjected to titration for total chloride content analysis. The chloride concentration analysis was performed by using FDOT method 5-516 (FM 5-516).[121] Chloride profiles were obtained by plotting chloride concentration vs. depth. Figure 4.7shows typical chloride profiles from specimens with FA and Slag cured at RT for 28 days before the bulk diffusion test started.

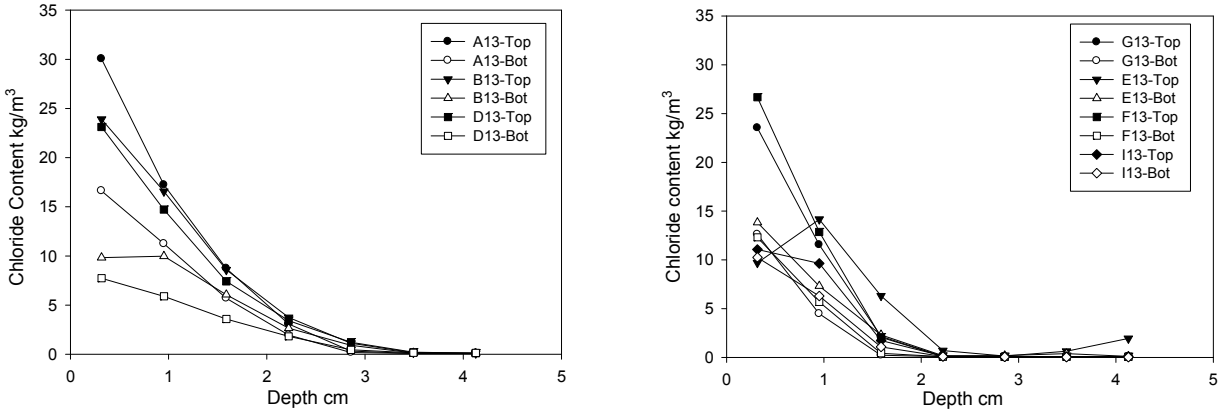

(a) (b)

Figure 4.7: Typical chloride profiles on specimens with FA/limestone (a) and specimens with Slag or Slag/FA (b)

The apparent diffusion coefficients (D_{app}) and the corresponding surface chloride content (C_s) were calculated by regression analysis to Fick's second law. The computed D_{app} values are listed in Table 4.8 for specimens immersed in 16.5% NaCl and in Table 4.9 for specimens immersed in 3% NaCl. In most instances the D_{app} values shown is the average of three D_{app} values for three specimens cured under the same conditions. Moreover, in a few cases the first layer was removed to obtain a better fit. This was done for cases in which the concentration at the first layer was less or about the same than the concentration observed at the second layer. Not all bulk diffusion test results were included due to time constraints or because the specimens were lost in transit (and hence no bulk diffusion tests were

performed). The different headers of each column describe the curing regime before starting the exposure in the sodium chloride solution. NC=AC correspond to specimens immerse in solution once $\rho_{RT} = \rho_{2RT/26ET}$. AC2/26, AC7/21 and AC14/14 correspond to specimens that were cured for 26, 21 and 14 days respectively in the elevated temperature room. These were sent to SMO for exposure and due to transport time, it was decided for these to be immersed for some additional time before exposure began, usually until reaching 170 days of age. 1yrRT corresponds to specimens cured at RT in calcium hydroxide solution for one year before starting the bulk diffusion test.

Table 4.8: Apparent diffusion coefficients on specimens cured as indicated in 16.5% NaCl and exposed for 1 year

		NC=AC	NC	AC2/26	AC7/21	AC14/14	1yrRT
Ai	20%FA-L	1.48E-12	3.16E-12	2.90E-12			1.16E-12
Bi	40%FA-L	7.43E-13	3.05E-12	1.88E-12			8.63E-13
		NC=AC	**NC**	**AC2/26**	**AC7/21**	**AC14/14**	**1yrRT**
A	20%FA-L	1.52E-12	3.19E-12	1.26E-12	1.44E-12	1.48E-12	9.87E-13
J	30%FA-L	1.19E-12	3.13E-12	1.54E-12	2.12E-12	1.90E-12	7.25E-13
B	40%FA-L	1.27E-12	3.59E-12	1.36E-12	1.40E-12	1.20E-12	9.84E-13
D	50%FA-L	8.90E-13	3.14E-12	1.10E-12	1.01E-12	1.82E-12	6.37E-13
		NC=AC	**NC**	**AC2/26**	**AC7/21**	**AC14/14**	**1yrRT**
E	50%SLAG-L	1.08E-12	1.83E-12	1.12E-12	1.34E-12	1.71E-12	1.09E-12
F	70%SLAG-L	8.02E-13	1.47E-12	N/A	N/A	N/A	7.95E-13
I	10FA-60Slag-L	7.76E-13	1.65E-12	N/A	N/A	N/A	6.31E-13
H	20FA-50Slag-L	4.07E-13	1.47E-12	7.19E-13	7.59E-13	6.56E-13	5.13E-13
G	50%SLAG-G	8.43E-13	1.32E-12	8.86E-13	8.92E-13	1.08E-12	1.02E-12
		NC=AC	**NC**	**AC2/26**	**AC7/21**	**AC14/14**	**1yrRT**
C	20%FA-G	8.12E-13	2.18E-12	8.34E-13	8.48E-13	7.43E-13	7.38E-13
K	30%FA-G	7.08E-13	2.81E-12	1.07E-12	7.15E-13	9.05E-13	4.70E-13
L	50%FA-G	5.28E-13	2.11E-12	6.81E-13	7.99E-13	6.78E-13	8.58E-13

Note: Units are in m^2/s

Figure 4.8 and Figure 4.9 show the average calculated chloride surface concentration on the plots on the left column and on the plots on the right column show the measured chloride concentration on the first layer for each corresponding case (i.e. curing regime and mix). The measured values were lower (as the position is assumed to be at half the thickness of the first layer). The plots in Figure 4.8 shows the corresponding values for those exposed in high chloride concentration (nominal 16.5 percent NaCl), whereas Figure 4.9 shows the corresponding cases for those exposed in 3% NaCl solution. In general, the concentration of the first layer and calculated surface concentration for those immersed in 16.5 NaCl ranged between 15 and 30 kg/m^3 for those measured and between 25 and 40 Kg/m^3 for the calculated surface concentrations. For those immersed in 3% the first layer chloride concentration ranged between 5

and 15 kg/m^3 (a few exceptions reached close to 20) and the calculated surface concentration values ranged between 10 and 20 kg/m^3. The concentration measured on the first layer tended to decrease as the amount of fly ash increased for those specimens with limestone, but not as clear trend was observed for those with granite as coarse aggregate. In general NC Specimens had the higher concentrations when compared to specimens that were subjected to accelerated curing, however prolonged RT curing (NC=AC or 1yrRT) did not seem to significantly reduce the concentration measured on the first layer.

Table 4.9: Apparent diffusion coefficients on specimens cured as indicated in 3% NaCl and exposed for 1 year

		NC=AC	NC	AC2/26	1yrRT
Ai	20%FA-L	1.25E-12			1.76E-12
Bi	40%FA-L	1.47E-12			1.51E-12
		NC=AC	NC	AC2/26	1yrRT
A	20%FA-L	9.11E-13	3.37E-12	2.98E-12	1.30E-12
J	30%FA-L	1.39E-12	2.48E-12	1.59E-12	1.01E-12
B	40%FA-L	1.27E-12	5.86E-12	3.31E-12	1.16E-12
D	50%FA-L	8.90E-13	4.76E-12	2.47E-12	4.90E-13
		NC=AC	NC	AC2/26	1yrRT
E	50%SLAG-L	1.13E-12	1.91E-12	1.84E-12	1.19E-12
F	70%SLAG-L	6.33E-13	1.16E-12	1.51E-12	6.51E-13
I	10FA-60Slag-L	5.45E-13	1.52E-12	1.09E-12	5.06E-13
H	20FA-50Slag-L	3.18E-13	1.26E-12	7.20E-13	6.86E-13
G	50%SLAG-G	9.31E-13	9.00E-13	7.66E-13	1.69E-12
		NC=AC	NC	AC2/26	1yrRT
C	20%FA-G	8.12E-13	1.46E-12	1.23E-12	1.03E-12
K	30%FA-G	8.53E-13	2.45E-12	1.01E-12	7.21E-13
L	50%FA-G	5.39E-13	3.87E-12	1.21E-12	1.34E-12

Note: Units are in m^2/s

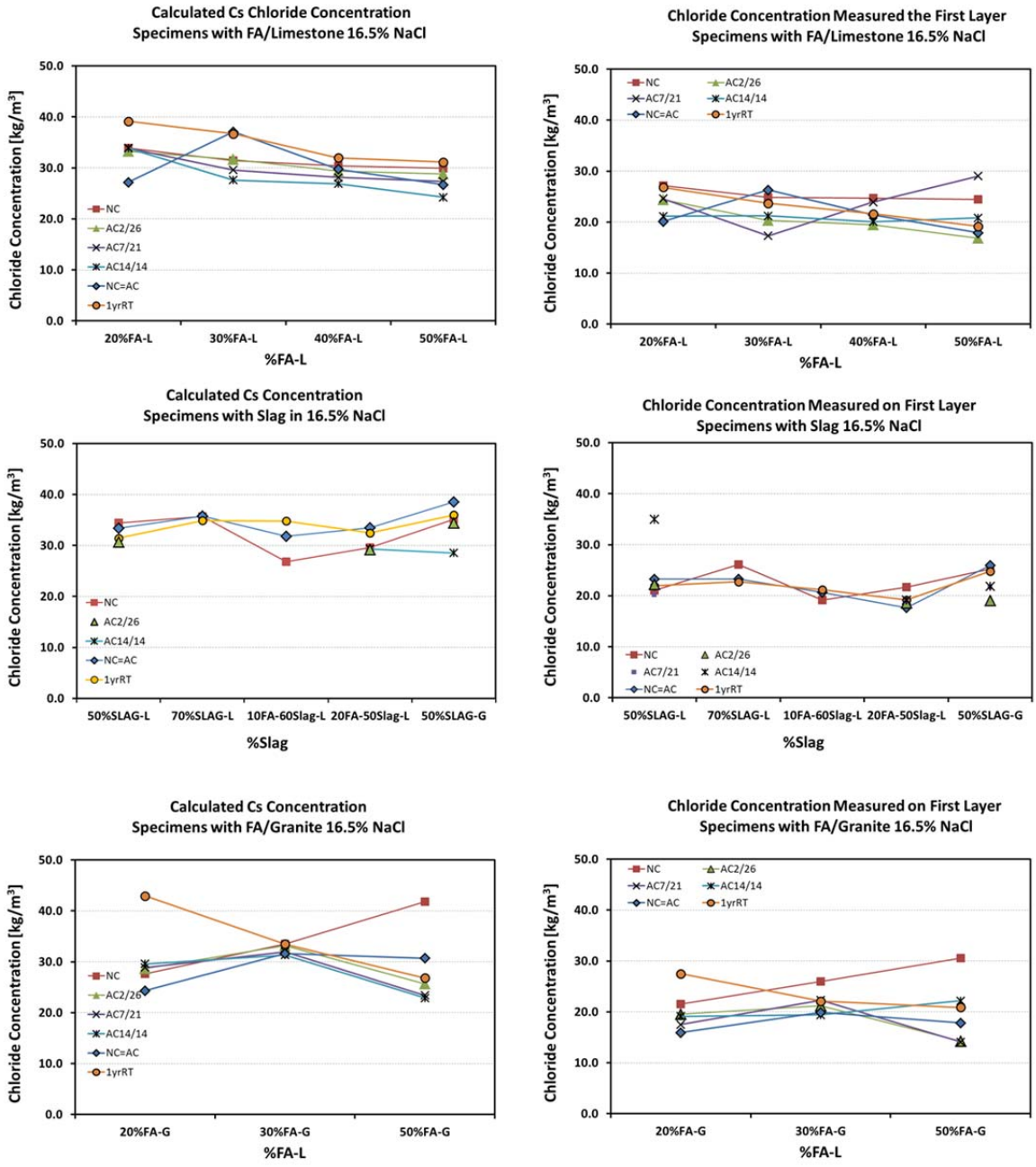

Figure 4.8: Average calculated surface concentration and measured concentration at the first layer for each one of the processed cases on specimens immersed in 16.5% NaCl

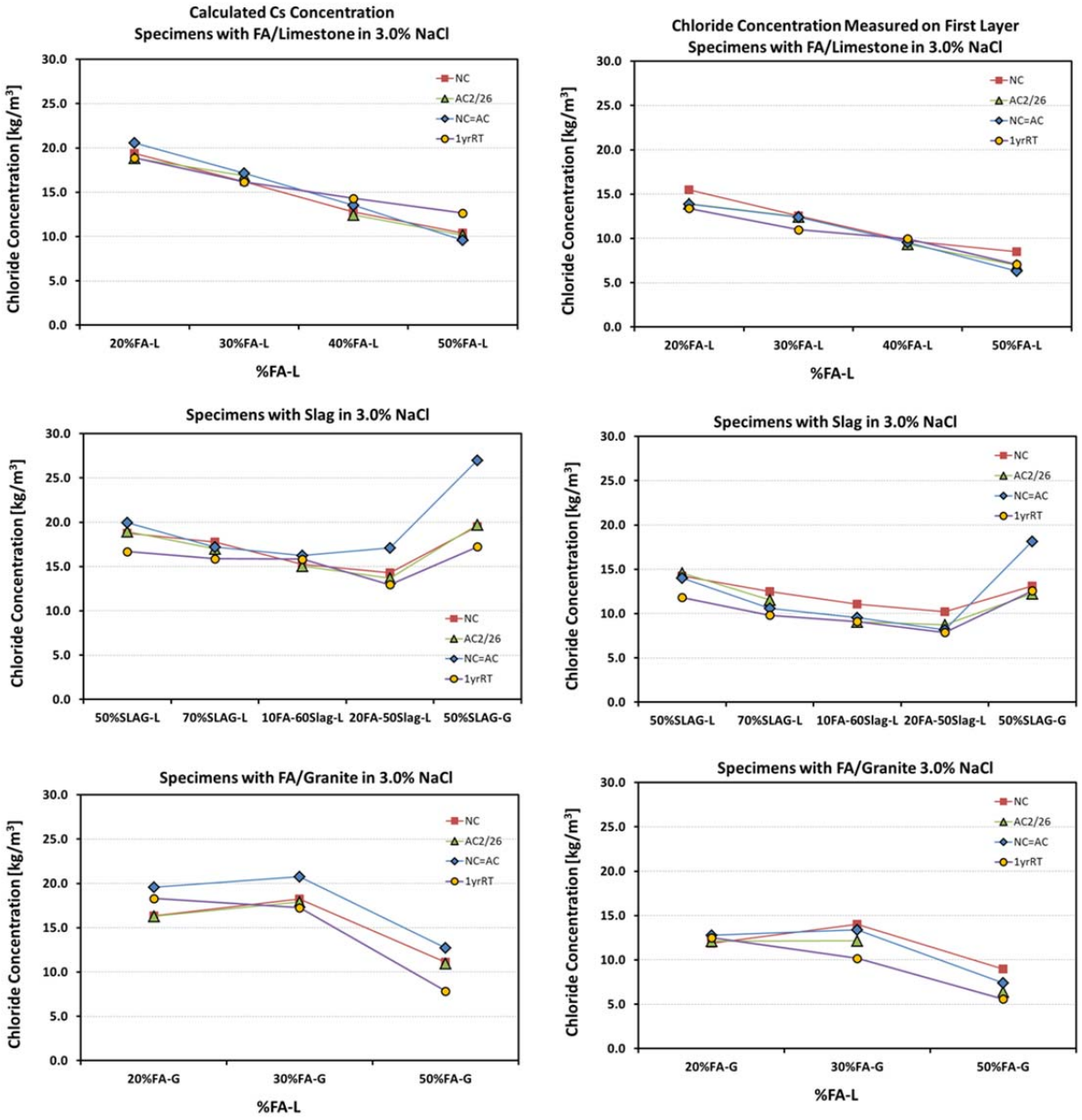

Figure 4.9: Average calculated surface concentration and measured concentration at the first layer for each one of the processed cases on specimens immersed in 3% NaCl

4.3.5 Discussion

4.3.5.1 Effect of Curing Regimes on Resistivity Development

Specimens with FA

During the early age up to 91 days, ET curing produced significant effects on resistivity development of all the specimens.

Figure 4.10 shows the early age resistivity development of concrete with 20%FA and limestone under different curing regimes. At 28 days, specimens cured under 2RT/26ET and 7RT/21ET showed the highest resistivity values and specimens cured under RT showed the lowest. For specimens cured under 14RT/ET, the resistivity value reached that of specimens under 2RT/ET and 7RT/ET at around 91 days. For the specimens exposed to ET curing and then moved back to RT curing at 28 days, the resistivity values continued increasing at RT; however, the rates of resistivity development at RT is much lower than at ET. As shown in Figure 4.8, the 28-day resistivity at RT is about 4 kΩ cm; however, the resistivity of 2RT/26ET, 7RT/21ET and 7RT/21ET is 15 kΩ cm, 14 kΩ cm and 10 kΩ cm, respectively.

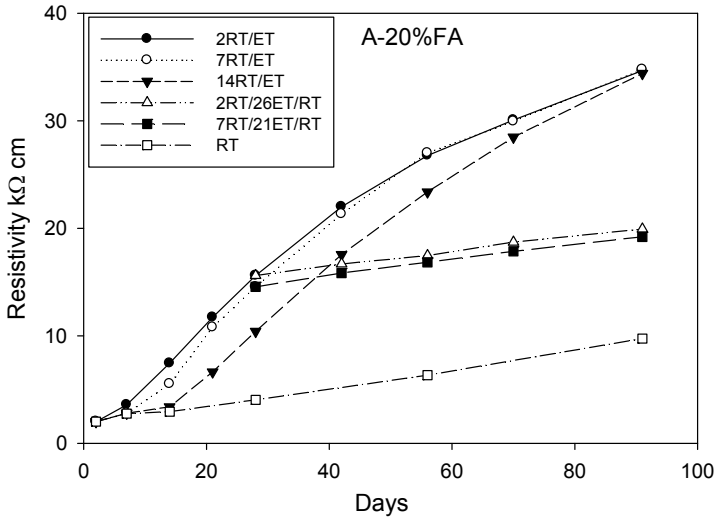

Figure 4.10: Resistivity evolution of concrete with 20% FA and limestone up to 91 days (Mix A)

Figure 4.11(a) shows 28-day resistivity values of specimens with FA/ limestone under different curing regimes. It is observed that at RT, specimens with higher replacement ratio of FA showed lower resistivity values. Whereas, under 2RT/26ET curing, specimens with higher replacement ratio of FA showed higher resistivity values and specimens with 50% FA showed the highest resistivity values. For

specimens under 7RT/21ET and 14/RT/14ET, specimens with higher amount of FA showed higher resistivity values, however, specimens with 40% FA showed the highest resistivity values. Similar results were also found on specimens with FA and granite as shown in Figure 4.11(b). It was found that the use of granite showed significant effects on resistivity. Under RT and with the same replacement ratio of FA, the 28-day resistivity of specimens with limestone is slightly higher than those with granite; however, under ET curing, resistivity of specimens with granite is significantly higher than that of specimens with limestone.

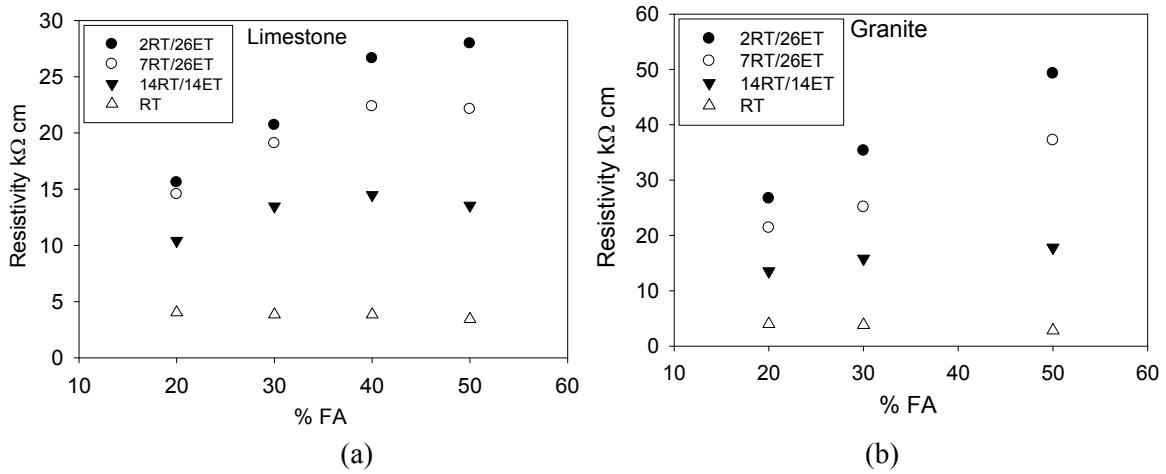

Figure 4.11: 28-day resistivity of specimens with (a) FA/limestone and (b) FA/granite under different curing regimes

Figure 4.12 shows the resistivity values at different age on specimens with limestone and FA under RT (a) and 2RT/ET (b) curing regimes. It indicates that for specimens under RT curing, at 91 days, specimens with 30% FA showed the highest resistivity, but after 1 year, specimens with 50% FA showed the highest resistivity. Under 2RT/ET curing and at 28 days, specimens with higher replacement ratio of FA showed higher resistivity; the benefits of higher resistivity with increasing replacement ratio FA become more significant at later ages (up to 500 days). For example, at 28-day, the resistivity value was 16 kΩ cm for 20%FA specimens and 28 kΩ cm for 50%FA specimens; whereas at 505 days, the resistivity value was 58 kΩ cm for 20%FA specimens and 229 kΩ cm for 50%FA specimens.

For specimens with granite, under RT, specimens with 50% FA showed similar resistivity to specimens with 30% FA at 505-day; however, under 2RT/ET curing, specimens with higher replacement ratio of FA showed higher resistivity both during short term and long term, as shown in Figure 4.13.

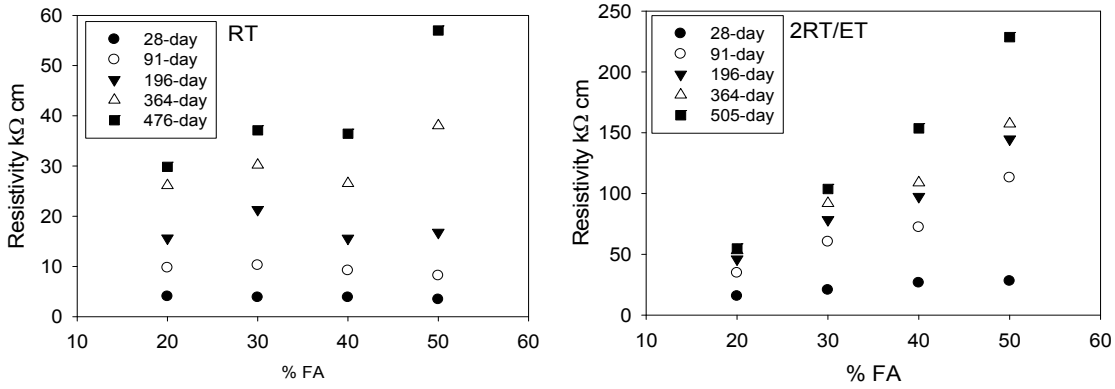

(a) (b)

Figure 4.12: Resistivity at different ages for specimens with FA/limestone under RT and ET

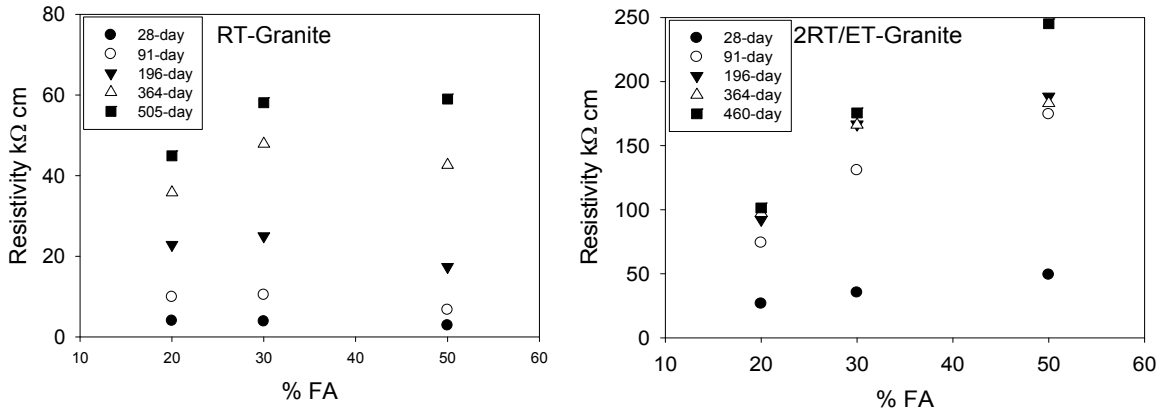

(a) (b)

Figure 4.13: Resistivity at different age for specimens with FA/granite cured under RT (a) and 2RT/ET (b)

Specimens with Slag or Slag+FA

Figure 4.14 shows comparison of resistivity development between specimens with 20%FA and 50%Slag under RT and ET curing regimes. Specimens with 50%Slag showed higher resistivity during the early age (28 days) than specimens with 20%FA under both RT and ET curing regimes; however, at the long term age, specimens with 20 FA showed higher resistivity than specimens with 50%Slag at both RT and ET curing regimes. This indicates that specimens with Slag have higher hydration rates during the early age than specimens with FA, which is more likely attributed to the high content of CaO in Slag than FA.

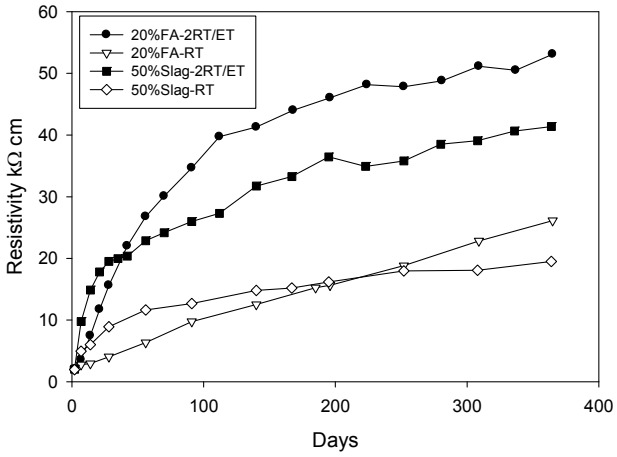

Figure 4.14: Comparison of resistivity evolution between specimens with 20% FA and 50% Slag under RT and ET curing regimes

Figure 4.15 shows the resistivity of specimens with Slag or Slag/FA at 28-day and 365-day under RT and ET curing regimes. At 28 days, under RT, specimens from Mix G (50% Slag and granite) showed the lowest resistivity(6 kΩ cm), and all the other groups (E, F, I, H) showed similar resistivity (9 to 12 kΩ cm); however, under ET, specimens from Mix H (50%Slag/20%FA and limestone) showed the highest resistivity (45 kΩ cm); specimens from Mix E (50%Slag and limestone) showed the lowest (19 kΩ cm). At 365 days, under RT, specimens from Mix G still showed the lowest resistivity (15 kΩ cm) and specimens from Group H (50%Slag/20%FA and limestone) showed the highest resistivity (40 kΩ cm); however, under ET curing, specimens with 50%Slag (Mix G and E) showed the lowest resistivity (41 kΩ cm), and specimens from Mix H (50%Slag+20%FA and limestone) showed the highest resistivity (139 kΩ cm).

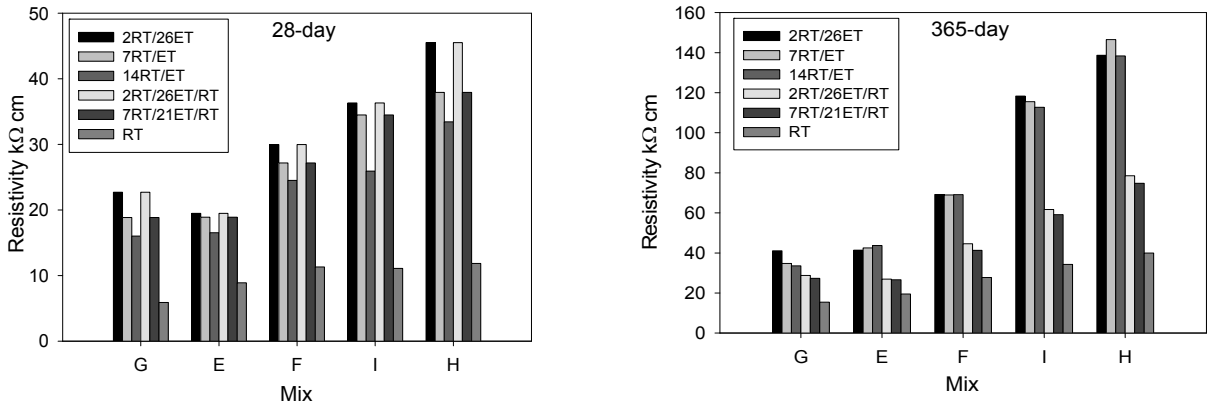

(a) (b)

Figure 4.15: Resistivity of specimens with Slag or Slag/FA under RT and ET curing regimes at 28 days and 365 days

4.3.5.2 Effect of Curing Regimes on 28-day Compressive Strength

Specimen with FA

Figure 4.16 shows the compressive strength on specimens with FA and limestone at 28 days. Under RT, compressive strength of all the specimens was over 30 MPa, ranging from 31.8 MPa to 48.1 MPa. Specimens with 20% FA (Mix A) showed the highest compressive strength (48 M Pa) and specimens with 50% FA showed the lowest compressive strength. Under RT and at 28 days, the compressive strength was lower for specimens with higher amount of FA. Under ET curing, compressive strength of all the specimens exceeded 51 MPa, ranging from 51 MPa to 68 MPa. However, 20%FA (Mix A) and 30% FA (Mix J) specimens showed similar compressive strength ranging from 65 MPa to 68 MPa. 40%FA (Mix B) and 50%FA (Mix D) specimens showed lower compressive strengths ranging from 51 MPa to 59 MPa.

At 28 days and under ET, specimens with 30% FA showed the highest compressive strength. For specimens with 20%FA and 30%FA, similar compressive strength was obtained from the same Mix under various ET curing regimes (2RT/26ET, 7RT/21ET and 14RT/14ET) at 28 days, however, for specimens with 40%FA and 50%FA, the longer the specimens were exposed under ET curing, the higher 28-day compressive strength was obtained, as shown in Figure 4.17.

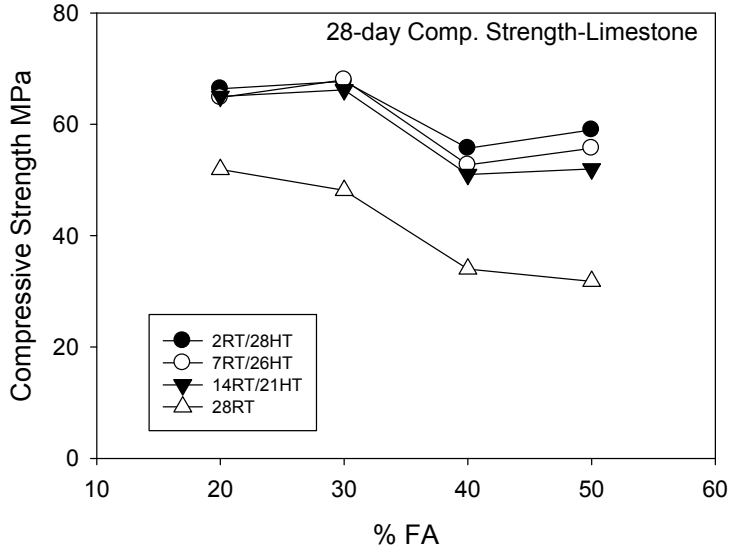

Figure 4.16: Compressive strength of specimens with FA/ limestone at 28 days

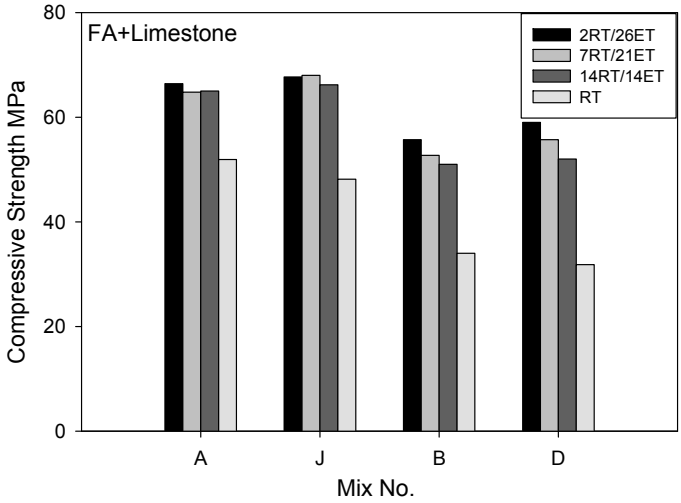

Figure 4.17: Comparison of 28-day compressive strength on specimens with FA and limestone

Specimen with FA + granite

Figure 4.18 shows the compressive strength of specimens with FA and granite at 28 days. Under both RT and ET curing, specimens with high amount of FA showed lower compressive strength. Under RT, specimens with 20%FA (Mix C) showed compressive strength of 47 MPa and specimens with 50% FA (Mix L) showed compressive strength of 24 MPa. Under ET curing regimes, specimens with 20%FA showed compressive strength between 73MPa (2RT/26ET) to 78MPa (14RT/14ET), and specimens with 50%FA showed compressive between 48Mpa (14RT/14ET) to 51MPa (2RT/26ET).

Under ET curing, for specimens with 20%FA, specimens curing under 14RT/14ET showed higher compressive strength (78MPa) than that of under 2RT/26ET (73MPa) and 7RT/21ET (77Mpa); however, for specimens with 50%FA, the compressive strength of specimens under 2RT/26ET (51MPa) was higher than that of under 7RT/14ET (49MPa) and 14RT/14ET (48Mpa), as is shown in Figure 4.19.

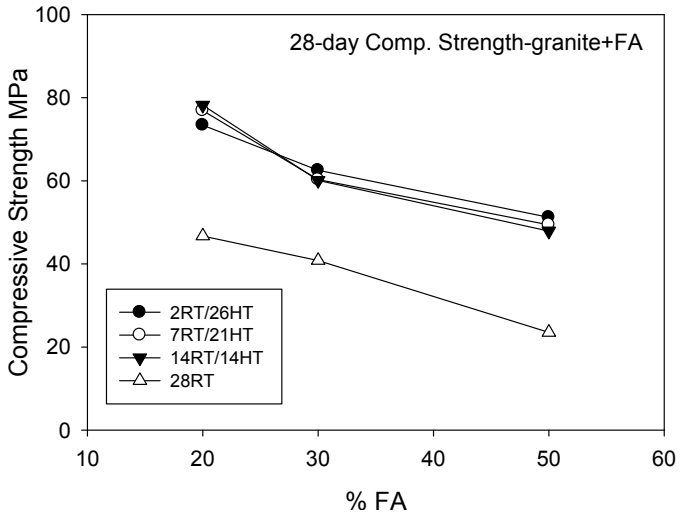

Figure 4.18: Compressive strength of specimens with FA and granite at 28 days

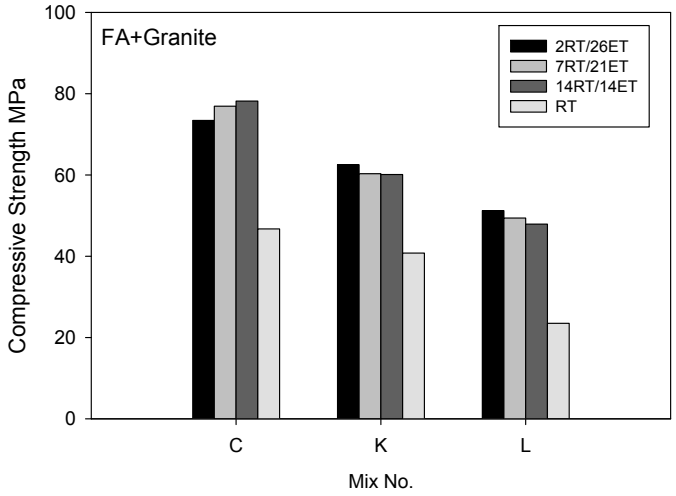

Figure 4.19: Compressive strength on specimens with FA/ granite at 28 days

Specimen with Slag or FA+Slag

Figure 4.20 shows the compressive strength of specimens with Slag or FA/Slag and limestone or granite. At 28 days, the compressive strength of all the specimens, either under RT curing or ET curing, was over 56 MPa. Under RT, specimens with 50%Slag/granite (Mix G) and specimens with

50%Slag/20%FA /limestone (Mix H) showed the lowest compressive strength (around 56 MPa to 58 MPa), and specimens with 70%Slag (Mix F) showed the highest compressive strength (67MPa).

Under ET curing regimes, specimens with 50%Slag/granite (mix G) showed the lowest compressive strength, ranging from 58 MPa to 65 MPa, and specimens with 50% Slag/limestone (Mix E) showed the highest measured compressive strength ranging from 78 MPa to 82 MPa. In general, the compressive strength of specimens under ET curing was higher than that of specimens under RT curing. However, the effect of temperature on 28-day compressive strength of specimens with Slag or Slag/FA was not as significant as at observed on specimens with FA only.

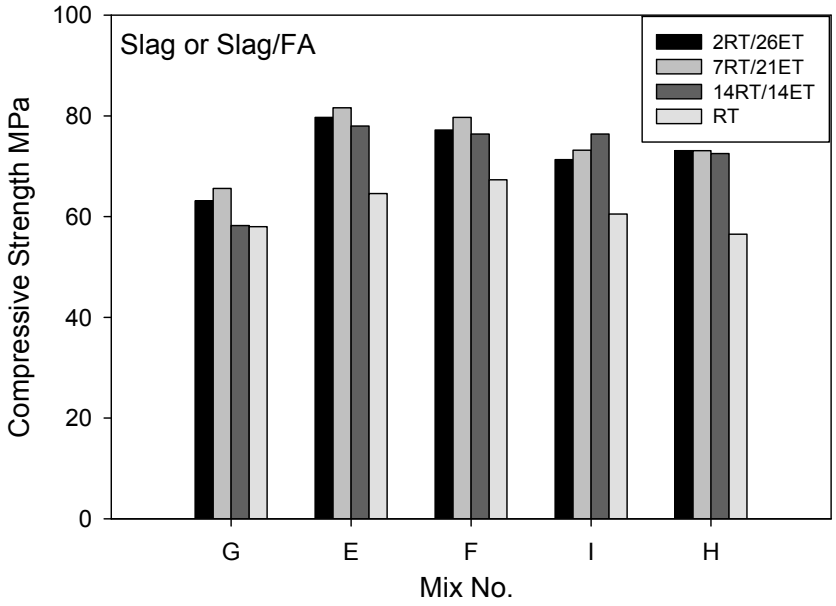

Figure 4.20: Compressive strength of specimens with Slag or Slag/FA at 28 days

4.3.5.3 Comparison of Resistivity and Compressive Strength under ET and RT

As indicated in

Figure 4.10, compressive strength tests were performed at 28 days on specimens under 2RT/26ET curing regimes, and also on specimens under RT at the time when $\rho_{RT} = \rho_{2RT/26ET}$, where ρ_{RT} is the resistivity of specimens cured under RT and $\rho_{2RT/26ET}$ is the 28-day resistivity of specimens under 2RT/26ET curing regimes. Figure 4.21 shows the age of specimens under RT curing when $\rho_{RT} = \rho_{2RT/26ET}$. Except for Mix G, the target resistivity of all other mixes was reached within 6 months (Mix A) to 14 moths (Mix L, I, F, and H) (Table 4.4). When comparing the mixes with the same

replacement ratio of FA, it took longer time to reach the target resistivity ($\rho_{2RT/26ET}$) for specimens with granite than those with limestone. For specimens with Slag or Slag/FA, it took 370 to 420 days for $\rho_{RT} = \rho_{2RT/26ET}$, which was longer than most of specimens with FA only (except Mix L).

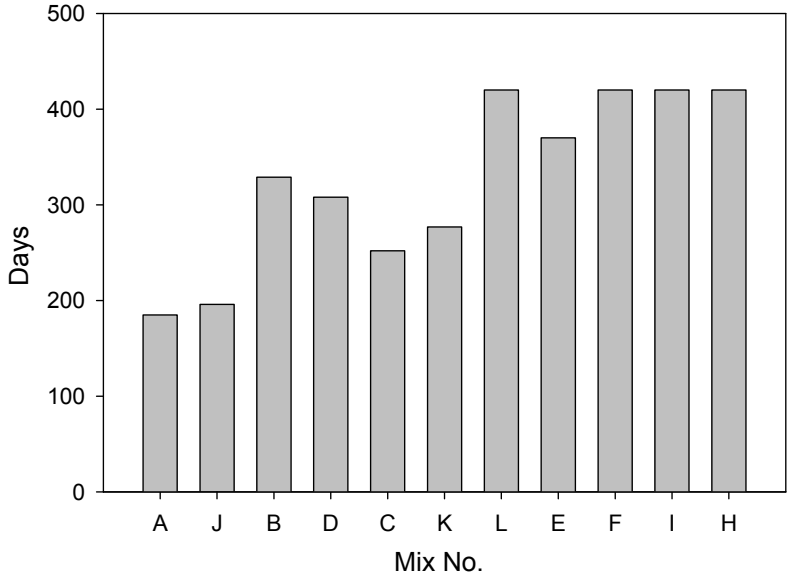

Figure 4.21: Age of specimens i.e., $t_{equivalent}$ cured under RT when $\rho_{RT} = \rho_{2RT/26ET}$ (See Table 4.3)

Due to the slower hydration rate of specimens under RT and the schedule of the resistivity measurement, it was hard to detect the exact days ($t_{equivalent}$) when $\rho_{RT} = \rho_{2RT/26ET}$, that is, the days shown in Figure 4.21 (or in Table 4.3) were not the exact days when $\rho_{RT} = \rho_{2RT/26ET}$, but the days when $\rho_{RT} \approx \rho_{2RT/26ET}$. Figure 4.22 shows comparisons between 2RT/26ET resistivity values and the RT resistivity values (Figure 4.22a) and between 2RT/26ET compressive strength and RT compressive when $\rho_{RT} = \rho_{2RT/26ET}$ (Figure 4.22b). The plots show that at the age when $\rho_{RT} \approx \rho_{2RT/26ET}$, the compressive strength of specimen cured under RT was 95% (Mix C) to 109% (Mix L) of the 28-day compressive strength of specimens cured under 2RT/26ET. Most of the compressive of specimens (at the age of $t_{equivalent}$) under RT curing was higher than the 2RT/26ET specimens except Mix A and Mix C. Figure 4.23 shows the actual ρ_{RT} vs. $\rho_{2RT/26ET}$ (Figure 4.23a) and 2RT/26ET compressive strength vs. RT compressive strength at age of $t_{equivalent}$ (Figure 4.23b). The above results indicate that, the 28-day electrical resistivity and compressive strength of specimens under 2RT/26ET curing regimes could be considered comparable to the corresponding values measured on specimens cured under RT at age of $t_{equivalent}$.

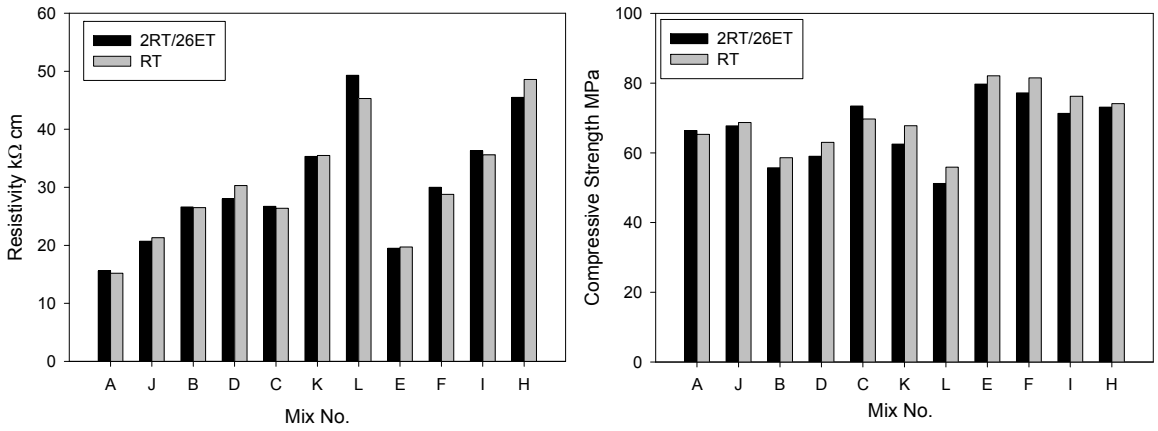

(a) (b)

Figure 4.22: Comparison between (a) ρ_{RT} *and* $\rho_{2RT/26ET}$, and (b)between 28-day compressive strength for samples cured 2RT/26ET and RT when $\rho_{RT} = \rho_{2RT/26ET}$

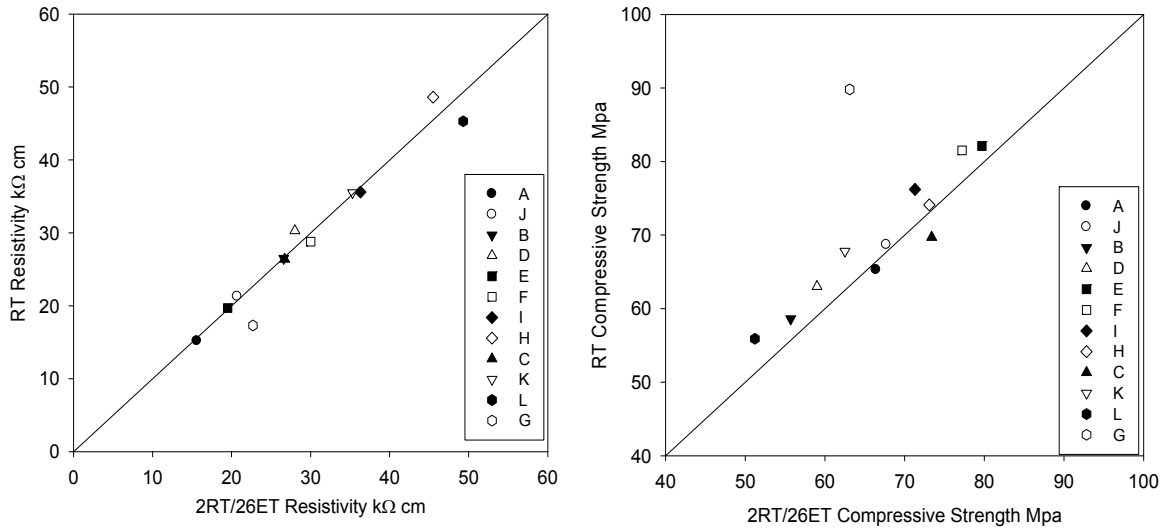

(a) (b)

Figure 4.23: Comparison between (a) ρ_{RT} vs. $\rho_{2RT/26ET}$ and (b) 28-day compressive strength under 2RT/26ET vs. RT when $\rho_{RT} \approx \rho_{2RT/26ET}$

Compressive Strength vs. Equivalent Age

Equivalent age is usually defined as "the duration of the curing at a reference temperature that would result in the same maturity as the curing period at other temperatures" (Malhotra & Carino, 2004). The equivalent age can be calculated by Equation (4-1)

$$\text{Equivalent Age} = \frac{\sum_{0}^{t}(T - T_0)\Delta t}{T_{ref} - T_0} \qquad \text{Equation (4-1)}$$

Where Δt= elapsed time in days at temperature T, T = average temperature during Δt, t = time after pour in days, T_o = datum temperature, in here T_o=10 °C, The reference temperature (T_{ref}) chosen was 20 °C. Equivalent age values were calculated for the different compression tests performed. The compression strength values were plotted vs. the calculated equivalent age in days. Figure 4.24 shows a compilation of all measured compressive strength values vs. calculated equivalent age grouped by concrete compositions. No attempt was made to obtain maturity indexes as there were not enough early compression tests performed at an early age. Instead, Figure 4.24 shows plots of the long-term compressive behavior not usually found in the literature for concrete with mineral admixtures. The left plot in Figure 4.24a shows the results for mixtures with FA at different replacements of cement by mass. Concrete with 30% FA (limestone or granite) showed the higher compressive strength at the age equivalent of 2000 days, whereas concrete specimens with 40% and 50% FA showed the lower compressive strength. Compressive strength values continue to increase monotonically with time on specimens with FA. The trends shown on Figure 4.24b suggests that there is not much difference in ultimate compressive strength (~83 MPa) on specimens with only slag at the equivalent age of 2000 days; slightly lower ultimate compressive strength (~79 MPa) is observed in specimens with both FA and Slag. No significant increase in compressive strength was observed after an equivalent age of 90 days in specimens with Slag and Slag/FA; i.e., short-term accelerated curing allowed these concrete specimens to reach their ultimate (limiting) compression strength due to the Slag faster reaction rate.

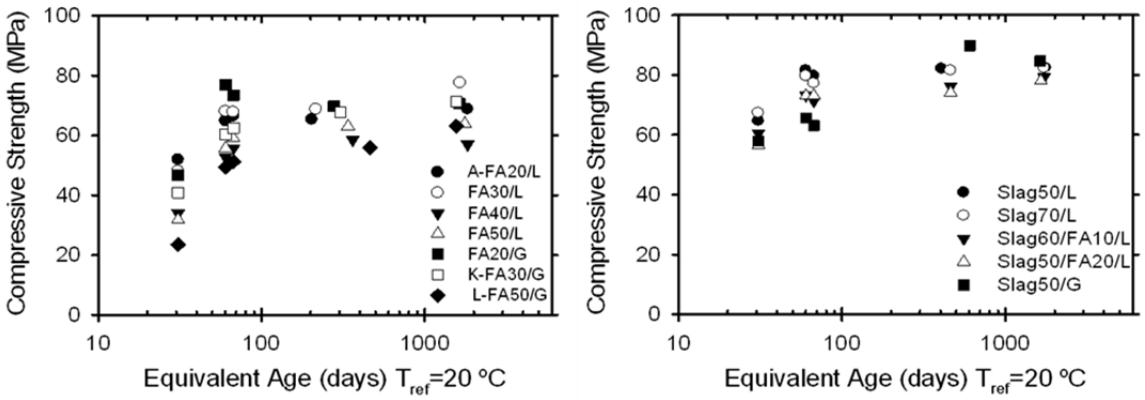

(a) (b)

Figure 4.24: Compressive Strength vs. Equivalent Age. (Note: 1 MPa=145 psi)

4.3.5.4 Effect of Curing Regimes on Non-Steady-State Migration Coefficients

Figure 4.25 shows the D_{nssm} at 1 year on specimens with FA+ limestone (a) and FA+ granite (b). For specimens with FA/limestone and under RT curing, specimens with 50%FA showed the lowest diffusion coefficients ($2.1\times10^{-12}m^2/s$) and specimens with 20%FA showed the highest ($3.5\times10^{-12}m^2/s$); under the same ET curing regimes, specimens with higher amount of FA showed lower diffusion coefficients. However, specimens under 2RT/ET and 7RT/ET showed lower diffusion coefficients than those of specimens under 2RT/26ET/RT and 7RT/21ET/RT. Specimens with 50%FA/limestone under 2RT/ET and 7RT/ET showed diffusion coefficients as low as $0.60\times10^{-12}m^2/s$, and those under 2RT/26ET/RT and 7RT/21ET/RT showed diffusion coefficient between $0.94\times10^{-12}m^2/s$ to $1.04\times10^{-12}m^2/s$.

Similar results were found on specimens with FA/ granite under ET curing regimes: specimens with higher amount of FA showed lower diffusion coefficients, and the D_{nssm} of specimens under 2RT/ET and 7RT/ET were lower than those of specimens under 2RT/26ET/RT and 7RT/21ET/RT. Under 2RT/ET and 7RT/ET curing regimes, specimens with 50%FA+granite (Mix L) showed diffusion coefficients as low as 0.22 to $0.24\times10^{-12}m^2/s$. For specimens with FA +granite and under RT, specimens with 30%FA showed the lowest diffusion coefficient ($1.0\times10^{-12}m^2/s$) than those with 20%FA ($1.5\times10^{-12}m^2/s$) and 50%FA ($1.4\times10^{-12}m^2/s$). For specimens with the same FA replacement ratio and under the same curing regimes, specimens with granite showed much lower diffusion coefficients than those with limestone. For specimens with 20%FA and under 2RT/ET curing regimes, the diffusion coefficient was $2.1\times10^{-12}m^2/s$ for specimens with limestone and $0.95\times10^{-12}m^2/s$ for specimens with granite, moreover, for specimens with

50%FA and under 2RT/ET curing regimes, the diffusion coefficient was $0.60\times10^{-12}m^2/s$ for specimens with limestone and $0.24\times10^{-12}m^2/s$ for specimens with granite.

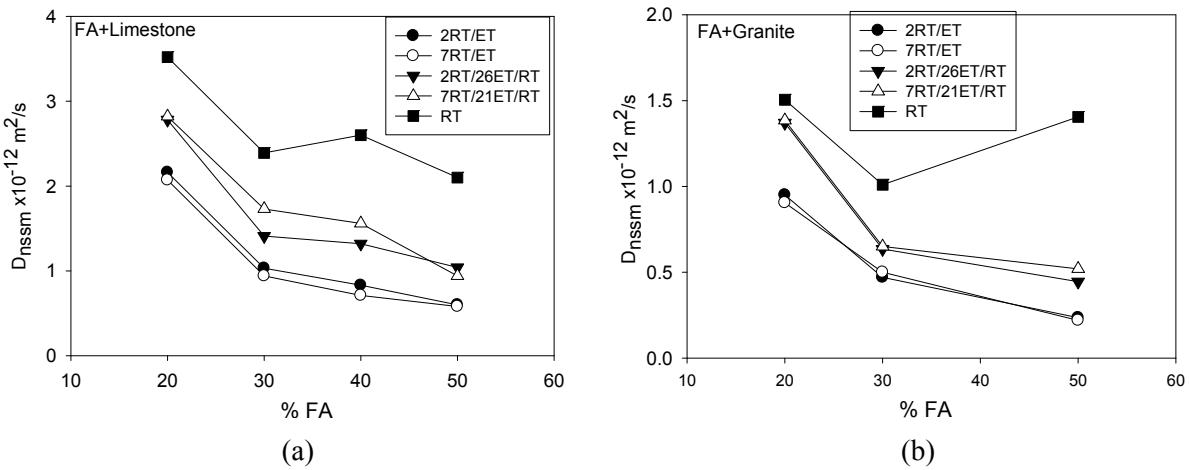

Figure 4.25: D_{nssm} of specimens with (a) FA/limestone and (b) FA/granite

Figure 4.26 shows the D_{nssm} obtained at one year of age on specimens with Slag or Slag/FA. Under RT, specimens from Mix G (50%Slag+limestone) showed the highest diffusion coefficients ($3.7\times10^{-12}m^2/s$), and specimens from Mix I (60%Slag+10FA) and Mix H (50%Slag+10%FA) showed the lowest diffusion coefficients (around $2.2\times10^{-12}m^2/s$). Similar results were also found on specimens under ET curing regimes: specimens from Mix H showed the lowest diffusion coefficients and specimens from Mix E showed the highest. For specimen with 50%Slag, specimens with granite showed lower diffusion coefficients under most of curing regimes except 7RT/ET. The reason that makes the diffusion coefficient of Mix G higher than Mix E under 7RT/ET is still unclear.

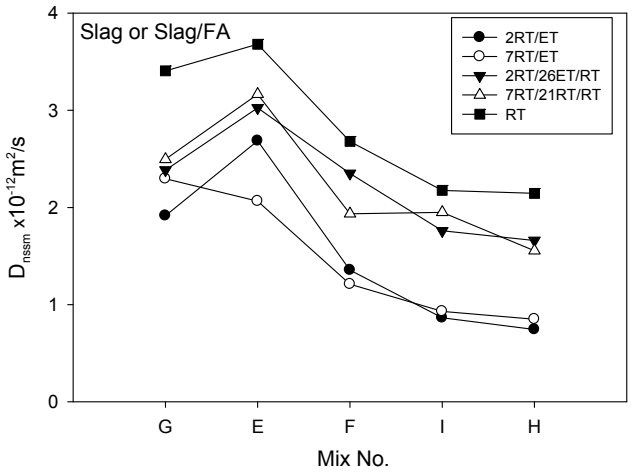

Figure 4.26: D_{nssm} of specimens with Slag or Slag/FA

Further discussion between D_{nssm} and Resistivity (including compositions effect) will be presented in the next chapter where results of tests on specimens from other mixes and those described above will be combined.

4.3.5.5 Effect of Pozzolanic Admixtures on Apparent Diffusion Coefficients

Figure 4.27 summarizes how the average calculated D_{app} varied depending on concrete composition, solution and curing regime. The three plots on the left column correspond to D_{app} values obtained from specimens exposed in 16.5% NaCl solution, whereas the D_{app} values shown on the three plots on the right correspond to D_{app} values obtained from specimens exposed in 3% NaCl.

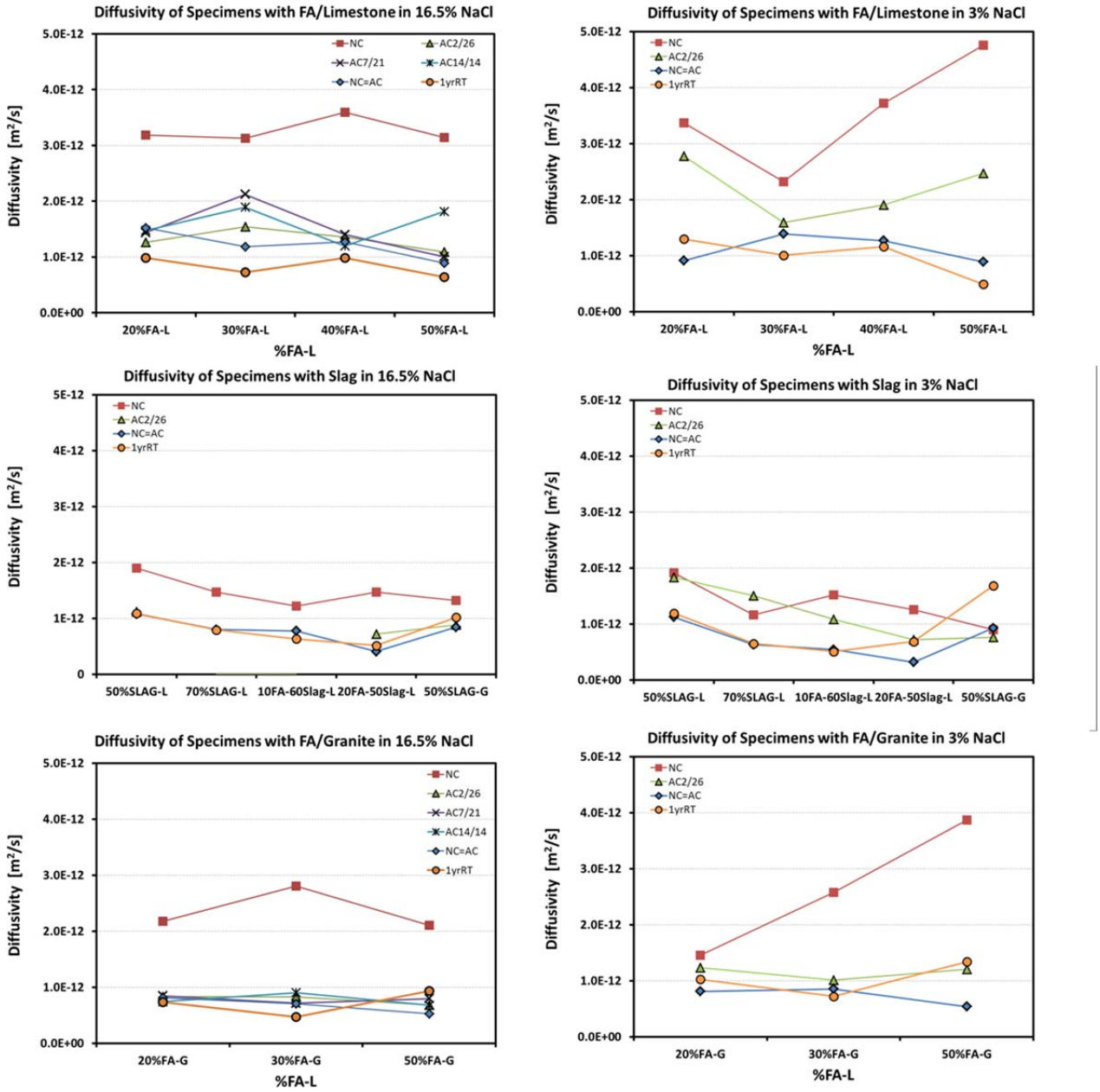

Figure 4.27: Calculated Apparent diffusion coefficients

The D_{app} obtained on specimens immersed in 16.5% NaCl after 28RT (labeled in here NC) does not appear to decrease as the FA increased, in fact on those immersed in 3% the opposite was observed (however, see note below). The D_{app} obtained for NC specimens immersed in 16.5 NaCl ranged between 1.5 and 3.5 $\times$ 10^{-12} m^2/s, whereas NC=AC specimens had an average D_{app} that ranged between 0.5 $\times$ 10^{-12}

m^2/s and 1.5×10^{-12} m^2/s. Specimens AC cured had similar or slightly larger D_{app} than those NC=AC cured. Specimens RT cured for 1 year before immersion had smaller Dapp for cases in tapparent was smaller than one year. Comparable Dapp values were observed when tapparent did not differ significantly from 1 year.

The D_{app} calculated for those specimens immersed in 3% NaCl was of the same order of magnitude than the D_{app} calculated on specimens immersed in 16.5% NaCl, but in some cases it was larger (see below).

Similar to what was observed for D_{nssm} values, the D_{app} measured on specimens cured for 28 RT showed the largest D_{app} values when comparing any given composition. The D_{app} values obtained after NC=AC and those exposed to AC and then immersed at an age of 170 days following 2RT/26ET/RT exposure were comparable for those specimens immersed in 16.5% NaCl. However, the D_{app} for those specimens immersed in 3% NaCl after AC curing were larger than those obtained after NC=AC. This apparent difference is likely due to the significantly longer time that elapsed from removal from the exposure solution to the moment the specimens were sliced. During this waiting period, the specimens are exposed in a low humidity chamber (50% RH) and room temperature, and additional chloride transport likely took place even if the moisture content was low close to the surface (as a result of the low relative humidity). It is known that the humidity inside the concrete could be > 80% RH at depths of 2 to 3 cm and depends on the w/cm, composition, porosity and tortuosity of the concrete. A personal communication with Dr. Sagues [e-mail, October 2013], reports that modeling suggest that if the concrete moisture is the same than while immersed and exposed for a year before slicing after a year of exposure. If one uses the profile to calculate D_{app} and assumes 1 year exposure, the calculated value would suggest a D_{app} three times larger than that would be obtained if the specimen had been sliced shortly after reaching one year of exposure. Using the D_{app} values for specimens cured NC=AC as a reference, the results suggest that D_{app} for those cured AC were anywhere from 1.1 times to close to 3 times larger. In many instances the D_{app}(AC) was about twice that for D_{app}(AC=NC). Those that were comparable were due to the shorter waiting time between removing from solution and slicing.

In addition to bulk diffusion test on specimens once the resistivity NC=AC, bulk diffusion was also performed both testing solutions on specimens RT cured for 1 year (series 1yrRT). However, not all profiles and fittings were completed due to time constrains. When comparing the D_{app} from 1yrRT and NC=AC specimens immersed in 16.5% NaCl, for series that were prepared withFA and Limestone, it is evident that additional curing time allow for additional hydration which resulted in lower D_{app}. NC=AC was usually reached after < 200 days for those with FA<=30%. In the case of those specimens with Slag

there was not much difference, suggesting that most of the slag had reacted by one year (for 4 of the mixes with slag NC=AC took >400 days).

The following figures show the correlation between the Dapp measured and measured ρ(initial) and Dapp vs. ρ(final). The Dapp values are influenced by microstructure changes during the exposure period as well as per binding and $C_s(t)$. Considering the specimens for which the resistivity change very little, it appears that the dominant microstructure/resistivity is that observed upon exposure. The values shown in here continue to carry the effects of the delay before slicing particularly for AC2/26. The plot also contains a series for specimens with 19% Fly ash labeled D_{app_ASR}, which were cured in the elevated temperature room in High Humidity for about six years before starting the bulk diffusion test. This series actually align close to most of the D_{app} from series Rf (final resistivity) particularly NC=AC, and some of RT-30dRf. NOTE mark those with Slag with a different color for all subgroups. Or create additional plots that only show FA+L, FA+G, and Slag (or Slag+FA)

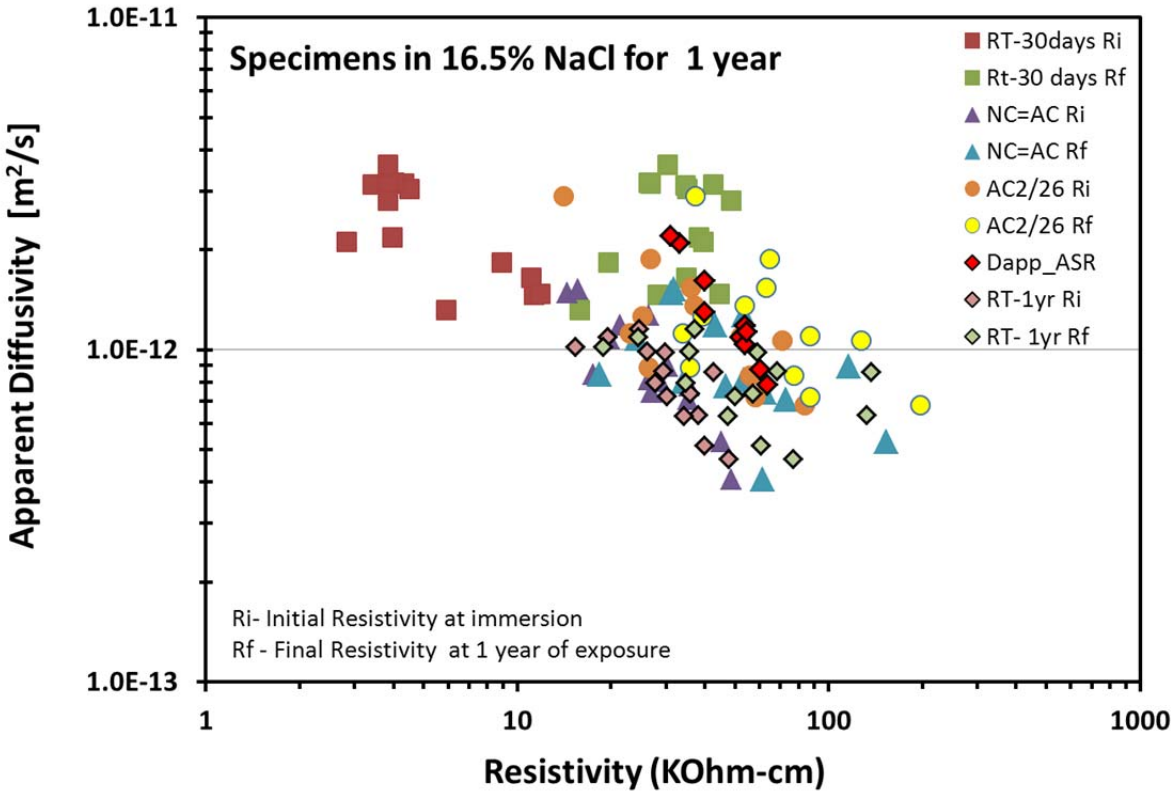

Figure 4.28: Apparent diffusivity vs. resistivity (initial and final ρ) for specimens immersed in 16.5% NaCl

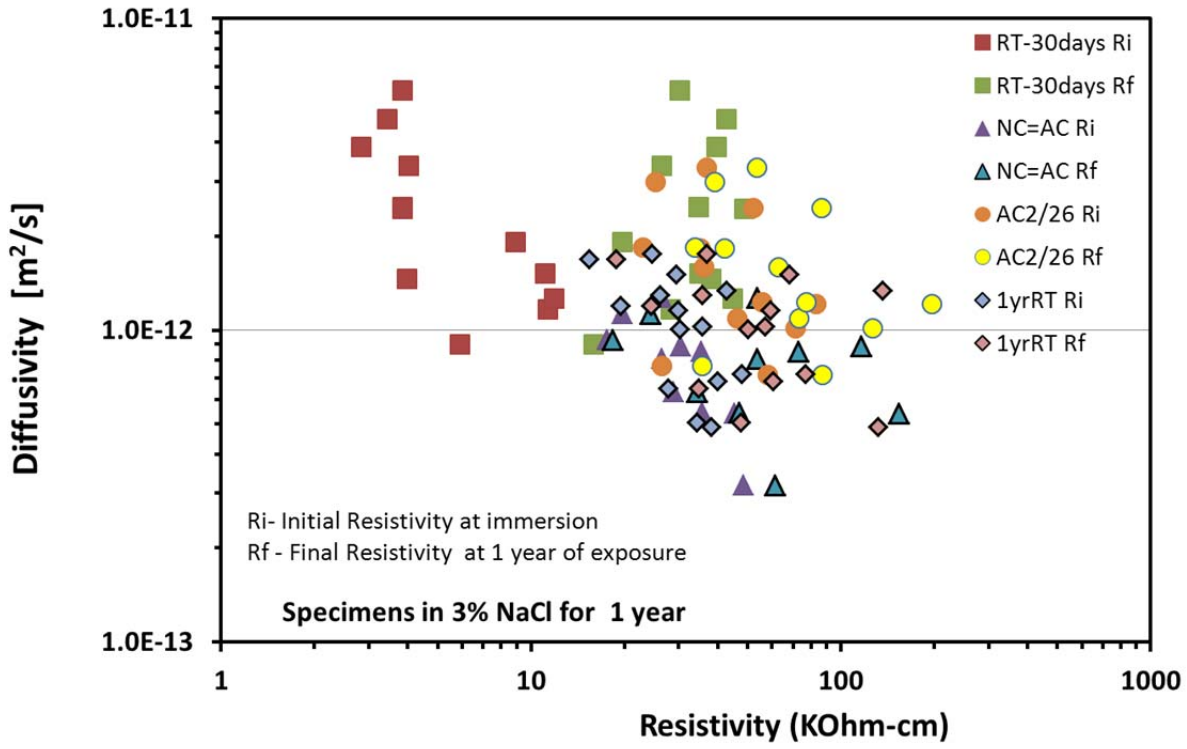

Figure 4.29: Apparent diffusivity vs. resistivity (initial and final ρ) for specimens immersed in 3% NaCl

Figure 4.29 compares the D_{app} vs Resistivity (initial and final ρ) for specimens immersed in 3% NaCl. In this case there is significant more scatter than what was observed on specimens exposed in 16.5% NaCl, and it is likely due to the gap/lag in time between removal from solution and slicing of specimens.

4.3.5.6 Chloride Aging Factor

With the correlation between resistivity and diffusivity, the diffusivity could be calculated using Equation 2-22 introduced in chapter 2:

$$D(t) = \frac{K_{D,\rho}}{\rho(t)} \tag{4-2}$$

Where $D(t)$ is the diffusivity at age t (days); $\rho(t)$ is the resistivity at age t, and $K_{D,\rho}$ is the constant of diffusivity and resistivity. Combine Equation 4-2 and Equation 2-14, and take t_0 as 28 days, then the following equation is obtained:

$$\frac{\rho(28)}{\rho(t)} = \left(\frac{28}{t}\right)^{m} \tag{4-3}$$

With Equation 4-3, the aging factor is calculated as:

$$m = -\frac{\log_{10}\left[\rho(t)/\rho(28)\right]}{\log_{10}\left(t/28\right)} \tag{4-4}$$

Aging Factor for Specimens under RT

An alternate to visualize what was described above;

Figure 4.30 shows the results of the correlation between $\log_{10}\left(t/28\right)$ and $\log_{10}\left[\rho(t)/\rho(28)\right]$ obtained from resistivity values measured on specimens of Group A for three curing conditions. It indicates that only specimens cured under RT show a linear correlation overtime, that is, a constant (or close to constant) m value was observed from the measurements performed on Group A specimens cured under RT conditions, but not for those cured 2RT/26ET/RT or 2RT/ET. Figure 4.30 shows results from specimens cured under RT including results from OPC concrete (mix 1C). A good linear relationship is found for most of specimens with OPC, Slag, Slag/FA, or < 30% FA, suggesting that m is constant vs. time for these compositions when cured immersed in lime water. The m value was not constant vs. time on specimens with ≥40%FA.

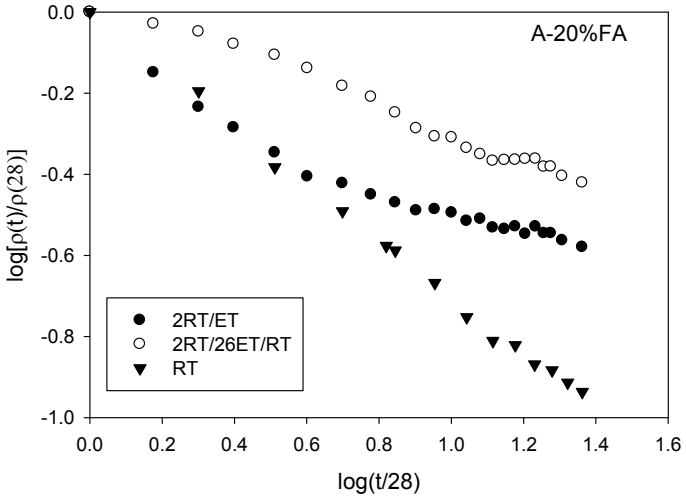

Figure 4.30: Correlation between and on specimens in Group A

Table 4.10 lists the aging factors calculated from the results shown in Figure 4.31. The value of *m* ranges from 0.1 to 1.14, which is in partial agreement with the reported values (0.32 to 0.91).[8, 21, 34, 36]. OPC concrete showed the lowest value (*m* =0.1) and specimens with large volume of FA (≥30%) showed the largest values (m≥0.8). However, *m* values calculated from Mix L (*m*=1.14) was larger than 1. The large value of *m* obtained from Mix L (50%FA/granite) is believed to be caused by the high replacement ratio of FA, at an early age hydration reaction rate proceeds at a similar rate than 40%FA, but as the concrete ages a higher reaction rate happens later due to the pozzolanic reaction and larger amount of FA.

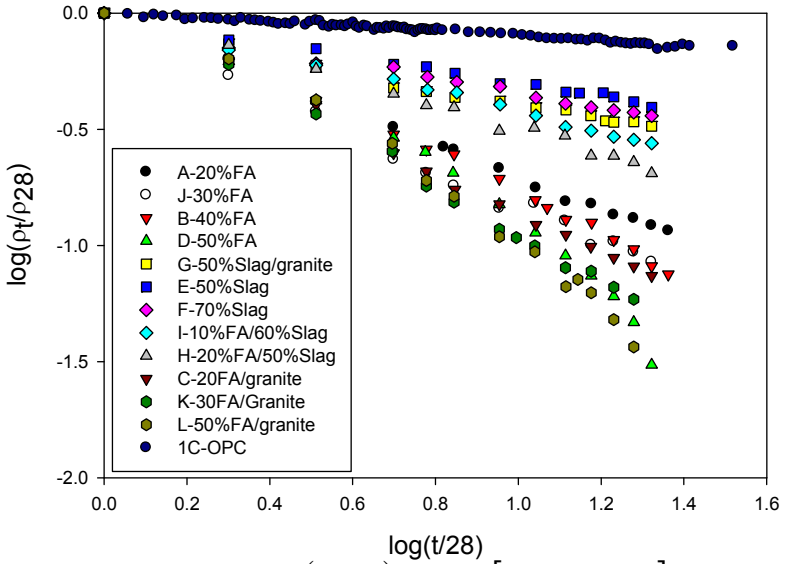

Figure 4.31: Correlation between $\log(t/28)$ and $\log[\rho(t)/\rho(28)]$ on specimens cured under RT.

The results in Table 4.10: Values of *m* calculated from specimens cured under RT indicate that, that as a result of using pozzolanic admixtures, the m value increases. The value of m also increases with increasing replacement ratio of FA. It is suggested that caution should be used when using the aging method to predict the diffusivity coefficients evolution with time, as the value of m could be significantly different depending on the replacement ratio and type of pozzolanic admixtures.

Table 4.10: Values of *m* calculated from specimens cured under RT

Mix	A	J	B	D	G	E	F	I	H	C	K	L	1C	2C
m	0.70	0.80	0.82	0.82	0.35	0.29	0.32	0.42	0.51	0.88	1.00	1.14	0.10	0.56
R^2	1.00	0.98	0.98	0.85	0.91	0.98	0.94	0.99	0.99	0.99	0.98	0.88	0.96	0.94

Aging Factor for Specimens under 2RT/26ET/RT using $t_{equivalent}$

Table 4.5 shows that at the age of $t_{equivalent}$ the resistivity value of specimens cured under RT could reach the 28-day resistivity of specimen's cured under 2RT/26ET conditions. Figure 4.32 shows a comparison of resistivity evolution with time on specimens under RT and 2RT/26ET/RT. The resistivity values of 2RT/26ET/RT starts from 28 days (resistivity measure at day 28). However, the age in days for the 2RT/26ET/RT series shown in Figure 4.32 are ($t_{equivalent} + t - 28$). Figure 4.32 shows that the resistivity of 2RT/26ET/RT specimens after 28 days vs. ($t_{equivalent} + t - 28$) almost overlapped with the resistivity values measured on RT specimen's after $t_{predicted}$. With these results, it is possible to calculated and estimate the long term(after $t_{equivalent}$) aging factor *m* of RT specimens using the resistivity values measured on specimens cured 2RT/26ET/RT vs. ($t_{equivalent} + t - 28$).

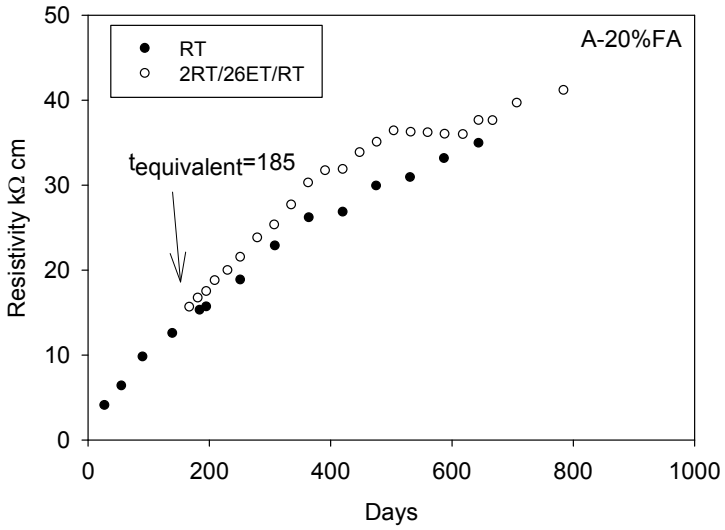

Figure 4.32: Comparison of resistivity evolution with time on specimens under RT and 2RT/26ET/RT

The correlation between $\log((t_{equivalent} + t - 28)/28)$ and $\log(\rho_{t_{equivalent}+t-28} / \rho_{t_{equivalent}})$ on 2RT/26ET/RT specimens from Mix A (20%FA) is shown in Figure 4.33. Table 4.11 lists and compares the *m* values calculated from the resistivity values measured on RT specimens (Table 4.10) and from 2RT/26ET/RT

specimens using $t_{equivalent}$ for the portion of the trend that is linear. Most *m* values calculated from 2RT/26ET/RT specimens were higher than the *m* values calculated from RT specimens using this approach. Some of the *m* values from 2RT/26ET/RT specimens were even higher than 1 (should be $0 \leq m \leq 1$). The results in Table 4.11 suggest that using the $t_{equivalent}$ method requires additional consideration when used to predict the long term *m* values of RT specimens. The m values > 1 are believed to be due to high hydration rates present while these specimens were in the ET and some latent effect upon moving these to RT curing. Below, we introduce an alternate method to monitor how m changes vs. time while exposed to the different curing regimes.

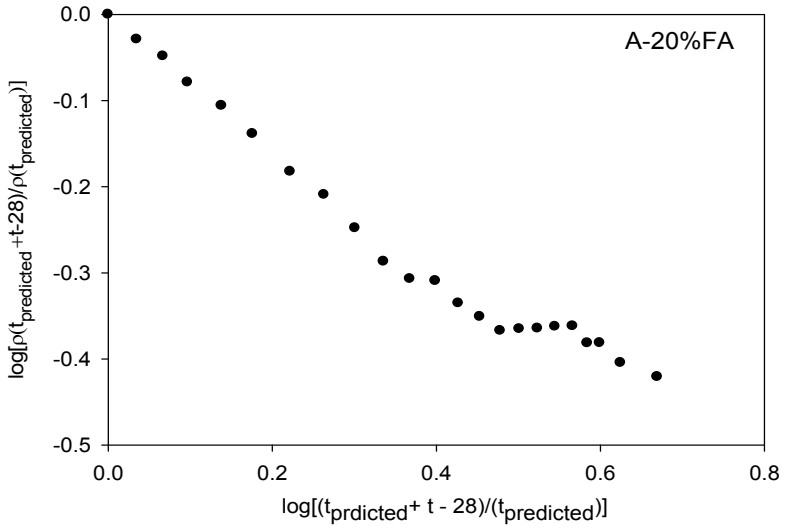

Figure 4.33: Correlation between $\log((t_{predicted}+t-28)/28)$ and $\log(\rho_{t_{predicted}+t-28}/\rho_{t_{predicted}})$

Table 4.11: Values of m calculated from RT and 2RT/26ET/RT using the equivalent days

Mix		A	J	B	D	G	E	F	I	H	C	K	L
RT	*m*	0.70	0.80	0.82	0.82	0.35	0.29	0.32	0.42	0.51	0.88	1.00	1.14
	R^2	1.00	0.98	0.98	0.85	0.91	0.98	0.94	0.99	0.99	0.99	0.98	0.88
2RT/26ET/RT	*m*	0.64	0.88	1.12	1.71	-	0.62	0.52	0.45	0.90	1.33	1.27	1.73
	R^2	0.91	0.96	0.98	0.97	-	0.95	0.89	0.94	0.97	0.91	0.93	0.97

4.3.5.7 Chloride Aging Factor vs. time

The aging factors of concrete specimens for the different mixes and curing regimes were calculated using equation (4-3) with a reference age of 28 days (t_0) and the corresponding concrete resistivity obtained at that age (ρ_0). This is an alternative method to that presented in the previous section.

Aging Factor for Specimens under RT

Figure 4.34 shows the aging factors of specimens in Group (Mix) Ai, A, J, Bi, B and D with the different fly ash ratio and limestone aggregate cured in room temperature (RT). Here t_0 =28 days. The y-axis shows the calculated aging factors (*m*) values and the x-axis shows t- t_0, all values will be mentioned with respect to this axis. For the specimen in Group (Mix) Ai (with 20% FA), the *m* value did not change much with time, during the first 168 days it oscillated between 0.615 and 0.685 and reached a maximum value of 0.696 on day 392. Thereafter, the *m* value decreased at a very slow rate and reached a value of 0.624 by day 999. The aging factor for specimens in Group A (20% FA and with a closer to target air content) evolved slightly different. The *m* value increased from 0.649 at day 28 to 0.727 at day 336 and then decreased at slow rate and by day 998 *m* reached a value of 0.623. For the specimen in Group J (30 % FA), the *m* value of specimen decreased with time and ranged from 0.83 to 0.9 during the first 120 days. After day 818, the *m* value ranged from 0.757 and 0.763 and appears to have reached a plateau. For the specimen in Groups Bi and B (40% FA), the trends of the *m* values vs time were similar but the former value was slightly lower than those for the latter before day 448. The *m* values increased with time from 0.7 to 0.77 by day 400 for specimens of group B, the m value continue to increase but the slope was less steep and reached a value of 0.85 by day 950. Compared to previous groups, the *m* value obtained on specimens of Group D (50 % FA) increased at higher rate from 0.690 to 1.111 and appears to have reached a plateau by day 616. After day 800, the *m* value decreased at a very slow rate and varied from 1.078 to 1.074, which might be considered constant. It would be apparent that the *m* values of specimens with higher replacement ratio of fly ash were larger than those of specimens with less fly ash. It is also observed that the air content did not play critical role for the *m* value after long term exposure (comparing Ai and A groups and Bi and B groups). Additionally, it can also be concluded that the *m* value for specimens cure in RT only becomes constant after a long term exposure.

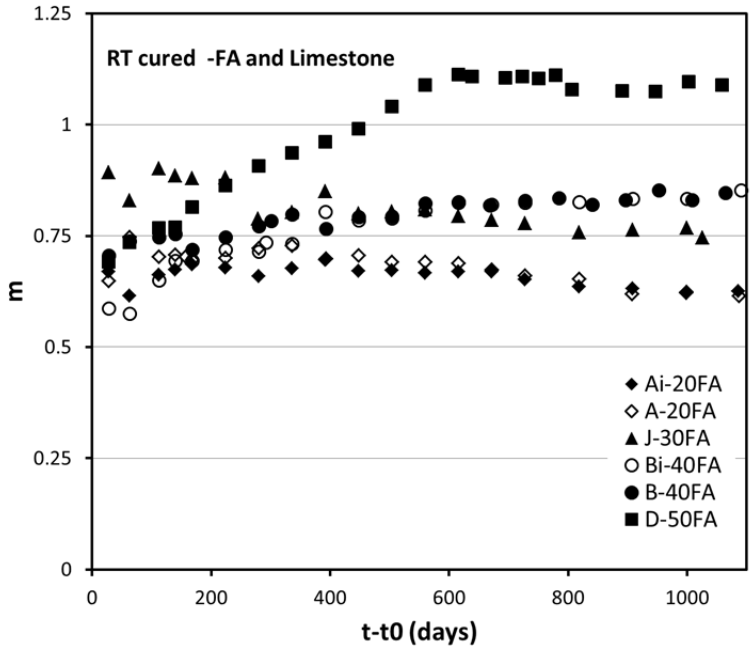

Figure 4.34: Aging factors of specimens in Groups Ai, A, J, Bi, B and D cured under RT

Figure 4.35 shows the aging factors of specimens in Group (Mix) C, K and L with the different fly ash ratio and granite cured in room temperature (RT). Here t_0 =28 days. It can be seen that the trends of the aging factors (*m*) are time-dependent. For the specimen in Group C with 20% fly ash, the *m* value increased with time and reached a value of 0.898 on day 168 and then slowly decreased to a value of 0.756 on day 909. The *m* value of specimen in Group K with 30% fly ash were larger than those observed for Group C (20% fly ash). The *m* value for Group K reached a value 0.974 on day 224 and then decreased slowly to a value of 0.914 on day 896. The *m* value for Group L with 50% fly ash evolved a bit different. It increased from 0.65 to a value of 1.00 by day 200 and then increased a lower rate and achieved a value of 1.222 by day 889. Similar to what was described above, it was evident that the higher fly ash ratio leads to the larger *m* values. The m value exceeded a value of 1 on specimens with 50% FA, and it is possible that this is because there is a larger amount of pozzolans and enough calcium hydroxide for the pozzolanic reaction to proceed for a longer time and even increases its rate as suggested by the steeper slope for both group D and L.

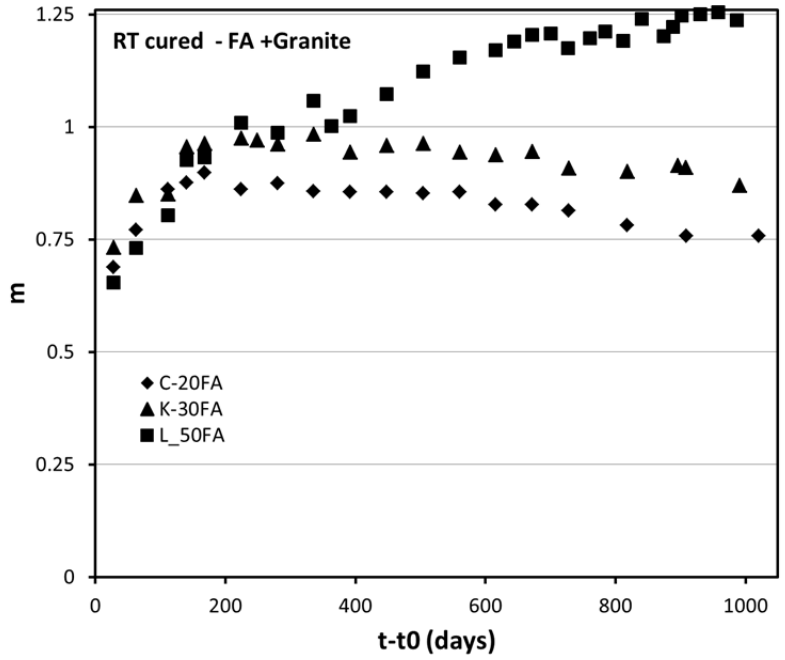

Figure 4.35: Aging factors of specimens in Groups C, K and L cured under RT

Figure 4.36 shows the aging factors of specimens in Group (Mix) E (50% slag + limestone), F(70% slag + limestone), I(10% FA+%60Slag), H(20% FA+%50Slag) and G (50% Slag+granite) cured in room temperature (RT). Here t_0 =28 days. For the specimens in Group E, the aging factor (*m*) decreased from 0.385 (day 28) to 0.299 (day 63) and then oscillated between 0.292 and 0.315 until day 968. Similarly, the *m* value on specimen in Group F also decreased from 0.534 (day 28) to 0.356(by day 169) and then oscillated between 0.336 and 0.354 which can be considered stable. However, the *m* value on specimen in Group F was generally larger than that on specimen in Group E due to the higher slag ratio on specimens in Group F. It is also seen that the *m* value on specimen in Group I decreased with time from 0.554 (day 28) to 0.415 (day 112) and from day 280 it ranged between 0.430 and 0.418. For the specimens in Group H, the *m* value gradually increased from 0.454 (day 28) to 0.510 (day 140) and then oscillated between 0.479 and 0.531. This *m* value for group H is somewhat larger than that observed on specimens in Group E,F, I and G. For the specimen in Group G, the *m* value increased slightly during the first 112 days and then decreased from 0.461 to 0.330. This change rate was higher than that observed for Groups E and F. It is clear that the *m* values on specimens in Group I and H were larger than those of specimens in Group E, F and G, suggesting that concrete specimens with FA and Slag generally have larger *m* values than those with only Slag after a long term exposure and cured immersed in limewater.

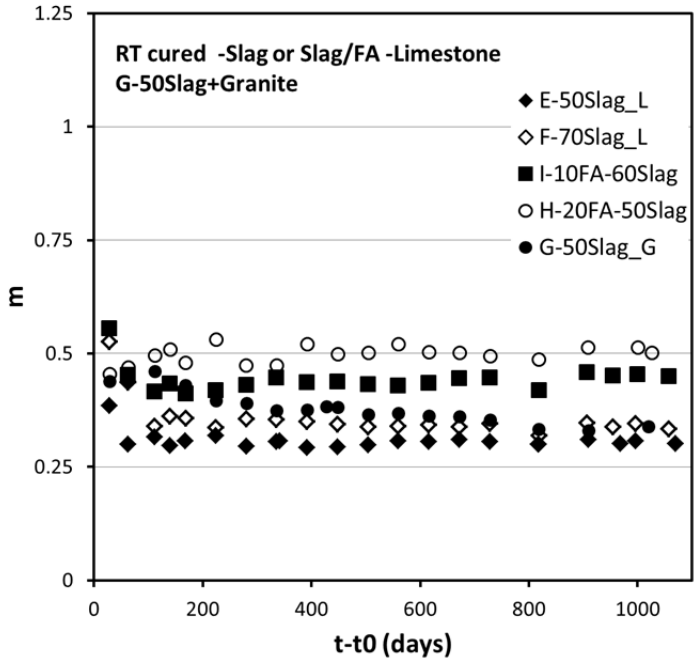

Figure 4.36: Aging factors of specimens in Groups E, F, I, H and G cured under RT

Comparing the results in Figure 4.34 and 4.35, it is evident that the *m* values of specimens with FA + Granite were generally larger than those on concrete with FA+ Limestone for the same FA ratio. Figure 4.36 shows that that the *m* vales of concrete with only slag tended to be smaller than those with FA+Slag and significantly lower than the m values observed for those with FA only.

Aging Factor for Specimens under 2RT/ET

Figure 4.37 shows the aging factors of specimens in Group (Mix) Ai, A, J, Bi, B and D with the different fly ash ratio and limestone aggregate cured in 2RT/ET. Here t_0 =28 days. Generally, the aging factors (*m*) of all specimens were time – dependent and most trends showed a decrease in the calculated *m* values vs. time. The maximum value shown is 1.25. All groups showed a monotonic decrease in the corresponding m values during the initial 200 (Group A) to 400 (Group D) days. The rate of change significantly slows down after that. By day 1000 the *m* value was 0.41 and 0.45 for specimens of Groups A and Ai respectively. The other three groups had m values that ranged from 0.52 to 0.53. Something that is not seen in Figure 5.28 is that by day t_0=28 a significant amount of hydration has taken place as all

these specimens had spent 26 days at ET. It appears that the 26 days in the ET room allows most of the pozzolanic reaction to take place.

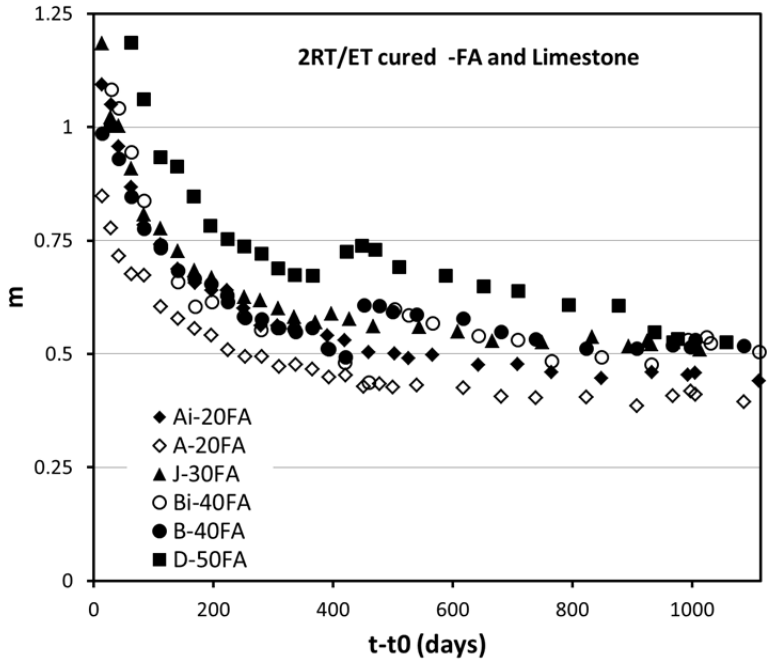

Figure 4.37: Aging factors of specimens in Groups Ai, A, J, Bi, B and D cured under 2RT/ET

Figure 4.38 shows the aging factors of specimens in Group (Mix) C, K and L with the different fly ash ratio and granite cured in 2RT/ET. Here t_0 =28 days. Obviously, the aging factors (*m*) of all specimens were time – dependent and the trends showed a decrease in the calculated *m* values vs. time. It can also be seen that the *m* value obtained from specimens in Group C was generally lower when compared to m values of group K and L. Additionally, the *m* values of specimen in Groups L were influenced by refreshing the lime water on days 380 and 850, such increase in m value was not observed for Group K and L. The m value by day 850 was < 0.5 for K and C series.

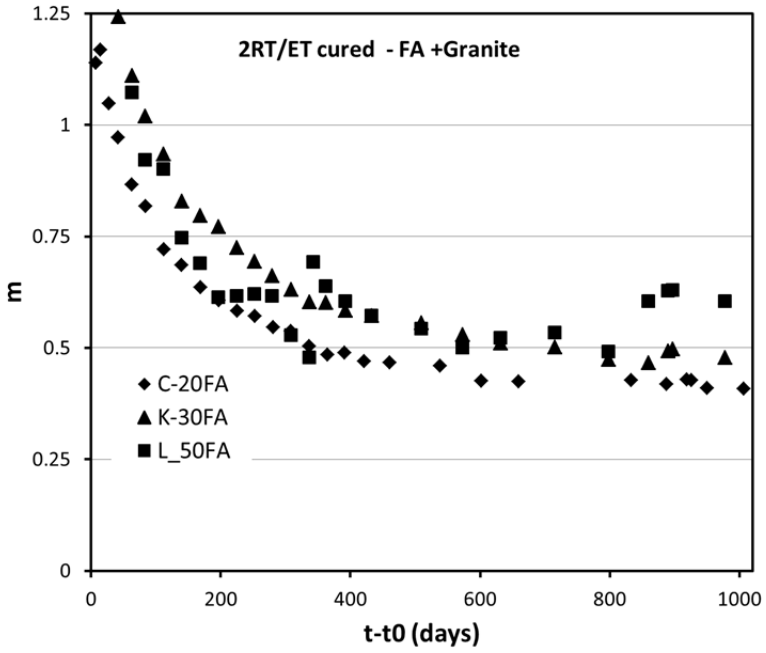

Figure 4.38: Aging factors of specimens in Groups C, K and L cured under 2RT/ET

Figure 4.39 shows the aging factors of specimens in Group (Mix) E (50% slag + limestone), F(70% slag + limestone), I(10% FA+%60Slag), H(20% FA+%50Slag) and G (50% Slag+Granite) cured in 2RT/ET. Here t_0 =28 days. It is observed that the *m* values of specimen in Groups E, F and G did not change much after 175 days. The latest obtained *m* values were 0.24, 0.31 and 0.33 for Groups G, E and F, respectively. For specimen in Groups I and H, the *m* values after day 170 decreased from 0.488 to 0.431 and 0.545 to 0.499, respectively. By day 930 the *m* values were 0.44 for mix I and 0.45 for mix H. Similarly to what was observed on specimens cured at RT all the time, the *m* values of specimens from groups containing both FA and Slag were generally larger than the *m* values of specimens in Group E, F and G due to the pozzolanic reaction for those with FA.

The results in Figure 4.37 and 4.38 have shown that the *m* values of specimens with FA+Limestone and FA + Granite currently had already decreased significantly under curing conditions of 2RT/ET for a given ratio of fly ash. It is also observed that the *m* values of specimen in Groups A, C and H (with 20% FA) in Figures 4.37, 4.38 and 4.39 were 0.385 (day 907), 0.433 (day 890) and 0.45 (day 930), respectively. The cause for this might be associated with high temperature which resulted in faster hydration of fly ash within concrete and that after this much time most of the pozzolanic reaction has been completed or is proceeding at a significantly slower rate.

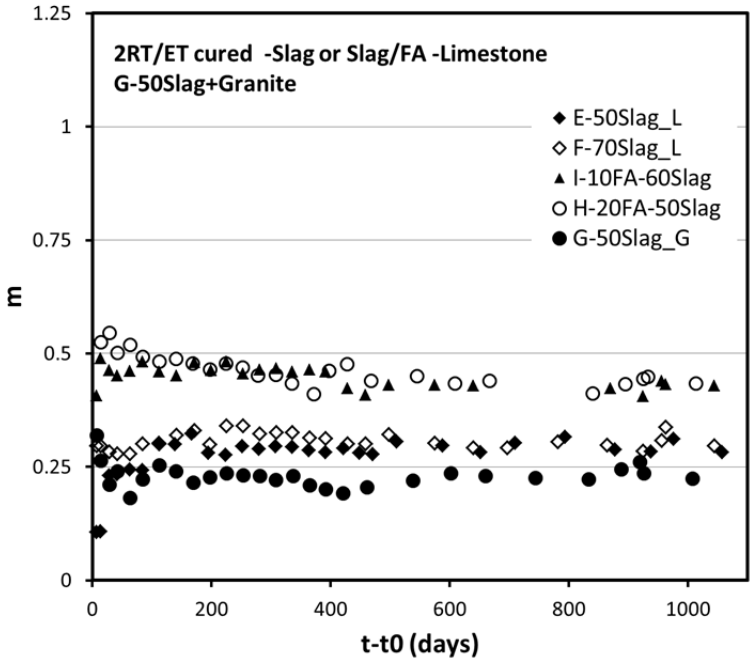

Figure 4.39: Aging factors of specimens in Group (Mix) E (50% slag + limestone), F(70% slag + limestone), I(10% FA+%60Slag), H(20% FA+%50Slag) and G (50% Slag+Granite) cured in 2RT/ET

Aging Factor for Specimens under 2RT/26ET/RT

Figure 4.37 shows the aging factors of specimens in Group (Mix) Ai, A, J, Bi, B and D with the different fly ash ratio and limestone aggregate cured in 2RT/26ET/RT. Here t_0 =28 days. It is important to note that all specimens described in this section spent 26 days in the ET room, which accelerated the hydration process and pozzolanic reaction (those with FA) or latent hydraulic (slag) reactions. Hence, upon transfer to the room temperature the resistivity was higher than for those cured in RT all the time. That is why the initial m values are small. In general, the trends showed a gradual increase and then a plateau was reached in the calculated *m* value vs. time. The time in which *m* value increases, strongly depends on the ratio of fly ash. Usually, the higher the ratio of fly ash in concrete the longer the period of time in which the *m* value increases. This is because it takes longer time to hydrate the larger amount of pozzolans present on those specimens with higher FA replacement at RT. In the present study, this time duration for the specimen in Group A (20% FA) was 224 days and its *m* values increased from 0.165 to 0.322 while it was 588 days for the specimen in Group D (50% FA) and its *m* values moved from 0.115 to 0.537. On specimens cured 2RT/26ET, the ρ_{21} at 28 days for each mix was significantly larger than the

corresponding ρ_{21} value measured on day 28 for those cured at RT. Upon transferring the specimens to RT from the ET, the reaction rates of the hydrating products likely are slowed down. Eventually, any un-hydrated products that need to hydrate would continue at RT rate. Note that these m values are smaller than those obtained on specimens cured at RT all the time or 2RT/ET curing described in the previous two sections.

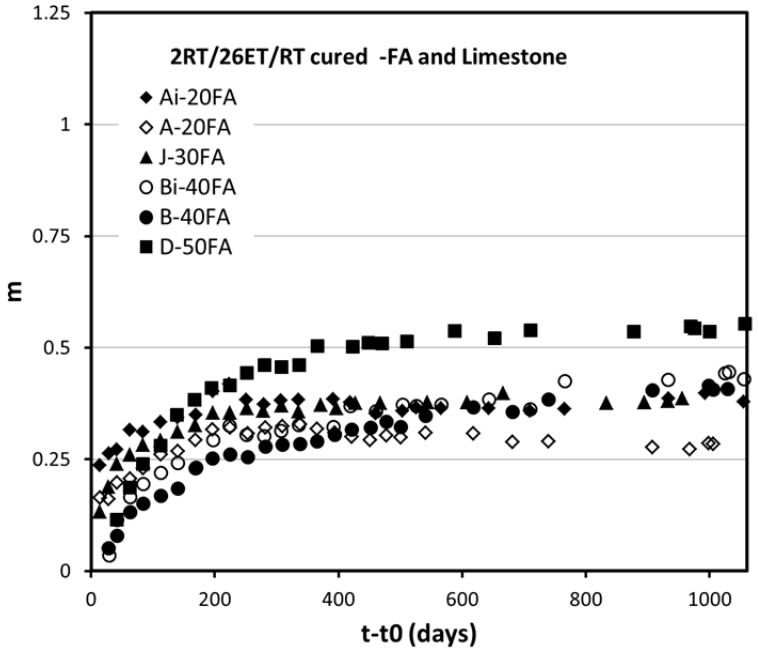

Figure 4.40: Aging factors of specimens in Group (Mix) Ai, A, J, Bi, B and D with the different fly ash ratio and limestone aggregate cured in 2RT/26ET/RT

Figure 4.41 shows the aging factors of specimens in Group (Mix) C, K and L with the different fly ash ratio and granite cured in 2RT/26ET/RT. Here t_0 =28 days. Similar to the previous results, the *m* value increased as time passed. However, the *m* values of specimen in Group C (20% FA+Granite) and K(30%+Granite) in Fig. 4.41 were slightly larger than those of specimen in Group A(20% FA+Limestone) and Group J (30% +Limestone), respectively whereas the *m* value of specimen from Group L (50% FA +Granite) was slightly smaller than the *m* value of specimens in Group D(50% FA+Limestone) for a given t-t0 time. It should be pointed out that this trend might change after a longer exposure.

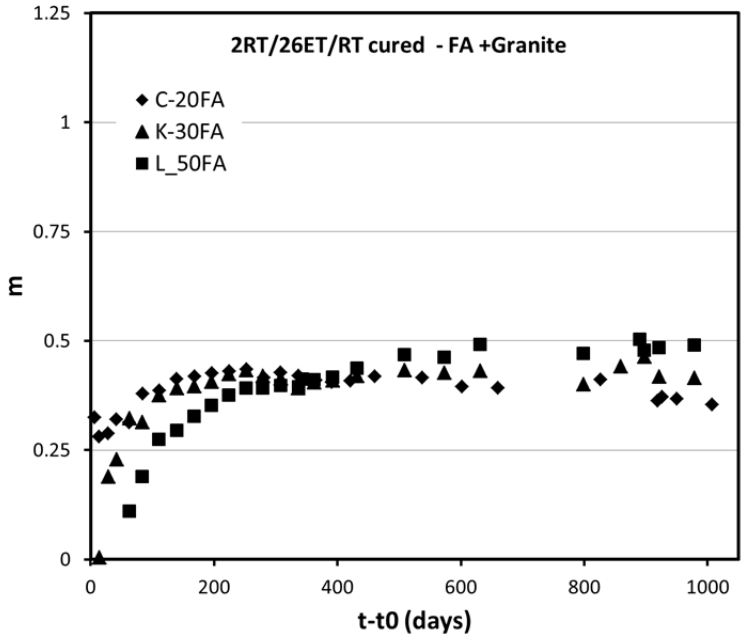

Figure 4.41: Aging factors of specimens in Group (Mix) C, K and L with the different fly ash ratio and granite cured in 2RT/26ET/RT

Figure 4.42 shows the aging factors of specimens in Group (Mix) E (50% slag + limestone), F(70% slag + limestone), I(10% FA+%60Slag), H(20% FA+%50Slag) and G (50% Slag+Granite) cured in 2RT/26ET/RT. Here t_0 =28 days. Generally, the m values increased with time development, which was different from what cured in RT and 2RT/ET. As can be observed from Figure 4.33, the *m* values were generally less than 0.25 before by day 1000. The aging factor evolution for each mix under the different tested curing conditions (including 7RT/21ET/RT and 7RT/ET and 14RT/14ET) is listed in Appendix B.

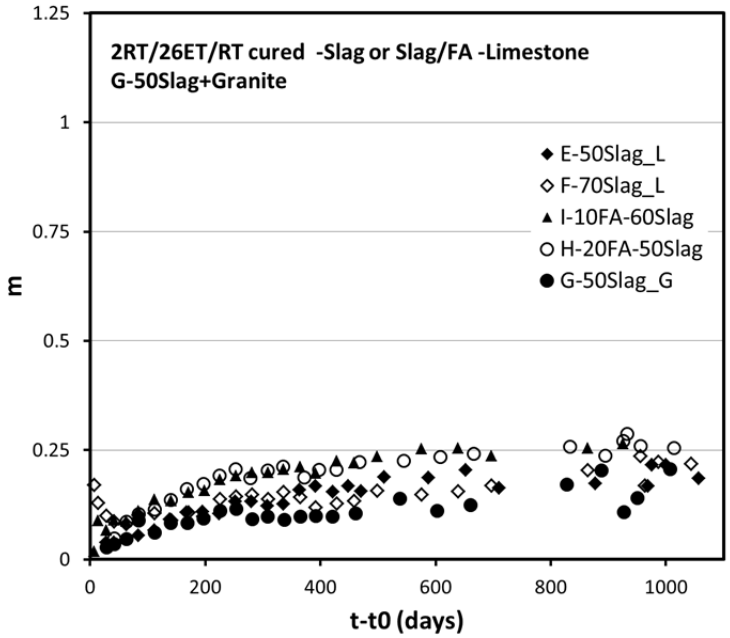

Figure 4.42: Aging factors of specimens in Group (Mix) E (50% slag + limestone), F(70% slag + limestone), I(10% FA+%60Slag), H(20% FA+%50Slag) and G (50% Slag+Granite) cured in 2RT/26ET/RT

4.3.5.7 Porous Surface Layer on Concrete with High Percentage of FA

After the exposure period of RCM test, the specimens were split and $AgNO_3$ was sprayed at the cross section. A phenomenon was observed on some specimens that had a porous surface layer which was less resistive to chloride penetration, as shown in Figure 4.43. This phenomena of porous surface layer was observed on specimens containing >30%FA, with a thickness between 1 mm to 20 mm. The thickness of surface layer increased with increasing replacement ratio of FA. This porous surface layer was not observed (or not obvious) on specimens with 20%FA or with Slag, as shown in Figure 4.44.

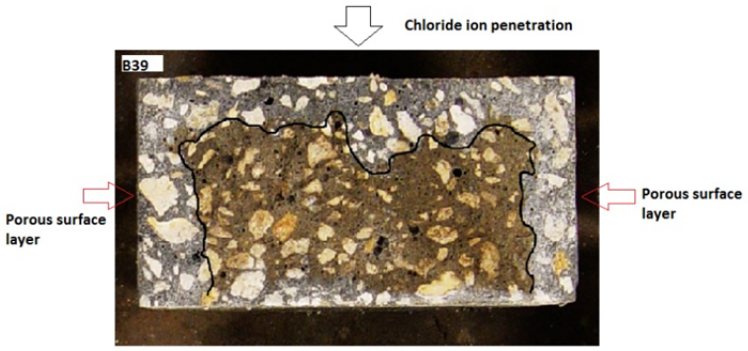

Figure 4.43: Indication of porous surface layer after RCM test on specimens with 40%FA

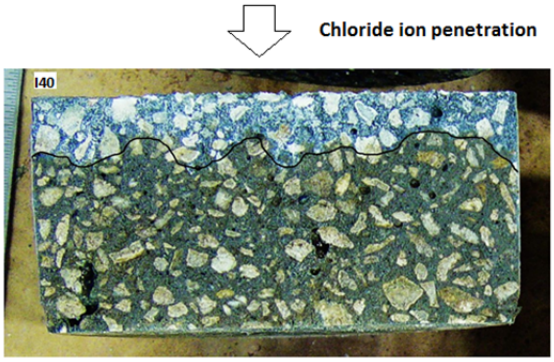

Figure 4.44: Profile of chloride penetration on specimens with 50%Slag/20%FA

The porous surface layer was also observed during resistivity measurement. When the curing lime water was changed to fresh water, there was a sharp increase of resistivity on specimens with ≥40%FA, whereas, this increase of resistivity was not observed on specimens with 20%FA, or with slag, as shown in Figure 4.45. More details are included in Appendix A. It is believed that when specimens with a porous surface layer were immersed in lime water, the surface layer was filled with lime water, which creates a relatively more conductive surface layer. However, when these specimens were immersed in fresh water, the lime in the porous surface layer leached quickly to the fresh water, which made the surface layer less conductive. As a result, the measured resistivity was significantly higher in fresh water than in lime water. For specimens without (or with little) surface layer, this change of pore solution in surface did not or was not obvious, so the resistivity change by changing lime water to fresh water was not observed.

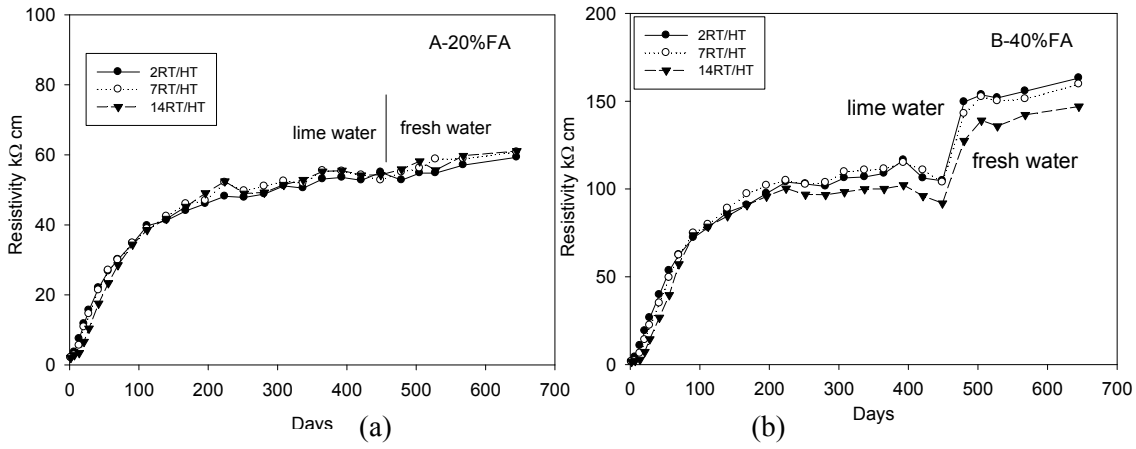

Figure 4.45: Resistivity change by changing lime water to fresh water

The porous surface layer has been reported on specimens cured in air without sufficient time of moist curing. The porous surface observed in this investigation was formed when concrete was cured in lime water. It is possibly because when large replacement ratios of FA were used, the hydration rate during the early age was significantly reduced. So the concrete was more porous during the early age. When these concrete specimens were cured in limewater, the un-hydrated cement grains and FA, as well as Ca $(OH)_2$ in the surface layer, could leach into the lime water. As a result, there was less cement, FA and $Ca(OH)_2$ at the surface, causing a significantly porous surface layer.

Cox et al. also reported the different property of surface layer which was more susceptible to freezing-thawing on concrete with high volume (≥35%) FA cured under 90% humidity[122]. However, the reason which caused the surface layer was not reported.

4.4 Conclusions

1. Accelerated curing by elevated temperature increased both 28-day electrical resistivity and compressive strength than RT curing.

2. Elevated temperature curing increased 1-year resistivity and decreased 1-year diffusion coefficients when compared to those cured all the time at RT. Intermediate resistivity and diffusivity values were observed on those cured for 26 days or 14 days in the elevated temperature room and then transferred to RT conditions.

3. Specimens cured under 2RT/26ET curing regimes were equivalent to 6 to 12 month specimens under RT in terms of both electrical resistivity and compressive strength.

4. The use of granite as coarse aggregate could increase compressive strength, electrical resistivity and decrease chloride ion diffusion coefficients, compared to those with limestone.

5. Under both RT curing regimes, specimens with higher amount of FA showed lower compressive strength and resistivity values, however, under ET curing regimes, specimens with higher amount of FA showed higher compressive strength and resistivity values.

6. Under both RT and ET curing regimes, specimens with Slag showed higher hydration rates then specimens with FA, which was reflected the evolution of electrical resistivity.

7. Aging factor method is applicable on specimens cured under RT for OPC concrete, Slag/FA(≤20%FA) concrete, and concrete with ≤20%FA, up to the test age of 700 days in this investigation.

8. Caution should be used when using aging factor method to predict diffusivity evolution with time, as the value of *m* could be significantly different depending on the replacement ratio and type of pozzolanic admixtures, and the curing regimes.

9. A porous surface layer up to 2 cm thick was observed on specimens with high replacement ratio (>30%) of FA. As concrete cover is most important for durability of concrete structures, attention should be paid on this porous layer when large volume of FA is used.

5. CORRELATION BETWEEN ELECTRICAL RESISTIVITY AND NON-STEADY-STATE MIGRATION COEFFICIENTS

5.1 Introduction and Objectives

The Rapid Chloride Migration (RCM) test (NT Build 492) is one of the most popular methods to determine chloride ion permeability in concrete. The non-steady-state migration coefficients (D_{nssm}) from RCM test have been used in predicting the service life of reinforced concrete structures[7]. Although the RCM test is a widely used and promising accelerated test method for chloride ion permeability, there is a need to develop an alternative non-destructive test (NDT) method as an alternative of the RCM test. According to Nernst-Einstein equation, chloride diffusion coefficient is inversed to the electrical resistivity of concrete as stated in Equation 2-22:

$$D_{Cl^-} = \frac{K_{D,\rho}}{\rho} \tag{5-1}$$

Experiments also have been performed by DuraCrete to study the correlation between concrete resistivity and D_{nssm}[7]. However, DuraCrete only reported concrete with resistivity from 5kΩ cm to 90 kΩ cm and the resistivity was measured using two-electrode method. As FDOT has replaced the Rapid Chloride Permeability (RCP) test with the four-point electrical resistivity method (Wenner method)[14], there is a desire to study the correlation between D_{nssm} from RCM test and electrical resistivity by four-point method.

In this investigation, the RCM test as well as resistivity measurement were conducted on specimens from various mix designs with electrical resistivity ranging from 5kΩ cm to 340 kΩ cm. Resistivity was measured according FM 5-578.

The objectives of this investigation include:

● Study the correlation between D_{nssm} from RCM test and electrical resistivity by four-point method.

● Study the possibility of using non-destructive resistivity measurement as an alternative method of RCM test to evaluate chloride permeability of concrete structures.

5.2 Experimental Procedure

5.2.1 Materials

Specimens used in this investigation were from the same mixes described in Chapter 3 and Chapter 4. Details of the mixes were given in Table 3.1 (Group1), Table 3.3(Group 2), Table 3.4 (Group 3) and Table 4.1 (Group 4). All the specimens were 10cm×20cm (4×8in) concrete cylinders. Two concrete cylinders were selected from each mix in Table 3.1; three concrete cylinders were selected from each mix in Table 3.2 and 3.3; ten cylinders (two per curing regime) were selected from each mix in Table 3.4, and the details of curing regimes for each cylinder is listed in Table 4.2.

5.2.1 Experimental Methods

All the specimens were immersed in water so that they were fully saturated prior to the tests. Resistivity was measured according to FM 5-578 and water temperature was recorded. The measured resistivity (ρ_{app}) was firstly corrected by geometry cell constant ($K_{\rho,g}$=1.89), and then the corrected resistivity was normalized to resistivity at 21°C (ρ_{21}) using general equations developed in Chapter 3.

RCM test was performed according to NT Build 492. However, preconditioning the concrete with a vacuum setup was not used in this experiment as the specimens were already saturated. The cylinders were were sliced using a wet saw and two slices (slice A and slice B) from each cylinder were subjected to RCM test, as illustrated in Figure 5.1. D_{nssm} of each cylinder was the average value of the two slices. Illustrations of slicing specimens with a wet saw and setup of RCM test are shown in Figure 5.2 and Figure 5.3, respectively.

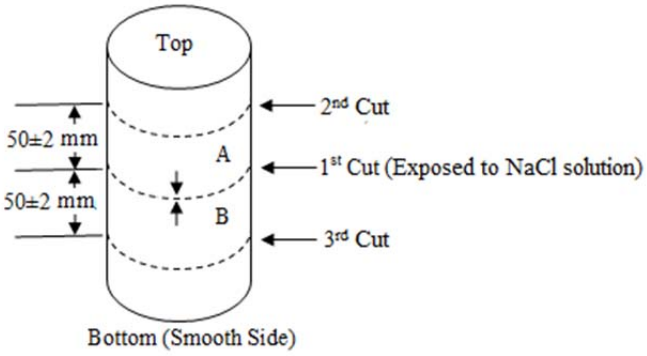

Figure 5.1: Procedure of slicing specimens

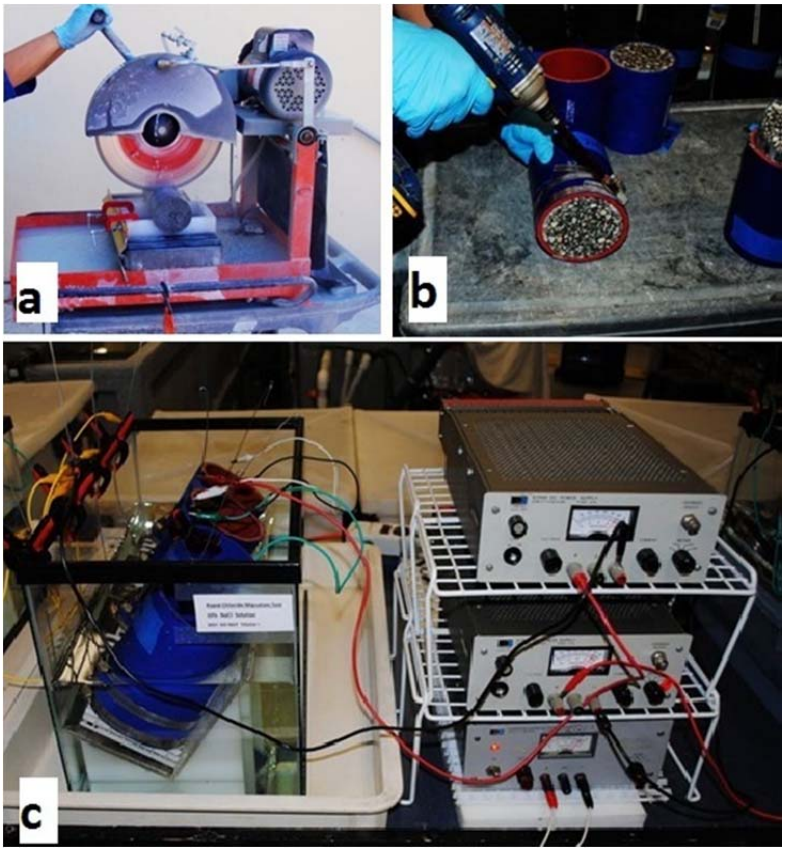

Figure 5.2: Illustration of (a)slicing specimens and (b, c) setup of RCM test

After the exposure period, the tested slices were split into halves and 0.1N $AgNO_3$ was sprayed at the cross section as indication of chloride ion penetration depth, and then a caliper was used to measure the penetration depth, as shown in Figure 5.3 and Figure 5.4. D_{nssm} was then calculated according to Equation 2-13.

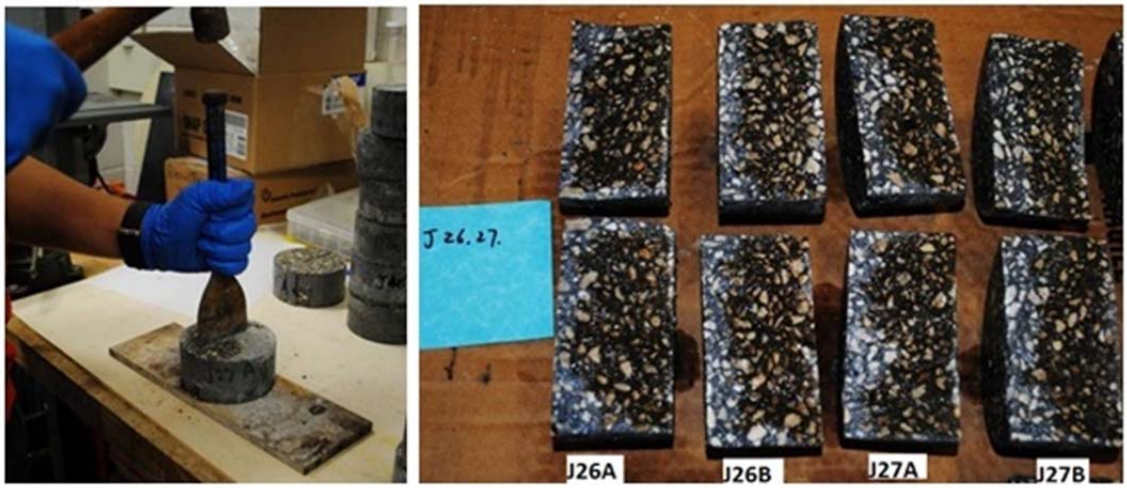

Figure 5.3: Illustration of splitting slices and spraying 0.1N AgNO3 at the cross section as indication of chloride ion penetration depth

Figure 5.4: Measurement of chloride ion penetration depth

5.3 Results and Discussion

5.3.1 Results

Table 5.1 shows an example of the procedure used to calculate 21°C resistivity and D_{nssm} on specimen J26. For all the tested specimens, D_{nssm} calculated from slice A and B were similar. Table 5.2 shows the results of D_{nssm} and ρ_{21} on specimens from Group 1 to Group 3. Results of D_{nssm} and ρ_{21} for specimens from Group 4 are shown in Table 4.5.

Table 5.1: Electrical resistivity and D_{nssm} of specimen J26

Specimen ID: J26

Resistivity - Wenner Method

Date: 1/24/2012

Spacing: 3.8 cm Geometry Factor: K=1.89

Water T: 21.2 ˚C

	0°	90°	180°	270°	0°	90°	180°	270°	ρ_{avg}	ρ_{avg}/K	ρ_{21}
Res. (kΩ cm)	96	97	90	90	88	91	91	91	91.8	48.5	48.9

Slice Thickness (mm)

	t_0	t_{90}	t_{180}	t_{270}	t_{avg}
Slice A	50.2	50.4	50.8	51.3	50.7
Slice B	49.9	51.4	50.2	50.1	50.4

Rapid Migration Test

	I_{30V} (mA)	Adjst V	Adjst I (mA)	Test t (hours)	$T_{initial}$ (˚C)	T_{end} (˚C)	T_{avg} (˚C)	Start Time	End Time	Start Date	End Date
Slice A	8	60	-	48	22.8	23.9	23.4	1:05 PM	1:05 PM	1/25/2012	1/27/2012
Slice B	8	60	-	48	22.8	23.5	23.2	1:05 PM	1:05 PM	1/25/2012	1/27/2012

Chloride Penetration Depth (mm)

	1	2	3	4	5	6	7	Average
Slice A	14.1	8.0	8.7	8.2	10.2	10.7	9.7	9.9
Slice B	12.6	12.4	9.9	11.7	11.8	12.8	14.6	12.3

No-steady-state Migration Coefficient

	D_{nssm} (x10^{-12} m^2/s)
Slice A	1.13
Slice B	1.40
Average	1.26

Table 5.2: D_{nssm} and 21°C resistivity of specimens from Group1, 2 and 3

Specimen No.	ρ_{21} kΩ cm	D_{nssm} $10^{-12}m^2/s$	Specimen No.	ρ_{21} kΩ cm	D_{nssm} $10^{-12}m^2/s$
1C1-11	4.8	31.87	2A	41.3	2.46
1C1-12	4.8	34.17	2B	49.2	2.37
1C2-1	28.5	2.97	7A	43.9	1.10
1C2-8	23.9	3.77	7B	46.1	2.07
1C3-2	58.6	1.39	31A	41.4	2.71
1C3-4	67.6	1.20	31B	43.4	2.06
R2-A	47.2	2.78	17A	107.3	1.09
R2-B	43.4	2.96	17B	110.9	0.95
R2-C	26.2	3.12	18A	94.1	0.99
R3-A	51.9	1.82	18B	99.3	1.15
R3-B	48.7	1.65	19A	89.8	0.91
R3-C	50.8	1.39	19B	85.2	0.75
R4-A	57.1	1.10	23A	109.0	0.99
R4-B	57.0	1.10	23B	99.0	0.90
R4-C	48.6	1.71	35A	81.8	1.69
R5-A	24.0	3.98	35B	82.4	1.74
R5-B	24.2	3.87	37A	58.7	1.99
R5-C	25.9	2.43	37B	55.9	1.96
R6-A	9.2	11.78	42A	108.4	1.15
R6-B	9.2	20.05	42B	109.0	0.84
R6-C	8.5	20.17	49A	24.6	4.54
R7-A	107.5	0.67	49B	25.4	3.81
R7-B	105.1	0.71	16A	84.6	1.12
R7-C	76.9	1.42	16B	89.2	1.25
R8-A	149.0	0.57	22A	75.9	1.21
R8-B	147.9	0.65	22B	89.6	1.07
R8-C	100.8	0.92	34A	87.5	1.42
R9-A	43.0	2.02	34B	86.6	1.58
R9-B	45.5	1.95	44A	19.8	9.26
R9-C	41.9	1.73	44A	16.4	6.31
R10-A	170.0	0.44	47A	23.0	5.43
R10-B	163.0	0.57	47B	21.6	3.87
R10-C	91.1	1.50	32B	40.3	2.75
R11-A	68.0	0.80			
R11-B	67.0	0.99			
R11-C	51.3	1.38			
R12-A	30.4	2.19			
R12-B	32.5	2.10			
R12-C	28.9	2.68			

5.3.2 Discussion

5.3.2.1 Correlation between D_{nssm} and ρ_{21}

The correlation between D_{nssm} and ρ_{21} is described in Equation 5-1. To verify this correlation, the values of parameter $K_{D,\rho}$ were obtained from the experimental results. Figure 5.5 shows the correlation between D_{nssm} and ρ_{21} on OPC concrete, including Mix 1C, R6 and results from test on specimens from previous FAU projects. It shows that for OPC concrete, the value of $K_{D,\rho}$ is 156.7. Figure 5.6 shows that the value of $K_{D,\rho}$ is 92.6 by fitting results from Group 1, Group2 and Group 3 excluding OPC specimens. Figure 5.7 shows results from Group 4 including specimens with moderate air content (Mix A-L) and high air content (Mix Ai and Bi), in which the value of $K_{D,\rho}$ was calculated separately. Results in Figure 5.7 show that, the value of $K_{D,\rho}$ is 120.1 for concrete with higher air content, however, the value of $K_{D,\rho}$ is 89.0 for concrete with moderate air content, which is similar to the value obtained by fitting the data shown in Figure 5.6 ($K_{D,\rho} = 92.1$). By combining data in Figure 5.6 and Figure 5.7 (excluding Mix Ai and Bi), a new fitting plot was calculated as shown in Figure 5.8, giving $K_{D,\rho} = 90.7$.

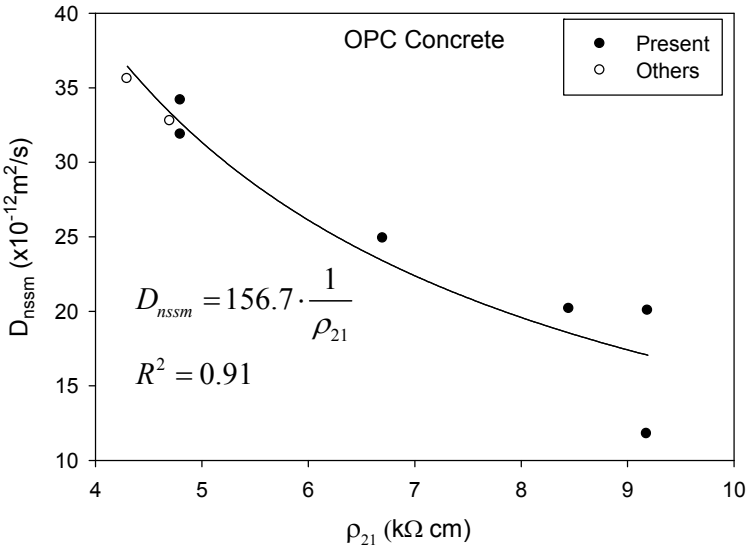

Figure 5.5: Correlation between D_{nssm} and ρ_{21} on OPC concrete specimens

By comparing the products of $K_{D,\rho} = D_{nssm} \times \rho_{21}$ from the test results, it is found that the value of K = 156 is significantly larger for concrete with OPC only. The K value of 120 for concrete with large air content (>10% Mixes Ai and Bi) is also high.

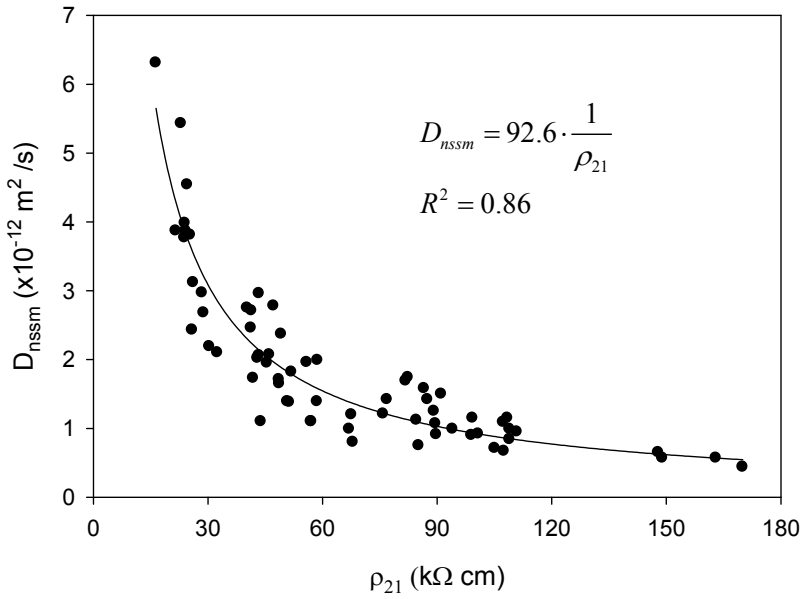

Figure 5.6: Correlation between D_{nssm} and ρ_{21} on specimens from Group 1, 2 and 3 excluding OPC specimens

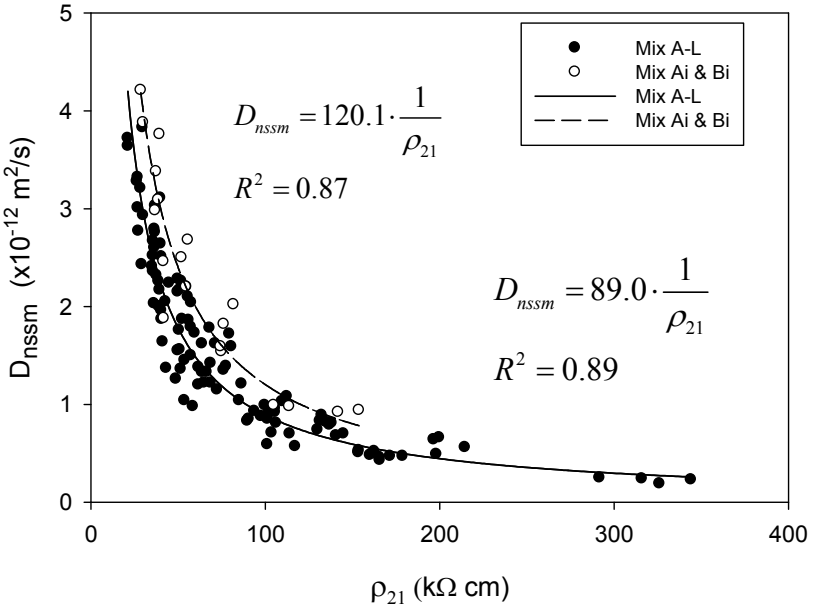

Figure 5.7: Correlation between D_{nssm} and ρ_{21} on specimens from Group 4

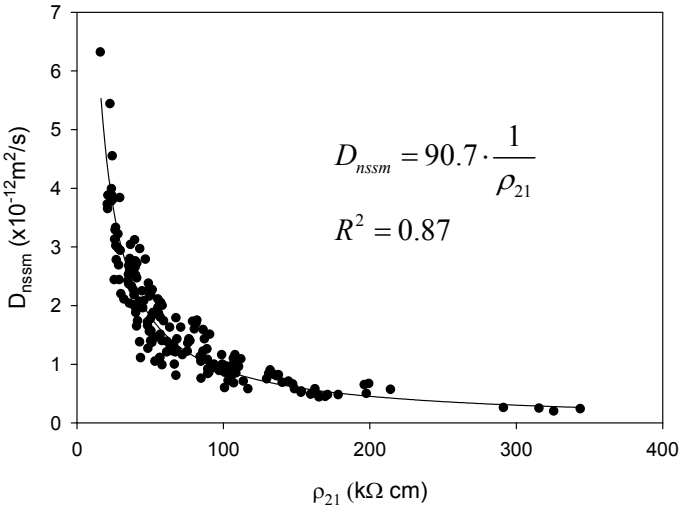

Figure 5.8: Correlation between D_{nssm} and ρ_{21} on specimens from Group 1 to Group 4 excluding OPC (Mix 1C) and high air content specimens (Mix Ai and Bi)

Figure 5.9 includes results from specimens in Group 1 to 4 and test on specimens from previous or parallel FAU projects (FAU-projects). The correlation between D_{nssm} and ρ_{21} based on the data shown in Figure 5.9 is:

$$D_{nssm} = 105.5 \cdot \frac{1}{\rho_{21}} \tag{5-2}$$

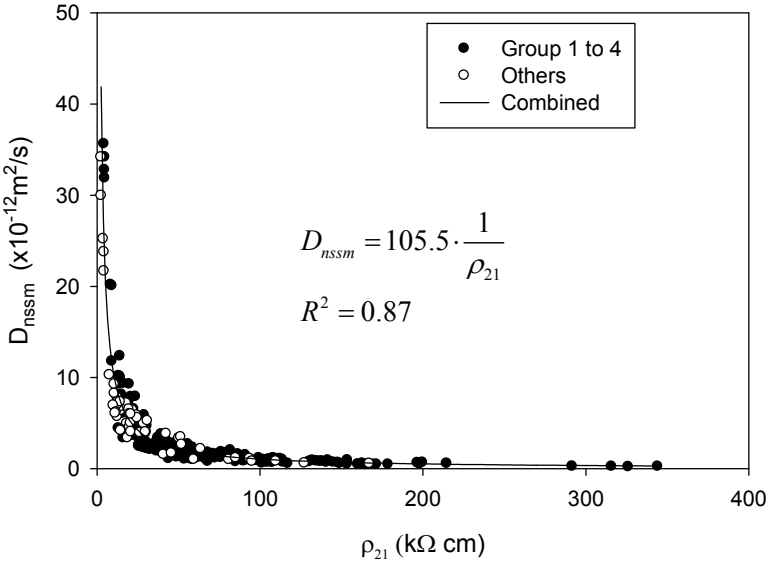

Figure 5.9: Correlation between D_{nssm} and ρ_{21} on specimens from Group 1 to Group 4 and other projects (FAU)

The values of parameter $K_{D,\rho}$ from the above correlations are summarized in Table 5.3.

Table 5.3: The values of parameter $K_{D,\rho}$ corresponding to Fig. 5.5 to Fig. 5.9

Group	$K_{D,\rho}$ (x 10-2 kΩ·m-3/s)	R^2	Residual	Fig. No.
OPC	156.70	0.91	7.64	Fig. 5.5
Groups 1, 2 & 3 excluding OPC	92.60	0.86	0.21	Fig. 5.6
Group 4i excluding Ai+Bi	89.03	0.89	0.09	Fig. 5.7
Ai + Bi	120.10	0.87	0.14	Fig. 5.7
Groups 1 to 4 excluding OPC & Ai+Bi	90.70	0.87	0.13	Fig. 5.8
Groups 1 to 4 & other FAU projects	105.50	0.87	3.76	Fig. 5.9

5.3.2.2 Correlation between D_{nssm}, ρ_{21} and Resistance to Chloride Penetration

Nilsson et al. [32] proposed a correlation between D_{nssm} and resistance to chloride penetration in concrete, and was included in chapter 2 as Table 2.4. Here the correlation is extended to include the corresponding electrical resistivity. Recall, that ρ_{21} and D_{nssm} are correlated by Equation 5-2. By combing the results from Table 2.4, and Equation 5-2, it is possible to evaluate concrete specimens' resistance to chloride penetration by resistivity measurement. The suggested correlation is shown in Table 5.4:

Table 5.4: Correlation between 28-day D_{nssm}, ρ_{21} and resistance to chloride penetration

D_{nssm} $\times 10^{-12}$ m^2/s	ρ_{21} kΩ cm	Resistance to chloride penetration
>15	<7	Low
10-15	7-11	Moderate
5-10	11-21	High
2.5-5	21-42	Very high
<2.5	>42	Extremely high

The correlation in Table 5.4 is based on the 28-day chloride diffusivity, a modified correlation is shown in Table 5.5 that extends to ρ_{21} and D_{nssm} obtained on mature concrete specimens.

Table 5.5: Modified correlation between D_{nssm}, ρ_{21} and resistance to chloride penetration regardless of concrete age

D_{nssm} $\times 10^{-12}$ m^2/s	ρ_{21} kΩ cm	Resistance to chloride penetration
>15	<7	Low
10-15	7-11	Moderate
5-10	11-21	High
1-5	21-106	Very high
<1	>106	Extremely high

5.3.2.3 Effect of Admixtures on Parameter $K_{D,\rho}$

In Section 5.3.2.1, $K_{D,\rho}$ was calculated and discussed for six different groups. Additional $K_{D,\rho}$ were calculated and are presented in this section. The $K_{D,\rho}$ values were calculated by grouping the results depending on the type and/or amount of admixture added to the concrete mix. The $K_{D,\rho}$ results of these additional computations are shown in Table 5.6. As it was indicated in the previous section, the specimens with OPC only had the largest $K_{D,\rho}$ value, which is 157.64×10^{-2} kΩ-m^3/s here. The, value of $K_{D,\rho}$ decreased on concrete specimens with mineral admixtures, for example, the value of $K_{D,\rho}$ was 94.00×10^{-2} kΩ-m^3/s for specimen with FA (18% to 39%) and the $K_{D,\rho}$, value was 83.30×10^{-2} kΩ-m^3/s for specimens with FA(20%) + Silica Fume (4% to 8%). It is also seen that the $K_{D,\rho}$ values of specimens with FA (20 to 50%) +Limestone ranged from 84 to 103×10^{-2} kΩ-m^3/s with an average $K_{D,\rho}$ value of 96.7×10^{-2} kΩ-m^3/s, which was very close to the average calculated $K_{D,\rho}$ value (97.08×10^{-2} kΩ-m^3/s) obtained from specimens with FA/Slag (20/50, 10/60). For the specimen with FA (20%-50%) + Granite, the $K_{D,\rho}$ values ranged between 80.99 and 74.39×10^{-2} kΩ-m^3/s with an average $K_{D,\rho}$ value of 75.16×10^{-2} kΩ-m^3/s suggesting that the presence of Granite and FA tend to lower the $K_{D,\rho}$, value more than the presence of limestone and FA. The lowest calculated $K_{D,\rho}$, value corresponded to that obtained on specimens with Slag and Granite. A graphical comparison of $K_{D,\rho}$ values for the various groupings can be seen in Figure 5.10.

Table 5.6: The values of parameter $K_{D,\rho}$ under different group*

Group	$K_{D,\rho}$ (x 10^{-12} kΩ - m^{-3}/s)	Residual
1. OPC	157.64	14.173
2. FA (18% to 39%)	94.00	0.239
3. FA 20%+SF(4% to 8%)	83.30	0.037
4. FA 20%+Limestone	103.72	0.065
5. FA 30%+Limestone	84.17	0.084
6. FA 40%+Limestone	95.86	0.030
7. FA 50%+Limestone	100.08	0.035
8.FA +Limestone - Average	96.75	0.067
9. FA/Slag (10/60)	91.82	0.067
10.FA/Slag (20/50)	103.91	0.068
11.FA/Slag - Average	97.08	0.072
12.FA 20 % +Granite	80.99	0.122
13.FA 30 % +Granite	66.52	0.019
14.FA 50 % +Granite	74.39	0.002
15.FA+Granite- Average	75.16	0.043
16.Slag 50%	83.81	0.166
17.Slag 70%	84.26	0.100
18.Slag - Average	83.96	0.118
19.Slag + Granite	62.62	0.105

Note:

1. OPC: 1C1; A6 in Table 5.2;
2. FA (18% to 39%): 1C2, R2,R3,R4, R5, R8C, R10,R11,2A,2B,7A,7B,31A,31B,35A,35B,37A,37B,49A,49B,44A,32B in Table 5.2;
3. FA (20%)+SF(4% to 8%): 1C3, R7, R9 in Table 5.2 ;
4. FA 20% +Limestone: A10, A11,A24,A25,A26,A27,A37,A38,A39,A40 in Table 4.7;
5. FA 30% +Limestone: J10, J11,J24,J25,J26,J27,J37,J38,J39,J40 in Table 4.7;
6. FA 40% +Limestone: B10, B11,B24,B25,B26,B27,B37,B38,B39,B40 in Table 4.7;
7. FA 50% +Limestone: D10, D11,D24,D25,D26,D27,D37,D38,D39,D40 in Table 4.7;
8. FA+Limestone – Average: All specimens from 4 to 7;
9. FA/Slag(10/60): I10, I11,I24,I25,I26,I27,I37,I38,I39,I40 in Table 4.7;
10. FA/Slag(20/50): H10, H11,H24,H25,H26,H27,H37,H38,H39,H40 in Table 4.7;
11. FA/Slag –Average: All specimens from 8 to 9;
12. FA 20% +Granite: C10, C11,C24,C25,C26,C27,C37,C38,C39,C40 in Table 4.7;
13. FA 30% +Granite: K10, K11,K24,K25,K26,K27,K37,K38,K39,K40 in Table 4.7;
14. FA 50% +Granite: L10, L11,L24,L25,L26,L27,L37,L38,L39,L40 in Table 4.7;
15. FA+Granite – Average: All specimens from 12 to 13;
16. Slag 50%: E10, E11,E24,E25,E26,E27,E37,E38,E39,E40 in Table 4.7;
17. Slag 70%: F10, F11,F24,F25,F26,F27,F37,F38,F39,F40 in Table 4.7;
18. Slag – Average: All specimens from 15 to 16;
19. Slag +Granite: G10, G11,G24,G25,G26,G27,G37,G38,G39,G40 in Table 4.7.

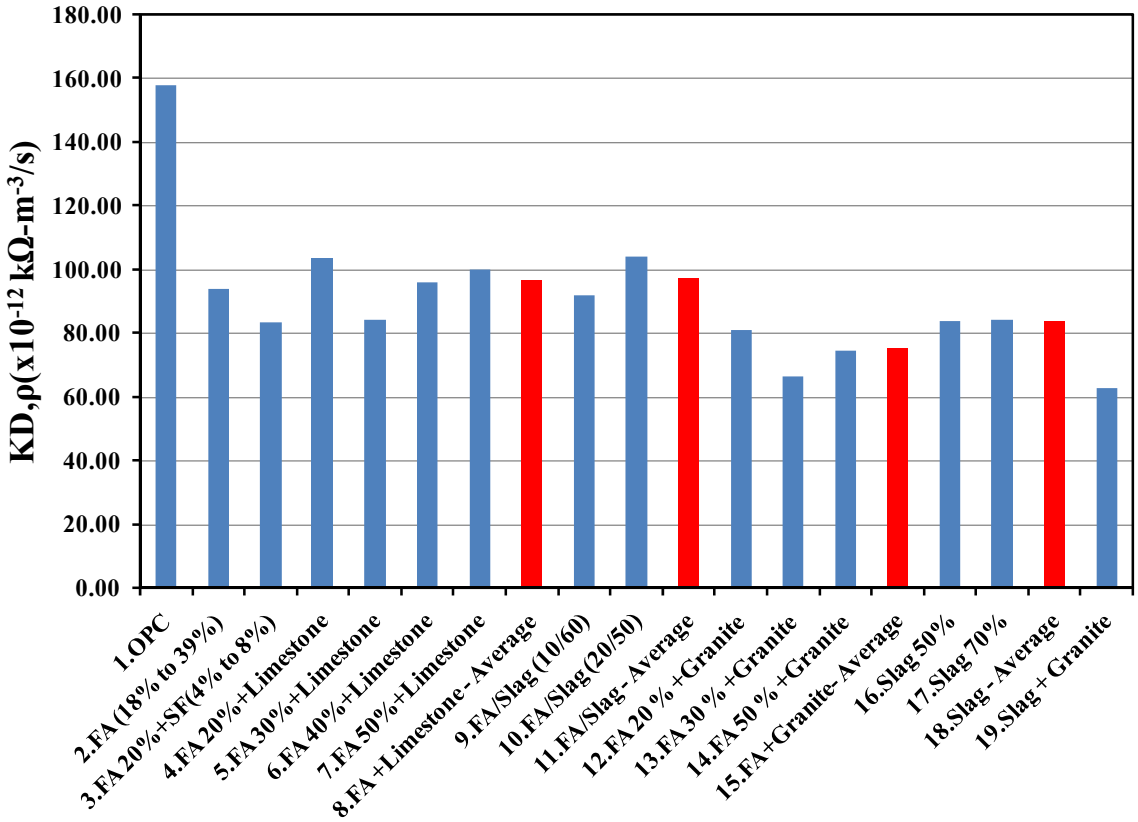

Figure 5.10: Effect of Admixtures on Parameter $K_{D,\rho}$

5.3.2.4 Comparison with Results Found in the Literature

The value of constant $K_{D,\rho}$ obtained in Equation 5-2 is 105.5, which is similar to the value by Dura Crete ($K_{D,\rho} = 96.5$) as shown in Figure 2.10. Table 5.5 shows comparison of chloride ion permeability classification based on the results from this investigation (Table 5.4) and results by FDOT (Table 2.5). In this investigation, the classification of resistance of chloride penetration was based on the correlation between D_{nssm} and resistivity. In FDOT's research, the classification of chloride ion permeability was based on the correlation between RCP and resistivity. By comparing the two classification methods in Table 5.7, it indicates that the classification of chloride permeability from the present investigation is in agreement with that from FDOT.

Table 5.7: Comparison of chloride ion permeability classification based on D_{nssm} vs. Resistivity (Table 5.4) and RCP vs. Resistivity (Table 2.5)

D_{nssm} vs. Resistivity			RCP vs. Resistivity		
D_{nssm} $\times 10^{-12}$ m^2/s	ρ_{21} kΩ cm	Resistance to chloride penetration	RCP test (coulombs)	ρ kΩ cm	Chloride ion permeability
>15	<7	Low	>4000	<6.7	High
10-15	7-11	Moderate	2000-4000	6.7-11.7	Moderate
5-10	11-21	High	1000-2000	11.7-20.6	Low
1-5	21-106	Very high	100-1000	20.6-141.1	Very low
<1	>106	Extremely high	<100	>141.1	Negligible

5.4 Conclusions

1. A correlation between D_{nssm} and ρ_{21} was obtained, and the value of $K_{D,\rho}$ is 105.5 for all the tested specimens. A value of $K_{D,\rho}$ = 90.7 was observed when the correlation included only values obtained on concrete with $\rho_{21} > 15$kΩ cm and moderate air content.

2. Based on the results from this investigation, it is possible to use resistivity measurement as a non-destructive method to replace (or be used as an alternative to) the RCM test to evaluate chloride ion permeability of concrete.

6. TEMPERATURE DEPENDENCE OF CHLORIDE DIFFUSIVITY IN CONCRETE

6.1 Introduction

Chloride diffusivity is an important parameter for service life of reinforced concrete structures. The time to corrosion initiation period (T_i) is fundamentally dependent on chloride diffusivity. RCM test (NT Build 492) is one of the most popular test methods to determine chloride diffusivity in concrete. DuraCrete has employed the non-steady-state migration coefficient (D_{nssm}) from the RCM test to predict service life of reinforced concrete structures[7]. However, chloride diffusivity in concrete has been found to be dependent on temperature, and usually diffusivity coefficients increase with increasing temperature. The Arrhenius equation (Equation 2-35) is widely accepted to describe the relationship between temperature and chloride diffusivity, moreover, the activation energy for diffusivity ($E_{a,D}$) has been found ranging from 15.5 kJ/mol to 45 kJ/mol[74-78].

Due to the importance of temperature effect on chloride diffusivity, it is necessary to consider the temperature effect while predicting the service life of reinforced concrete structures. Because of the large range of reported $E_{a,D}$ values, an adequate $E_{a,D}$ value should be used so that the temperature effect is precisely considered. However, how to choose the value of $E_{a,D}$ is still unknown.

The objectives of this investigation include:

● Study the temperature effect on chloride ion diffusivity in concrete by RCM test.

● Determine $E_{a,D}$ values on concrete with different diffusivity (or resistivity).

● Study the correlation of activation for resistivity ($E_{a,\rho}$) and activation for diffusivity ($E_{a,D}$).

● Find an alternative method to apply $E_{a,D}$ values in Arrhenius equation in prediction of service life of reinforced concrete structures.

6.2 Experimental Procedure

6.2.1 Materials

Six mix designs were used in this investigation, including a set of OPC specimens and specimens with pozzolanic admixtures. Mix 1C, 2C, and 3C were the same as listed in Table 3.4 and details of the other three mixes are shown in Table 6.1. All the specimens were 10cm ×20cm (4×8in) cylinders. Before the RCM tests were carried, specimens from Mix 1C, 2C and 3C were cured under high humidity (95%) environment for more than three years and then immersed in water for more than half a year. Specimens from Mix CRA, DCL1 and DCL10 were cured under RT in limewater for one week and then cured in 35°C from 1 month to three months to obtain different ranges of resistivity/diffusivity values.

Table 6.1: Mix design of specimens

Mix No.	Cement Type	Coarse agg. Type	Cement (kg/m^3)	FA (kg/m^3)	Water (kg/m^3)	Fine agg. SSD (kg/m^3)	Coarse agg. SSD (kg/m^3)	w/cm	% FA
CRA	type I/II	Limestone	351	39	163	721	951	0.42	10
DCL1	type I/II	Limestone	312	78	137	653	1063	0.35	20
DCL10	type I/II	Limestone	268	67	137	766	1009	0.41	20

6.2.2 Experimental Methods

According to the resistivity values, specimens from Mix DCL1 were separated into three groups (DCL1-I, DCL1-II and DCL1-III), and each group included eight cylinders. Totally eight groups from six mix designs were tested and each group included four to eight cylinders.

Prior to the RCM test, dynamic temperature tests (DTTs) were performed on two cylinders from each group (CRA, DCL1-I, DCL1-II, DCL1-III and DCL-10) to calculate the 21°C resistivity (ρ_{21}) and activation energy for resistivity ($E_{a,\rho}$). As DTTs were already performed on specimens from Mix 1C, Mix 2C and Mix 3C as presented in Chapter 3, the activation energy of specimens from these Mixes were calculated using Equation 3-3.

To investigate the temperature effect on chloride ion diffusivity, RCM tests were performed at 10°C, 23°C, 30°C and 40°C. Test setup and procedure were similar to those described in section 5.2.

23°C test environment was obtained by performing RCM test in the laboratory at room temperature as shown in Figure 5.2(c).

To obtain the 10°C test environment, a fresh water tank connected to a chiller was used, and the RCM test tank was immersed in the fresh water tank to 2/3 of the height. The temperature of the fresh water was controlled at around 8°C and temperature of the 10% NaCl in the RCM test tank was at around 10°C. A small pump was placed in the RCM test tank to circulate the salt water so that temperature in the tank was uniformly distributed. A schematic illustration of the test setup is shown in Figure 6.1. One day before the RCM test was conducted, a bottle filled with 0.1M NaOH as well as the concrete slices was immersed in the fresh water tank. At the same time, 10% NaCl solution was filled to the RCM test tank. The next day, when the NaOH solution, 10%NaCl solution and concrete sliced reached 10°C, the RCM test was set up and started.

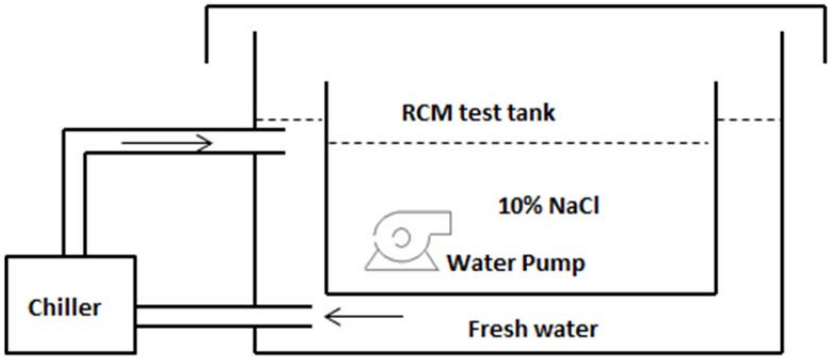

(a)

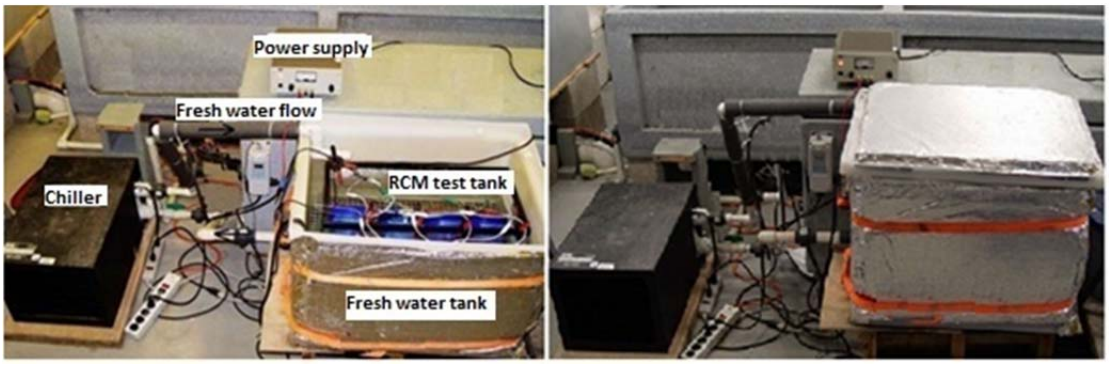

(b)

Figure 6.1: Schematic illustration of setup for RCM test at 10°C

The 30°C and 40°C test environments were obtained by performing RCM test in a room with air temperature at around 32°C and 42°C, respectively. The room temperature was controlled by heaters connected to digital thermostats. A fan was placed in the room to circulate the air. An illustration of the test setup is shown in Figure 6.2. One day before the RCM test was conducted, the solutions (0.1 M NaOH and 10% NaCl) filled in buckets with lids, together with the concrete slices immersed in lime water, were stored in the test room with elevated temperature. The RCM test was set up and performed the next day when the temperature of the solutions and concrete slices had reached the target test temperature.

Figure 6.2: Schematic illustration of setup for RCM test at 30°C and 40°C

6.3 Results and Discussion

6.3.1 Results

Non-steady-state migration coefficients (D_{nssm}) were calculated with Equation 2-13 and all the temperature T in the equation was set as 21°C. The average of the initial catholyte (0.1M NaOH) and anolyte (10% NaCl) temperature was taken as the initial test temperature and the average of the final catholyte and anolyte temperature was taken as the final test temperature. The test temperature was the average of the initial and final test temperatures. Activation energy for diffusivity ($E_{a,D}$) and D_{nssm} at 21°C ($D_{nssm,21}$) were calculated using the Arrhenius equation:

$$D_T = D_\infty \cdot \exp\left[-\frac{E_{a,D}}{R}\left(\frac{1}{T+273.15}\right)\right] \quad (6\text{-}1)$$

Where D_T is the diffusion coefficient at temperature T (°C); D_∞ is the diffusion coefficient when $T \to +\infty$. For specimens from Mix 1C, 2C and 3C, the values of ρ_{21} and $E_{a,\rho}$ were calculated by resistivity measured at room temperature using Equation 3-2. For specimens from the other groups, the values of ρ_{21} and $E_{a,\rho}$ were calculated by DTT tests performed at temperature between 10°C to 45°C.

Figure 6.3 shows results of D_{nssm} vs. temperature for all the tested groups. Details of the results and calculated parameters including $E_{a,D}$, ρ_{21} and $E_{a,\rho}$ are shown in Table 6.2.

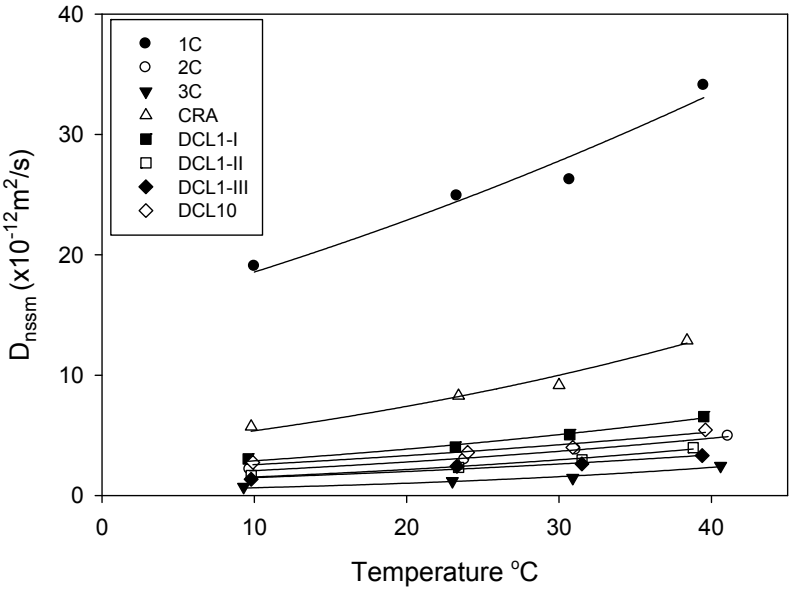

Figure 6.3: Evolution D_{nssm} of with temperature

Table 6.2: Chloride ion migration coefficients, resistivity and activation energy

Group ID	Number of cylinders	T °C	D_{nnsm} $x10^{-12}m^2/s$	$D_{nnsm,21}$ $x10^{-12}m^2/s$	$E_{a,D}$ kJ/mol	ρ_{21}* kΩ cm	$E_{a,\rho}$** kJ/mol	K $D_{nnsm,21}\times\rho_{21}$
1C	1	10.0	19.05	23.33	14.4	6.6	15.7	154
	1	23.3	24.90					
	1	30.7	26.23					
	2	39.5	34.08					
2C	2	9.7	2.15	2.87	19.4	25.2	23.7	72
	1	23.8	2.97					
	2	31.1	3.79					
	2	41.1	4.93					
3C	1	9.3	0.71	1.07	31.6	70.7	30.0	76
	1	23.0	1.20					
	1	30.9	1.46					
	1	40.6	2.46					
CRA	2	9.8	5.72	7.64	21.4	9.7	20.4	74
	2	23.4	8.29					
	2	30.0	9.16					
	2	38.4	13.12					
DCL1-I	2	9.6	3.03	3.96	20.1	23.2	23.8	92
	2	23.2	4.03					
	2	30.7	5.06					
	2	39.5	6.55					
DCL1-II	2	9.8	1.66	2.23	21.8	36.9	23.0	82
	2	23.4	2.33					
	2	31.5	2.97					
	2	38.8	3.97					
DCL1-III	2	9.8	1.34	2.05	20.7	42.3	22.9	87
	2	23.3	2.43					
	2	31.5	2.63					
	2	39.4	3.32					
DCL10	2	9.9	2.75	3.28	23.0	28.0	21.7	92
	2	24.0	3.59					
	2	30.9	4.00					
	2	39.6	5.45					

*: Average of all the tested cylinders;
**: Calculated with Equation 3-2 for 1C, 2C and 3C; others were calculated by dynamic temperature test.

6.3.2 Discussion

6.3.2.1 Correlation between D_{nssm} and Temperature

The plots in Figure 6.3 indicate that for all the tested groups, diffusivity coefficients were found to increase with increasing temperature. It also indicates that temperature effect seems to be more significant for specimens with higher diffusivity coefficients (1C) than those with lower diffusivity coefficients (3C), as the plot of 3C looks more "flat" than that of 1C. But comparing the diffusivity values in Table 6.2, the diffusivity value of Group 1C was about $19\times10^{-12}m^2/s$ at 10°C and $34\times10^{-12}m^2/s$ at 40°C,

so the diffusivity at 40°C was about 1.8 times of the diffusivity at 10°C; whereas, the diffusivity value of Group 3C at 40 °C ($2.46\times10^{-12}m^2/s$) was about 3.5 times of the diffusivity at 10°C ($0.71\times10^{-12}m^2/s$), which indicates that temperature effect should be more significant on specimens with lower diffusivity values than on those lower higher diffusivity values.

6.3.2.2 Correlation between D_{nssm} and $E_{a,D}$

The correlation between D_{nssm} at 21°C and $E_{a,D}$ is shown in Figure 6.4. Based on these test results, the correlation between $D_{nssm,21}$ and $E_{a,D}$ is described by the following equation:

$$E_{a,D} = -4.46\ln(D_{nssm,21}) + 27.92 \tag{6-2}$$

The values of $E_{a,D}$ range from 14.4 kJ/mol to 31.6 kJ/mol for all the tested groups. This relationship suggests that the value of $E_{a,D}$ is dependent on the intrinsic diffusivity. It also suggests that the value of $E_{a,D}$ decreases with increasing intrinsic D_{nssm} values.

Figure 6.5 shows comparison of correlation between $D_{nssm,21}$ and $E_{a,D}$ with results by Yuan [76]. It indicates that results from present investigation are in partial agreement with Yuan's results.

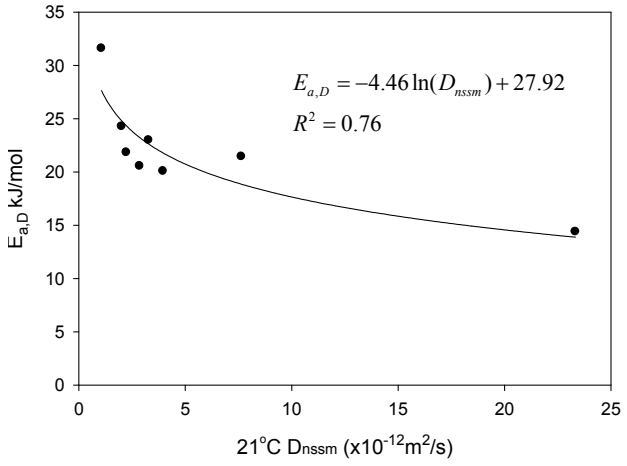

Figure 6.4: Correlation between $D_{nssm,21}$ and $E_{a,D}$

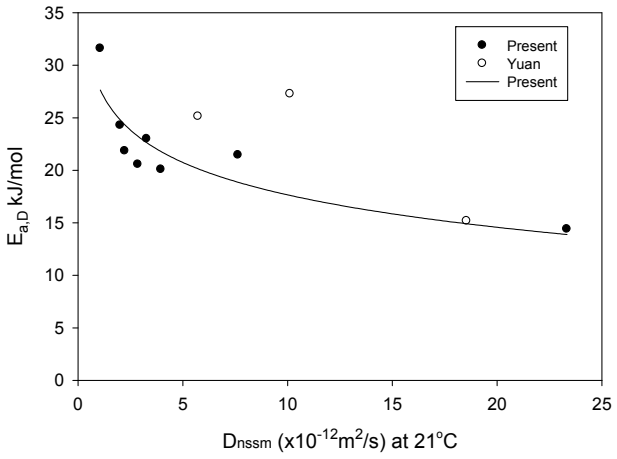

Figure 6.5: Comparison of correlation between $D_{nssm,21}$ and $E_{a,D,}$ and with results by Yuan

6.3.2.3 General Equations for Diffusivity Normalization

According to Arrhenius law, with a reference temperature of 21°C, the diffusivity coefficient at temperature T (°C) is:

$$D_T = D_{21} \exp\left[\frac{E_{a,D}}{R}\left(\frac{1}{294.15} - \frac{1}{T + 294.15}\right)\right] \tag{6-3}$$

Combine Equation 6-2 and Equation 6-3 and it leads to:

$$D_T = D_{21} \exp\left[\frac{-4.46\ln(D_{21}) + 27.92}{R}\left(\frac{1}{294.15} - \frac{1}{T + 294.15}\right)\right] \tag{6-4}$$

Equation 6-4 is a general equation with which it is possible to predict diffusivity coefficients at different temperatures if the D_{nssm} at 21°C is known. It is necessary to note that all the diffusion coefficients in Equation 6-3 and Equation 6-4 are non-steady-state migration coefficients (D_{nssm}). Figure 6.6 shows the temperature factor for diffusivity (D_T/D_{21}) generated from Equation 6-4. It indicates that temperature effect is more significant on concrete with lower diffusivity coefficients than on those with higher diffusivity coefficients. For concrete with $D_{nssm,21}$ =0.5×10^{-12}m^2/s, the migration coefficient at 45°C is 2.6 times the D_{nssm} at 21°C; whereas, for concrete with $D_{nssm,21}$ =30×10^{-12}m^2/s, the migration coefficient at 45°C is only 1.5 times the D_{nssm} at 21°C.

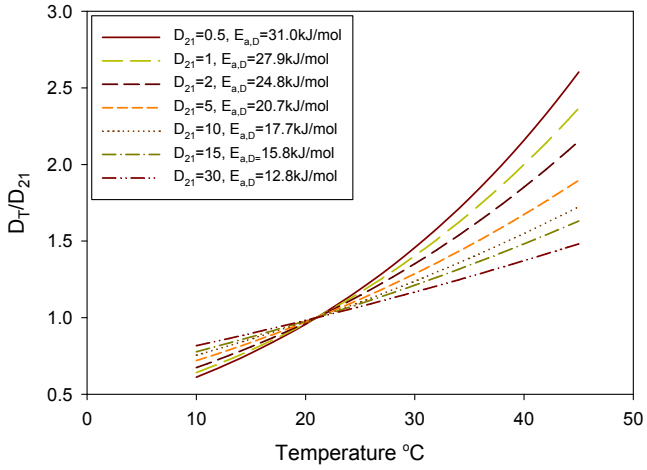

Figure 6.6: Temperature factor ($K_{D,T}$=D_T/D_{21}) on concrete with various diffusivity and $E_{a,D}$ values

Figure 6.7 shows comparison of the temperature factors calculated from present investigation and from Life-365 and LIFECON. [8, 80] It shows that when $T > 21$°C, the temperature factor (D_T / D_{21}) calculated from Life-365 and LIFECON are larger than those from present investigation, which is due to the larger $E_{a,D}$ employed by Life-365 and LIFECON (35kJ/mol and 39.9 kJ/mol) than the $E_{a,D}$ obtained from the present research (14.4kJ/mol to 31.6kJ/mol). As a result of this, the temperature effect calculated from Life-365 and LIFECON is more significant than using the method proposed from this investigation.

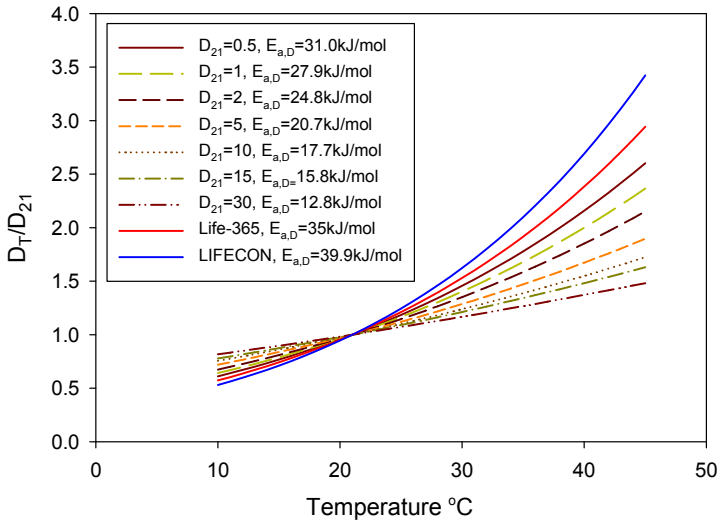

Figure 6.7: Comparison of temperature factors (D_T/D_{21}) from the present investigation with results from Life-365 and LIFECON [8, 80]

6.3.2.4 Correlation between $E_{a,D}$ and $E_{a,\rho}$

Theoretical Discussion

The temperature dependence of both resistivity and diffusivity follows the Arrhenius law. When taking 21°C as the reference temperature, the equations are:

$$\rho_T = \rho_{21} \cdot \exp\left[\frac{E_{a,\rho}}{R}\left(\frac{1}{T+273.15}-\frac{1}{294.15}\right)\right] \tag{6-5}$$

$$D_T = D_{21} \exp\left[\frac{E_{a,D}}{R}\left(\frac{1}{294.15}-\frac{1}{T+294.15}\right)\right] \tag{6-6}$$

Multiply Equation 6-5 and Equation 6-6 and it becomes:

$$\rho_T \cdot D_T = \rho_{21} \cdot D_{21} \exp\left[\frac{\left(E_{a,\rho}-E_{a,D}\right)}{R}\cdot\left(\frac{1}{T+273.15}-\frac{1}{294.15}\right)\right] \tag{6-7}$$

As previously stated in Equation 2-27 and Equation 5-2, it has been found both theoretically and experimentally that $\rho_T \cdot D_T = K_{\rho,D}$. By combing Equation 2-27 and Equation 6-7, it leads to:

$$\rho_T \cdot D_T = \rho_{21} \cdot D_{21} \exp\left[\frac{\left(E_{a,\rho}-E_{a,D}\right)}{R}\cdot\left(\frac{1}{T+273.15}-\frac{1}{294.15}\right)\right] = K_{\rho,D} \tag{6-8}$$

In order to make Equation 6-8 tenable, the following correlation should exist:

$$E_{a,\rho} - E_{a,D} = 0 \tag{6-9}$$

That is:

$$E_{a,\rho} = E_{a,D} \tag{6-10}$$

Experimental Discussion

Figure 6.8 shows the correlation of activation energy for resistivity and diffusivity and Figure 6.9 show comparison of $E_{a,D}$ and $E_{a,\rho}$. It indicates that, the values of $E_{a,D}$ and $E_{a,\rho}$ obtained from the same group of specimens were quite similar, which suggest that the correlation in Equation 6-10 might be valid.

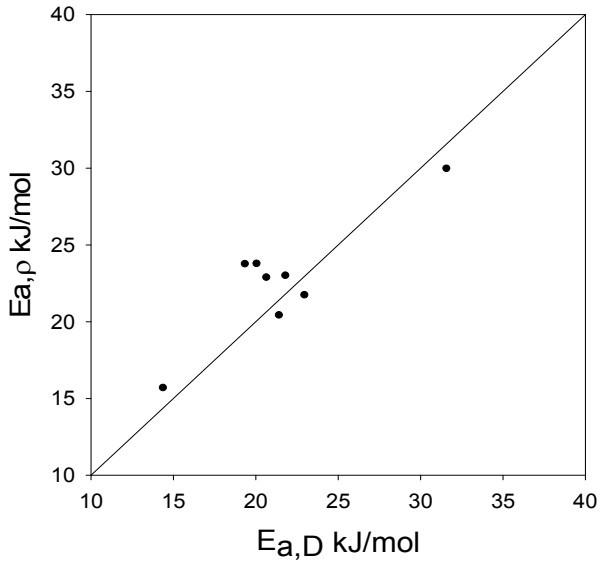

Figure 6.8: Correlation of $E_{a,D}$ and $E_{a,\rho}$

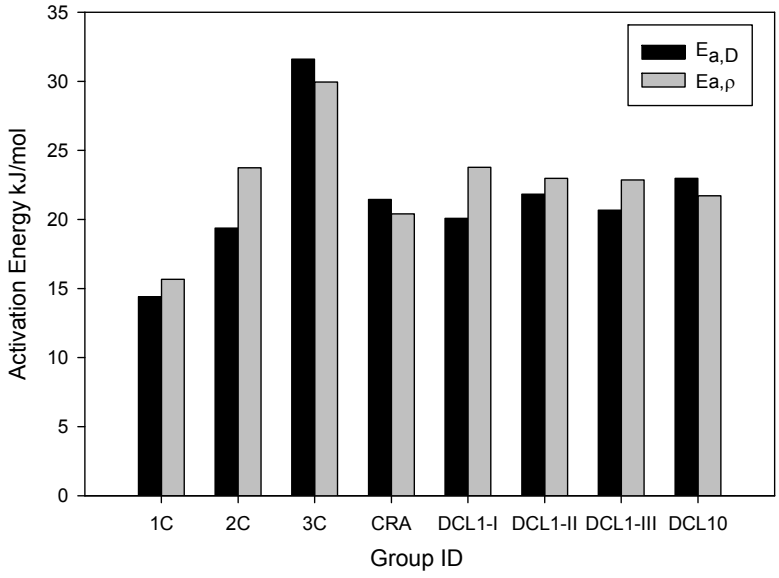

Figure 6.9: Comparison of $E_{a,D}$ and $E_{a,\rho}$ by groups

The correlation between ρ_{21} and $E_{a,\rho}$ for the tested groups is obtained by plotting the results from Table 6-2, which is shown in Figure 6.10

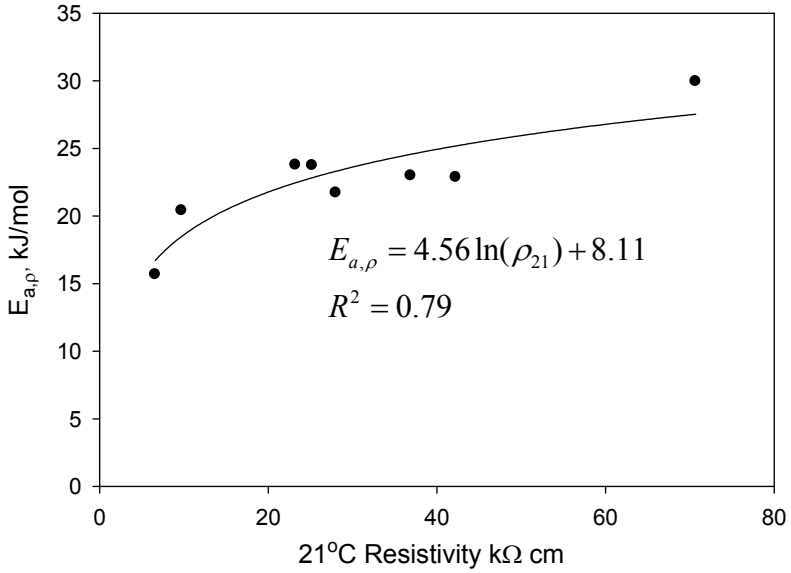

Figure 6.10: Correlation between $\boldsymbol{\rho_{21}}$ and $\boldsymbol{E_{a,\rho}}$ for tested groups in Table 6-2

As indicated in Figure 6.10, the correlation between ρ_{21} and $E_{a,\rho}$ for all the tested groups is described as:

$$E_{a,\rho} = 4.56\ln(\rho_{21}) + 8.11 \tag{6-11}$$

To prove the correlation in Equation 6-10 with the experimental results, combine Equation 6-2, Equation 6-10 and Equation 6-11, and it becomes:

$$4.56\ln(\rho_{21}) + 8.11 = -4.46\ln(D_{21}) + 27.92 \tag{6-12}$$

By applying $\rho_{21} \cdot D_{21} = K_{D,\rho}$ into Equation 6-12, it leads to:

$$4.56\ln(\rho_{21}) + 8.11 = -4.46\ln\left(\frac{K}{\rho_{21}}\right) + 27.92 \tag{6-13}$$

The solution of Equation 6-13 is:

$$K = \exp\left[-0.022 \cdot \ln(\rho_{21}) + 4.44\right] \tag{6-14}$$

The constant K in Equation 6-14 calculated with different values of ρ_{21} is shown in Table 6.3: Values of constant K calculated with Equation 6-13.

Table 6.3: Values of constant K calculated with Equation 6-13

ρ_{21} kΩ cm	K
1	85
10	81
50	78
100	77
200	75
300	75

As the resistivity value of the tested groups is between 7 kΩ cm to 71 kΩ cm, the value of K for the tested groups should be between 78 -81, which is in agreement with the K values (72-92) in Table 6-2 obtained by $D_{nssm,21} \times \rho_{21}$ except Group 1C (K=154).

6.3.2.5 Prediction of D_{nssm} by Resistivity Measurement

With the conclusions from this chapter and the previous chapters, the correlations between resistivity, chloride ion migration coefficient and temperature have been obtained. With these correlations, it is possible to predict not only resistivity values under different temperatures, but also chloride ion migration coefficients under different temperatures by resistivity measurement. The procedures for predicting chloride ion migration coefficients from resistivity measurement are shown in Figure 6.11: Procedure for prediction of chloride diffusivity at different temperatures by resistivity measurement. Although limited data was used to study the effect of temperature dependence of chloride ion diffusivity and the correlation between activation energy for resistivity and diffusivity, the resistivity measurement is still a promising method in estimating chloride ion diffusivity and predicting the service life of reinforced concrete structures.

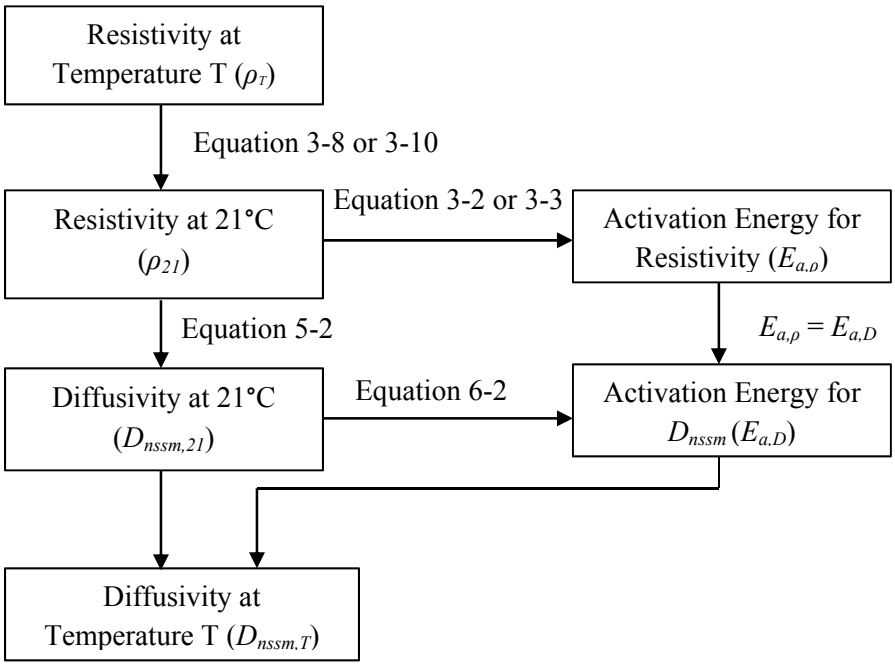

Figure 6.11: Procedure for prediction of chloride diffusivity at different temperatures by resistivity measurement

6.4 Conclusions

1. Chloride diffusivity in concrete increases with increasing temperature, however, the activation energy for diffusivity decreases with increasing diffusivity coefficient.

2. Temperature effect is more significant on concrete with lower D_{nssm} values.

3. Based on the correlation between $D_{nssm,21}$ and $E_{a,D}$ developed from this investigation, it is possible to predict chloride migration coefficients at different temperatures.

4. Activation energy for resistivity ($E_{a,\rho}$) and diffusivity ($E_{a,D}$) from the same concrete were found to be quite similar to each other.

5. Chloride ion migration coefficients as well as the temperature effect on diffusivity could be estimated by the resistivity measurement.

7. EFFECT OF POZZOLANIC ADMIXTURES ON pH and CONDUCTIVITY OF PORE SOLUTION

7.1 Introduction

Properties of the concrete pore solution, such as pH and conductivity, play an important role in durability of reinforced concrete structures. Due to the high pH (usually >12.5) of concrete pore solution, reinforcing steel bars in concrete are usually protected from corrosion. Presence of chloride ion exceeding a threshold [Cl_{th}^-] can depassivate the steel bars and initiate corrosion even at high pH. Therefore it is important to keep the pore solution at a high pH as it has been reported that [Cl_{th}^-] increases with an increase in pH [123, 124]. However, when alkali-silica-reaction (ASR) susceptible aggregates are used, the high pH of pore solution would increase the risk of ASR. In this case, it would be necessary to control the pH of concrete pore solution to a lower level. Conductivity of pore solution is important to concrete durability as it is possible to calculate the chloride ion diffusion coefficient by the conductivity of pore solution and bulk concrete using Nernst-Einstein equation (Equation 2-23)[54-56].

Pozzolanic admixtures have been widely used for producing high-performance concrete, especially for more durable concrete structures. The use of pozzolanic admixtures not only changes pore structures of concrete, but also the pH and conductivity of pore solution, as the pozzolanic reactions could consume and decrease the concentration of $Ca(OH)_2$ in the pore solutions[125, 126]. However, it has also been reported that a decrease of pH in pore solution could also be caused by the dilution effect of using fly ash as a replacement of cement in large amounts, especially when the alkalinity of FA is lower than the alkalinity of cement[25].

In this investigation, pH and conductivity of pore solution, porosity and electrical resistivity of concrete with different replacement ratios of pozzolanic admixtures were studied. The objectives of this investigation include:

- Study the effect of pozzolanic admixtures on pH and conductivity of concrete pore solution.
- Study the porosity of concrete with different resistivity values.

● Calculate chloride ion diffusion coefficients using the Nernst-Einstein equation and compare these coefficients with the migration coefficients obtained from RCM test.

7.2 Experimental Procedure

7.2.1 Materials

The concrete mix designs in this investigation were the same as those listed in Table 4.1 (excluding Mix Ai and Bi). Six cylinders were selected from each mix: cylinders #10 & #11, #24 & #25, and #26 & #27, which were cured under RT, 2RT/ET and 2RT/26ET/RT regimes, respectively.

7.2.2 Experimental Methods

At the age of one year, electrical resistivity was measured according to FM 5-578. Thereafter, the specimens were sliced as illustrated in Figure 7.1. The middle slices (slice A&B) were subjected to the RCM test as described in Chapter 5. The top and bottom slices (slice C&D) from cylinders #10, #24 and #26 were subjected to porosity test according to ASTM C642[127]. Because all the specimens were cured in limewater before porosity test (specimens were already water-saturated), the test procedure in ASTM C642 was slightly modified as follows:

1: Measure the saturated, surface-dried mass *C*.
2: Measure the apparent weight in water *D*.
3: Measure the oven-dry mass (*A*) at the time when the difference between the last two successive weight values is less than 0.5 % of the lowest value obtained.
4: Calculate the volume of permeable voids % = (C-A)/(C-D).

To avoid the evaporation of the gel water, the temperature in the oven was adjusted to 60°C - 70°C rather than using the temperature range in ASTM C642 (100°C - 110°C)[128]. The final porosity value for each cylinder was the average of the top and bottom slices.

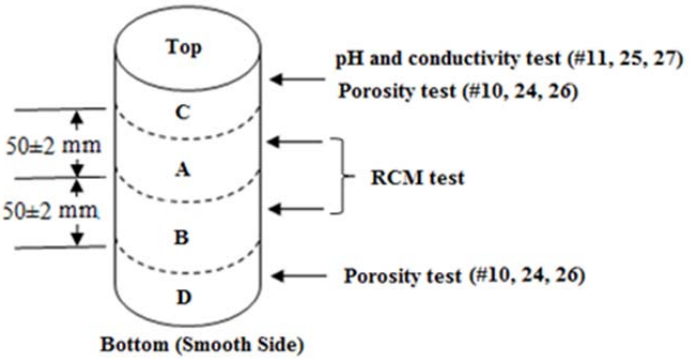

Figure 7.1: Illustration of specimen slices subjected to different tests

The pH of pore solution was measured using a leaching method developed by Sagüés et al.[129, 130] The pore solution conductivity was measured using the same setup used for pH measurement, but with a micro conductivity probe. Two holes were drilled from the cut section with diameter of 0.4cm and depths of 3cm. Plastic washers were glued to the mouth of the holes. The distance between center to center of the two holes was at least 2cm. The holes were then filled with 0.5 ml deionized (DI) water and closed with rubber stoppers. The specimens were then stored in high humidity containers. Schematic illustration of leaching method is shown in Figure 7.2. The concrete pore solution pH and conductivity was measured at 4, 7, 14, 21, 28 and 38 days. The pH measurement was performed by using a glass pH microelectrode (MI-405 from Microelectrodes, Inc.) and an Ag-AgCl reference microelectrode (MI-402). The conductivity was measured using a conductivity microelectrode (MI-905). All the measurements were performed at room temperature between 22°C to 23°C.

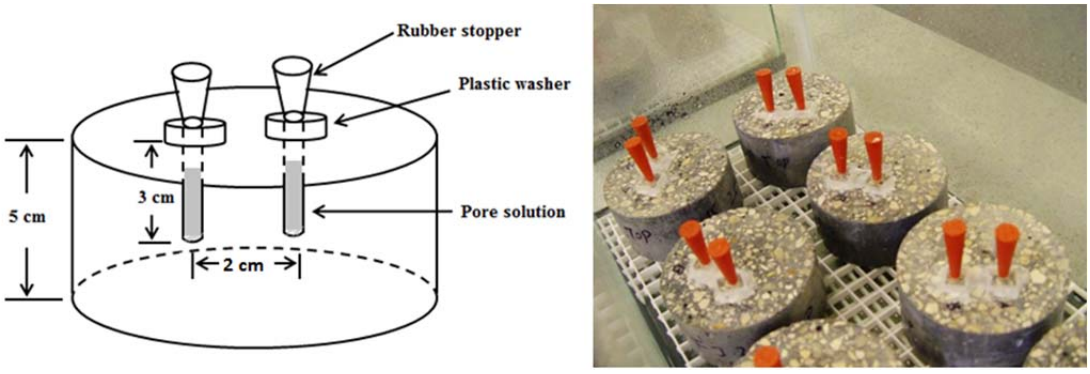

(a) (b)

Figure 7.2: Schematic illustration of (a) leaching method and (b) specimens in a high humidity container.

As the pH of the concrete pore solution is usually higher than 12, glass electrodes are subject to alkali ion error[129]. All measurements were recorded in mV (using a pH/mV meter). To minimize the effect of alkali ion error, the potential of reference buffer solutions with pH =12.45 and pH =13 were measured. The potential readings from the pore solutions were converted to pH values by a linear potential interpolation method using the pH/mV values from measured on the buffer solutions.

7.3 Results and Discussion

7.3.1 Results

7.3.1.1 ρ_{21} and D_{nssm}

Results of ρ_{21} and D_{nssm} from RCM test on cylinder #10 & #11, #24 & #25 and #26 & #27 were the same as reported in Table 4.6. The average values are shown in Table 7.1, in which the values of resistivity range from 29.1 kΩ cm (A10-11) to 330 kΩ cm (L24-25) and the values of D_{nssm} range from 0.24×10^{-12}m^2/s (L24-25) to 3.52×10^{-12}m^2/s (A10-11).

Table 7.1: Average values of ρ_{21} and D_{nssm} on tested specimens

Specimen No.	ρ_{21} kΩ cm	D_{nssm} 10^{-12}m^2/s	Specimen No.	ρ_{21} kΩ cm	D_{nssm} 10^{-12}m^2/s
A10-11	29.1	3.52	I10-11	37.0	2.18
A24-25	50.4	2.16	I24-25	106.0	0.87
A26-27	36.7	2.78	I26-27	58.5	1.76
J10-11	35.5	2.39	H10-11	43.9	2.15
J24-25	88.6	1.03	H24-25	140.9	0.75
J26-27	49.4	1.41	H26-27	80.1	1.66
B10-11	35.7	2.60	C10-11	42.3	1.51
B24-25	133.1	0.83	C24-25	103.3	0.95
B26-27	68.7	1.32	C26-27	76.9	1.37
D10-11	53.2	1.93	K10-11	56.2	1.01
D24-25	205.7	0.60	K24-25	175.2	0.47
D26-27	106.1	1.04	K26-27	115.7	0.64
E10-11	21.3	3.68	L10-11	52.7	1.41
E24-25	39.4	2.69	L24-25	330.1	0.24
E26-27	26.9	3.03	L26-27	165.7	0.45
F10-11	29.6	2.68	G10-11	16.4	3.41
F24-25	62.8	1.36	G24-25	37.5	1.92
F26-27	40.3	2.58	G26-27	28.3	2.39

7.3.1.2 Porosity

Table 7.2 shows the results of the porosity test. The average value of the top and bottom slices (slice C&D) was taken as the bulk porosity of each specimen. Results show that porosity of the top splice is higher than the porosity of the bottom on all the specimens. The bulk porosity ranges from 5.23% (H24) to 9.04% (B10).

Table 7.2: Porosity of tested specimens

Specimen ID	Porosity by volume %			Specimen ID	Porosity by volume %		
	Top	Bottom	Average		Top	Bottom	Average
A10	9.21	8.06	8.64	I10	7.61	6.20	6.90
A24	7.14	5.49	6.31	I24	5.96	4.77	5.36
A26	8.42	5.83	7.12	I26	6.32	5.29	5.81
J10	9.76	7.98	8.87	H10	7.53	5.88	6.70
J24	6.85	5.79	6.32	H24	6.02	4.44	5.23
J26	7.54	5.91	6.73	H26	6.01	4.96	5.48
B10	9.49	8.59	9.04	C10	8.34	7.00	7.67
B24	6.87	5.90	6.38	C24	6.78	4.94	5.86
B26	7.98	7.05	7.51	C26	6.50	4.64	5.57
D10	8.54	7.54	8.04	K10	7.89	6.61	7.25
D24	6.64	5.40	6.02	K24	5.90	4.72	5.31
D26	7.17	5.73	6.45	K26	6.25	5.24	5.74
E10	8.29	6.41	7.35	L10	8.17	7.63	7.90
E24	5.89	5.05	5.47	L24	5.43	5.05	5.24
E26	6.35	5.66	6.00	L26	5.94	5.09	5.51
F10	7.43	6.16	6.79	G10	8.53	6.33	7.43
F24	6.23	4.63	5.43	G24	5.89	4.43	5.16
F26	6.24	4.95	5.60	G26	5.94	4.54	5.24

NOTE: The number after the mix ID indicates cylinder # tested 10 RT, 24 2RT/ET, 26 2RT/26ET/RT

7.3.1.3 pH and conductivity of pore solution

Figure 7.3 to Figure 7.5 show the evolution of pore solution pH with time on all the tested specimens. It indicates that the pH of the pore solution became stable after 28 days and no significant change was found between 28 days and 38 days. However, it was found that there was an obvious mV drifting on the glass pH electrodes during the measurement, especially when the measurement period was over 20 minutes. It is suggested that the glass pH electrodes should be calibrated at least every 15 minutes.

Due to the mV drifting, errors could happen if the electrodes are not frequently calibrated, as can be observed in Figure 7.3 to Figure 7.5 where an oscillation of pH values occurred at 7 and 14 days.

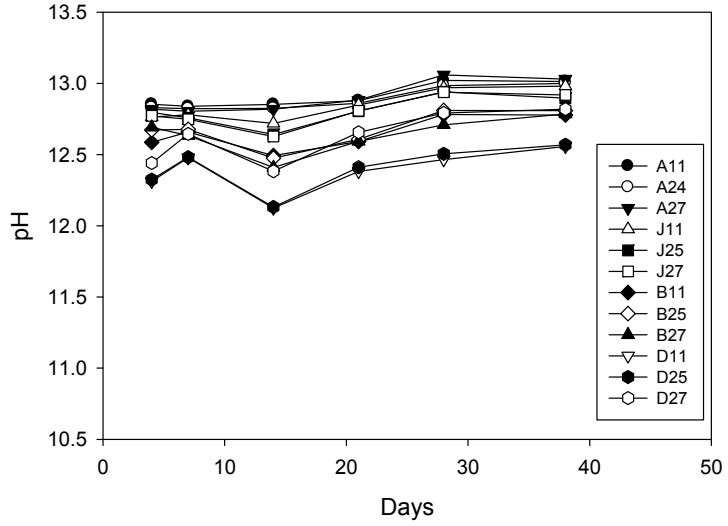

Figure 7.3: Evolution of pore solution pH with time on specimens with FA/limestone

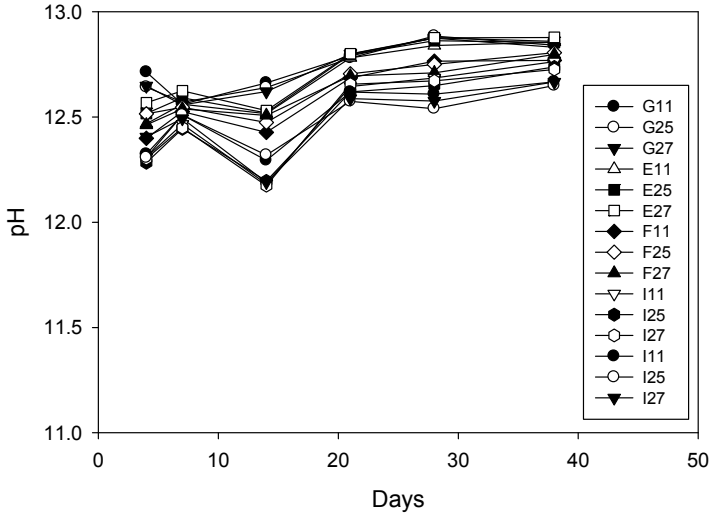

Figure 7.4: Evolution of pore solution pH with time on specimens with Slag or Slag/FA

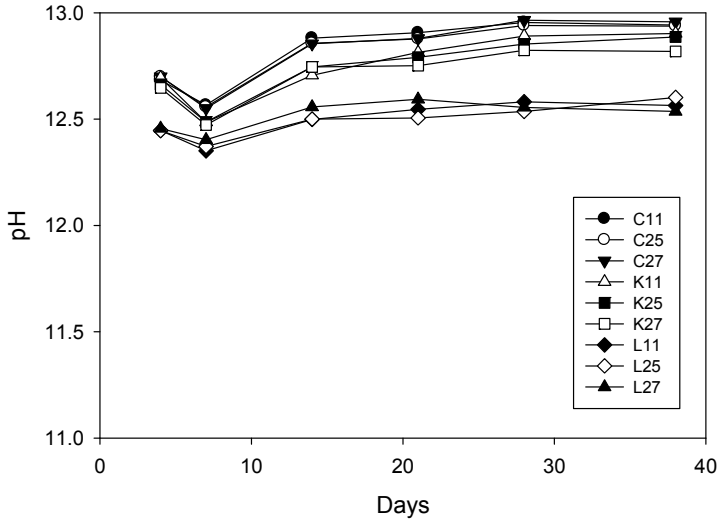

Figure 7.5: Evolution of pore solution pH with time on specimens with FA/Granite

Figure 7.6 to Figure 7.8 show evolution of pore solution conductivity with time on all the tested specimens. Similar to the observed evolution of pH values, the conductivity values on most of specimens tended to be stable after 28 days, however, a slight increase in conductivity was observed on some specimens even after 28 days.

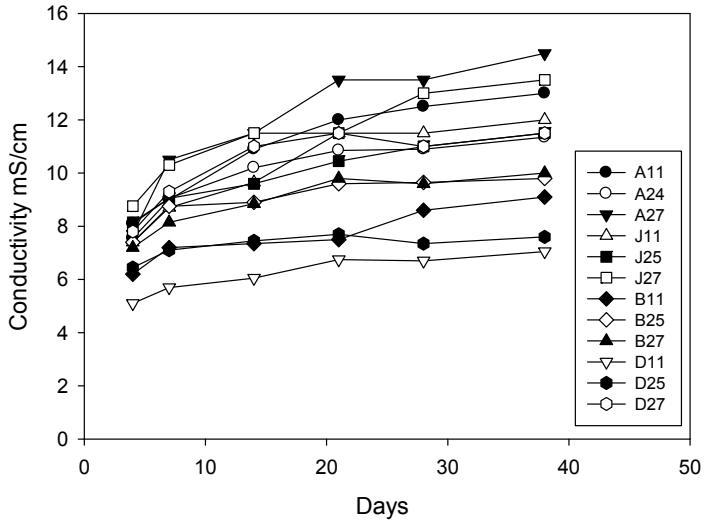

Figure 7.6: Evolution of pore solution conductivity with time on specimens with FA/limestone

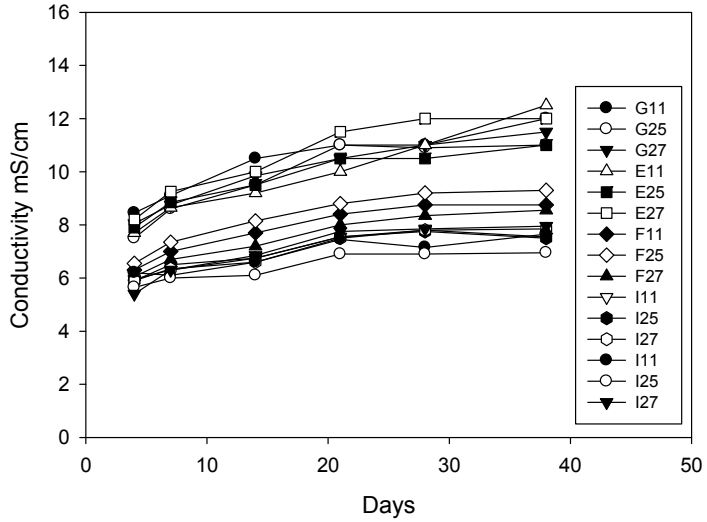

Figure 7.7: Evolution of pore solution conductivity with time on specimens with Slag or Slag/FA

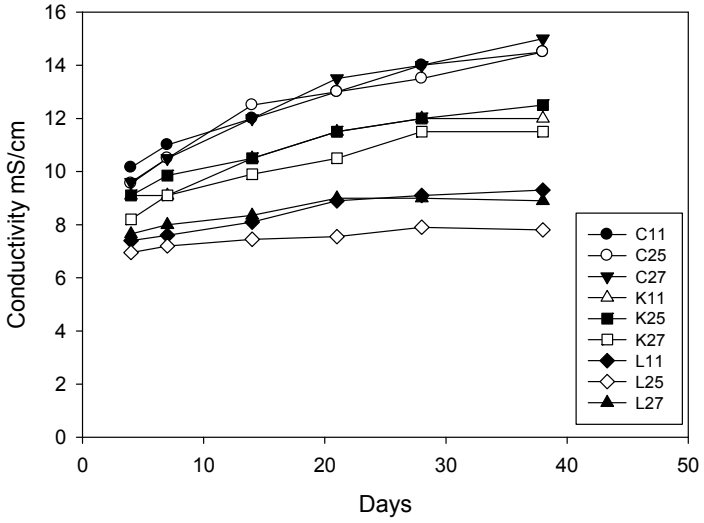

Figure 7.8: Evolution of pore solution conductivity with time on specimens with FA/granite

7.3.2 Discussion

7.3.2.1 Correlation between Resistivity and Porosity

Results in Table 7.2 show that the average porosity of the tested specimens ranged from 5% to 9%. However, the porosity of the top slices was about 1% to 2% higher than the porosity of the bottom

slices shown in Figure 7.9, which was believed to be mainly caused by consolidation and segregation while the cylinders were cast.

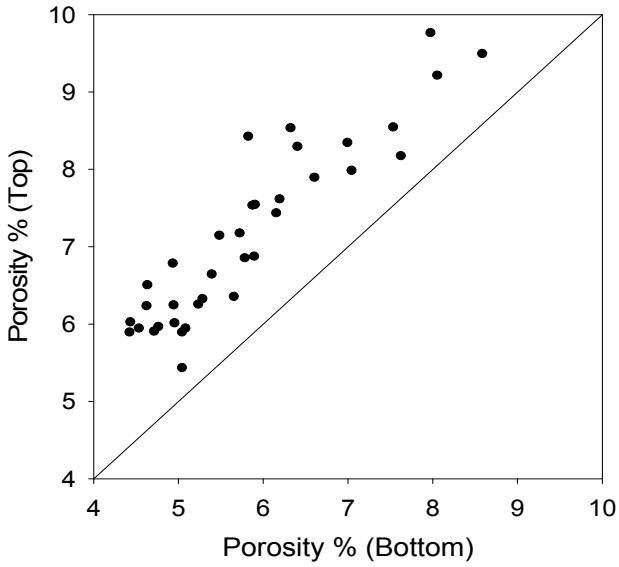

Figure 7.9: Comparison of porosity results from bottom slices and top slices

Results in Table 7.2 also show that, the average porosity of the specimens from the same mix was different depending on the curing regime (or degree of hydration). The specimens cured under RT all the time (cylinder #10) showed the highest porosity and the specimens cured under 2RT/ET (cylinder #24) showed the lowest. Figure 7.6 shows the correlation between porosity and resistivity (data from Table 7.1 and Table 7.2). The plots indicate that for specimens from the same mix, porosity decreased with increasing resistivity. Although the results in Figure 7.6 were from specimens cured under different curing conditions, the correlation between porosity and resistivity could also be used to describe the change of porosity during hydration. Concrete resistivity increases with time as a result of continuing hydration as was shown in Figure 4.5. The correlation in Figure 7.6 indicates that the increase in resistivity during hydration is accompanied by a decrease in porosity, which is caused by the refinement and lesser inter-connectivity of pore structures as a result of further pozzolanic reaction and hydration.

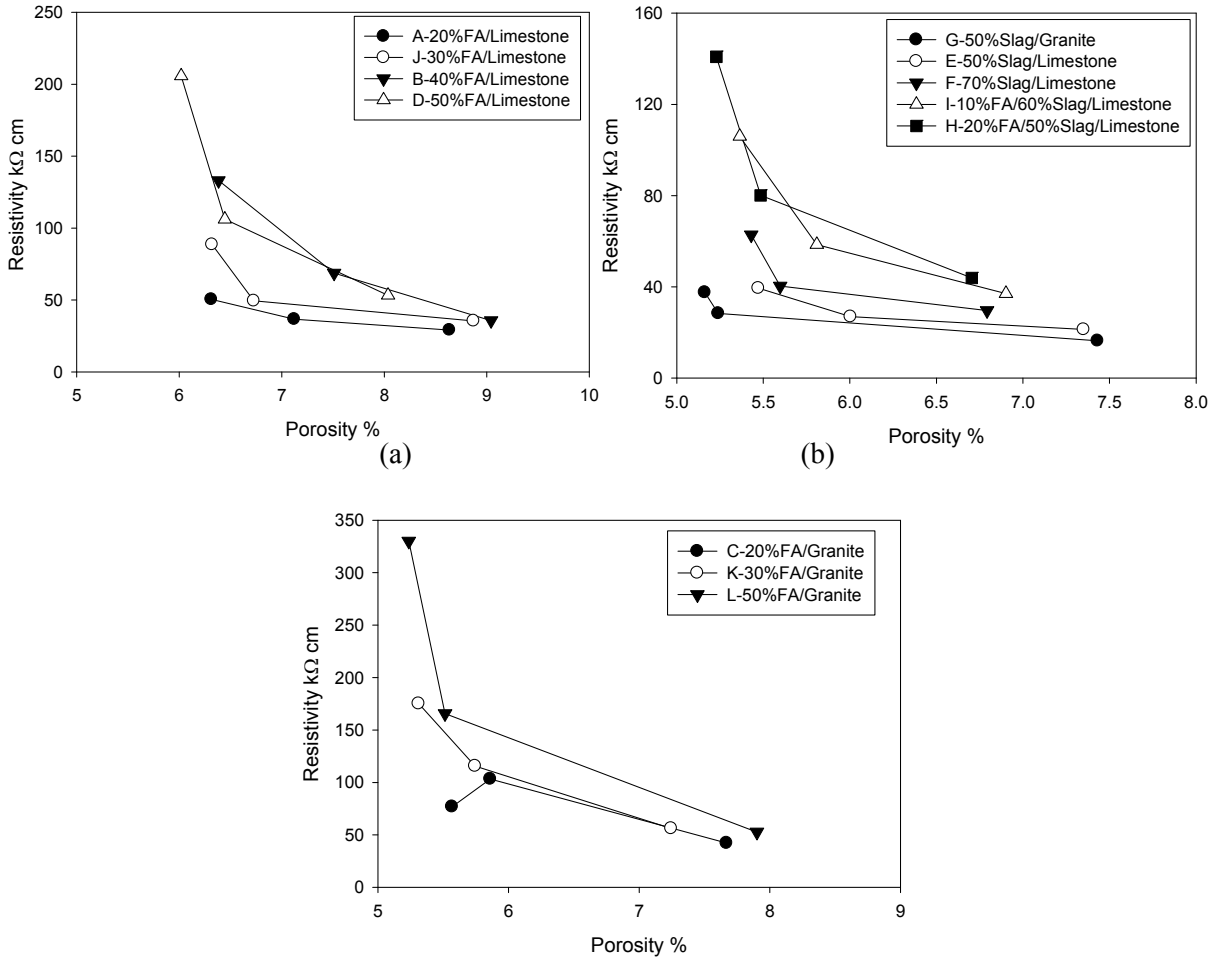

Figure 7.10: Correlation between porosity and electrical resistivity

7.3.2.2 Effect of Pozzolanic Admixtures on pH of Pore Solution

Figure 7.11 shows the measured pH on all the tested specimens, in which the pH value of each specimen was the average of the last two sets of measurements (28 days and 38 days). It shows that for specimens from the same mix, the values of pH were similar(with a maximum difference of 0.08 except Mix D), although the specimens were subjected to different curing regimes and showed different resistivity values (an indication of different degree of hydration), which indicates that pH of concrete with pozzolanic admixtures was stable at an a late age (after 1 year in this investigation) and the further hydration or pozzolanic reaction did not significantly change the pH of concrete.

The pH values of all the specimens ranged from 12.51(D11) to 13.05 (A27). Specimens with 20%FA (Mix A and Mix C) showed the highest pH values (12.9-13.0) and specimens with 50%FA (Mix D and Mix L) showed the lowest values (12.5-12.6). It also indicates that pH of specimens with 70%Slag (Mix F) was lower than pH of specimens with 50%Slag (Mix G and Mix E). Also, for specimens with total replacement of 70% (Slag+FA), the pH decreased with increasing replacement ratio of FA. D27 in Mix D was abnormally higher than the other two specimens and the reason is not clear. Results from D27 were omitted in the rest of discussion.

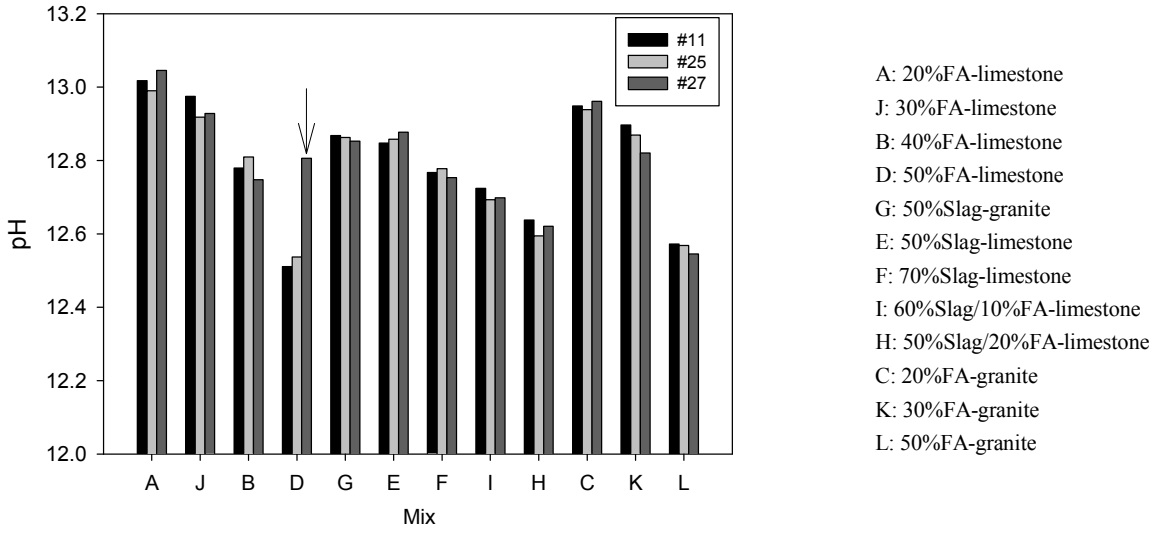

Figure 7.11: pH of pore solution on tested specimens (average of the last two measurements).

Figure 7.12 shows the correlation between pH of the pore solution and replacement ratio of FA on specimens with limestone and granite. From the observed trends, it shows that the pH of pore solution decreases with increasing replacement ratio of FA. The trend also indicates that decrease of pH in pore solution is more significant when larger amount of FA is used. However, as reported by Shehata et al. that the decrease of pH by using FA could be affected by both the dilution effect as well as the alkalinity of FA[25].

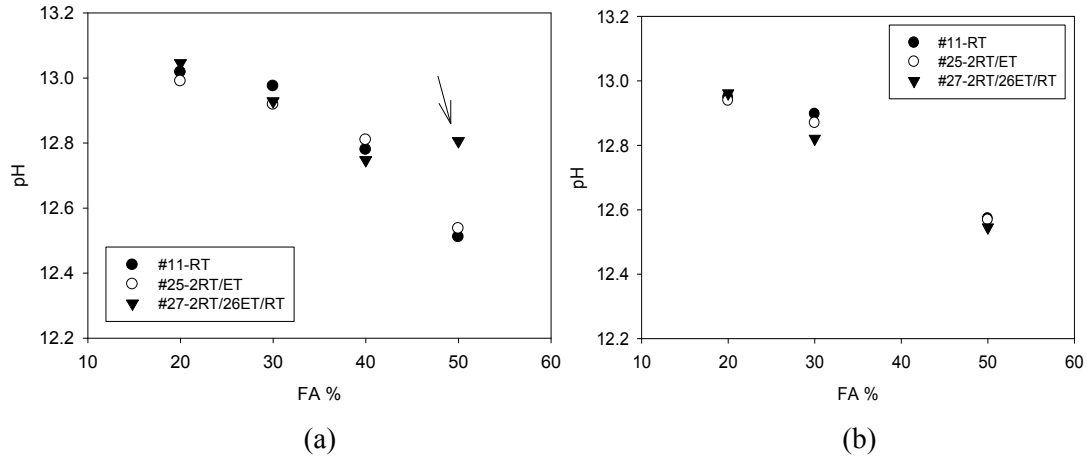

Figure 7.12: Correlation between pH of pore solution and replacement ratio of FA on specimens with (a) limestone and (b) granite

Figure 7.13 shows the correlation between replacement ratio of FA and concentration of OH^- in the pore solution. The straight line in Figure 7.13 shows the ideal dilution effect (assuming FA is an inert filler). The concentration of OH^- in OPC concrete was calculated from the pH measured from 1C (pH=13). It indicates that the smaller pH measured for specimens with increasing replacement ratio of FA is a complex process which involves both the alkalinity of the cement, the alkalinity of the admixture, the dilution effect, and the pozzolanic reaction. The results in Figure 7.13 are in agreement with the results from Medhat et al. as shown in Figure 2.18 [25].

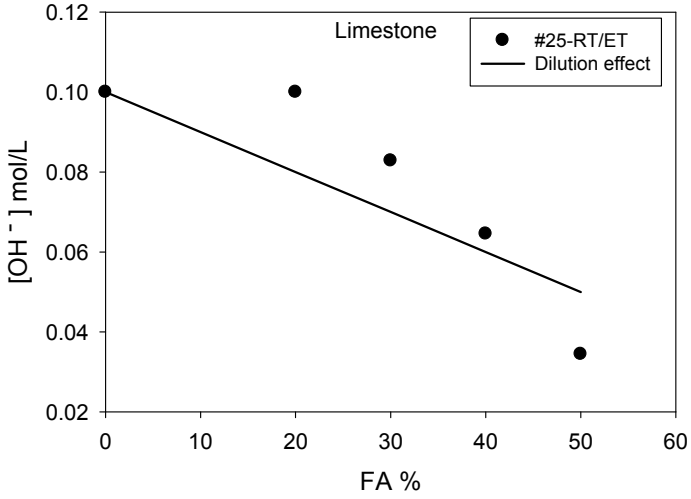

Figure 7.13: Correlation between replacement ratio of FA and concentration of OH- in the pore solution

7.3.2.3 Effect of Pozzolanic Admixtures on Conductivity of Pore Solution

Figure 7.14 shows the measured conductivity of the pore solution on all the tested specimens at 38 days. The values of pore solution ranged from 7.0 mS/cm (H25) to 15 mS/cm (C27). The pore solution conductivity measured on the specimens from the same mix was similar. Specimens with 20%FA (Mix A & Mix L) showed the highest pore solution conductivity and specimens with 50%FA (Mix D), 10%FA/60%Slag (Mix I) and 20%FA/50%Slag(Mix H) showed the lowest pore solution conductivity, which was similar to the trend found on the measured pH values. The pore solution of specimens with 50%Slag (Mix G & E) showed higher conductivity values than specimens with 70%Slag (Mix F). However, with the same total replacement ratio (70%) of pozzolanic admixture, the pore solution conductivity of specimens with 70%Slag (Mix F) was higher than that with 10%FA/60%Slag (Mix I) and 20%FA/50%Slag (Mix H).

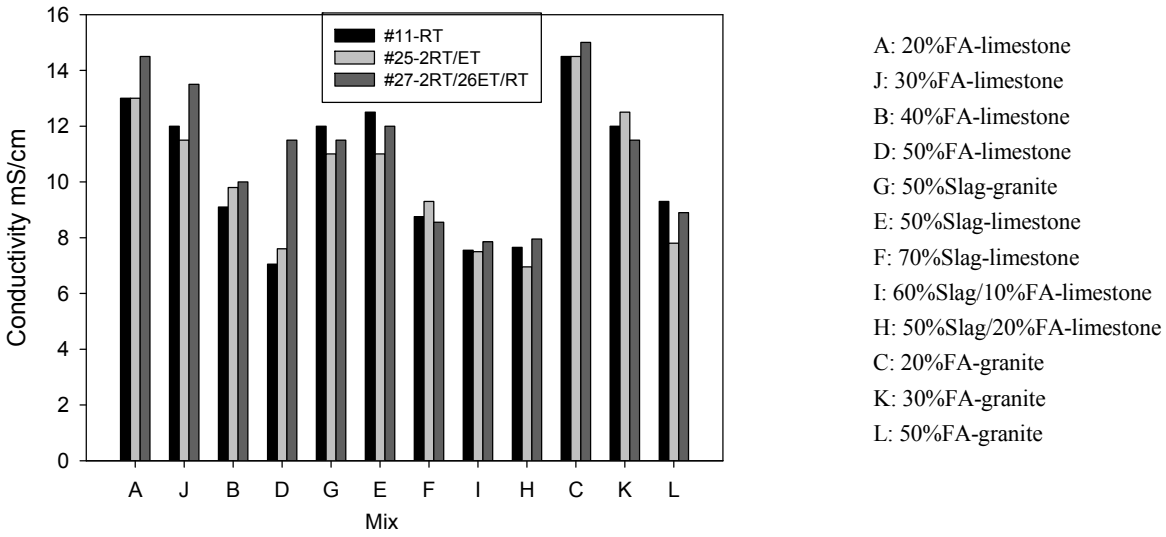

Figure 7.14: Conductivity of pore solution on tested specimens

Figure 7.15 shows correlation between pore solution conductivity and replacement ratio of FA on specimens with limestone and granite. The trends in the plots indicate that the pore solution conductive of specimens was lower for specimens with higher amount of FA, which is in agreement with the correlation between pH and replacement ratio of FA as shown in Figure 7.12. The lower pH and conductivity values measured on the specimens with higher replacement ratio of FA is believed to be caused by a combination of both the dilution effect and the pozzolanic reaction which consumed and reduced the concentration of Ca $(OH)_2$ in the pore solution.

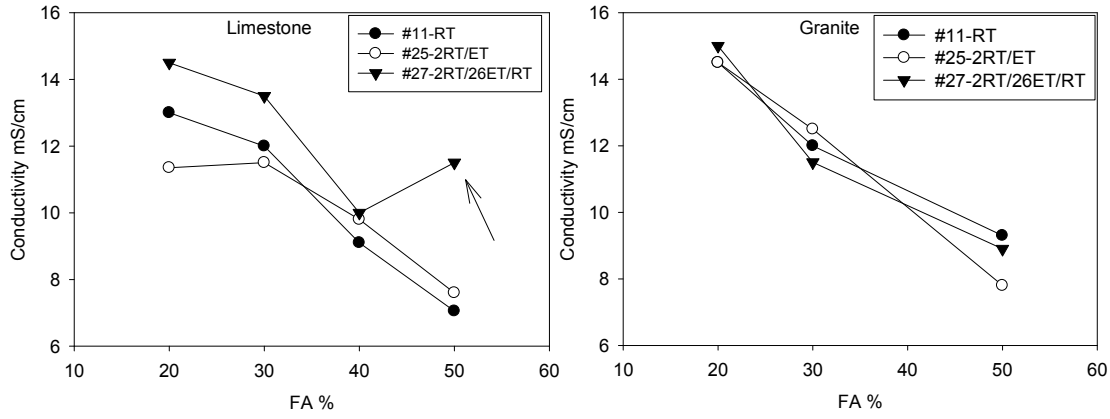

(a) (b)

Figure 7.15: Correlation between pore solution conductivity and replacement ratio of FA for specimens with (a) limestone and (b) granite

7.3.2.4 Correlation between pH and Conductivity of Pore Solution

Figure 7.16 shows the correlation between pH and conductivity on all the tested specimens. The good correlation confirms that conductivity of pore solution is mainly governed by the pH (or concentration of OH^-).

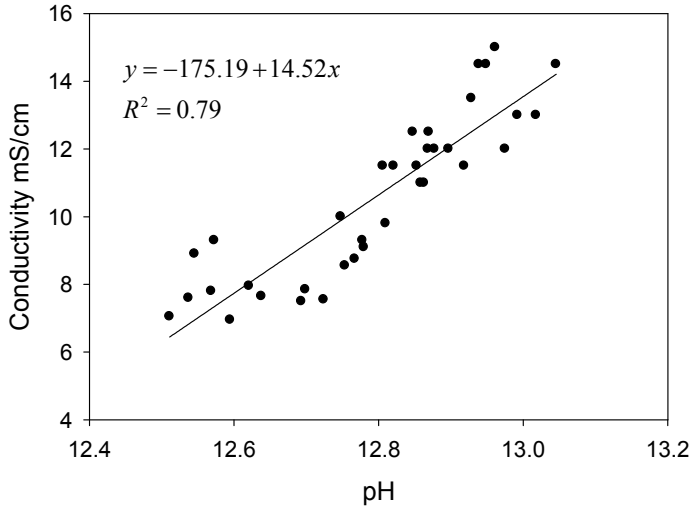

Figure 7.16: Correlation between pH and conductivity of pore solution

7.3.2.5 Application of Nernst-Einstein Equation and Archie's Law in Concrete

Pore Solution Conductivity Analysis

As described by the Nernst-Einstein Equation (Equation 2-23), the diffusivity of chloride ions in concrete can be calculated by knowing the pore solution conductivity, bulk conductivity and chloride ion diffusivity in the pore solution. In this investigation, the pore solution conductivity is known as shown in Figure 7.14 and the bulk conductivity can be obtained from the 21°C resistivity values listed in Table 7.1. Whereas, the diffusivity of chloride ions in pore solution is complex as there are multiple ions in the pore solution, such as Na^+, K^+, Ca^{2+},OH^- and SO_4^{2-}. The conductivity of pore solution can be expressed as[131]:

$$\sigma_0 = \sum_i z_i c_i \lambda_i \tag{7-1}$$

where σ_0 is the conductivity of pore solution; z_i, c_i and λ_i are the valence, concentration and equivalent conductivity of species *i*, respectively. Recall that the pH-pore-solution values measured on tested specimens ranged from 12.51 to 13.05; thus the concentration of OH^- in the pore solutions should be between 0.032mol/L to 0.112mol/L. According to the results by Snyder, the most significant contributor to the pore solution conductivity is OH^-, and Na^+ and K^+ are secondary contributors[131]. Snyder stated that the contribution of Ca^{2+} to the conductivity was in the order of 0.0003 mS/m, so the contribution of Ca^{2+} to the overall conductivity could be neglected. Snyder also stated that the contribution of SO_4^{2-} was less than 2% of the total conductivity.

To simplify the calculation of conductivity, it is assumed all the cation in the pore solution is Na^+ and the concentration of NaOH in the pore solution was between 0.032 mol/L to 0.112 mol/L. The molar conductivity of NaOH as a function of concentration at 25°C is listed in Table 7.3 [132].

Table 7.3: Molar conductivity of NaOH as a function of concentration at 25°C [132]

Concentration (mol L^{-1})	Λ(ohm^{-1} cm^2 mol^{-1})
0.001	244.5
0.010	238.0
0.050	227.6
0.100	221.2
0.200	213.0

The molar conductivity and conductivity of NaOH for concentrations between 0.032mol/L and 0.112mol/L is calculated in Table 7.4 by an interpolation method using the values shown in Table 7.3. This interpolated values indicate that the conductivity of NaOH solution between 0.032mol/L to 0.112mol/L is between 7.3 mS/cm to 23.9 mS/cm, which is in agreement with the conductivity values measured on the pore solution of specimens (7.0 mS/cm to 15.0 mS/cm). However, there is a significant difference between 23.9 mS/cm (calculated) and 15.0 mS/cm (measured) when comparing the calculated and measured pore solution conductivity on concrete with the higher pore solution pH and conductivity. To explain this, more investigation is necessary to analyze the chemical compositions in the pore solution. It is speculated that for these concrete other ions might have a significant contribution.

Table 7.4: Molar conductivity and solution conductivity of NaOH at 25°C

concentration (mol L^{-1})	Λ ($ohm^{-1}\,cm^2\,mol^{-1}$)	σ (mS/cm)
0.032	229.5	7.3
0.112	213.0	23.9

Calculated Diffusion Coefficients vs. D_{nssm}

The concentration of NaCl used for the RCM test is about 1.9 mol/L (10% NaCl by mass in water). It has been reported that diffusivity coefficients of NaCl with concentration between 0.1mol/L to 1mol/L in diluted solutions is between $1.483\times10^{-9}m^2/s$ to $1.484\times10^{-9}m^2/s$[133]. Neglecting the ion strength effect to the NaCl diffusivity in pore solution, the diffusivity coefficient of 1.9 mol/L NaCl in pore solution can be estimated as $1.484\times10^{-9}m^2/s$. Then the diffusivity of chloride ions in concrete can be calculated using Nernst-Einstein (Equation 2-23):

$$D_c = D_0 \frac{\sigma}{\sigma_0} \tag{7-2}$$

Where D_C the calculated diffusion coefficient; D_0 is the diffusion efficient of Cl^- in the concrete pore solution ($1.484\times10^{-9}m^2/s$); σ is the bulk conductivity of concrete and σ_0 is the conductivity of pore solution. The calculated values of D_C and the measured values of D_{nssm} from RCM test are listed in Table 7.5

Table 7.5: Calculated diffusion coefficients, formation factor, tortuosity constant and tortuosity

Specimen No.	ρ_{21} kΩ cm	ϕ %	σ S/m	σ_0 S/m	D_c $10^{-12}m^2/s$	D_{nssm} $10^{-12}m^2/s$	F	m	τ
A10-11	29.1	8.64	3.436E-03	1.30	3.92	3.52	378	2.42	32.67
A24-25	50.4	6.31	1.984E-03	1.30	2.26	2.16	655	2.35	41.37
A26-27	36.7	7.12	2.725E-03	1.45	2.79	2.78	532	2.38	37.90
J10-11	35.5	8.87	2.817E-03	1.20	3.48	2.39	426	2.50	37.79
J24-25	88.6	6.32	1.129E-03	1.15	1.46	1.03	1018	2.51	64.37
J26-27	49.4	6.73	2.024E-03	1.35	2.22	1.41	667	2.41	44.87
B10-11	35.7	9.04	2.801E-03	0.91	4.57	2.60	325	2.41	29.38
B24-25	133.1	6.38	7.516E-04	0.98	1.14	0.83	1304	2.61	83.25
B26-27	68.7	7.51	1.456E-03	1.00	2.16	1.32	687	2.52	51.61
D10-11	53.2	8.04	1.881E-03	0.71	3.96	1.93	375	2.35	30.12
D24-25	205.7	6.02	4.863E-04	0.76	0.95	0.60	1563	2.62	94.09
D26-27	106.1	6.45	9.425E-04	1.15	1.22	1.04	1220	2.59	78.65
G10-11	16.4	7.43	6.116E-03	1.20	7.56	3.41	196	2.03	14.58
G24-25	37.5	5.16	2.667E-03	1.10	3.60	1.92	413	2.03	21.29
G26-27	28.3	5.24	3.534E-03	1.15	4.56	2.39	325	1.96	17.06
E10-11	21.3	7.35	4.695E-03	1.25	5.57	3.68	266	2.14	19.57
E24-25	39.4	5.47	2.538E-03	1.10	3.42	2.69	433	2.09	23.72
E26-27	26.9	6.00	3.717E-03	1.20	4.60	3.03	323	2.05	19.38
F10-11	29.6	6.79	3.378E-03	0.88	5.73	2.68	259	2.07	17.59
F24-25	62.8	5.43	1.592E-03	0.93	2.54	1.36	584	2.19	31.71
F26-27	40.3	5.60	2.481E-03	0.86	4.31	2.58	345	2.03	19.29
I10-11	37.0	6.90	2.703E-03	0.76	5.31	2.18	279	2.11	19.28
I24-25	106.0	5.36	9.438E-04	0.75	1.87	0.87	795	2.28	42.62
I26-27	58.5	5.81	1.709E-03	0.79	3.23	1.76	459	2.15	26.68
H10-11	43.9	6.70	2.281E-03	0.77	4.42	2.15	335	2.15	22.49
H24-25	140.9	5.23	7.100E-04	0.70	1.52	0.75	979	2.33	51.19
H26-27	80.1	5.48	1.249E-03	0.80	2.33	1.66	636	2.22	34.90
C10-11	42.3	7.67	2.367E-03	1.45	2.42	1.51	613	2.50	46.98
C24-25	103.3	5.86	9.685E-04	1.45	0.99	0.95	1497	2.58	87.74
C26-27	76.9	5.57	1.300E-03	1.50	1.29	1.37	1154	2.44	64.23
K10-11	56.2	7.25	1.781E-03	1.20	2.20	1.01	674	2.48	48.82
K24-25	175.2	5.31	5.708E-04	1.25	0.68	0.47	2190	2.62	116.34
K26-27	115.7	5.74	8.647E-04	1.15	1.12	0.64	1330	2.52	76.40
L10-11	52.7	7.90	1.898E-03	0.93	3.03	1.41	490	2.44	38.73
L24-25	330.1	5.24	3.029E-04	0.78	0.58	0.24	2575	2.66	134.82
L26-27	165.7	5.51	6.037E-04	0.89	1.01	0.45	1474	2.52	81.29

Note: $\sigma=1/\rho_{21}$; $D_c=D_0.\sigma/\sigma_0$;$F= \sigma_{0/} \sigma$; $m=\ln(F)/\ln(\phi)$; $\tau=F\cdot\phi$

Figure 7.11 shows the comparison between D_c and D_{nssm}. It indicates that for specimens with 20% FA, the values of D_c were almost the same to the values of D_{nssm}. However, in most cases the values of D_c were higher than D_{nssm}, and the ratio of D_c/D_{nssm} ranged from 1 to 2. A possible explanation which makes $D_c > D_{nssm}$ is that the binding effect which was not considered during the calculation of D_c. However, chloride binding possible happened during the RCM test which resulted in a lower D_{nssm} than the calculated D_c.

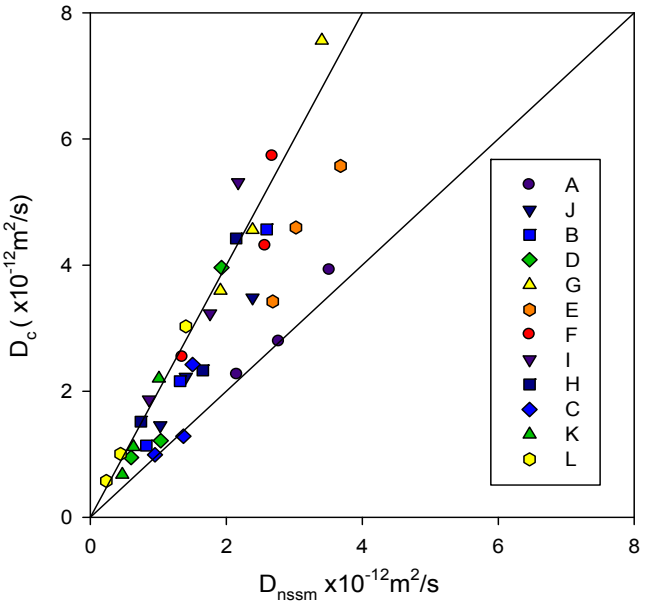

Figure 7.17: Comparison between D_C and D_{nssm}

Formation Factor vs. D_{nssm}

The formation factor was calculated using Equation 2-24, and the results are listed in Table 7.5. The values of F ranged from 196 to 2575, which are in agreement with the reported values.[56, 57] Moreover, an interesting and good correlation between formation factor and migration coefficients is observed as shown in Figure 7.18. This correlation confirms the validation of Equation 2-25 and it also proves that the migration coefficients could possibly be calculated by the formation factor of concrete.

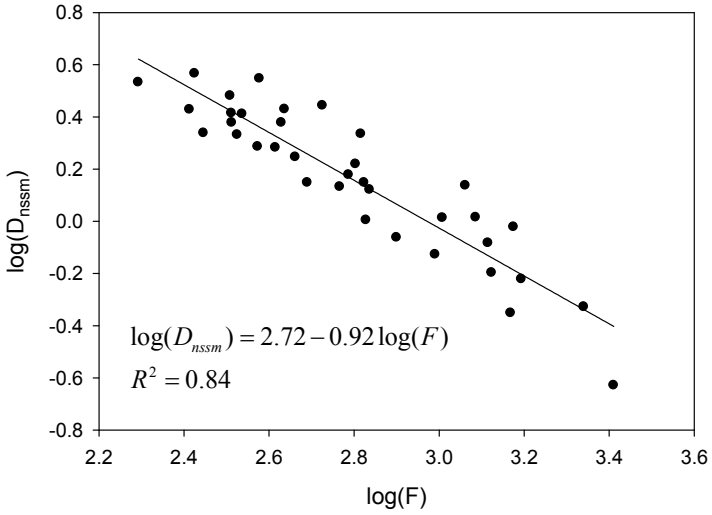

Figure 7.18: Correlation between D_{nssm} and F

Formation Factor, Porosity and Tortuosity Constant

The correlation between formation factor and porosity is described by Equation 2-24 as:

$$F = a \cdot \phi^{-m} \tag{7-5}$$

In some investigations, the value of *a* was set to 1, and Equation 7-5 becomes:[44, 88]

$$m = -\frac{\ln(F)}{\ln(\phi)} \tag{7-6}$$

The calculated value of *m* is listed in Table 7.5. It shows that the value of *m* calculated by Equation 7-6 ranged from 1.96 to 2.66, which is in partial agreement with the reported *m* values in the literature[44, 54, 57, 88]. However, the *m* values for specimens with FA (Mix A, J, B, D, C, K, L) ranged from 2.35 to 2.66, which is larger than the *m* values (1.96 to 2.33) obtained from specimens with Slag or FA/Slag (Mix G, E, F, I, H).

Some authors suggested that Equation 7-6 should be applied to calculate the value of *m* [44, 57]. Figure 7.19 shows results of regression analysis for constant *a* and *m* using Equation 7-5, in which the specimens were separated to two groups (specimens with FA only and specimens with Slag or FA/Slag). In Figure 7.14, *m* = 3.22 and *a* = 0.11 for specimens with FA, and *m* = 2.59 and *a* = 0.27 for specimens

with Slag or FA/Slag, which is in partial agreement with results reported by Backe (m=5.77, a=0.126) and Tumidajski (m=2.55, a=0.64 for cement paste and m=2.14, a=0.02 for mortar) [44, 57].

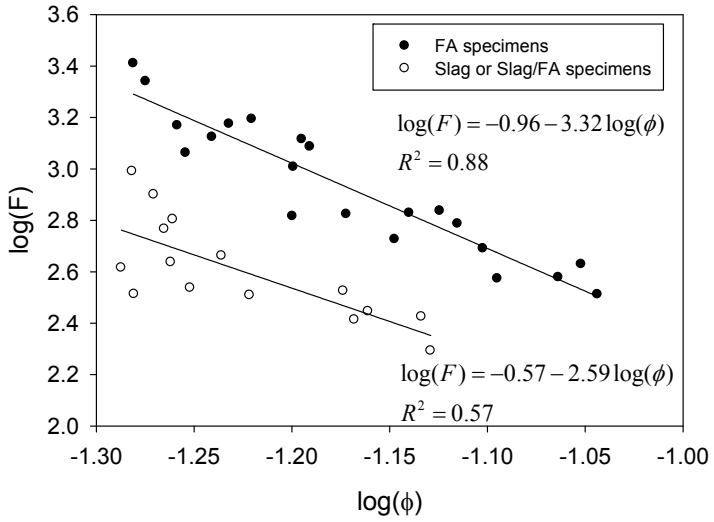

Figure 7.19: Calculation of a and m by regression analysis

Tortuosity vs. D_{nssm}

Tortuosity of the tested specimens was calculated using Equation 2-25:

$$\tau = F \cdot \phi \tag{7-7}$$

The calculated τ is listed in Table 7.5 and the τ values ranged from 14.6 to 135. The τ values in this investigation are in agreement with the results from Ahman et al (38 to 275) obtained through gas diffusion test and pore properties of concrete[134]. Low τ values (3 to 5) were reported on blended cement paste with high porosity (0.1 to 0.5) by Zeng, et al.[135].

A good correlation between tortuosity and. D_{nssm} is found as shown in , which is similar to the results reported by Ahman as shown in Figure 7.21 [134].

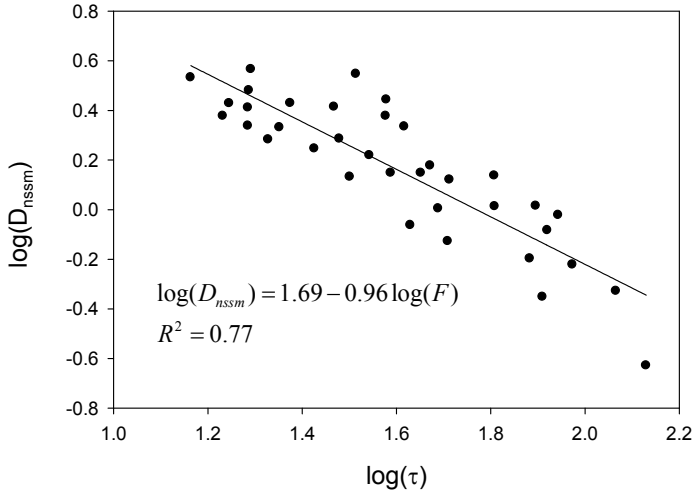

Figure 7.20: Correlation between D_{nssm} and tortuosity

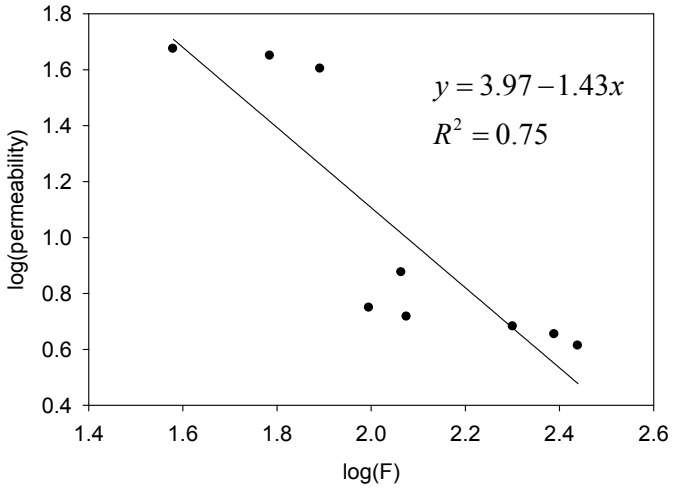

Figure 7.21: Correlation between tortuosity and permeability[134]

The correlation shown in Figure 7.21 indicates that tortuosity plays an important role in affecting the chloride ion diffusivity in concrete. During the hydration period, porosity, tortuosity as well as pore solution change with time, which together affect the diffusivity properties of concrete. However, the correlation shown in Figure 7.21 could provide a method to analyze the independent effect of tortuosity on chloride diffusivity in concrete. It is important to note that all the above applies for concrete under saturated conditions that have been cured for more than a year. The correlations and findings reported

here might not apply to fresh concrete (as values for these types of concrete were not included in the correlations).

7.4 Conclusions

1. The leaching method could provide a direct technique to measure pH and conductivity of concrete pore solutions. Leaching for pH measurement has been reported before, but not for conductivity.

2. Use of pozzolanic admixtures decreases both the pH and conductivity of concrete pore solutions.

3. Archie's law could be applied to analyze the correlation of porosity and formation in concrete. A good correlation is found between migration coefficients and formation factor.

4. A good correlation is found between tortuosity and migration coefficients, and based on this correlation; it is possible to study how tortuosity affects diffusion of chloride in concrete.

8. CONCLUSION

This investigation presents the results of temperature effect on durability properties (resistivity and diffusivity) and the compressive strength of concrete with pozzolans, and the effect of pozzolanic admixtures on microstructure and chemical compositions of concrete pore solution. Based on the results and discussion presented in the previous chapters (Chapters 3 to 7), the following conclusions are reached:

1. A resistivity-dependent method based on Arrhenius equation has been developed to normalize the temperature effect or electrical resistivity of concrete. This method could be applied on saturated concrete as well as concrete subjected to a fixed RH condition. Compared with traditional methods, the resistivity-dependent method is more precise in normalizing temperature effect on concrete. Also, this method could provide more precise results in predicting service life of reinforced concrete structures exposed to environments with different temperatures.

2. The accelerated curing regimes significantly increased the 28-day compressive strength. The 2RT/26ET curing regime could provide 28-day compressive strength and resistivity equivalent to the 6 to 14 months of specimens cured under RT. With the resistivity measurements, it was found that the accelerated curing regimes could increase concrete's resistance to chloride ion penetration at both short-term (28 days) and long-term (up to 700 days in this investigation).

3. A correlation between electrical resistivity and migration coefficients has been developed. Based on this correlation, electrical resistivity measurement could be an alternative of the RCM test to evaluate concrete's resistance to chloride ion permeability. A further application of this correlation is to estimate the migration coefficients by electrical resistivity measurement, which could be employed in predicting service of concrete structures.

4. A correlation between migration coefficients (D_{nssm}) and activation energy for diffusivity ($E_{a,D}$) has been developed, which indicates that the temperature effect on diffusivity of chloride ions in concrete is dependent on the intrinsic diffusivity of concrete. With this innovative correlation, the temperature effect on chloride diffusivity in concrete could be more precisely described, providing a more precise prediction of service life of concrete structures.

5. For saturated concrete with the same resistivity (or diffusivity), the values of activation energy obtained from resistivity and diffusivity are the same or very similar. As the activation energy

for resistivity could be calculated by 21°C resistivity, the activation energy for diffusivity (D_{nssm}) could also be calculated by resistivity values.

6. Regarding pH and conductivity: the leaching method could provide a direct way to measure both pH and conductivity of saturated concrete from leached pore solution. The use of SCMs admixtures reduce significantly the pH and conductivity of pore solution, and this effect is more pronounced for concrete mixes with high replacement ratio of SCMs. The observed effect of FA on pH and conductivity is more significant than that observed on concrete specimens with Slag. The decrease of pH and conductivity of pore solution is due to both dilution effect and pozzolanic reactions.

7. The diffusivity of concrete is greatly correlated to the microstructure properties of concrete, such as porosity, formation factor and tortuosity.

REFERENCES

1. Mohamed, A.E., (2008) *Steel-reinforced concrete structures: assessment and repair of corrosion*. Boca Raton, FL, CRC Press.

2. Mindess, S., Young, J. F. (1981), *Concrete*: Englewood Cliffs, N.J. : Prentice-Hall.

3. Broomfield, J.P., (2007) *Corrosion of Steel in Concrete: understanding, investigation and repair* 2nd ed. Boca Raton, FL, CRC Press.

4. Tutti, K., (1982) "*Corrosion of Steel in Concrete"*, , Swedish Cement and Concrete Research Institute, Stockholm.

5. CHLOREST, "*Guideline for Practical Use of Methods for Testing the Resistance of Concrete to Chloride Ingress"*. EU-Project G6RD-CT-2002-00855 Resistance of concrete to chloride ingress - from laboratorytests to in-field performance (CHLORTEST), Swedish National Testing and Research Institute, Boras,Sweden, 2005.

6. Böhni, H., (2005) "*Corrosion in Reinforced Concrete Structures*" Boca Raton, FL, CRC Press.

7. DuraCrete, (2000) *Statistical Quantification of the Variables in the Limit State Functions.* The European Union-Brite EuRam III.

8. Lay, S. and Schiebl, P., (2003) *Service Life Models: Instructions on Methodology and Application of Models for the Prediction of the Residual Service Life for Classified Environmental Loads and Types of Structures in Europe.* LIFECON.

9. Alonso, M.C., Andrade, C. and Gonzalez, J. A., (1988), *Relation between Resistivity and Corrosion Rate of Reinforcement in Carbonated Mortar with Several Cement Types.* Cement and Concrete Research, Vol **8**: p. 687-698.

10. AASHTO T277, (2002) *Standard Method of Test for Resistance of Concrete to Chloride Ion Penetration.* American Association of State Highway and Transportation Officials, Washington, D.C.

11. ASTM C1202, (2010) *Standard Test Method for Electrical Indication of Concrete's Ability to Resist Chloride Ion Penetration, ASTM International, West Conshohocken, PA*.

12. NTBuild 443, (1995) *Concrete, Hardened: Accelerated Chloride Penetration*, Nordtest Method.

13. NTBuild 492, (1999) *Concrete, Mortar and Cement-based Repair Materials: Chloride Migration Coefficient from Non-steady-state Migration Experiments*, Nordtest Method.

14. FM5-578 FDOT, (2004) *Florida Method of Test For Concrete Resistivity as an Electrical Indicator of its Permeability*.

15. Kessler, R. J., Powers, R. G. and Paredes, M. A. (2005), *Resistivity Measurements of Water-Saturated Concrete as an Indicator of Permeability*, in *Corrosion/*2005.

16. Langford, P. and Broomfield, J., (1987) *Monitoring the Corrosion of Reinforcing Steel.* Construction Repair, **1**(2): p. 32-36.

17. Ozyildirim, H.C., (1998) *Effects of temperature on the development of low permeability in concretes*. Feb, Virginia Transportation Research Council.

18. Ahmed, H.E.H., (2005) *Early Prediction of Concrete Compressive Strength through Accelerated Curing Regime*, in *Eleventh International Colloquium on Structural and Geotechnical Engineering*. Cairo.

19. Liu, Y., (2008) *Experiments and Modeling on Resistivity of Multi-layer Concrete with and without Embedded Rebar*. Ms. Thesis, Florida Atlantic University: Boca Raton, FL.

20. Uysal, M., Kemalettin, Y. and Metin, I., (2012) *The Effect of Mineral Admixtures on Mechanical Properties, Chloride Ion Permeability and Impermeability of Self-compacting Concrete.* Construction and Building Materials, Vol. **27**: p. 263-270.

21. Nokken, M., Boddy, A., Hooton, R. D. and Thomas, M.D.A., (2006) *Time Dependent Diffusion in Concrete - Three Laboratory Studies.* Cement and Concrete Research, Vol. **36**: p. 200-207.

22. ASTM C684 (1999), *Standard Test Method for Making, Accelerated Curing, and Testing Concrete Compression Test Specimens*, ASTM International, West Conshohocken, PA.

23. Hooton, R.D. and Titheringtonb, M.P. , (2004) *Chloride Resistance of High-performance Concretes Subjected to Accelerated Curing.* Cement and Concrete Research, Vol. **34**: p. 1561-1567.

24. Stephanie, C., (1999) *Influence of Pozzolanic Admixtures on Concrete Pore Water pH, Chloride Diffusion and Chloride Binding.* Ms Thesis, Florida Atlantic Universitiy: Boca Raton, FL.

25. Shehata, M.H., and Thomas, M. D. A., (1999) Roland F. Bleszynski, *The Effects of Fly Ash Composition on the Chemistry of Pore Solution in Hydrated Cement Pastes.* Cement and Concrete Research, Vol. **29**: p. 1915-1920.

26. Diamond, S., (1981) *Effects of Two Danish Flyashes on Alkali Contents of Pore Solutions of Cement-Flyash Pastes.* Cement and Concrete Research, Vol. **11**: p. 383-394.

27. Mehta, P.H., (1986) *Concrete: Structure, Properties, and Materials* Englewood Cliffs, N.J. : Prentice-Hall.

28. Groose, C.U., (2007) *Advances in Construction Materials 2007*. : Berlin, Heidelberg : Springer-Verlag Berlin Heidelberg.

29. Bertolini, L.E., B., Pedeferri, P. and Polder, (2004) R, *Corrosion of steel in concrete: Prevention, diagnosis, repair*: Weinheim ; Cambridge : Wiley-VCH.

30. ASTM C1556, (2004) *Standard Test Method for Determining the Apparent Chloride Diffusion Coefficient of Cementitious Mixtures by Bulk Diffusion, ASTM International, West Conshohocken, PA*.

31. Stanish, K.D., Hooton.R.D. and M.D.A. Thomas, *Testing the Chloride Penetration Resistance of Concrete: A Literature Review*, Department of Civil Engineering, University of Toronto.

32. Nilsson, L., Ngo, M.H. and Gjorv, O.E. (1998) *High-performance Repair Materials for Concrete Structures in the Port of Gothenburg*. in *Second International Conference on Concrete Under Severe Conditions: Environment and Loading*.

33. Mangat, P.S. and Molloy, B.T., (1994) *Prediction of Long Term Chloride Concentration in Concrete.* Materials and Structures, Vol. **27**: p. 338-346.

34. Andrade, C., Castellote, M. and d'Andrea, R., (2011) *Measurement of Aging Effect on Chloride Diffusion Coefficients in Cementitious Matrices.* Journal of Nuclear Materials, Vol. **412**: p. 209-216.

35. Tang, L. and Gulikers, J., (2007) *On the Mathematics of Time-dependent Apparent Chloride Diffusion Coefficient In Concrete.* Cement and Concrete Research, Vol. **37**: p. 589-595.

36. Stanish, K. and Thomas, M., (2003) *The Use of Bulk Diffusion Tests to Establish Time-dependent Concrete Chloride Diffusion Coefficients.* Cement and Concrete Research, Vol. **33**: p. 55-62.

37. Andrade, C., Castellote, M. and d'Andrea, R., (2011)*Chloride Aging Factor of Concrete Measured by Means of Resistivity*, in *International Conference on Durability of Building Materials and Components*: Porto-Portugal.

38. Polder, R.B., (2001) *Test Methods for on Site Measurements of Resistivity of Concrete-a RILEM TC-154 Technical Recommendation.* Construction and Building Materials Vol. **15**: p. 125-131.

39. Castellote, M., Andrade, C. and Alonso, M. C. (2002), *Standardization, to a Reference of 25°C, of Electrical Resistivity for Mortars and Concretes in Saturated or Isolated Conditions.* ACI Materials Journal, Vol. **99**(2).

40. Büteführ, M., Fischer, C., Gehlen, C., Menzel, K., and Nürnberger, U., (2006) *On-site Investigation on Concrete Resistivity- A Parameter of Durability Calculation of Reinforced Concrete Structures.* Materials and Corrosion, Vol. **57**(12).

41. Langford, P. and Broomfield, J., (1987) *Monitoring the Corrosion of Reinforcing Steel.* in Constr. Repair, May: p. 32-36.

42. Bertolini, L. and Polder, R. B., (1997) *Concrete Resistivity and Reinforcement Corrosion Rate as a Function of Temperature and Humidity of the Environment*, in *TNO report 97-BT-R0574*.

43. McCarter, W.J., (2006) *Monitoring the Influence of Water and Ionic Ingress on Cover-Zone Concrete Subjected to Repeated Absorption.* Cement and Concrete Research, Vol. **18**.

44. Tumidajski, P.J., Schumacher, A. S., Perron, S., Gu, P. and Beaudoin, J. J, (1996) *On the Relationship between Porosity and Electrical Resistivity in Cementitious System.* Cement and Concrete Research, Vol. **25**(4): p. 539-544.

45. Elkey, W. and Sellevold, E. J, (1995) *Electrical Resistivity of Concrete*, Norwegian Public Roads Administration Publication.

46. Shi, C., Stegemann, J. A., and Caldwell, R. J., (1998) *Effect of Supplementary cementing Materials on the Specific Conductivity of Pore Solution and its Implications on the Rapid Chloride Permeability Test (AASHTO T277 and ASTM C1202) Results.* ACI Materials Journal, Vol. **95**(4).

47. McCarter, W.J., Starrs, G. and Chrisp, T.M, (2000) *Electrical Conductivity, Diffusion, and Permeability of Portland Cement-based Mortars.* Cement and Concrete Research, Vol. **30**: p. 1395-1400.

48. Villagrán Zaccardi, Y.A., Fullea García, J., Huélamo, P. and Di Maio, Á. A, (2009) *Influence of Temperature and Humidity on Portland Cement Mortar Resistivity Monitored with Inner Sensors.* Materials and Corrosion, Vol. **60**(4).

49. Gjørv, O.E., Vennesland, Ø., and El-Busaidy, A. H. S., (1977) *Electrical Resistivity of Concrete in the Oceans*, in *Offshore Technology Conference*. Houston, TX. p. 581-588.

50. Wenner, F., (1916) *A Method of Measuring Earth Resistivity*, Bulletin of Bureau of Standards p. 469-478.

51. Morris, W., Moreno, E.I. and Sagüés, A. A. , (1996) *Practical evaluation of resistivity of concrete in test cylinders using a Wenner array probe.* Cement and Concrete Research, Vol. **26**(12): p. 1779-1787

52. Lu, X., (1997) *Application of the Nernst-Einstein Equation to Concrete.* Cement and Concrete Research, Vol. **27**(2): p. 293-302.

53. Sengul, O. and Gjørv, O. E., (2008) *Electrical Resistivity Measurement for Quality Control During Concrete Construction.* ACI Materials Journal, Vol. **105**(6).

54. McCarter, W.J., Starrs, G., Kandasami, S., Jones, R. and Chrisp, M., (2009) *Electrode Configurations for Resistivity Measurements on Concrete.* ACI Materials Journal, May-June, Vol. **106**(3).

55. Klinghoffer, O. and Rislund, E. (1995) *Determination of Chloride Diffusivity in Matured Concrete Based on Electrical Conductivity Measured Hardening Material*. in *International Symposium Non-Destructive Testing in Civil Engineering (NDT-CE)*.

56. Promentilla, M.A.B., Sugiyama, T., Hitomi, T. and Takeda, N., (2009) *Quantification of Tortuosity in Hardened Cement Pastes Using Synchrotron-based X-ray Computed Microtomography.* Cement and Concrete Research, Vol. **39**: p. 548-557.

57. Backe, K.R., Lile, O.B. and Lyomov, S.K., (2001) *Characterizing Curing Cement Slurries by Electrical Conductivity* SPE Drilling & Completion, Vol. **16**(4).

58. Rupnow, T.D. and Icenogle, P., (2011) *Evaluation of Surface Resistivity Measurements as an Alternative to the Rapid Chloride Permeability Test for Quality Assurance and Acceptance*. Final Report, Louisiana Transportation Research Center.

58b. Paredes, M.; Jackson, N.M.; El Safty, A.; Dryden, J.; Joson, J.; et al., (2012) "Precision Statements for the Surface Resistivity of Water Cured Concrete Cylinders in the Laboratory", Advaces in Civil Engineering, Vol, **1**(1)

59. AASHTO TP-95, (2011) *Surface Resistivity Indication of Concrete's Ability to Resist Chloride Ion Penetration.*

60. Presuel-Moreno, F., Suarez, A. and Liu, Y., (2010) *Characterization of New and Old Concrete Structures Using Surface Resistivity Measurements*. Final Report BD546-08 Tallahassee, FL Florida Department of Transportation Research Center..

61. Vries, H.D. (2002) *Durability of Concrete: A Major Concern to Owners of Reinforced Concrete Structures.* in *Concrete for Extreme Conditions Proceedings of the International Conference held at the University of Dundee, Scotland, London : Thomas Telford*.

62. Andrade, C. and Alonso, C., (1996) *Corrosion Rate Monitoring in the Laboratory and On-site.* Construction and Building Materials, Vol. **10**(5): p. 315-328.

63. Bentur, A., Berke, N. and Diamond, S., (1998) *Steel Corrosion in Concrete: Fundamentals and civil engineering practice* London ; New York : E & FN Spon.

64. Glass, G.K., Page, C.L. and Short, N. R. , (1991) *Factors Affecting the Corrosion Rate of Steel in Carbonated Mortars.* Corrosion Science, Vol. **32**(12): p. 1283-1294.

65. Morris, W., Vico, A., Vazquez, M. and de Sanchez, S. R., (2002) *Corrosion of Reinforcement Steel Evaluated by Means of Concrete Resistivity Measurements.* Corrosion Science, Vol. **44**: p. 81-99.

66. Gulikers, J., (2005) *Theoretical Considerations on the Supposed Linear Relationship Between Concrete Resistivity and Corrosion Rate of Steel Reinforcement.* Materials and Corrosion, Vol. **56**(6): p. 293-403.

67. Andrade, C. and Alonso, C., (2004) *Test Methods for on-site Corrosion Rate Measurement of Steel Reinforcement in Concrete by Means of the Polarization Resistance Method.* Materials and Structures, Vol. **37**: p. 623-643.

68. Gowers, K. R. and Millard, S. G., (1999) *Measurement of Concrete Resistivity for Assessment of Corrosion Severity of Steel Using Wenner Technique.* ACI Materials Journal, Vol. **96**(5).

69. Chrisp, T.M., Starrs, G., McCarter, W. J., Rouchotas, E. and Belewett, J., (2001) *Tempreature-conductivity Relationships for Concrete: An Activation Energy Approach.* Journal of Materials Science Letters Vol. **20**: p. 1085-1087.

70. McCarter, W.J., Chrisp, T. M., Starrs, G., Basheer, P. A. M. and Blewett, J., (2005) *Field Monitoring of Electrical Conductivity of Cover-zone Concrete.* Cement & Concrete Composites Vol. **27**: p. 809-817.

71. Pour-Ghaz, M., Isgor, O. B., and Ghods, P, (2009) *The Effect of Temperature on the Corrosion of Steel in Concrete. Part 1: Simulated Polarization Resistance Tests and Model Development.* Corrosion Science, Vol. **51**: p. 415-425.

72. Julio-Betancourt, G.A. and Hooton, R. D., (2003) *Study of the Joule Effect on Rapid Chloride Permeability Values and Evaluation of Related Electrical Properties of Concretes.* Cement and Concrete Research, Vol. **34**: p. 1007-1015.

73. Bockris, J.O. and Reddy, A. K., (2002) *Modern Electrochemistry, Volume 1*. New York : Kluwer Academic.

74. Lin, S.H., (1993) *Chloride Diffusion in Porous Concrete Under Conditions of Variable Temperature* Heat and Mass Transfer Vol. **28**(7): p. 411-415.

75. Xi, Y. and Bazant, Z.P., (1999) *Modeling Chloride Penetration in Saturated Concrete.* Journal of Materials in Civil Engineering, Vol. **11**(1): p. 58-65.

76. Yuan, Q., Shi, C., Schutter, G. D. and Audenaert, K. (2008) *Effect of Temperature on Transport of Chloride Ions in Concrete*. in *Concrete Repair, Rehabilitation and Retrofitting II*. Cape Town, South Africa.

77. Page, C.L., Short, N. R., and Tarras, A. (1981) *Diffusion of Chloride Ions in Hardened Cement Pastes.* Cement and Concrete Research, Vol. **11**(3): p. 395-406.

78. Nguyen, T.S., Lorent, S. and Carcasses, M., (2009) *Effect of the Environment Temperature on the Chloride Diffusion through CEM-I and CEM-V Mortars: An Experimental Study.* Construction and Building Materials, Vol. **23**: p. 795-803.

79. Samson, E. and Marchand, J., (2007) *Modeling the Effect of Temperature on Ionic Transport in Cementitious Materials.* Cement and Concrete Research, Vol. **37** pp. 455-467.

80. Benz, E.C., Thomas, M. D. A. and Ehlen, M.A., (2012) *Life-365 Service Life Prediction Model for Reinforced Concrete Exposed to Chlorides*.

81. ASTM C618, (2008) *Standard Specification for Coal Fly Ash and Raw or Calcined Natural Pozzolan for Use in Concrete,* ASTM International, West Conshohocken, PA.

82. Neville, A.M., (2000) *Properties of Concrete*. Harlow, England ; New York : Prentice Hall/Pearson Education.

83. ASTM C989, (1999) *Standard Specification for Ground Granulated Blast-Furnace Slag for Use in Concrete and Mortars*, ASTM International, West Conshohocken, PA.

84. Ramachandran, V.S., (1995) *Concrete Admixtures Handbook: Properties, Science and Technology*. Second Edition ed. Park Ridge, N.J., U.S.A. : Noyes Publications.

85. FDOT, (2000) *Standard Specifications for Road and Bridge Construction*.

86. Newman, J., Choo, B. S., (2003) *Advanced Concrete Technology: Constituent Materials*. Oxford : Elsevier Science & Technology.

87. Canham, I., Page, C. L. and Nixon, P. J., (1987) *Aspects of the Pore Solution Chemistry of Blended Cements Related to The Control of Alkali Silica Reaction.* Cement and Concrete Research, Vol. **17**: p. 839-844.

88. Nokken, M.R. and Hooton, R.D., (2008) *Using Pore Parameters to estimate Permeability or Conductivity of Concrete.* Materials and Structures, Vol. **41**: p. 1-16.

89. ACI, *Building Code Requirements for Structural Concrete and Commentary*. 2008.

90. Goto, S. and Roy, D.M., (1981) *The Effect of w/c Ratio and Curing Temperature on the Permeability of Hardened Cement Paste.* Cement and Concrete Research, Vol. **11**(4): p. 575-579.

91. Williams, J.T. and Owens, P.L. (1982) *The Implications of a Selected Grade of United Kingdom Pulverized Fuel Ash on the Engineering Design and Use in Structural Concrete*. in *Proceedings of International Symposium on the Use of PFA in Concrete*. Leeds, U.K.: Department of Civil Engineering, University of Leeds.

92. Ozturan, T. and Bastopcu, M. E., (2003) *SP212-23 Effects of Curing on Durability of Fly Ash Concrete*, in *Sixth CANMET/ACI International Conference on Durability of Concrete*. p. 353-368.

93. ACI, (1978) *Accelerated Strength Testing*. Publication SP-56.

94. Freyne, S.F. and Russell, B. W. and Bush Jr, T. D., (2003) *Heat Curing of High-Performance Concrete Containing Type III Cement.* ACI Materials Journal, Vol. **100**(6).

95. Verbeck, G. J., Helmuth, R. A, (1969) *Structures and Physical Properties of Cement Paste*, in *Proceedings of the Fifth International Symposium on the Chemistry of Cements*. Tokyo. p. 1-32.

96. Detwiler, R.J. and Kjellsen, K. O., and Gjorv. O. E., (1991) *Resistance to Chloride Intrusion of Concrete Cured at Different Temperatures.* ACI Materials Journal, Vol. **88**(1).

97. Detwiler, R.J. and Fapohunda, C. A. and Natale, J, (1994) *Use of Supplementary Cementing Materials to Increase the Resistance to Chloride Ion Penetration of Concretes Cured at Elevated Temperatures.* ACI Materials Journal, Vol. **91**(1).

98. Ezziane, K., Kadri, E., Bougara, A. and Bennacer, R, (2010) *Analysis of Mortar Long-Term Strength with Supplementary Cementitious Materials Cured at Different Temperatures.* ACI Materials Journal, Vol. **107**(4).

99. ASTM C684, (1999) *Standard Test Method for Making, Accelerated Curing and Testing Concrete Compression Test Specimens*. ASTM International, West Conshohocken, PA.

100. ACI-517, (1970) *Recommended Practice for Atmospheric Pressure Steam Curing of Concrete*.

101. Kosmatka, S.H., Kerkhoff, B. and Panarese, W. C., (2003) *Design and Control of Concrete Mixtures*. 14th ed. EB 001.: Portland Cement Association.

102. Klieger, P., (1958) *Effect of Mixing and Curing Temperature on Concrete Strength.* Journal of American Concrete Institute, Vol. **54**: p. 1063-1081.

103. Gardner, N.J., (1990) *Effect of Temperature on the Early-age Properties of Type I, Type II, and Type III/fly ash concretes with temperature.* ACI Materials Journal, Vol. **87**(1).

104. Ozyildirim, C. and Halstead, W. J., (1991) *Optimum Mixture Proportions for Concrete Containing Fly Ash and Silica Fume*. Final Report VTRC 91-R21 for VDOT.

105. Tokyay, M., (1999)*Strength Prediction of Fly Ash Concretes by Accelerated Testing.* Cement and Concrete Research, Vol. **29**: p. 1737-1741.

106. Yazici, H., Aydin, S., Yigiter, H., and Baradan, B., (2005) *Effect of Steam Curing on Class C High-Volume Fly Ash Concrete Mixtures.* Cement and Concrete Research, Vol. **35**: p. 1122-1127.

107. Ozkul, M.H., (2001) *Efficiency of Accelerated Curing in Concrete* Cement and Concrete Research, Vol. **31**: p. 1351-1357.

108. Siviero, E., (1994) *Evaluation of Early Concrete Strength* Materials and Structures, Vol. **27**: p. 273-284.

109. Naik, T.R., (1979) *Effect of Cement Types in Accelerated Compressive Strength Testing of Concrete.* Cement and Concrete Research, Vol. **9**(3): p. 377-386.

110. Chini, A.R., Muszynski, L. C., Acquaye, L. and Tarkhan, S. (2003), "*Determination of the Maximum Placement and Curing Temperatures"* Final Report BC 354-29, Tallahassee, FL Florida Department of Transportation Research Center.

111. Newlon Jr, H., (1970) *Evaluation of Several Types of Curing and Protective Materials on Concrete. Final Report On Part II Installation Report and Initial Condition Survey of Bridge Decks*. Virginia Highway Research Council.

112. Nasser, K.W. and Marzouk, H. M.., (1979) *Properties of Mass Concrete Containing Fly Ash at High Temperatures.* ACI Materials Journal, Vol. p. 537-550.

113. Johnston, C.D. (1992) *Durability of High Early Strength Silica Fume Concretes Subjected to Accelerated and Normal Curing*. in *CANMET/ACI 4th International Conference on Fly Ash, Silica Fume, Slag and Natural Pozzolans in Concrete*. Istanbul.

114. Kanda, T.S., F. and Suzuki, K. (1992) *Compressive Strength of Silica Fume Concrete at Higher Temperatures*. in *CANMET/ACI 4th International Conference on Fly Ash, Silica Fume, Slag and Natural Pozzolans in Concrete*. Istanbul.

115. Poon, C.S., Wong, Y. L., and Lam, L., (1997) *The Influence of Different Curing Conditions on the Pore Structure and Related Properties of Fly-ash Cement Pastes and Mortars.* Constrction and Building Materials, Vol. **11**(7-8): p. 383-393.

116. Ozyildirim , H. C. and Halstead, W. J., (1994) *Improved Concrete Quality with Combinations of Fly Ash and Silica Fume* ACI Materials Journal, Vol. **91**(6).

117. Hou, W., Chang, P., and Hwang, C., (2004) *A Study on Anticorrosion Effect in High-performance Concrete by the Pozzolanic Reaction of Slag.* Cement and Concrete Research, Vol. **34**: p. 615-622.

118. Ma, W., Liu, C., Brown, P. W., and Komarneni, S., (1995) *Pore Structures of Fly Ashes Activated by $Ca(OH)_2$ and $CaSO_4 \cdot 2H_2O$.* Cement and Concrete Research, Vol. **25**(2): p. 417-425.

119. Hartt, W.H. and Suarez, J. A., (2007) *Utility of High Alkalinity Cements for Control of Reinforcing Steel Corrosion in Concrete*. Final Report BD 546-01 Tallahassee, FL Florida Department of Transportation Research Center.

120. Jackson, N.M. and Beach, P.V., (2011) *Results of Round-Robin Testing for the Development of Precision Statements for the Surface Resistivity of Water-Saturated Concrete,* Ponte Vedra Beach, FL.

121. FM5-516 FDOT, (2000) *Florida Method of Test For Determining Low-Levels of Chloride in Concrete and Raw Materials* in *FM 5-516*.

122. Cox, K. and De Belie, N. , (2007) *Durability Behaviour of High Volume Fly Ash Concrete*, in *International Conference on Sustainable Construction Materials and Technologies*. Coventry, UK.

123. Nam, J., (2004) *Effect of Alkalinity, Exposure Conditions and Steel-Concrete Interface on the Time-to-Corrosion and Chloride Threshold for Reinforcing Steel in Concrete*. 2004, Florida Atlantic University: Boca Raton.

124. Li, L. and Sagüés, A., (2001) *Metallurgical Effects on Chloride Ion Corrosion Threshold of Steel in Concrete*. Final Report WPI 0510806 Tallahassee, FL Florida Department of Transportation Research Center..

125. Shehata, M. H. and Thomas, M. D. A., (2000) *The Effect of Fly Ash Composition on the Expansion of Concrete Due to Alkali-silica Reaction.* Cement and Concrete Research, Vol. **30**: p. 1063-1072.

126. Hussain, S.E. and Rasheeduzzafar, (1994) *Corrosion Resistance Performance of Fly Ash Blended Cement Concrete.* ACI Materials Journal, Vol **91**(3).

127. ASTM C642, (2006) *Standard Test Method for Density, Absorption, and Voids in Hardened Concrete*, ASTM International, West Conshohocken, PA.

128. Moreno, E.I., (1999) *Carbonation of Blended-cement Concretes*. Ph.D. Dissertation, University of South Florida, Tampa, FL.

129. Sagüés, A.A., Moreno, E. I. and Andrade, C., (1997) *Evolution of pH During In-situ Leaching in Small Concrete Cavities.* Cement and Concrete Research, Vol. **27**(11): p. 11747-1759.

130. Cáseres, L., Sagüés, A. A., Kranc, S. C. and Weyersb, R. E., (2006) *In Situ Leaching Method for Determination of Chloride in Concrete Pore Water.* Cement and Concrete Research, Vol. **36**: p. 492-503.

131. Snyder, K.A., Feng, X. and Keen, B. D., Mason, T. O., (2003) *Estimating the Electrical Conductivity of Cement Paste Pore Solutions from OH^-, K^+ and Na^+ concentrations.* Cement and Concrete Research, Vol **33**: p. 793-798.

132. Mortimer, R.G., (2008) *Physical Chemistry* Third Edition Academic Press.

133. Batchelor, B., (1997) *Discussion of The Paper "On the Relationship Between the Formation Factor and Diffusivity in Mortars".* Cement and Concrete Research, Vol. **27**(6): p. 963-964.

134. Ahman, S., Azad, A. K., and Loughlin, K. F. (2005) *A Study of Permeability and Tortuosity of Concrete*. in *30th conference on OUR WORLD IN CONCRETE & STRUCTURES*. Singapore.

135. Zeng, Q., Li,K., Fen-Chong, T. and Dangla, P. (2012), *Analysis of Pore Structure, Contact Angle and Pore Entrapment of Blended Cement Pastes from Mercury Porosimetry Data.* Cement & Concrete Composites, Vol **34**: p. 1053-1060.

136. Roy, Della M., Karen Luke, and Sidney Diamond. (1985) "Characterization of fly ash and its reactions in concrete." In Mater. Res. Soc. Symp. Proc. Vol 43, pp. 3-20.

APPENDIX A: PLOTS OF RESISTIVITY EVOLUTION WITH TIME

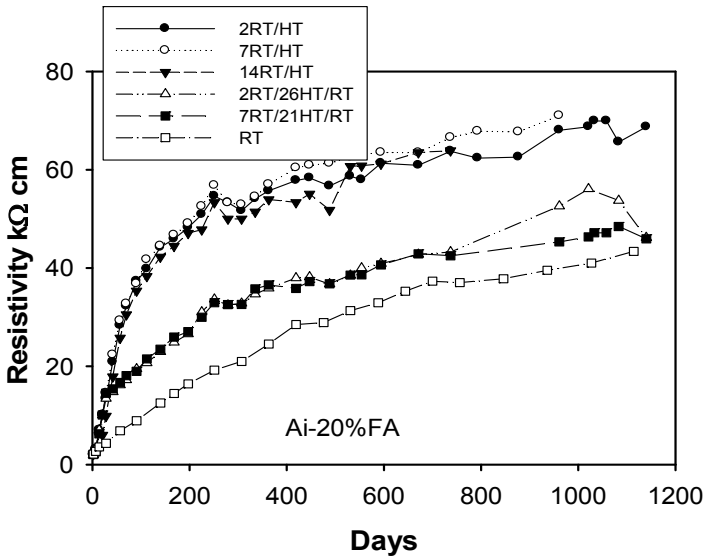

Note: Lime water was changed to fresh water for specimens under 2RT/HT, 7RT/HT, and 14RT/HT at the age of 505 days. Water was refreshed with tap water for specimens under 2RT/HT and 7RT/HT at age of 877 (Mix Ai)

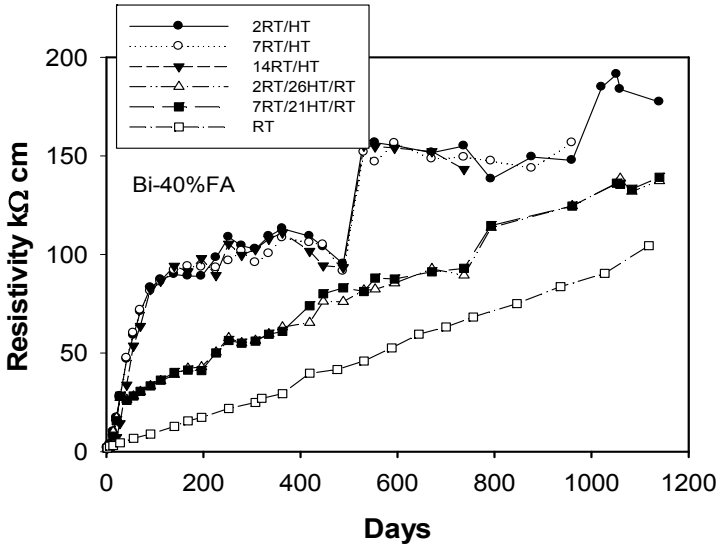

Note: Lime water was changed to fresh water for specimens under 2RT/HT, 7RT/HT, and 14RT/HT at the age of 505 days. Water was refreshed with tap water for specimens under 2RT/HT and 7RT/HT at age of 960 (Mix Bi)

Note: : Lime water was changed to fresh water for specimens under 2RT/HT, 7RT/HT, and 14RT/HT at the age of 479 days (Mix A & Mix B) and 406 days (Mix J)

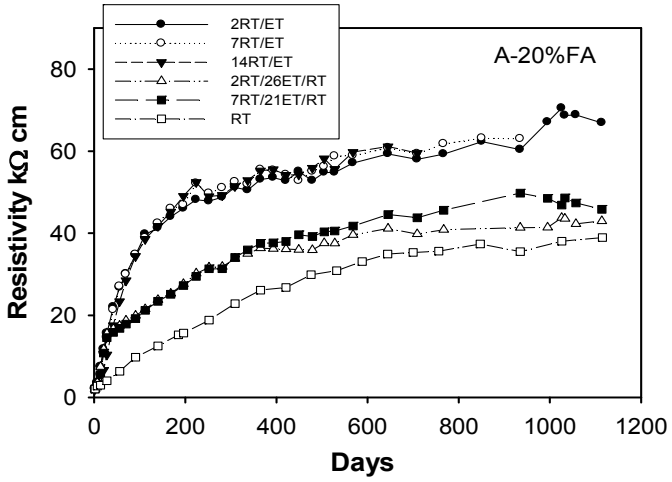

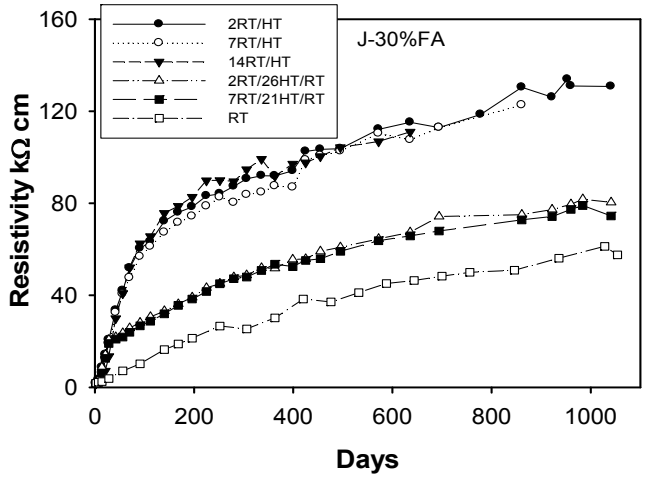

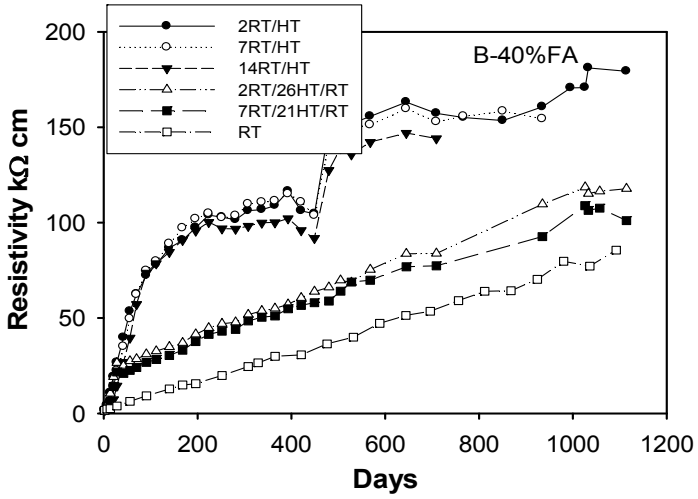

Note: Lime water was changed to fresh water for specimens under 2RT/HT, 7RT/HT, and 14RT/HT at the age of 450 days (Mix D & Mix E) and 400 days (Mix G).

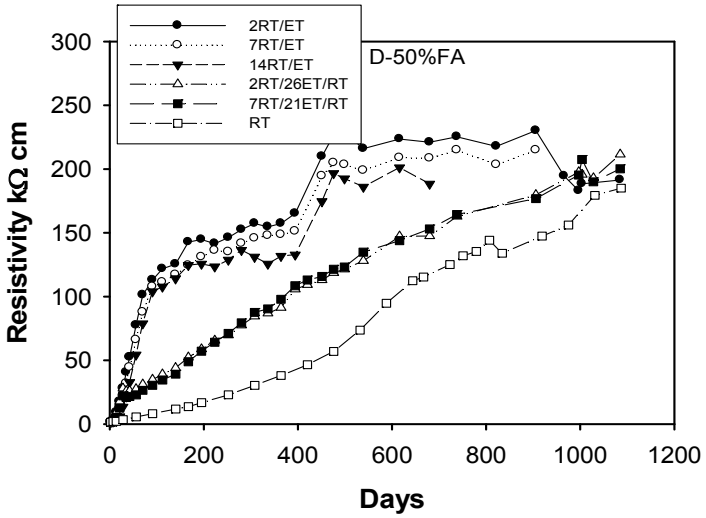

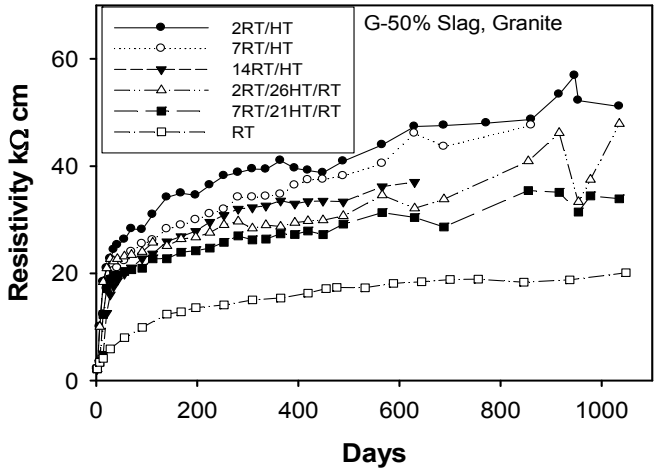

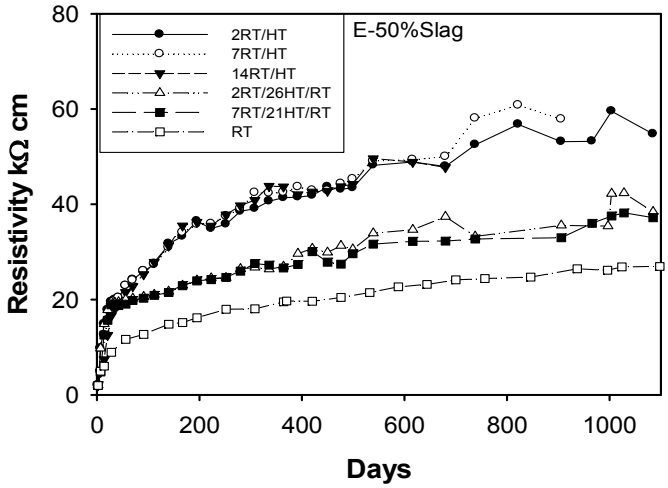

Note: Lime water was changed to fresh water for specimens under 2RT/HT, 7RT/HT, and 14RT/HT at the age of 437 days (Mix F & Mix I) and 406 days (Mix H).

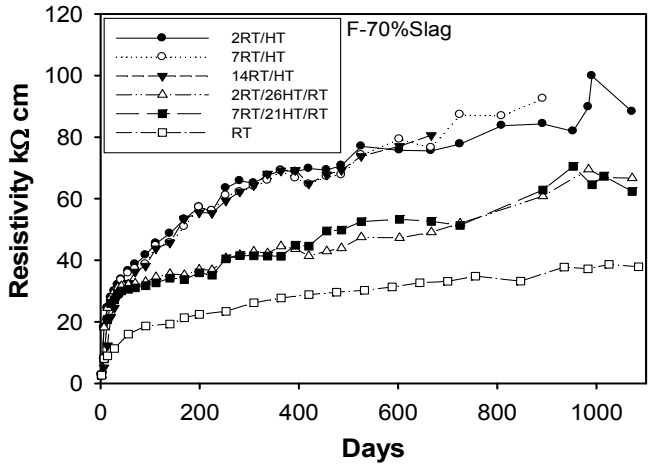

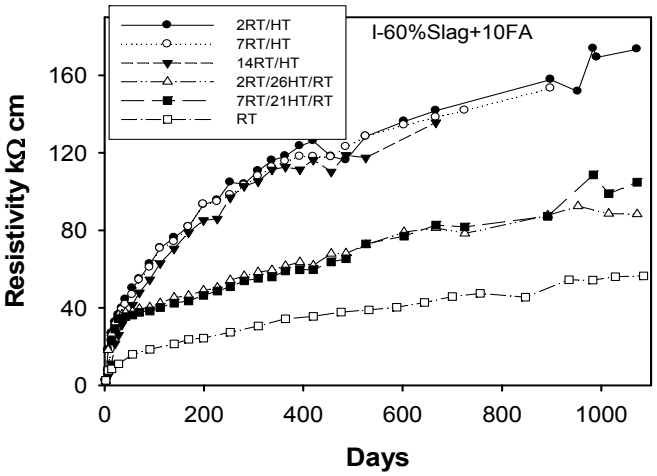

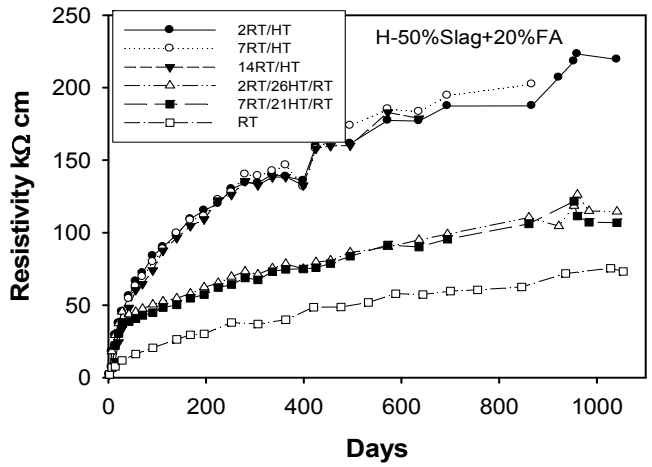

Note: Lime water was changed to fresh water for specimens under 2RT/HT, 7RT/HT, and 14RT/HT at the age of 371 days (Mix K & Mix L) and 400 days (Mix C)

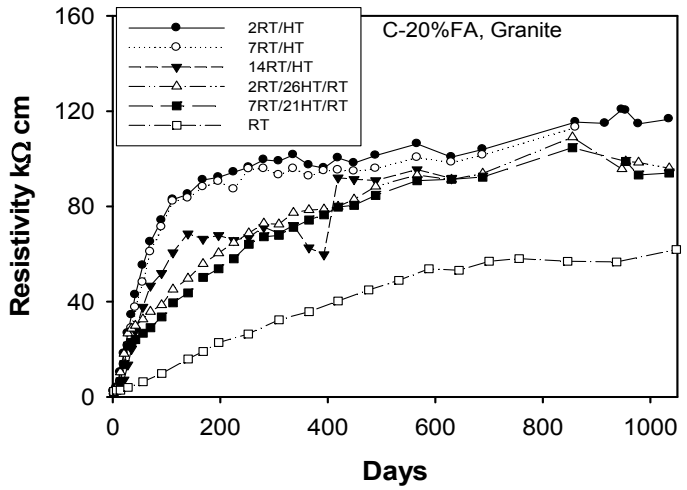

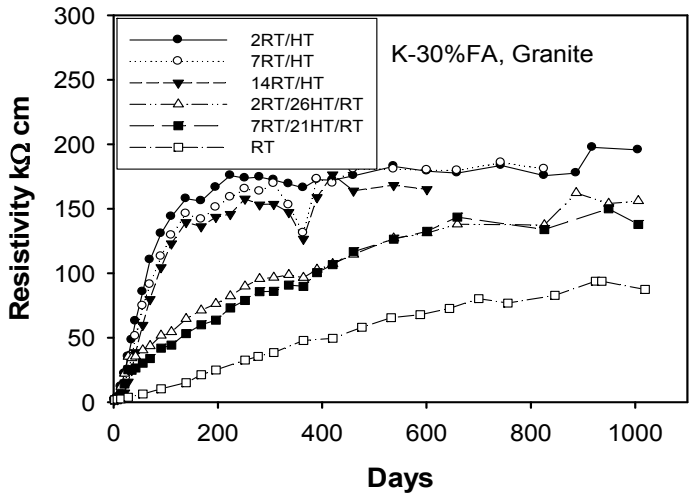

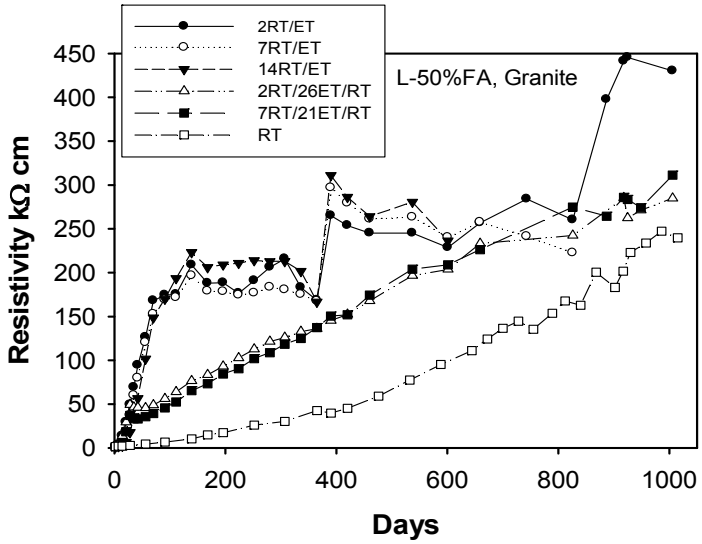

APPENDIX B: AGING FACTOR OF EACH CONCRETE MIX UNDER DIFFERENT CURING CONDITIONS

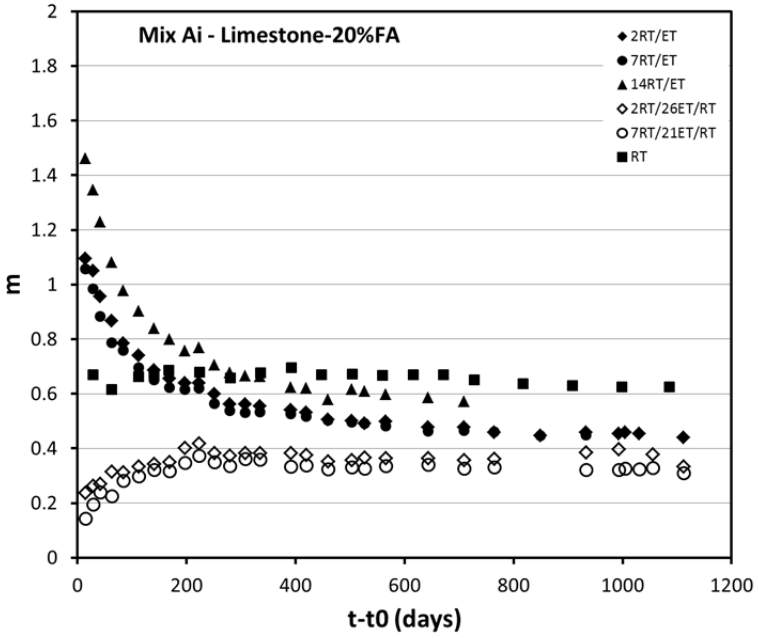

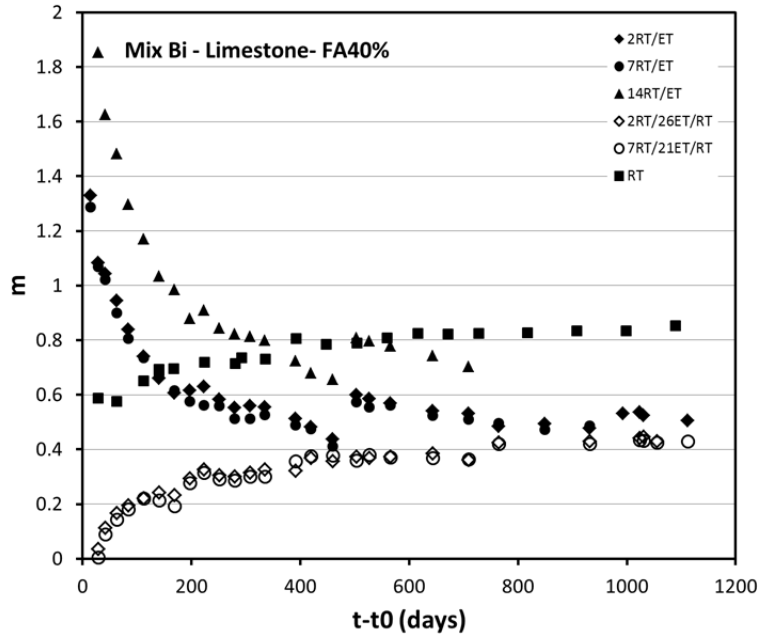

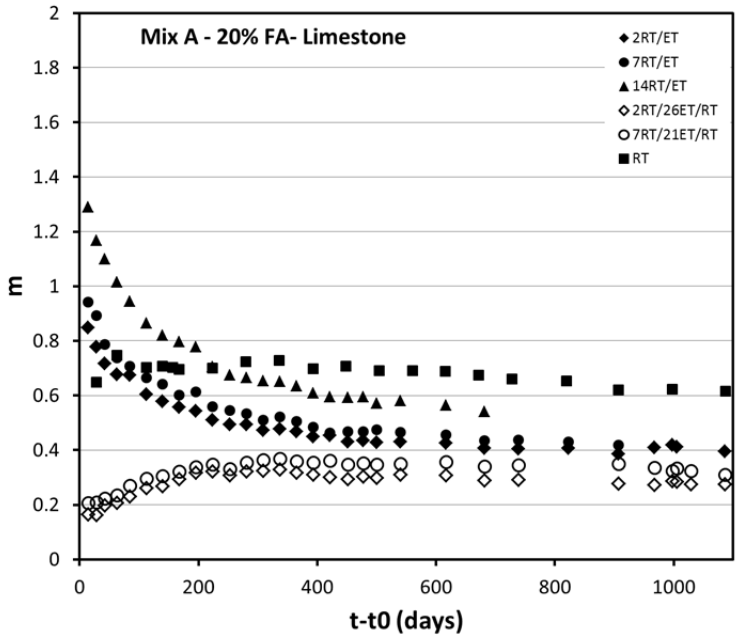
Mix A - 20% FA- Limestone
2RT/ET
7RT/ET
14RT/ET
2RT/26ET/RT
7RT/21ET/RT
RT
m
t-t0 (days)
0
0.2
0.4
0.6
0.8
1
1.2
1.4
1.6
1.8
2
0
200
400
600
800
1000

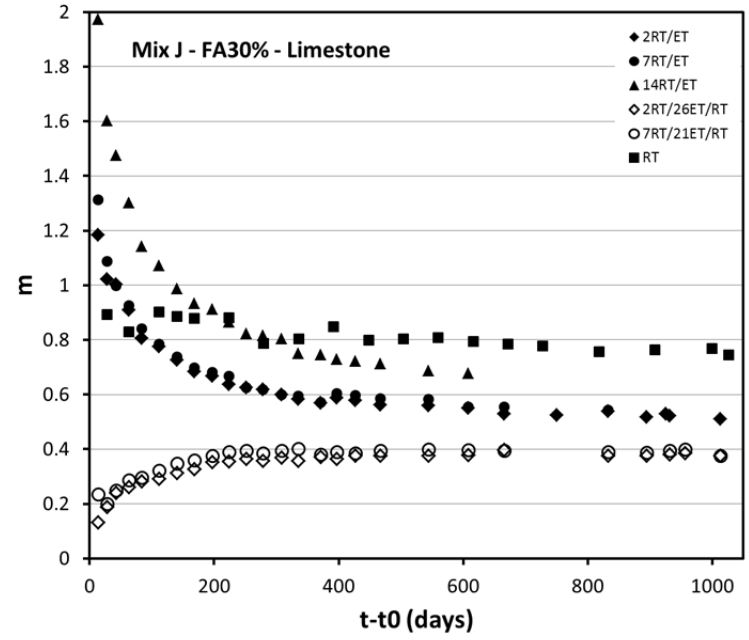
Mix J - FA30% - Limestone
2RT/ET
7RT/ET
14RT/ET
2RT/26ET/RT
7RT/21ET/RT
RT
m
t-t0 (days)
0
0.2
0.4
0.6
0.8
1
1.2
1.4
1.6
1.8
2
0
200
400
600
800
1000

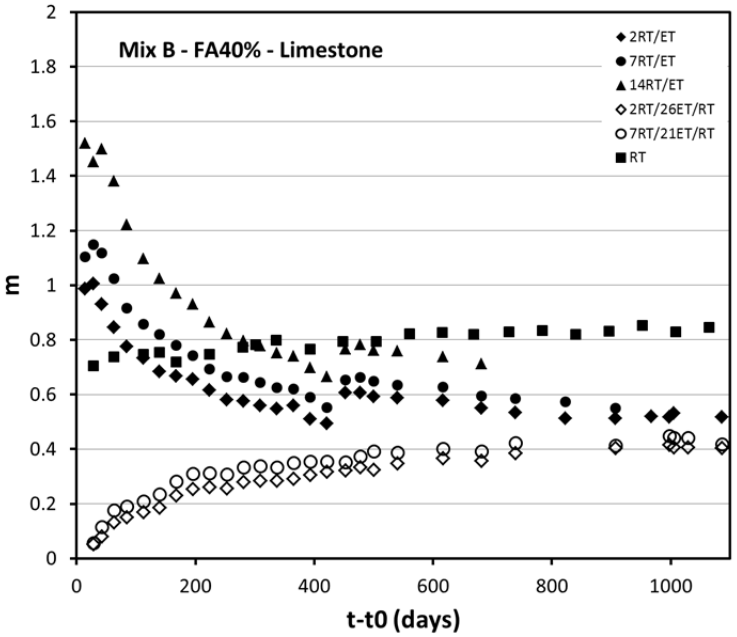
Mix B - FA40% - Limestone
2RT/ET
7RT/ET
14RT/ET
2RT/26ET/RT
7RT/21ET/RT
RT
m
t-t0 (days)
0
0.2
0.4
0.6
0.8
1
1.2
1.4
1.6
1.8
2
0
200
400
600
800
1000

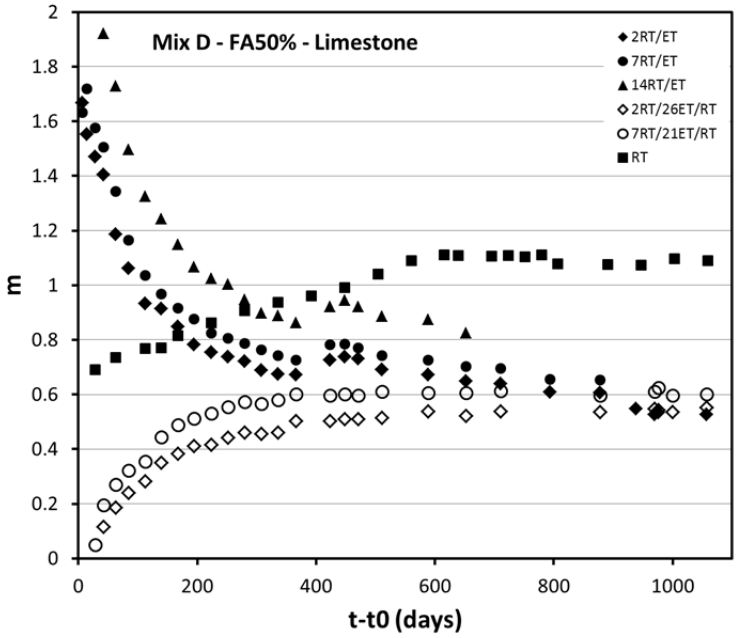
Mix D - FA50% - Limestone
2RT/ET
7RT/ET
14RT/ET
2RT/26ET/RT
7RT/21ET/RT
RT
m
t-t0 (days)
0
0.2
0.4
0.6
0.8
1
1.2
1.4
1.6
1.8
2
0
200
400
600
800
1000

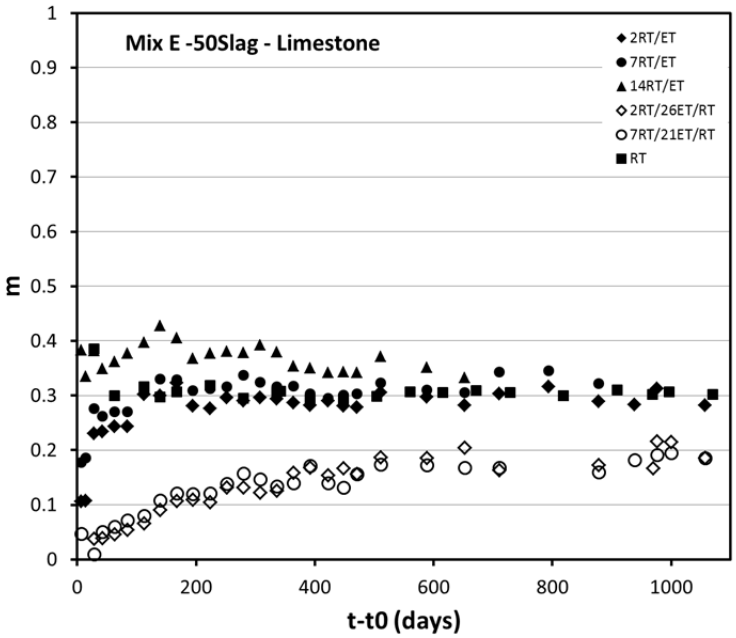
Mix E -50Slag - Limestone
2RT/ET
7RT/ET
14RT/ET
2RT/26ET/RT
7RT/21ET/RT
RT
m
t-t0 (days)
0
0.1
0.2
0.3
0.4
0.5
0.6
0.7
0.8
0.9
1
0
200
400
600
800
1000

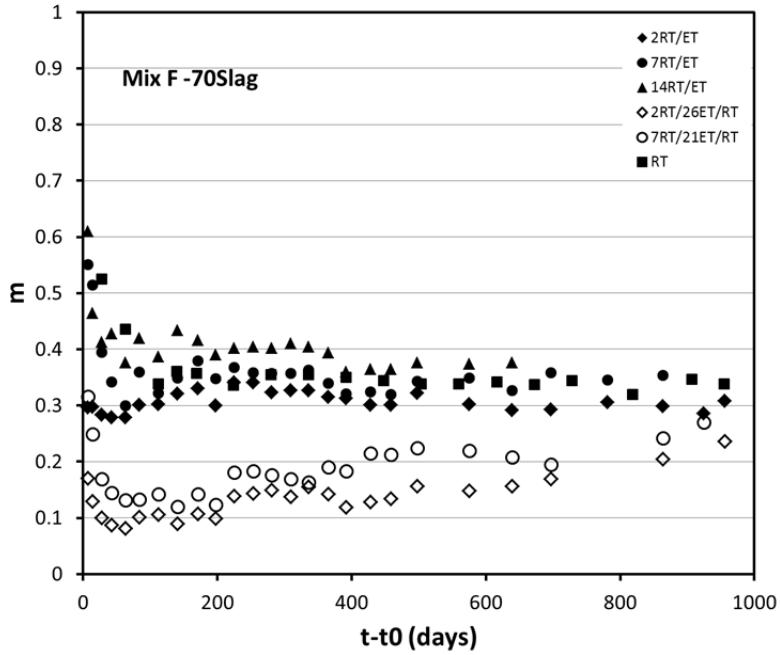
Mix F -70Slag
2RT/ET
7RT/ET
14RT/ET
2RT/26ET/RT
7RT/21ET/RT
RT
m
t-t0 (days)
0
0.1
0.2
0.3
0.4
0.5
0.6
0.7
0.8
0.9
1
0
200
400
600
800
1000

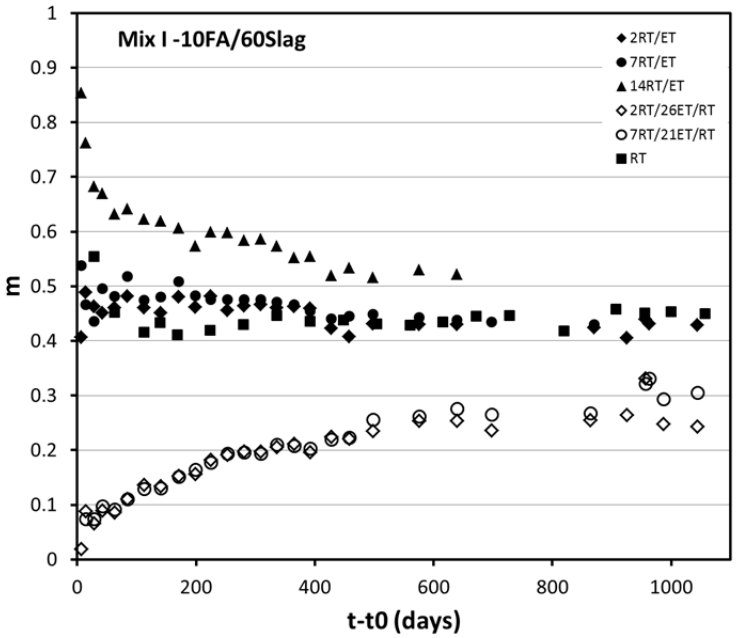
Mix I -10FA/60Slag
2RT/ET
7RT/ET
14RT/ET
2RT/26ET/RT
7RT/21ET/RT
RT
m
t-t0 (days)
0
0.1
0.2
0.3
0.4
0.5
0.6
0.7
0.8
0.9
1
0
200
400
600
800
1000

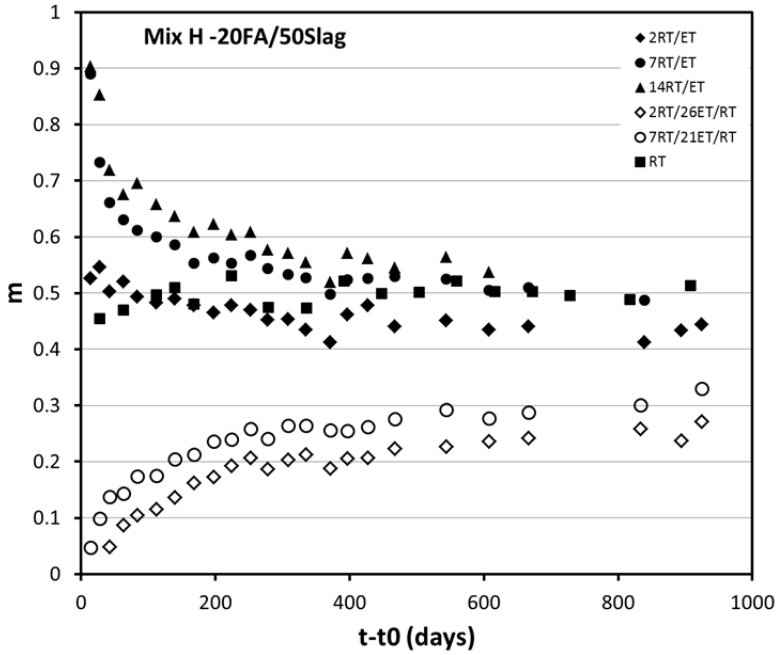
Mix H -20FA/50Slag
2RT/ET
7RT/ET
14RT/ET
2RT/26ET/RT
7RT/21ET/RT
RT
m
t-t0 (days)
0
0.1
0.2
0.3
0.4
0.5
0.6
0.7
0.8
0.9
1
0
200
400
600
800
1000

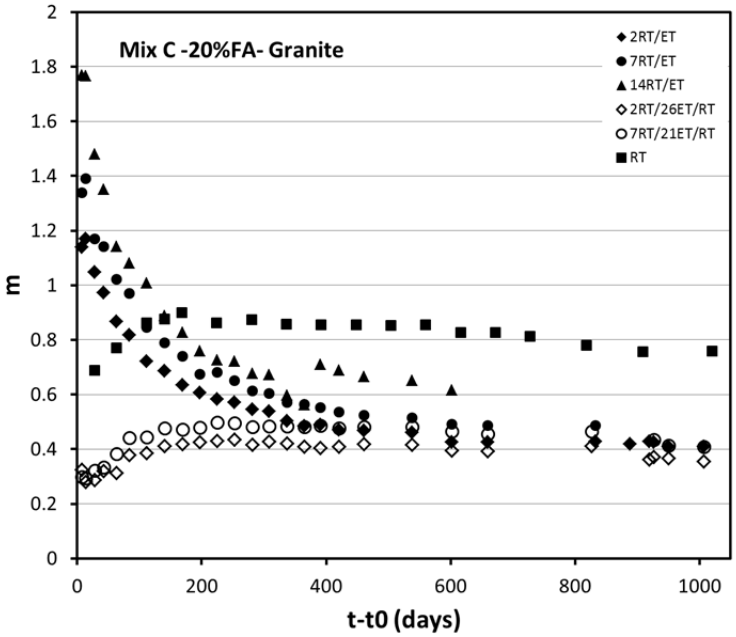
Mix C -20%FA- Granite
2RT/ET
7RT/ET
14RT/ET
2RT/26ET/RT
7RT/21ET/RT
RT
m
t-t0 (days)
0
0.2
0.4
0.6
0.8
1
1.2
1.4
1.6
1.8
2
0
200
400
600
800
1000

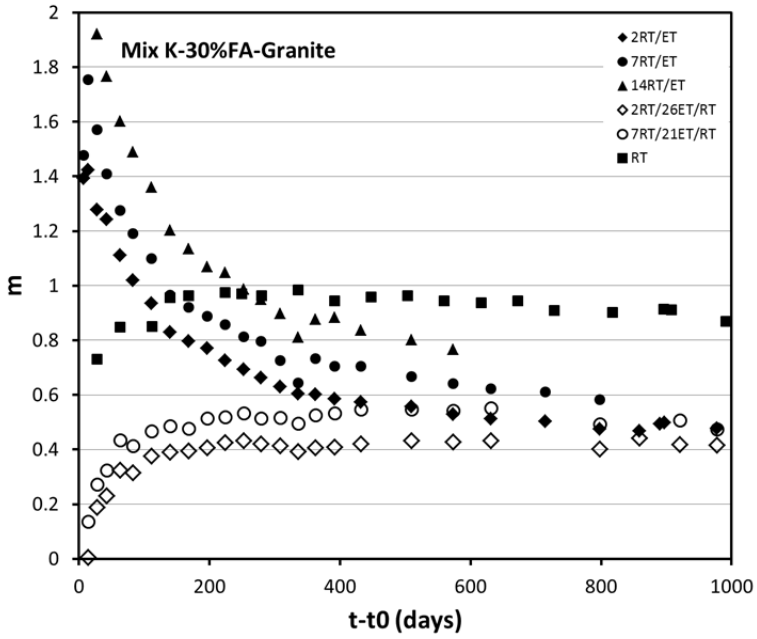
Mix K-30%FA-Granite
2RT/ET
7RT/ET
14RT/ET
2RT/26ET/RT
7RT/21ET/RT
RT
m
t-t0 (days)
0
0.2
0.4
0.6
0.8
1
1.2
1.4
1.6
1.8
2
0
200
400
600
800
1000

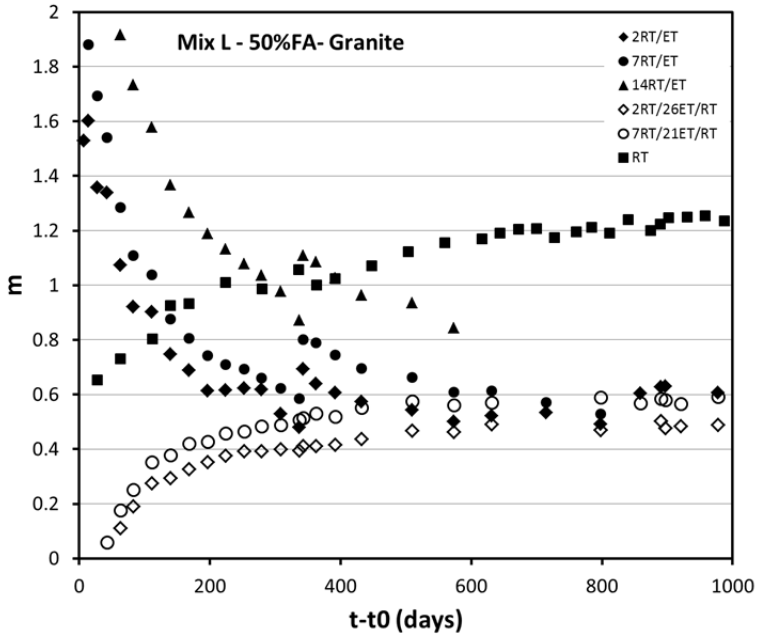
Mix L - 50%FA- Granite
2RT/ET
7RT/ET
14RT/ET
2RT/26ET/RT
7RT/21ET/RT
RT
m
t-t0 (days)
0
0.2
0.4
0.6
0.8
1
1.2
1.4
1.6
1.8
2
0
200
400
600
800
1000

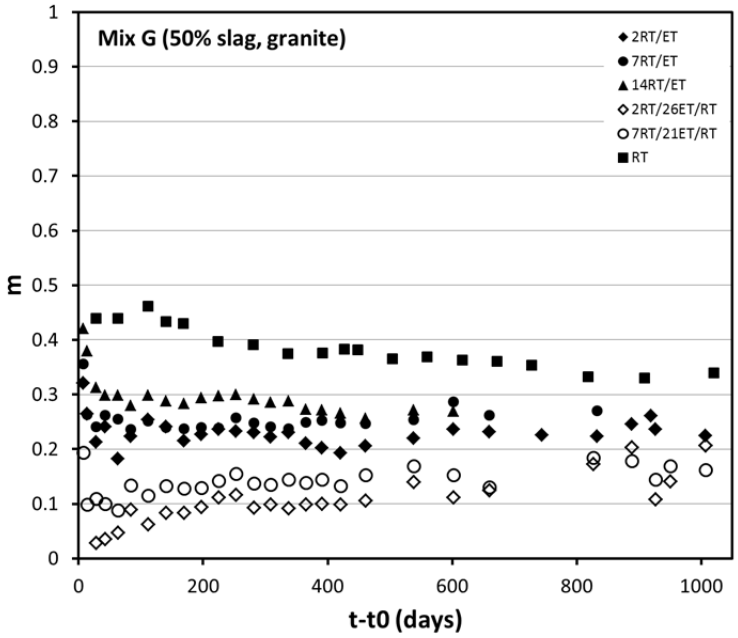
Mix G (50% slag, granite)
2RT/ET
7RT/ET
14RT/ET
2RT/26ET/RT
7RT/21ET/RT
RT
m
t-t0 (days)
0
0.1
0.2
0.3
0.4
0.5
0.6
0.7
0.8
0.9
1
0
200
400
600
800
1000

APPENDIX C: RESULTS OF COMPRESSIVE STRENGTH TEST

Specimen No.	psi	Mpa
Ai-29	6066	41.8
Ai-30	7251	50.0
Ai-31	6227	42.9
Ai-42	6228	42.9
Ai-43	6206	42.8
Ai-44	6127	42.3
Ai-50	5222	36.0

Specimen No.	psi	Mpa
Bi-28	4964	34.2
Bi-30	5426	37.4
Bi-31	5138	35.4
Bi-42	5650	39.0
Bi-43	5465	37.7
Bi-44	5255	36.2
Bi-50	4852	33.5

Specimen No.	psi	Mpa
A-29	9438	65.1
A-30	9641	66.5
A-31	9802	67.6
A-42	9143	63.1
A-43	9488	65.4
A-44	9555	65.9
A-50	9367	64.6

Specimen No.	psi	Mpa
J-29	9499	65.5
J-30	9830	67.8
J-31	10124	69.8
J-42	9745	67.2
J-43	10112	69.7
J-44	9726	67.1
J-50	9697	66.9
J-52	9511	65.6

Specimen No.	psi	Mpa
B-29	8074	55.7
B-30	7990	55.1
B-31	8173	56.4
B-42	7220	49.8
B-43	7997	55.2
B-44	7724	53.3
B-50	7392	51.0

Specimen No.	psi	Mpa
D-29	8667	59.8
D-30	8395	57.9
D-31	8596	59.3
D-42	8088	55.8
D-43	8088	55.8
D-44	8046	55.5
D-50	7601	52.4

Specimen No.	psi	Mpa
G-29	8892	61.3
G-30	9120	62.9
G-31	9440	65.1
G-42	9738	67.2
G-43	9431	65.0
G-44	9368	64.6
G-50	8445	58.2

Specimen No.	psi	Mpa
E-29	11581	79.9
E-30	11682	80.6
E-31	11421	78.8
E-42	12003	82.8
E-43	11585	79.9
E-44	11900	82.1
E-50	11290	77.9

Specimen No.	psi	Mpa
F-29	10962	75.6
F-30	11558	79.7
F-31	11045	76.2
F-42	11695	80.7
F-43	11605	80.0
F-44	11372	78.4
F-50	11084	76.4

Specimen No.	psi	Mpa
I-29	10329	71.2
I-30	10356	71.4
I-31	10311	71.1
I-42	10791	74.4
I-43	9794	67.5
I-44	10423	71.9
I-50	11084	76.4

Specimen No.	psi	Mpa
H-29	10899	75.2
H-30	10109	69.7
H-31	10778	74.3
H-42	11028	76.1
H-43	10407	71.8
H-44	10347	71.4
H-50	10208	70.4
H-52	10817	74.6

Specimen No.	psi	Mpa
C-29	10846	74.8
C-30	10356	71.4
C-31	10722	73.9
C-42	11414	78.7
C-43	10893	75.1
C-44	11132	76.8
C-50	11333	78.2

Specimen No.	psi	Mpa
K-29	8877	61.2
K-30	9341	64.4
K-31	8982	61.9
K-42	8547	58.9
K-43	8897	61.4
K-44	8806	60.7
K50	8710	60.1

Specimen No.	psi	Mpa
L-29	7178	49.5
L-30	7588	52.3
L-31	7503	51.7
L-42	7193	49.6
L-43	7087	48.9
L-44	7221	49.8
L-50	6948	47.9

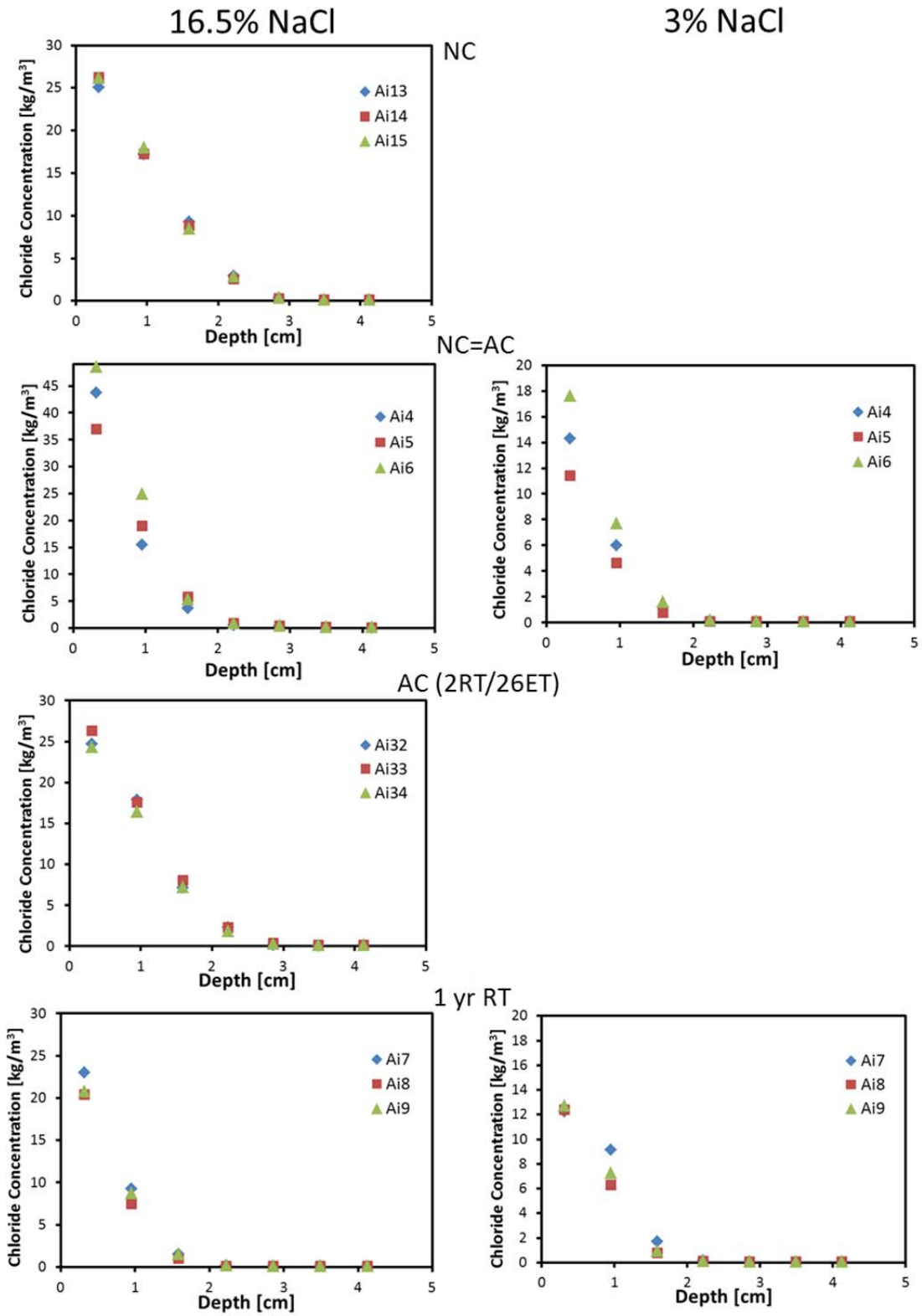
16.5% NaCl
3% NaCl
NC
NC=AC
AC (2RT/26ET)
1 yr RT
Chloride Concentration [kg/m³]
Depth [cm]
Ai13
Ai14
Ai15
Ai4
Ai5
Ai6
Ai32
Ai33
Ai34
Ai7
Ai8
Ai9

16.5% NaCl

3% NaCl

NC

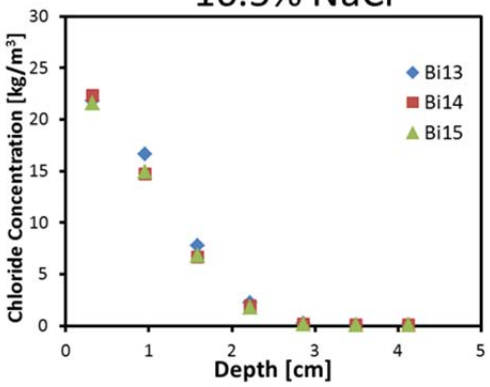

NC=AC

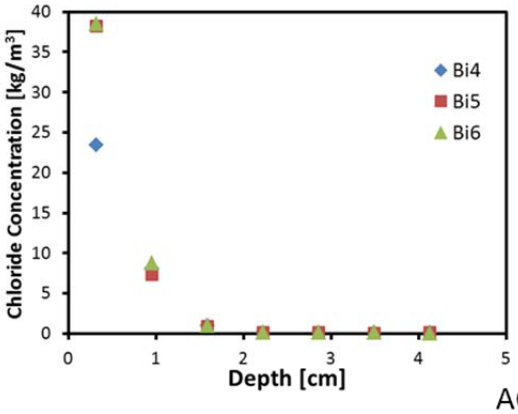

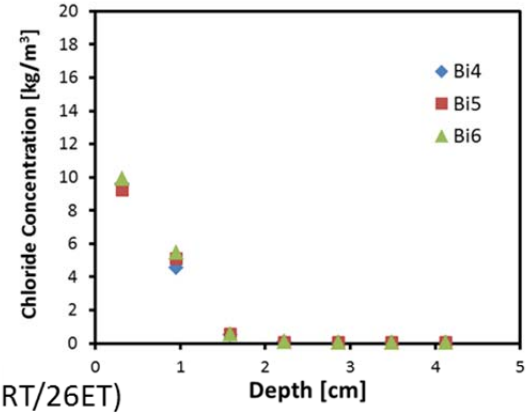

AC (2RT/26ET)

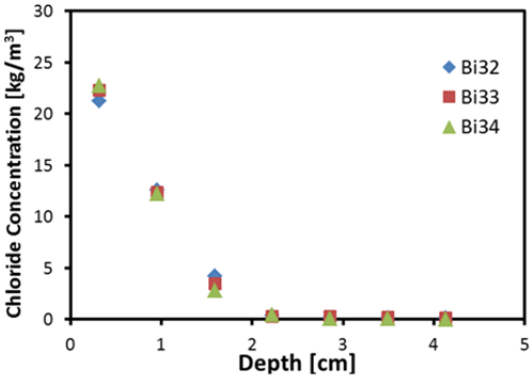

1 yr RT

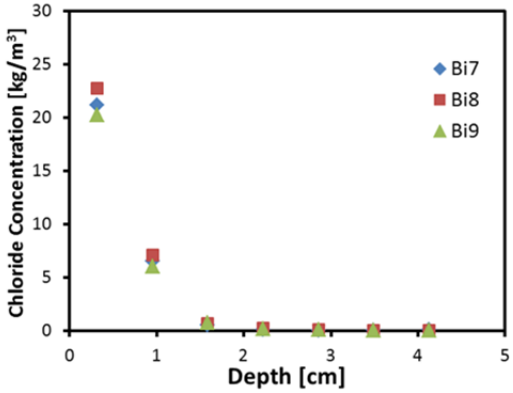

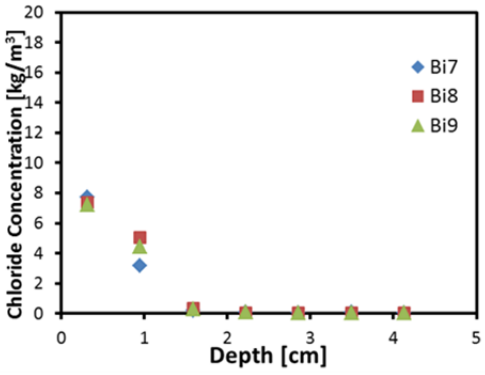

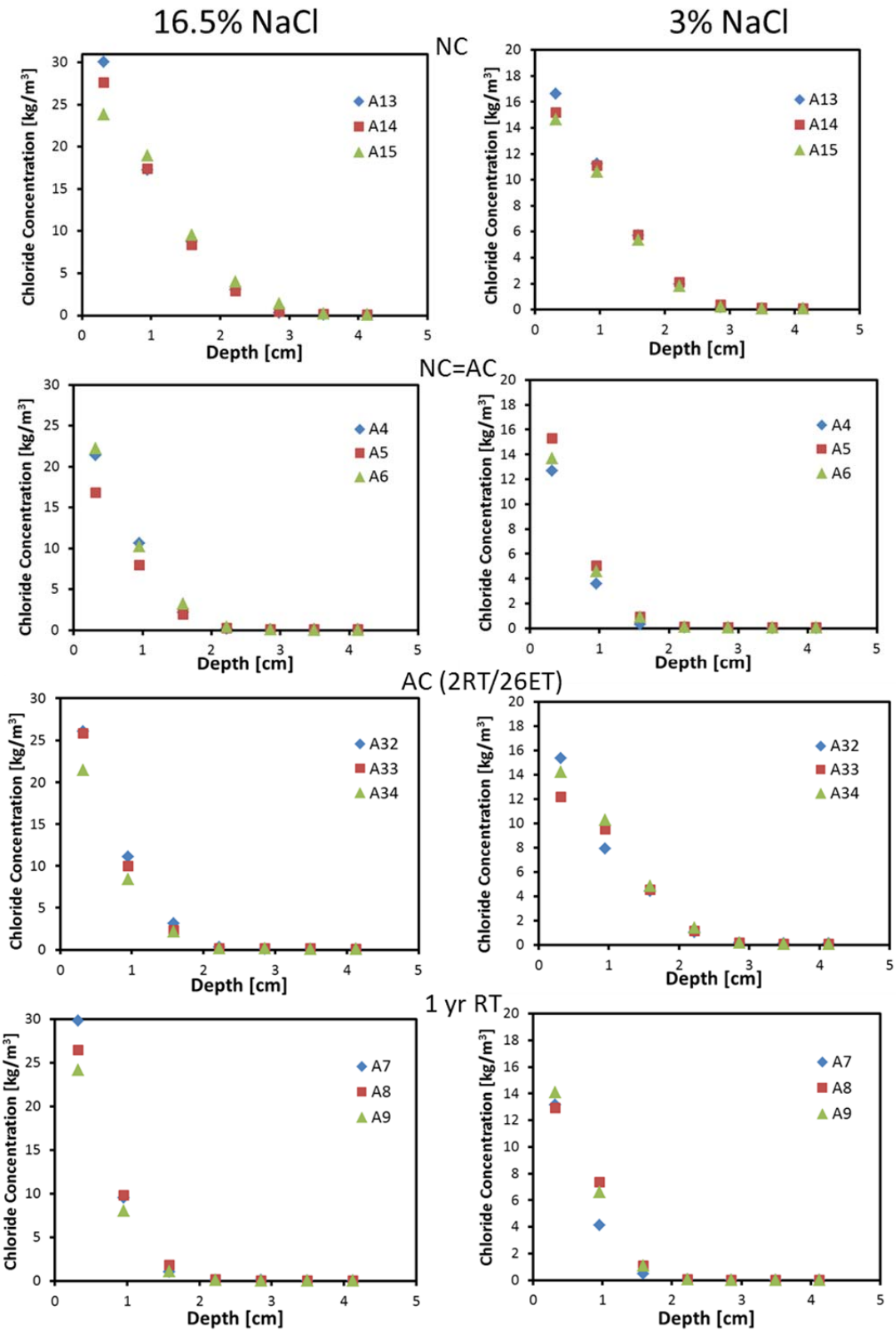
16.5% NaCl
3% NaCl
NC
NC=AC
AC (2RT/26ET)
1 yr RT
Chloride Concentration [kg/m³]
Depth [cm]
A13
A14
A15
A4
A5
A6
A32
A33
A34
A7
A8
A9

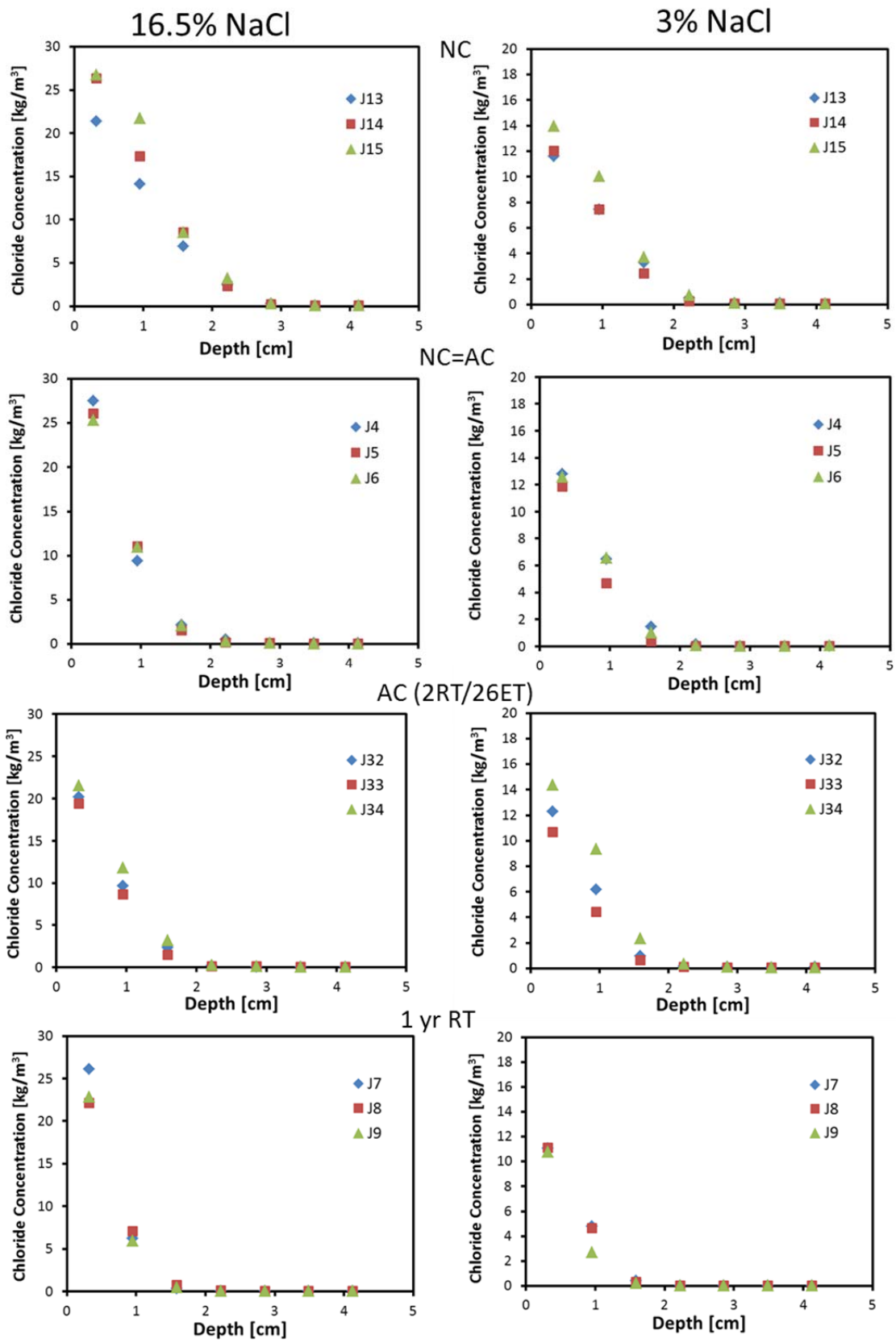
16.5% NaCl
3% NaCl
NC
NC=AC
AC (2RT/26ET)
1 yr RT
Chloride Concentration [kg/m³]
Depth [cm]
J13
J14
J15
J4
J5
J6
J32
J33
J34
J7
J8
J9

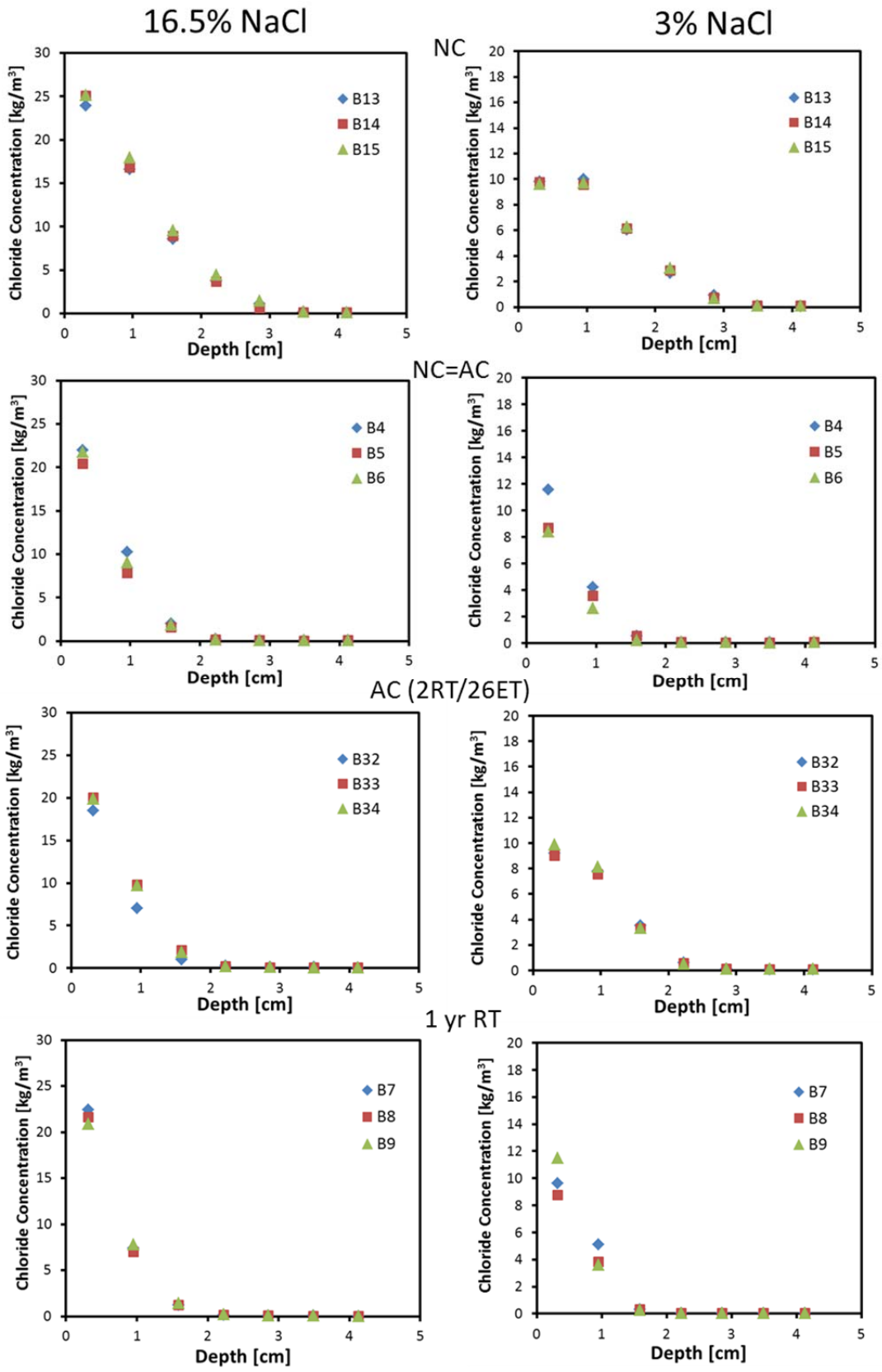
16.5% NaCl
3% NaCl
NC
NC=AC
AC (2RT/26ET)
1 yr RT
Chloride Concentration [kg/m³]
Depth [cm]
B13
B14
B15
B4
B5
B6
B32
B33
B34
B7
B8
B9

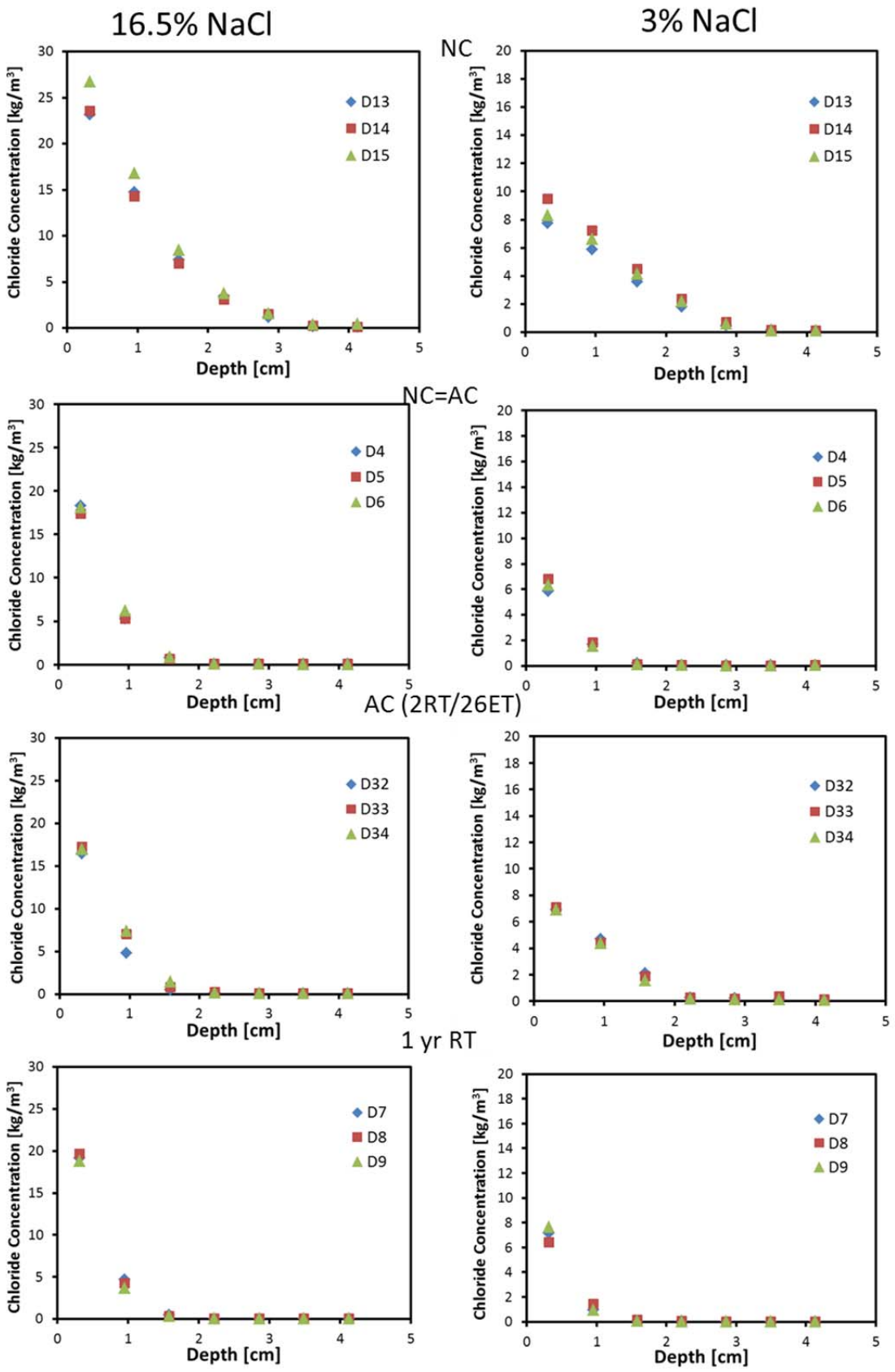
16.5% NaCl
3% NaCl
NC
NC=AC
AC (2RT/26ET)
1 yr RT
Chloride Concentration [kg/m³]
Depth [cm]
D13
D14
D15
D4
D5
D6
D32
D33
D34
D7
D8
D9

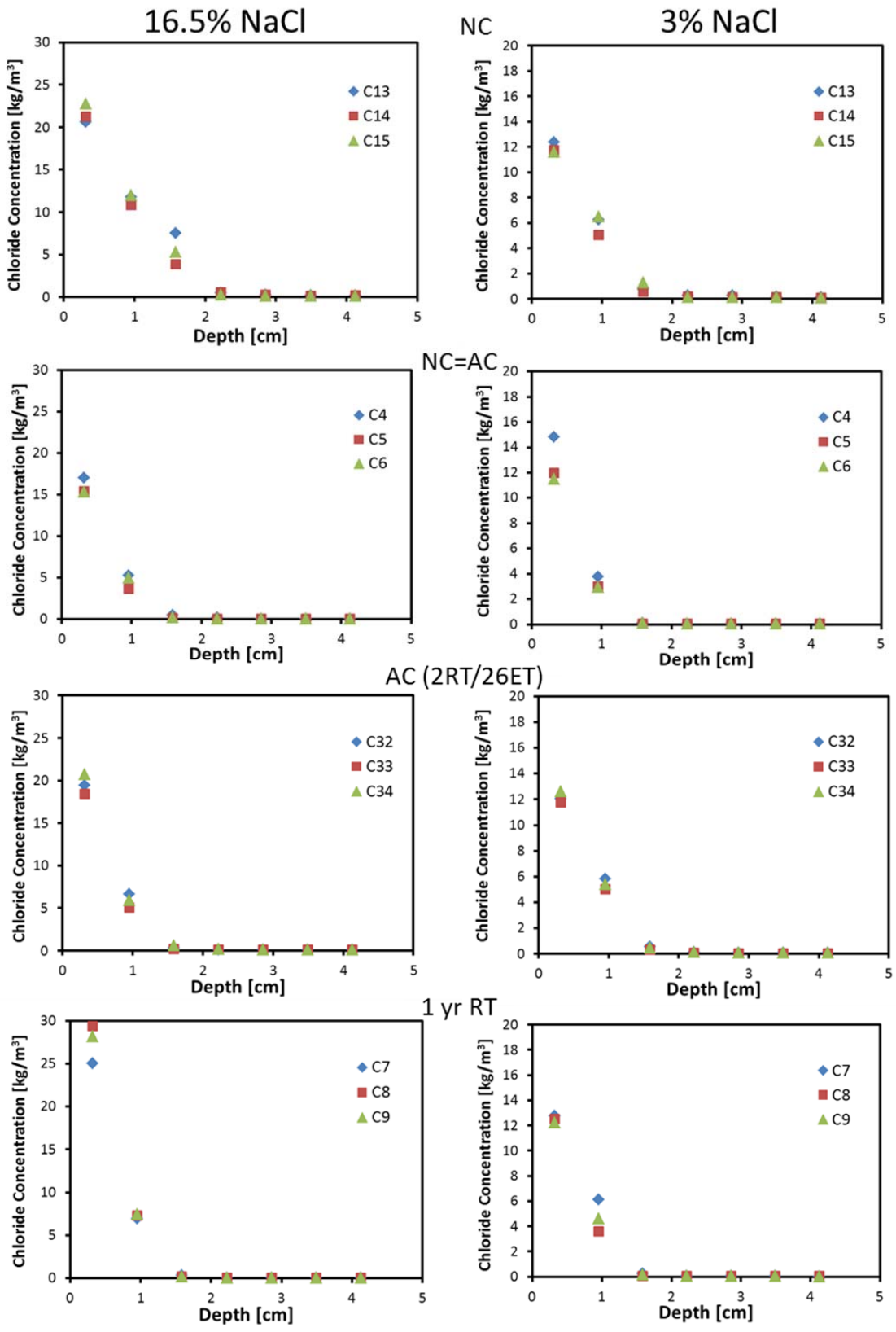
16.5% NaCl
NC
3% NaCl
NC=AC
AC (2RT/26ET)
1 yr RT
Chloride Concentration [kg/m³]
Depth [cm]
C13
C14
C15
C4
C5
C6
C32
C33
C34
C7
C8
C9

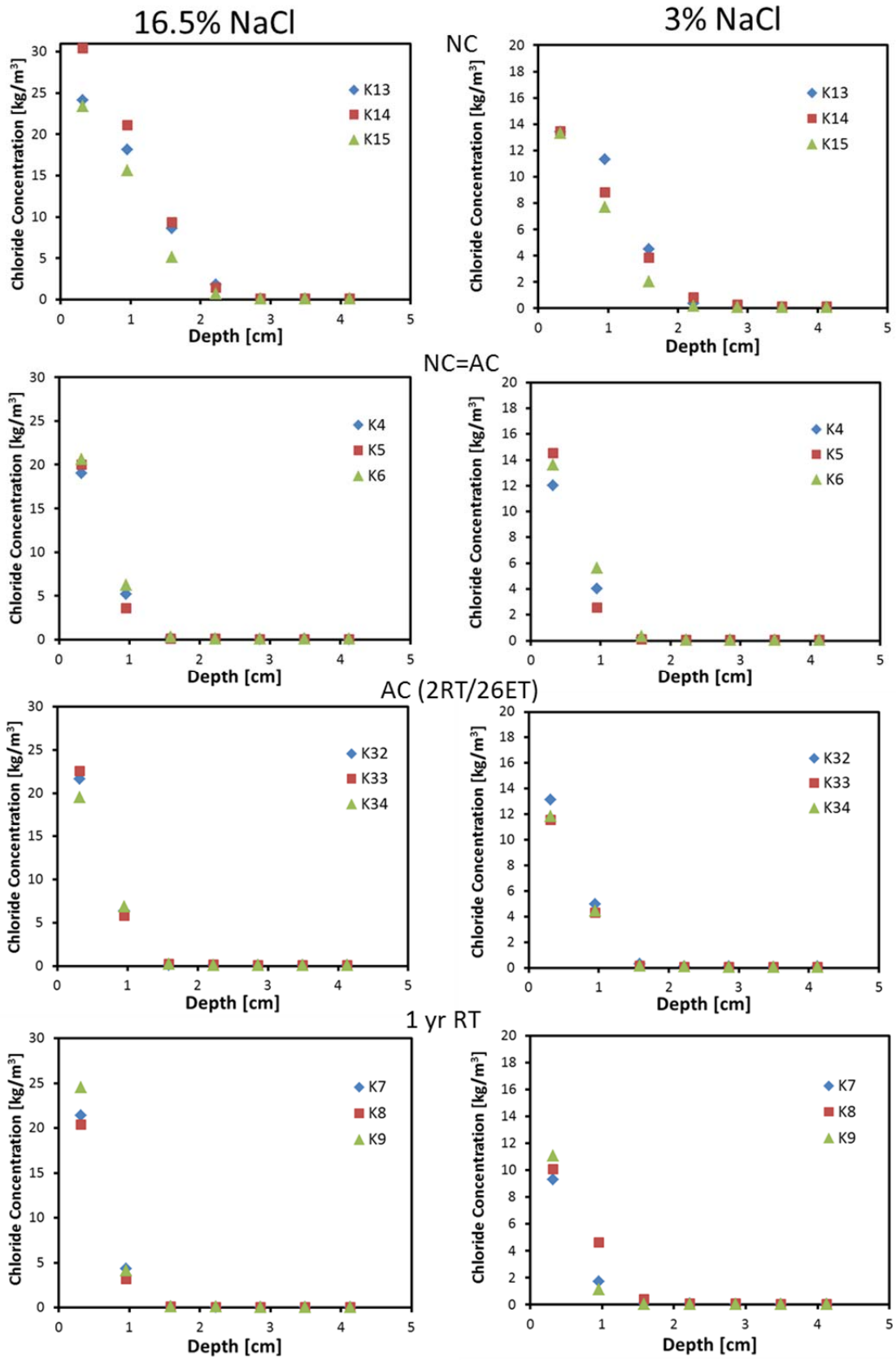
16.5% NaCl
3% NaCl
NC
NC=AC
AC (2RT/26ET)
1 yr RT
Chloride Concentration [kg/m³]
Depth [cm]
K13
K14
K15
K4
K5
K6
K32
K33
K34
K7
K8
K9

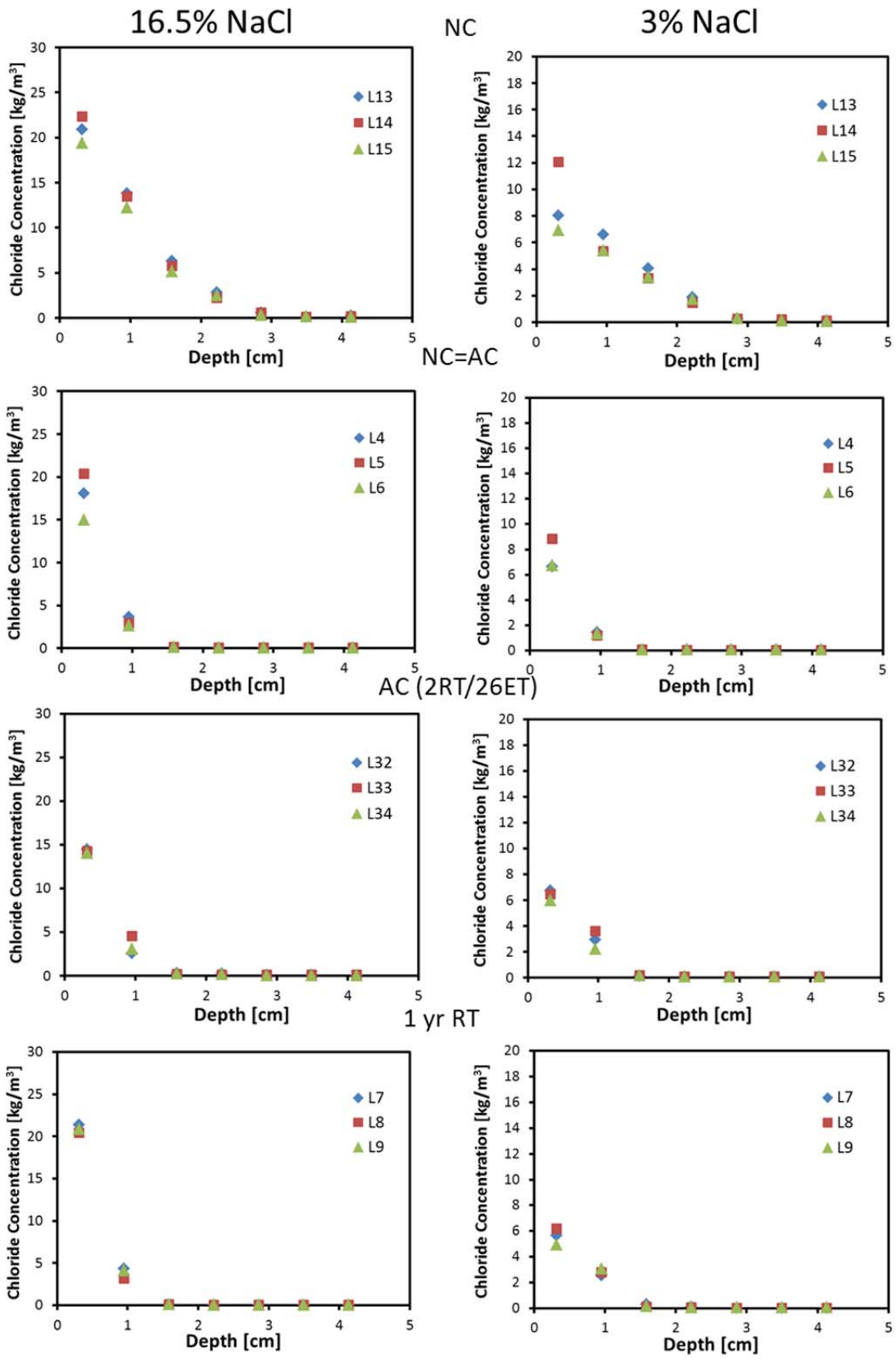
16.5% NaCl
NC
3% NaCl
NC=AC
AC (2RT/26ET)
1 yr RT
Chloride Concentration [kg/m³]
Depth [cm]
L13
L14
L15
L4
L5
L6
L32
L33
L34
L7
L8
L9

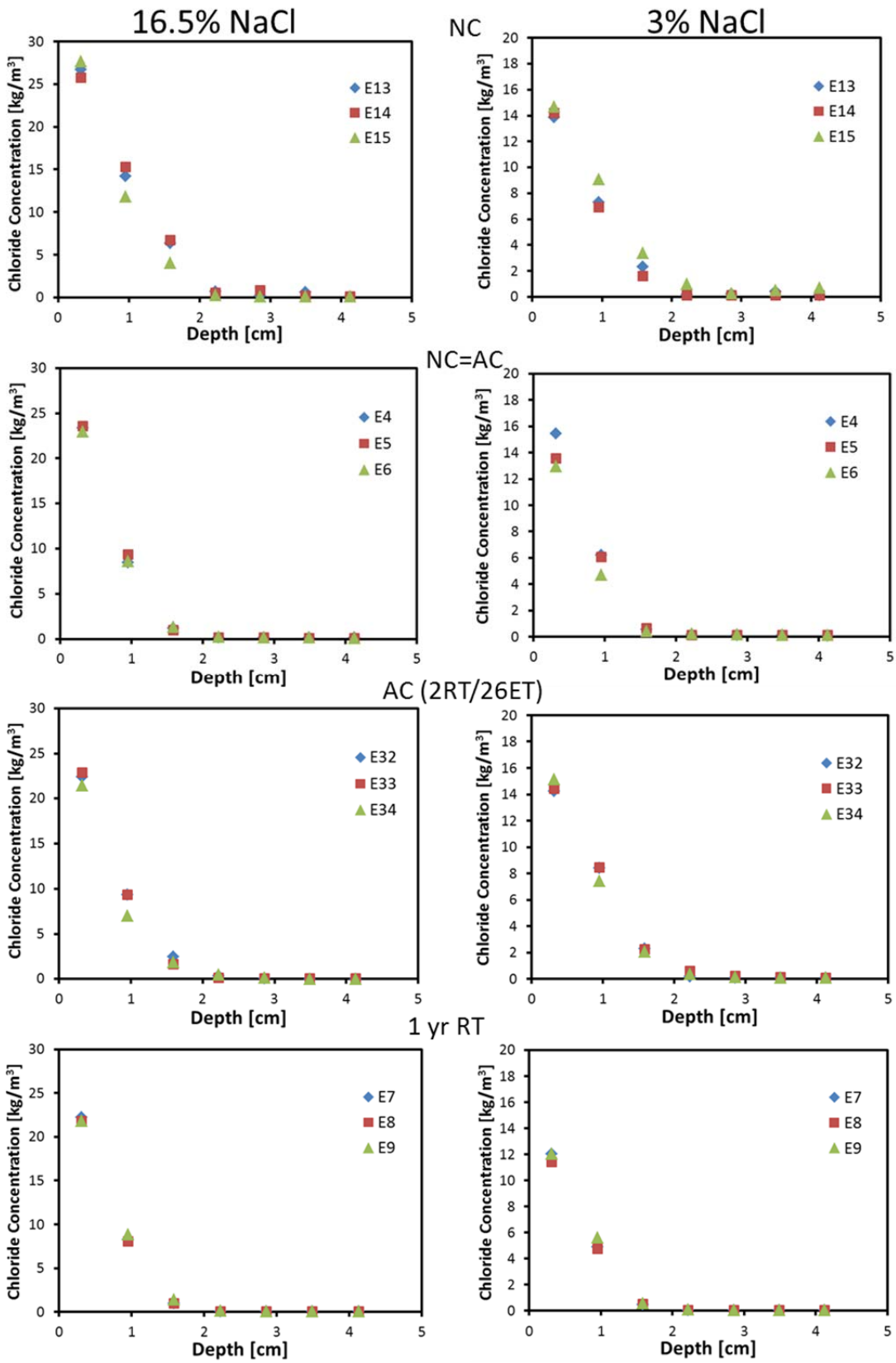
16.5% NaCl
NC
3% NaCl
NC=AC
AC (2RT/26ET)
1 yr RT
Chloride Concentration [kg/m³]
Depth [cm]
E13
E14
E15
E4
E5
E6
E32
E33
E34
E7
E8
E9

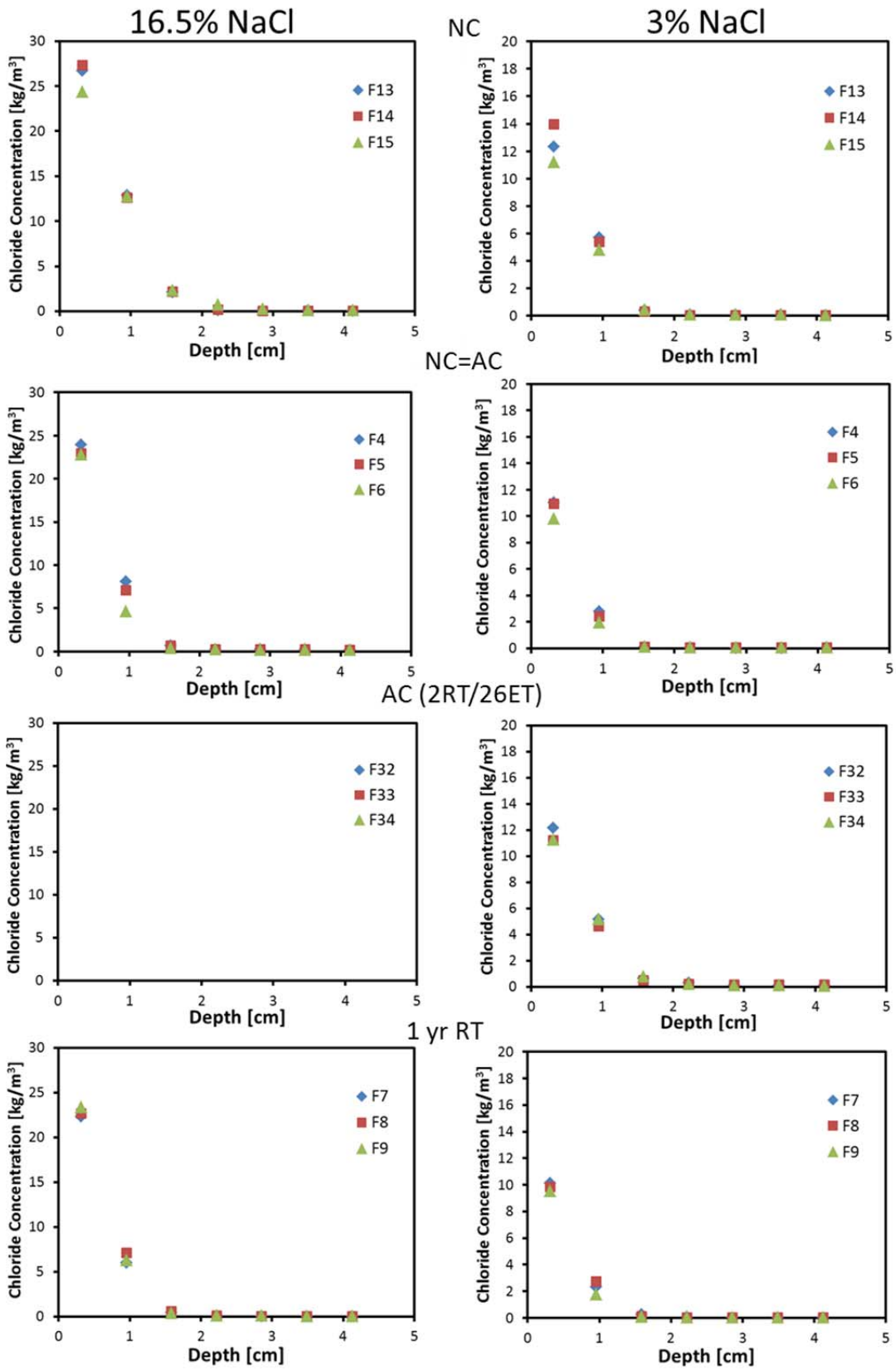
16.5% NaCl
NC
3% NaCl
NC=AC
AC (2RT/26ET)
1 yr RT
Chloride Concentration [kg/m³]
Depth [cm]
F13
F14
F15
F4
F5
F6
F32
F33
F34
F7
F8
F9

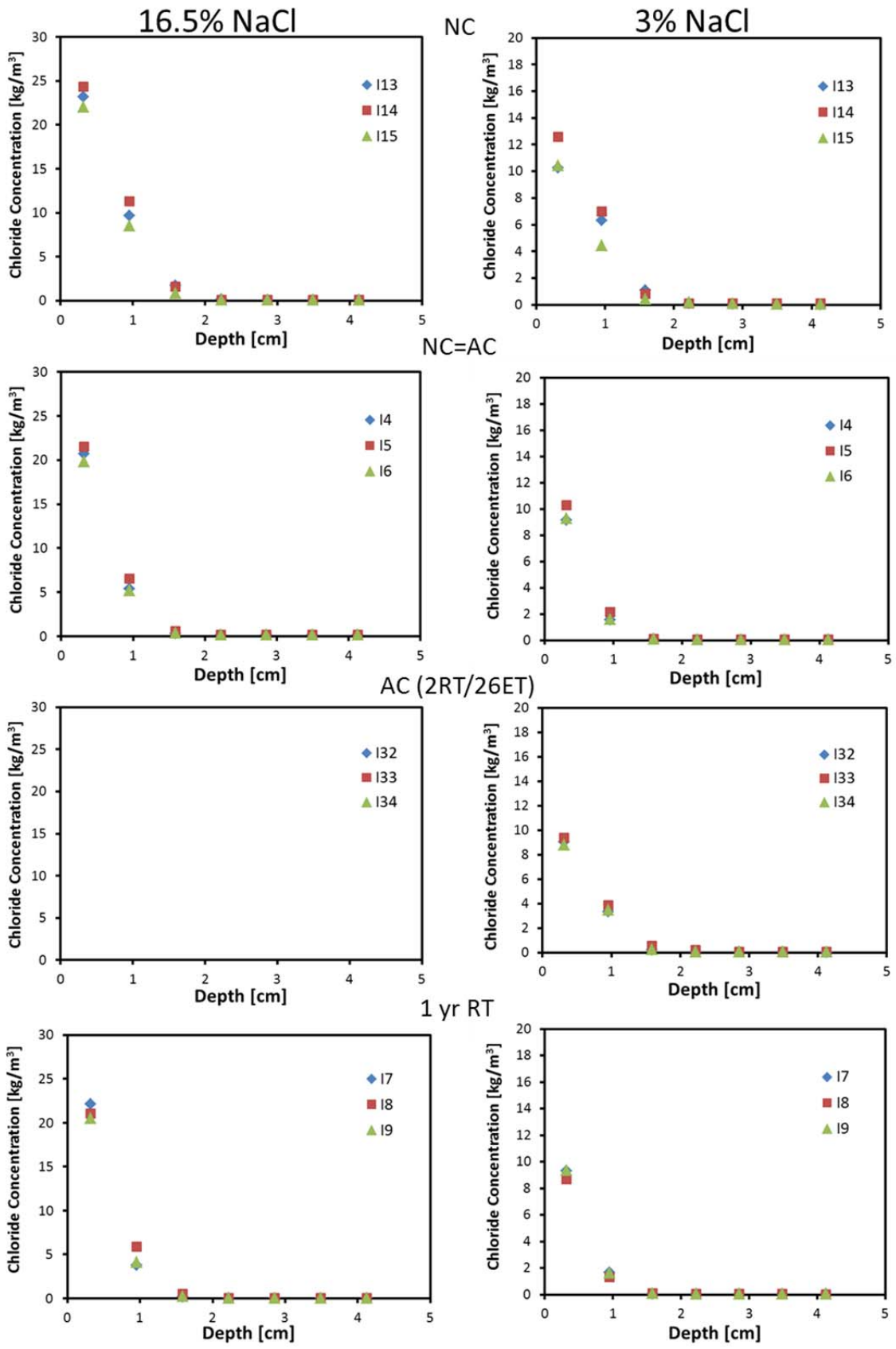
16.5% NaCl
NC
3% NaCl
NC=AC
AC (2RT/26ET)
1 yr RT
Chloride Concentration [kg/m3]
Depth [cm]
I13
I14
I15
I4
I5
I6
I32
I33
I34
I7
I8
I9

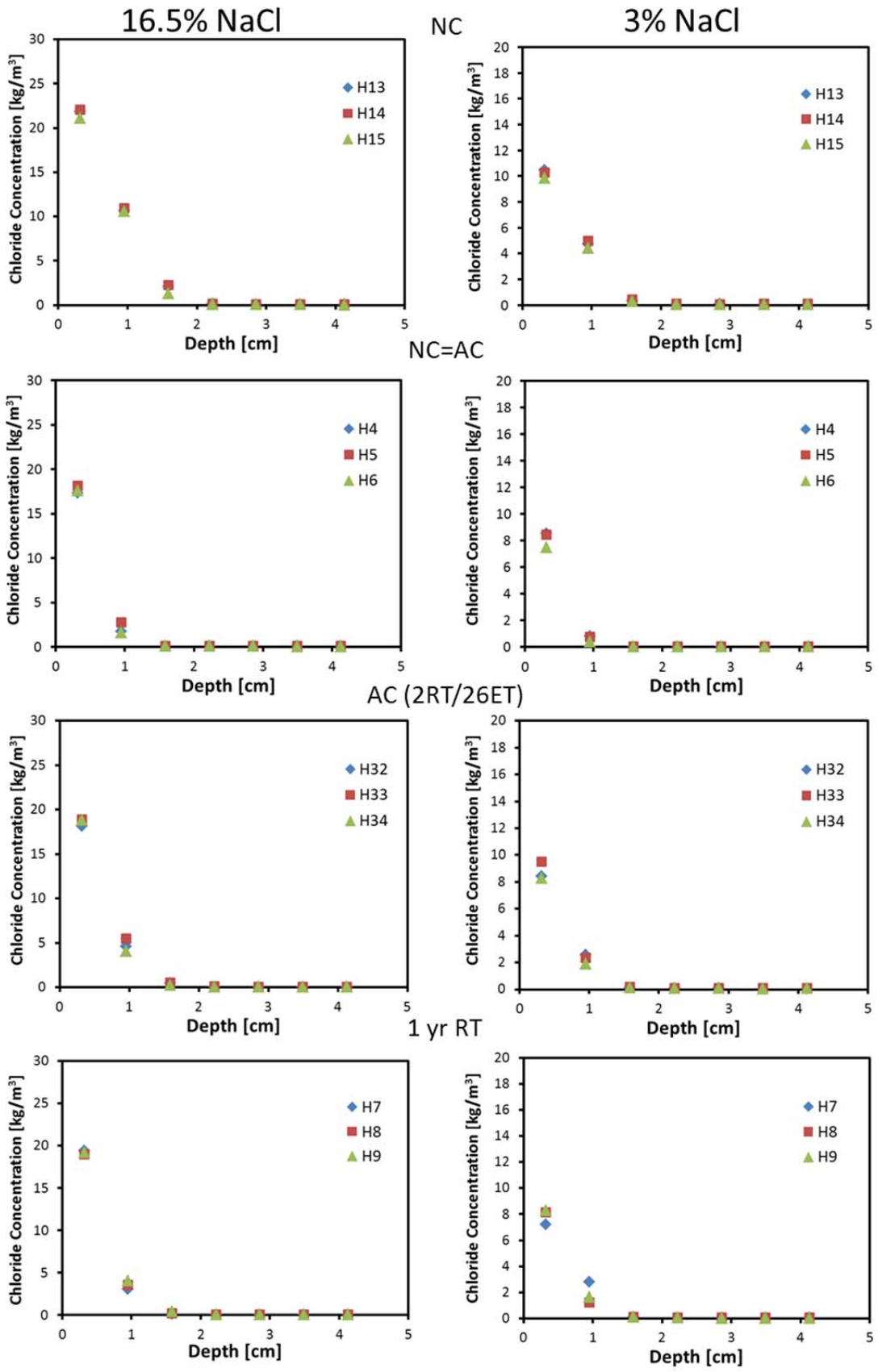
16.5% NaCl
NC
3% NaCl
NC=AC
AC (2RT/26ET)
1 yr RT
Chloride Concentration [kg/m³]
Depth [cm]
H13
H14
H15
H4
H5
H6
H32
H33
H34
H7
H8
H9

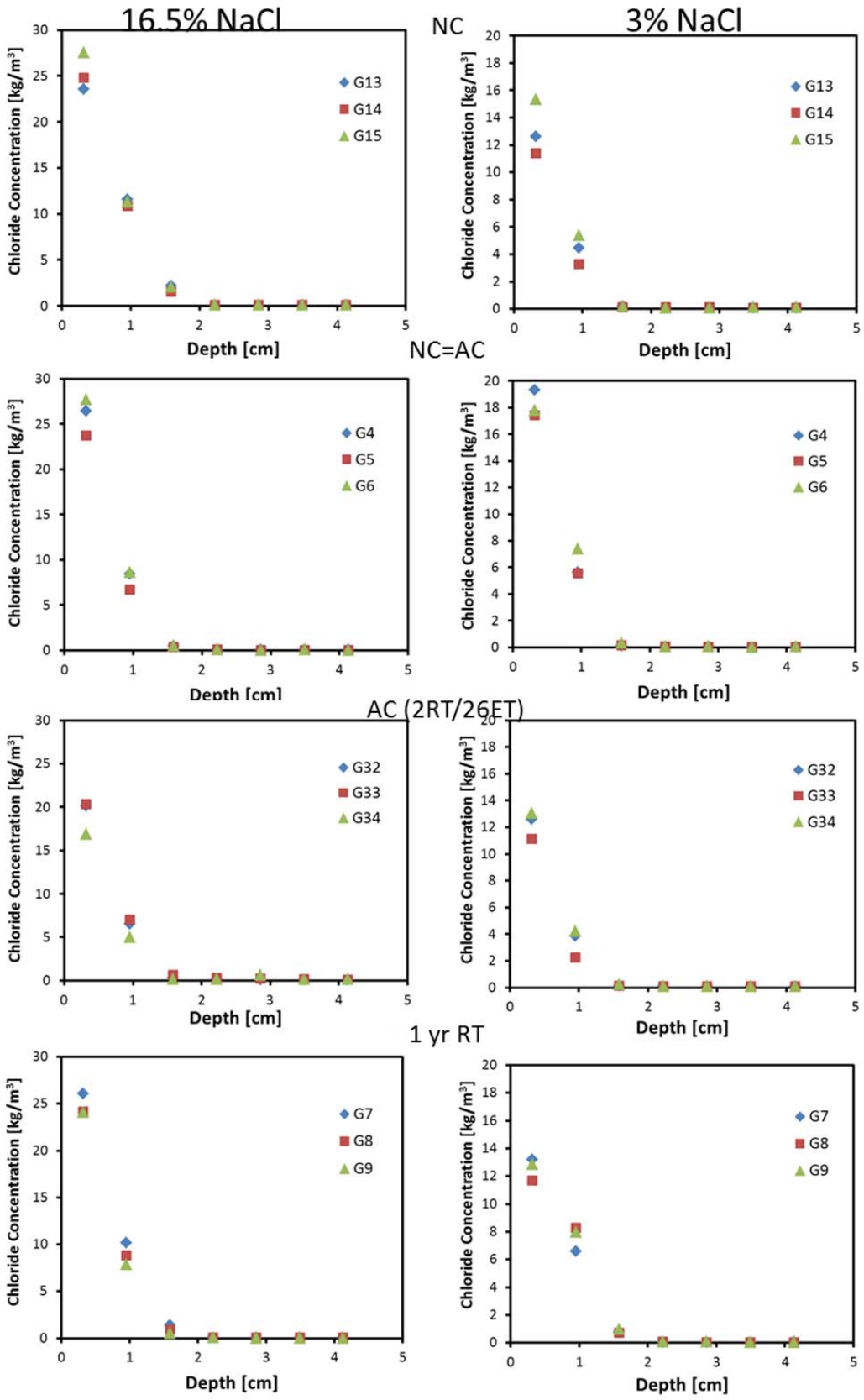
16.5% NaCl
NC
3% NaCl
NC=AC
AC (2RT/26ET)
1 yr RT
Chloride Concentration [kg/m³]
Depth [cm]
G13
G14
G15
G4
G5
G6
G32
G33
G34
G7
G8
G9